Azaphosphatranes derivetives : studies on their halogen donor properties, their behavior as confined frustrated Lewis acid/bronsted pairs and the chiral recognition properties

Chunyang Li

École Doctorale des Sciences Chimiques (ED250)

L'Institut des Sciences Moléculaires de Marseille (iSm2)

THÈSE DE DOCTORAT

pour obtenir le grade de

DOCTEUR de l'ÉCOLE CENTRALE de MARSEILLE

Discipline : Chimie

Azaphosphatranes et dérivés : propriétes comme donneurs de liaison halogen, comme paires de Lewis/bronsted frustrées et propriétés chirales

Par

Madame **LI Chunyang**

Directeur de thèse : Pr. MARTINEZ Alexandre

Co-directeur de thèse : Pr. BUGAUT Xavier

Soutenue le 07 octobre 2021

devant le jury composé de :

M. VIVES Guillaume, Maître de Conférences de *l'Université Sorbonne*	Rapporteur
Mme. GENIN Emilie, Associate Professor de *l'Université de Bordeaux*	Rapporteur
M. BROTIN Thierry, Directeur de recherché à *l'École normale supérieure de Lyon*	Examinateur
Mme DUFAUD Véronique, Directeur de recherché à *CPE Lyon*	Examinateur
Mme FERAY Laurence, Professeur de *l'Université de Aix-Marseille*	Examinateur
M. CHATELET Bastien, Maître de Conférences de *l'École Centrale de Marseille*	Membre invité
M. BUGAUT Xavier, Maître de conférences de *l'Université de Aix-Marseille*	Co-directeur de thèse
M. MARTINEZ Alexandre, Professeur de *l'École Centrale de Marseille*	Directeur de thèse

Acknowledgements

I would like to, first and foremost, sincerely express my gratitude to my Ph.D. supervisor, Professor Alexandre Martinez, for his continuous academic support, encouragement, and guidance throughout my Ph.D. career. I am very grateful to him for the trust and confidence that he had in me even in times when research results came slowly, and for giving me the freedom and understanding to do the research. I realize that not every Professor does that! Meanwhile, I also want to thank him for letting me know how to write scientific papers and supporting information, for polishing my presentations and of course, this thesis, and for allowing me to visit my home country. I have to say that I have been quite lucky in this regard.

Next, I would like to acknowledge my co-supervisor: Professor Xavier Bugaut, he is very knowledgeable, and help me a lot, especially in our first research topic! My special thanks to Dr. Bastien Chatelet and Dr. Anne-Doriane Manick. Bastien, an associate professor in our group, he taught me how to perform the experiments for the first day and gave me many suggestions in my manuscript and publications, he is smart and has a solid background in chemistry! Anne-Doriane, a post-doctor in our group, she put a lot energies in our first research project, without her help, I wouldn't finish this part so smoothly! She is a very good collaborator! Many thanks!

I would also like to thank the past and present Chiroscience group members: Dr. Cedric Colomban, a former post-doc in our group, he is very nice and patient. I am sincerely thankful to Dr. Gege Qiu, who is post-doctor in our group, for not only discussing chemistry with me, but also for teaching me how to do it. I also wish to thank Dr. Sabine Michaud-Chevallier, for helping me detect the mass of products. I warmly thank other members: Dr. Jian Yang, Dr. Marc Hennebelle, Dr. Oriane Della-Negara, Donglin Diao, Yoann Cyrillo, Jingke Hou, Yajie Chou and Louise Miton, thanks for your friendly help, you are very nice! It's my pleasure to work with you! I wish all the best to the rest members in our group.

My sincerely appreciate to Dr. Roseline Rosas and Dr. Julien Chiron for liquid NMR; Dr. Gaelle Hisler and Valérie Monnier for HRMS; Dr. Michel Giorgi for single crystal X-ray diffraction; Dr. Nicolas Vanthuyne and Marion Jean for HPLC.

I would now like to especially thank my parents and my younger sister for their never-ending love and support, my sister and I, we both agree that a doctoral degree is only a

recognition of a certain stage of life, this is still a long journey of life and new challenges come soon.

I also thanks to my friends who will give defense soon: Qiaoqiao Sun, Na Shao, Fangfang Yang, Jiaqi Yang, I have spent very enjoyable time with you! I wish you find a suitable faculty position soon!

Finally, I want to thank the jury members of my PhD defense: M. VIVES Guillaume, Mme. GENIN Emilie, M. BROTIN Thierry, Mme DUFAUD Véronique, Mme FERAY Laurence, for their examination and comments on my PhD work, that I appreciate so much!

I wish you all the best!

Table of contents

List of abbreviation

Ac = acetyl

aq = aqueous

Bn = benzyl

cat. = catalyst

CTV = cyclotriveratrylene

CuAAC = copper(I)-catalyzed alkyne-azide cycloaddition

d = doublet

DCC = dynamic covalent chemistry

DCM = dichloromethane

DFT = density functional theory

DMF = *N*, *N*-dimethylformamide

δ = chemical shift

ECD = electronic circular dichroism

ee = enantiomeric excess

Et = ethyl

ESI = electrospray ionization

h = hour

Hz = hertz

HPLC = High Performance Liquid Chromatography

HRMS = High Resolution Mass Spectroscopy

IR = infrared spectroscopy

J = coupling constant in hertz

m = multiplet

Me = methyl

NMR = Nuclear Magnetic Resonance spectroscopy

Ph = phenyl

ppm = parts per million 5

rt = room temperature

s = singlet

t = triplet

t-Bu = tertbutyl

THF = tetrahydrofuran

TLC = thin film chromatography

TON = turnover number

TOF = turnover frequency

tren = tris(2-aminoethyl)amine

General introduction

This thesis contains four chapters. Except chapter **1**, all the other chapters are based on papers that have either been published or accepted for publication in scientific journals. The ^{I}H, ^{13}C, and ^{31}P NMR spectra for the reaction products have been compiled in appendices, which appear at the end of the thesis. Also, since several chapters have the same reaction products, efforts have been made to avoid duplication of the spectra and thus have been provided only once.

Firstly, we discussed chloroazaphosphatranes, the corresponding halogenophosphonium cations of the Verkade's superbases, which were evaluated as a new motif for halogen bonding (XB). Their modulable synthesis allowed for synthetizing chloroazaphosphatranes with various substituents on the nitrogen atoms. Binding constants were determined from ^{1}H NMR titration experiments for Cl^{-}, Br^{-}, I^{-}, AcO^{-} and CN^{-} anions and are comparable to those obtained with conventional iodine-based monodentate XB receptors. Remarkably, the protonated azaphosphatrane counterparts display no affinity for anions under the same conditions. The strength of the XB interaction is, to some extent, related to the basicity of the corresponding Verkade's superbase. Moreover, the binding constants remain close to those obtained with conventional iodine-based monodentate XB receptors. The halogen bonding abilities of this new class of halogen donor motif were also revealed by the $\Delta\delta$ (^{31}P) NMR shift that observed in CD_2Cl_2 solution in the presence of triethylphosphine oxide (TEPO). Thus, chloroazaphosphatranes appear as a new class of halogen bond donors, expanding the repertory of XB motifs mainly based on C_{Ar}-I bonds, based on these results, we have published the first paper.

Secondly, two new enantiopure hemicryptophanes combining a cyclotriveratrylene unit with either an amino-trisamide or a tris-(2-aminoethyl)amine(tren) moiety have been synthesized. Although the conventional synthesis approach was used, the molecular cages obtained are devoid of the expected C_3 symmetry. NMR analyses and X-ray crystal structure determination showed that these hemicryptophanes exhibited C_1 symmetry due to the unusual arrangement of the substituents of the cyclotriveratrylene unit. We hypothesize that this unprecedented arrangement, is related to a change in the regioselectivity of the last Friedel-Crafts reaction that leads to the CTV cap. This constitutes an original approach to access to enantiopure chiral molecular cages with low symmetry. Reaction with $PCl(NMe_2)_3$ failed to give encaged

azaphosphatrane, but, an unusual reactivity of the tren unit was observed: a secondary phosphine oxide was formed, highlighting how the arrangement of the tren unit, controlled by the CTV cap, affects the reactivity, based on these results, we have another paper under review now.

Thirdly, three different endohedrally functionalized cage molecules were designed in order to study the effect of size of their cavities on their acid-base Lewis/Bronsted frustrated behavior and catalytic activities. The shape of the inner space above the reactive center was found to strongly affect these properties: once an acidic azaphosphatrane is encaged in the smallest cage and associated to *t*-BuOK or $^{-}CD_2CN$ bases, a frustrated Bronsted pairs are obtained. In contrast, when encapsulated in the medium and large cage, the azaphosphatrane acid is easily deprotonated under the same conditions. The two resulting supramolecular Verkade's superbases lead to FLP systems in the presence of $TiCl_4$. Furthermore, the larger cage displays a better catalytic activity when associated to $TiCl_4$, in the MBH reaction. This highlights that a small change in the cage size -they only differ by one methylene in their linkers- can influence the frustrated properties of the related systems and that a right balance between frustrated behavior and flexibility has to be reached to obtain optimal systems for catalytic applications.

Chapter 1: Proazaphosphatranes: a highly effective class of triaminophosphine ligands in chemistry

1.1 Introduction

Atrane **1** is the ring structure compound that contain two atoms (one of which is a nitrogen atom) at the bridgehead connected by three units, each unit consist of three atoms. Since the 1960s, it has been primarily used to refer to the transannular bond, which is related to a tricyclic structure if the atoms at the bridgehead interact (Figure 1.1.1). The transannular coordinate bond in atrane **1** can be considerably stretched to quasi tricyclic structure with a bond between the two bridging atoms, quasi-atrane **2,** and if there is no interacts between two atoms, atrane structure would be broken to give pro-atrane **3** through imposing stereoelectronic constraints on the Y and Z substituents for several main group elements E. The first well-substantiated example of such structure was studied in details by Voronkov with silatranes wherein E = Si, Y = O and Z was an organic substituent.[1] It was subsequently proposed to give the name azatrane to the type **1** structures when Y was replaced by NR. Up to now, many elements groups were introduced in atrane-type structures, such as bismuth, titanium, vanadium, boron, aluminum and iron[2]. The properties of azatrane can be modulated more easily since one can easily change the steric and electronic properties of R groups on nitrogen atoms. It is in particular the nature of the E atom and the properties of the groups on the nitrogen atoms which govern the properties of azatranes as we will see with azaphosphatranes.

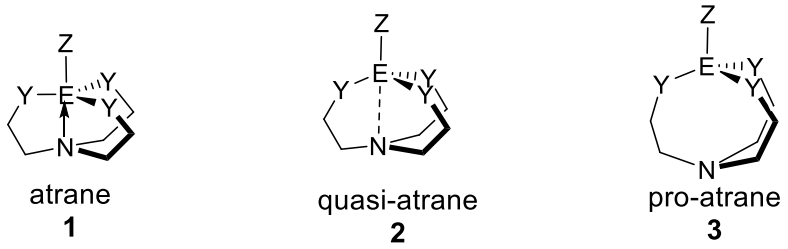

Figure 1.1.1 Structure of atrane **1**, quasi-atrane **2** and pro-atrane **3**.

In 1976, professor Verkade's research team synthesized the first phosphatrane, they used triethanolamine as ligand, let it reacted with tris(dimethylamino)phosphine in order to generate the compound **4,** hopefully, they attempted to isolate **4** by evaporating the solvent, but an intractable material which decomposed violently was produced. Later, their attempts to alkylate **4** by using Et_3OBF_4 or Me_3OBF_4, however the reaction did not produce expecting compound of alkylation, either, instead only **5-BF$_4$** was isolated (Figure 1.1.2), which was identified by

[1] *Voronkov M. G., Pure Appl. Chem., 1966, 13, 35-59.*

[2] *Verkade J.G., Acc. Chem. Res., 1993, 26, 412-489.*

high field ^{31}P nuclear magnetic resonance (NMR) shift (-20.9 ppm), and one-bond P-H coupling constant (790 Hz), and its structure was further confirmed by X-ray crystallography (P-N bond length 1.986 Å). [3] It was shown that the R_3OBF_4 alkylated the unreacted $(HOCH_2CH2)_3N$, releasing protons that surprisingly gave rise to a transannulated structure wherein the proton resides in such a position.[4]

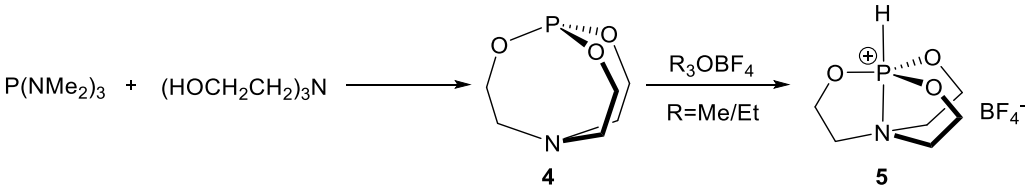

Figure 1.1.2 Synthesis of phosphatrane **5-BF_4** cation.

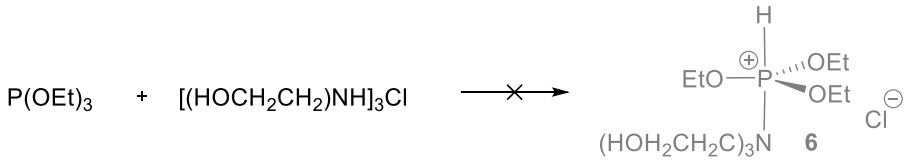

Figure 1.1.3 Chelation experiment to prove the stability of **5-BF_4**.

Verkade assumed that although coordination of the bridgehead nitrogen of **4** to a proton was expected in the basic condition, such a kinetically generated cation must rearrange to cation **5-BF_4**, because of the stability upon transannulation where the three chelating five-membered rings formed, meanwhile, relief of strain in the formation of additional bonds toward the bridgehead atoms in going from **4** to **5-BF_4** probably also played a role.[5] Then an experiment (Figure 1.1.3) was performed to demonstrate the main effect of chelation, where a P-H coupling would have been expected for the product salt **6**,[6] but they failed to obtain it.

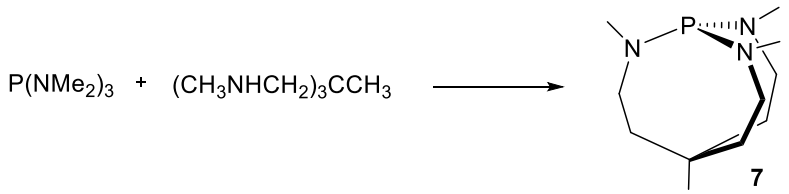

Figure 1.1.4 Synthesis of compound **7.**

[3] *Clardy, J.C.; Milbrath, D.S., Springer, J.P. and Verkade, J.G., J. Am. Chem. Soc., 1976, 98, 624-625.*

[4] *Carpenter, L. E.; Verkade, J. G. J. Org. Chem., 1986, 51, 4287.*

[5] *W. Alder, Tetrahedron, 1990, 46, 321.*

[6] *D.S. Milbrath and J.G. Verkade, J. Am. Chem. Soc., 1977, 99, 6607.*

There are further evidences to prove the stability of the phosphorus coordination compound **5-BF_4**, in the presence of sodium methoxide (CH_3ONa), the strong base 1,8-bis (dimethylamino) naphthalene (proton sponge), and magic acid HSO_3F-SbF_5 were considered. However, compound **5-BF_4** doesn't react under these conditions: no protonation of the quaternary nitrogen by magic acid or deprotonation of the phosphorus atom by strong bases was observed.[6] Since cation **5** was found to be a very weak acid, Verkade decided to synthesize other compounds that possessed similar structures but in azaphosphatrane's version. Firstly, $(MeHNCH_2)_3CMe$ was used to generate the more rigid molecule **7** (Figure 1.1.4) with a surprising yield of 90% within a few hours.[7] Then, they hoped to synthesize proazaphosphatranes and attempted to isolate proazaphosphatrane structures such as **8-10** which are analogues of unstable **4**. Figure 1.1.5 showed the synthesis pathway, whereas the synthesis of **8** only resulted in the formation of polymer, **9** and **10** could be synthesized in yields ranging from 20 to 50% over a period of a few weeks.[8] The slowness of the reaction was surprising since the reaction with the ligand $(MeNCH_2)_3CMe$ led to the product **7** with a very high yield in a few hours.

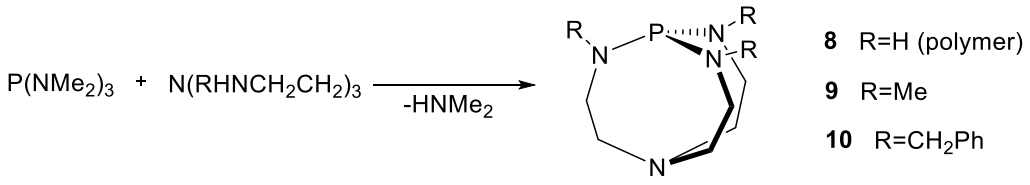

Figure 1.1.5 Synthesis of compounds **8-10.**

It was reasonable that the slow rate of reaction was probably associated with strain in the eight-membered ring bicyclic products, so some efforts were performed to increase the rate of formation of **9** or **10**, the more reactive phosphorus reagent $PCl(NMe_2)_2$ (a mixture of PCl_3 and $P(NMe_2)_3$) in Figure 1.1.6 was employed. To their surprise, this reaction took a different course, they did not observe the compound **8-10,** instead, producing nearly quantitative yields of **11-$H^+ \cdot Cl^-$**, **12a-$H^+ \cdot Cl^-$** and **12c-$H^+ \cdot Cl$** within about 1 hour at room temperature.[9] In this reaction, trimethylamine is the base to avoid deprotonating the phosphorus atom. The salts have very weak acidity, it was supported by the fact that, no proton was exchanged by a deuterated proton when mixed with deuterated trifluoroacetic acid.

---

[7] *B.L. Laube, R.D. Bertrand, G.A. Casedy, R.D. Compton and J.G. Verkade, Inorg. Chem., 1967, 6, 173.*

[8] *(a) C.L. Frye, G.E. Vogel and J.A. Hall, J. Am. Chem. Soc., 1961, 12, 996. (b) M.G. Voronkov, V.M. Dyakov and S.V. Kirpichenko, J. Organomet. Chem., 1982, 233, 1. (c) N. Stanislav, M.G. Voronkov and N.V. Alekseev, Topics Curr. Chem., 1986, 131, 99.*

[9] *M.A.H. Laramay and J.G. Verkade, J. Am. Chem. Soc., 1990, 112, 9421.*

It was therefore necessary to use strong ionic bases to deprotonate azaphosphatranes such as potassium tert-butoxide (*t*-BuOK). Competition deprotonation experiments were performed to compare the acidities of azaphosphatranes **11-H$^+$·Cl$^-$, 12a-H$^+$·Cl$^-$** and **12c-H$^+$·Cl$^-$** by ^{31}P NMR spectrum by using *t*-BuOK in DMSO,[9] it turned out that the acidity follows the order **11-H$^+$·Cl$^-$** > **12a-H$^+$·Cl$^-$** > **12c-H$^+$·Cl$^-$**, the observed acidity order is supported by the parallel decrease in $^1J_{PH}$ coupling (506, 491 and 453 Hz respectively), the decrease in steric hindrance around the axial proton in the order CH_2Ph > Me > H in **12c-H$^+$·Cl$^-$**, **12a-H$^+$·Cl$^-$** and **11-H$^+$·Cl$^-$**, therefore the domination of electronic effects could explain the relative acidity of cations. The pKa of **11-H$^+$·Cl$^-$** was evaluated at 26.8,[9] this increased basicity of proazaphosphatranes was due to the stability of the penta-coordinationated structures of their conjugated acids. The trans-annulation thanks to the lone pair of the nitrogen atom makes phosphorus very rich in electrons and gives stability to the cation, forming a 4-electron bond delocalized on three centers along the C_3 axis.

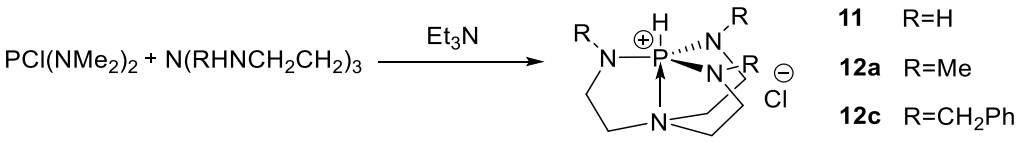

Figure 1.1.6 Synthesis of compound **11-H$^+$·Cl$^-$** or **12a-H$^+$·Cl$^-$** or **12c-H$^+$·Cl$^-$**.

1.2 Azaphosphatranes

It should be noticed that conjugated acids (PH^+) actually have received little attention, but recently new aspects have been developed, such as their use as organocatalysts to enhance the phase-transfer-catalysts (PTC) and the synthesis of cyclic carbonates from CO_2 and epoxides; otherwise confined catalysts in hemicryptophanes for the synthesis of cyclic carbonates with CO_2 and epoxides; as hydrogen-bonding organocatalysts for the activation of carbonyl groups, also azaphosphatranes could be used to recognize anions.

1.2.1 Azaphosphatranes as organocatalysts for PTC and CO_2

The use of azaphosphatrane derivatives in phase-transfer-catalysts (PTC) was studied by Martinez and coworkers.[10] The efficiency of a phase-transfer catalyst generally depends on its partial solubility both in aqueous and organic phases, as well as on its ration of lipophilicity and hydrophilicity. Thus, three azaphosphatranes acidic counterparts of the well-known proazaphosphatrane superbases **12a-H$^+$·Cl$^-$**, **12c-H$^+$·Cl$^-$** and **13-H$^+$·Cl$^-$** were considered as the phase-transfer catalysts in biphasic heterogeneous media (Figure 1.2.1), these azaphosphatrane cations bearing different alkyl or benzylic side chains were used to facilitate the migration of a reactant from one phase into another phase where the reaction occurs.

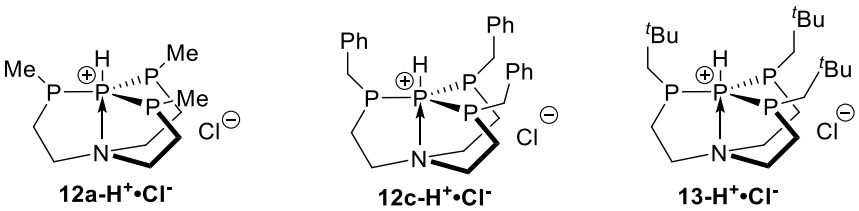

Figure 1.2.1 Azaphosphatranes involved in the catalytic studies.

PTC process can achieve faster reactions, obtain higher conversions or yields, and make fewer byproducts, so the authors firstly investigated the benzylation to give compound **16** by using the product **14** (methyl 1-oxo-2, 3-dihydro-1H-indene-2-carboxylate) and **15** (Figure 1.2.2). This classic reaction of PTC is a good example of C-C bond formation that involve the creation of a quaternary carbon center, and it have been used several times as a PTC standard.[11]. Three

[10] *P. Dimitrov-Raytchev, J.-P. Dutasta, A. Martinez. ChemCatChem 2012, 4, 2045 – 2049.*

[11] *a) K. Fuji, Chem. Rev. 1993, 93, 2037 – 2066; b) E. J. Corey, A. GuzmanPerez, Angew. Chem. 1998, 110, 402 – 415; Angew. Chem. Int. Ed. 1998, 37, 388 – 401; c) U. H. Dolling, P. Davis, E. J. J. Grabowski, J. Am. Chem. Soc. 1984, 106, 446 – 447; d) C. Nicolas, J. Lacour, Org. Lett. 2006, 8, 4343 – 4346; e) X. Wang, Q. Lan, S. Shirakawa, K. Maruoka, Chem. Commun. 2010, 46, 321 – 323.*

solvents (CH_2Cl_2, $CHCl_3$, and toluene) were considered to test this reaction: tetrabutylammonium bromide (TBAB) was monitored as a reference catalyst, three azaphosphatranes were efficient phase-transfer catalysts. They found that the most lipophilic azaphosphatrane derivative **13**-$H^+ \cdot Cl^-$ was the best catalyst among the three azaphosphatranes when the organic phase was toluene as the yield achieved to 95%.

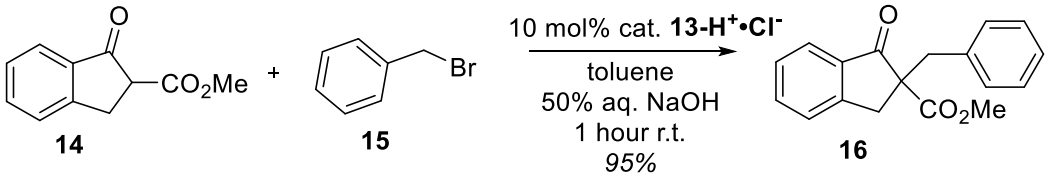

Figure 1.2.2 Benzylation of the methyl 1-oxo-2-indanecarboxylate.

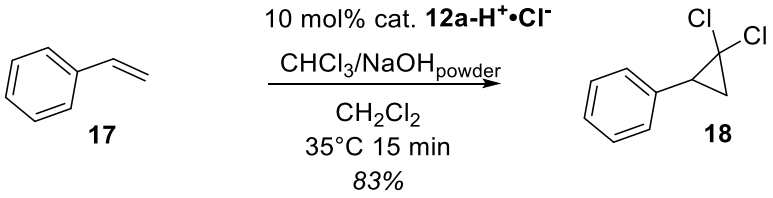

Figure 1.2.3 Cyclopropanation of styrene.

The second approach, which involved with a solid/liquid PTC protocol, was tested in the context of the cyclopropanation reaction of styrene **17** (Figure 1.2.3).[7] These experimental conditions required strong base, thus solid powdered potassium hydroxide was spread in an organic phase, and carbene derivative **18** was generated from chloroform. This reaction needed controlled conditions as well, because the generation of **18** was a very exothermic process. Among the catalysts, **12a-$H^+ \cdot Cl^-$** achieved the best yield in dichloromethane (12%).

The third example is to form a C-C bond through the alkylation of a Schiff base.[12] The possibility to easily deprotect the resulting alkylation product allows for an access to a wide variety of a-amino acids. The experimental conditions required the product **20**, a concentrated solution of NaOH (50%) and benzyl bromide or methyl iodide **19** in the presence of CH_2Cl_2 (Figure 1.2.4), **21** is isolated in a good yield (63%). It was surprising that the reactivity tendencies for the three azaphosphatranes were different, **12a-$H^+ \cdot Cl^-$** appeared to be slightly more efficient than **13-$H^+ \cdot Cl^-$** and **12c-$H^+ \cdot Cl^-$** in the benzylation reaction, whereas **13-$H^+ \cdot Cl^-$**

[12] *a) D. Hoppe, Angew. Chem. 1975, 87, 450-451; Angew. Chem. Int. Ed. Engl. 1975, 14, 426 – 427; b) M. J. O'Donnell, J. M. Boniece, S. E. Earp, Tetrahedron Lett. 1978, 19, 2641-2644; c) M. J. O'Donnell, R. L. Polt, J. Org. Chem. 1982, 47, 2663-2666; d) M. J. O'Donnell, W. D. Bennett, S. Wu, J. Am. Chem. Soc. 1989, 111, 2353-2355; e) K. Maruoka, T. Ooi, Chem. Rev. 2003, 103, 3013-3028; f) M. J. O'Donnell, Acc. Chem. Res. 2004, 37, 506-517. g) U. H. Dolling, P. Davis, E. J. J. Grabowski, J. Am. Chem.*

was more active than **12c-H$^+$·Cl$^-$** and **12a-H$^+$·Cl$^-$** in the methylation reaction.

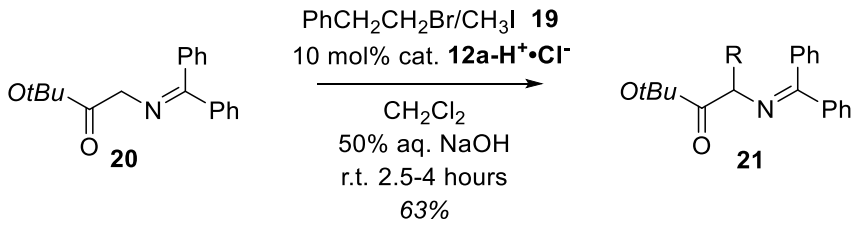

Figure 1.2.4 Alkylation of Schiff bases.

The use of azaphosphatranes as organocatalysts to synthesize cyclic carbonates from CO_2 and epoxides has been reported.[13] Since CO_2 is thermodynamically very stable, and its activation requires the use of high-energy substrates or electro reductive processes, [14] three azaphosphatranes (**12a-H$^+$·Cl$^-$, 13-H$^+$·Cl$^-$, 12d-H$^+$·Cl$^-$**) were considered as catalysts to synthesize the cyclic carbonates from CO_2 and epoxide **22** (Figure 1.2.5). These azaphosphatranes were proved to be efficient single-component, metal-free catalysts for the reaction of simple or activated epoxides, with CO_2 under mild conditions, displaying high stability and productivity over several days of reaction (Figure 1.2.6).

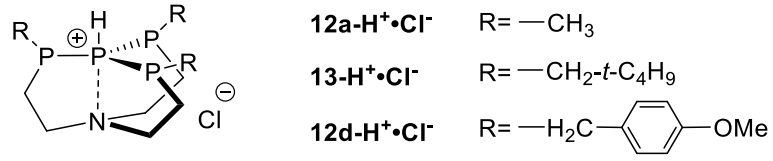

Figure 1.2.5 Structure of the azaphosphatranes **12a-H$^+$·Cl$^-$, 13-H$^+$·Cl$^-$, 12d-H$^+$·Cl$^-$**.

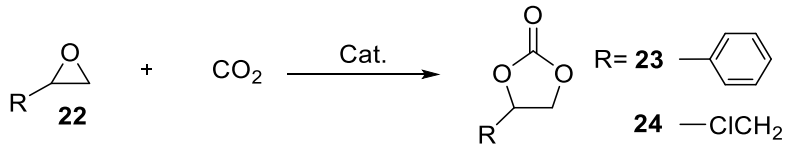

Figure 1.2.6 Synthesis of cyclic carbonates from epoxides and carbon dioxide.

The authors consider three azaphosphatranes with various electronic and steric properties, with Cl^- as counter anion, to explore the influence of the structural features on the catalytic behavior. Firstly, the reaction of styrene oxide (SO) with carbon dioxide is catalyzed by the methyl substituted azaphosphatrane **12a-H$^+$·Cl$^-$**, it gives low carbonate yield (11%), and the conversion stopped after a few hours, The ^{31}P NMR spectrum analysis of the crude mixture

[13] *B. Chatelet, L. Joucla, J.-P. Dutasta , A. Martinez , K. C. Szeto, V. Dufaud J. Am. Chem. Soc., 2013, 135, 5348.*

[14] *a) Sakakura, T.; Choi, J.-C.; Yasuda, H. Chem. Rev. 2007, 107, 2365. b) Jessop, P.; Ikariya, T.; Noyori, R. Chem. Rev. 1995, 95, 259.*

revealed that apart from the catalyst signal at -11.0 ppm, there are two other downfield signals at 7.3 and 5.6 ppm, meaning some catalyst degradation which may be from the insertion of CO_2 into the P-N bond, as previously reported for aminophosphane derivatives and also observed with CS_2.[15]

These results encouraged authors to explore the reaction with bulkier electron substrates azaphosphatranes, as expected, more sterically congested azaphosphatranes **12d-H$^+$·Cl$^-$**, and **13-H$^+$·Cl$^-$** give good results with 50% yields after 7 hours. The ^{31}P NMR spectra showed that the crude mixtures present only the initial signals of catalysts **12d-H$^+$·Cl$^-$**, and **13-H$^+$·Cl$^-$**, whose resonance lies at -12 ppm and 2.1 ppm, respectively. This supported their assumption which connected their stability to the bulkiness around the N-P-H bonds.

The second series of reactions is carried out with **12d-H$^+$·Cl$^-$**, and **13-H$^+$·Cl$^-$** under solvent-free conditions, a much higher substrate-to-catalyst ratio (1000:1) for a much longer period was applied. The progress of each reaction is monitored by ^{1}H NMR analysis of aliquots taken every 24 hours. After that, an appropriate amount of styrene oxide is added to bring the substrate-to-catalyst ratio back up to 1000. A marked difference between**12d-H$^+$·Cl$^-$** and **13-H$^+$·Cl$^-$** is clearly clarified. **12d-H$^+$·Cl$^-$** was initially active, but its activity decreased over the four-day test. **13-H$^+$·Cl$^-$** shows an almost constant reactivity through the four-day experiment. After this period the crude reaction mixtures were analyzed by ^{31}P NMR spectroscopy, several downfield signals, including signal of **12d-H$^+$·Cl$^-$**, were observed, whereas the spectrum with catalyst **12d-H$^+$·Cl$^-$** remained very clean.

Based on these results and previous literature,[16] a proper mechanism (Figure 1.2.7) was proposed, styrene oxide firstly forms adduct with the catalyst through oxygen via a hydrogen bond to the phosphonium cation. A tricyclic phosphoryl carbamate structure was then obtained by inserting carbon dioxide into the P-N bond. This species was highly reactive and very sensitive to hydrolysis and could lead to degradation as mainly observed with **12a-H$^+$·Cl$^-$**.[17] The bulkier substituents in **12d-H$^+$·Cl$^-$** and **13-H$^+$·Cl$^-$** acted as protecting groups which could avoid degradation. For this scheme, the observed first-order rate dependences on catalyst, CO_2, and styrene oxide seemed to show that the formation of adduct is in fast equilibrium with free azaphosphatrane and styrene oxide, and the carbon oxide step is rate-determining. The reaction

[15] *(a) Oertel, G.; Malz, H.; Holtschmidt, H. Chem. Ber. 1964, 97,891. (b) Jensen, K. A.; Dahl, O. Acta Chem. Scand. 1970, 24, 1179.(c) Pudovik, M. A.; Kibardina, L. K.; Aleksandrova, I. A.; Khairullin, V.K.; Pudovik, A. N. Zh. Obshch. khim. 1981, 51, 530.*

[16] *Yang, Z.-Z.; He, L.-N.; Miao, C.-X.; Chanfreau, S. Adv. Synth. Catal. 2010, 352, 2233. North, M.; Pasquale, R. Angew. Chem., Int. Ed. 2009, 48, 2946.*

[17] *Oertel, G.; Malz, H.; Holtschmidt, H. Chem. Ber. 1964, 97, 891.*

proceeded to product by the nucleophilic attack of the chloride at the secondary carbon of the epoxide and subsequent attack of the resultant alkoxide moiety on the activated carbon dioxide. The proximity of the two activated moieties might also suggest that these steps are concerted. Subsequent ring-closure would form the cyclic carbonate and regenerate the azaphosphatrane catalyst.

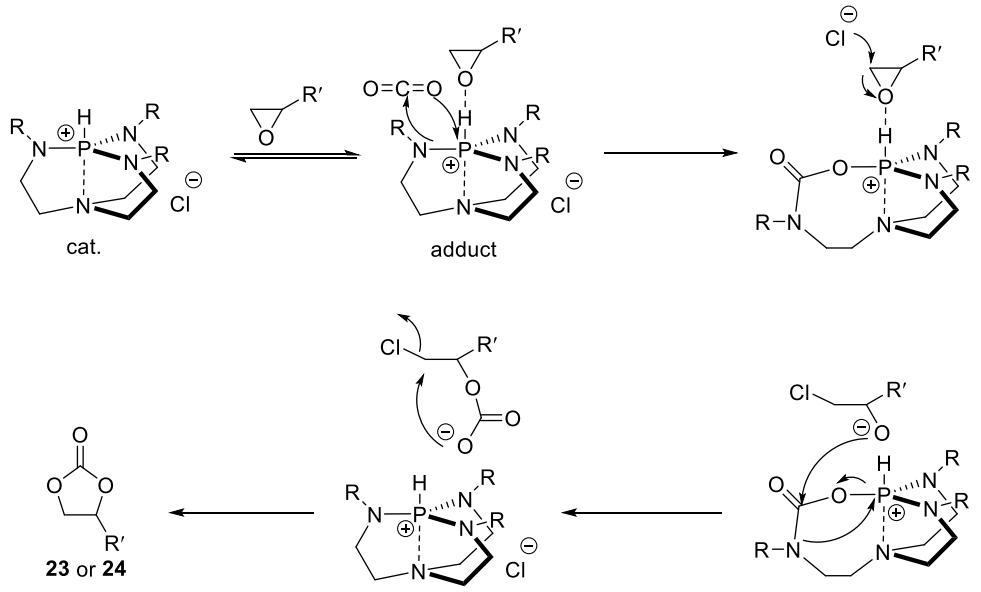

Figure 1.2.7 Example of proposed mechanism for cyclic carbonates synthesis catalyzed by azaphosphatrane derivatives.

Another study using various N-substituted azaphosphatranes as catalysts for the synthesis of styrene carbonates from carbon dioxide and epoxides is reported (Figure 1.2.6 and Figure 1.2.8). Enhancement of the catalytic properties of the azaphosphatrane is achieved upon pre-organization of the active site through hydrogen-bonding.[18] Azaphosphatranes possessed a few excellent properties that make them very interesting candidates for the activation of both carbon dioxide and epoxides. First of all, the structure presenting a well-defined tricyclic framework around the phosphorus atom was built from the tris (2-aminoethyl)-amine (tren) scaffold, which allowed for greater stability. The soft organic cation, where the charge is delocalized around the H-P-N core, does not strongly bind to the hard halide anion (chloride); thus, the anion is free to perform as a nucleophile role to initiate the epoxide ring-opening step. In the end, the nature of the lipophilic pocket formed by a ring of amino groups around the central P-H unit provided a unique catalytic space to probe the structure/activity effects. So, based on these reasonable hypotheses, **12d-H$^+$·Cl$^-$**, which contained a *p*-methoxybenzyl

[18] *B. Chatelet et al. Catalysis Communications 52 (2014) 26–30.*

substituent, is chosen as a benchmark structure, two other N-substituted azaphosphatranes are considered (Figure 1.2.8): **25-H $^{+}$·Cl^{-}**, bearing benzyl rings ortho-substituted by fluorine atoms, **26-H $^{+}$·Cl^{-}**, with a methoxy group. Probably these substituents could favor intramolecular hydrogen bonds with the cation moiety, and provide a cavity above the reactive center which may protect it from degradation.

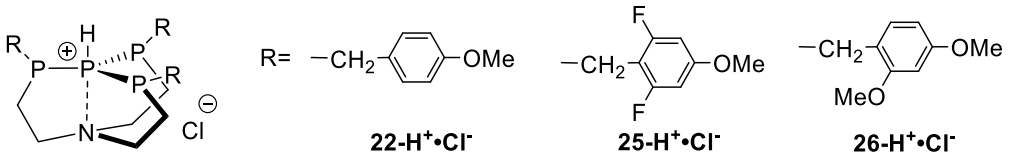

Figure 1.2.8 Targeted azaphosphatranes to probe the structure–activity relationships.

The authors have already explored the effect of the catalyst structure on the catalytic performance in detail by using the coupling of styrene oxide with carbon dioxide to produce styrene carbonate as a model reaction.[14] In order to meet the requirements of sustainable green methodologies, they also worked close to atmospheric pressure (1 bar CO_2) at relatively low temperatures (100 °C) and catalyst loadings (0.1% or 1 mol%). Catalytic tests were first performed over a 24-hour period with a catalyst loading of 1 mol%. All catalysts showed good catalytic activities with respectively 73% (**12d-H^{+}·Cl^{-}**), 86% (**25-H^{+}·Cl^{-}**) and 92% (**26-H^{+}·Cl^{-}**) yields in styrene carbonate. It demonstrated that intramolecular hydrogen bonding between the OMe group in ortho position and the PH^{+} center, that stabilizes the whole structure, could account for the better catalytic activity and stability of **26**-H^{+}·Cl^{-}.

1.2.2 Azaphosphatranes as organocatalysts in confined space

Up to now, a lot of azaphosphatranes as organocatalysts have been investigated. Hemicryptophane, which contains a rigid bowl shape cyclotriveratrylene (CTV) and a tren unit, was synthesized as encaged azaphosphatrane, the CTV is derived from cryptophane, while the tren part is the derivative of azaphosphatranes. Since azaphosphatranes could be used as catalysts, the application of encaged azaphosphatrane (hemicryptophane) as the catalyst have been reported as well. It is noted that hemicryptophanes provide a cavity for the reactions, such as for efficient conversion of carbon dioxide into cyclic carbonates[19].

[19] *B. Chatelet, L. Joucla, J.P. Dutasta, A. Martinez, V.R. Dufaud Chem. Eur. J. 2014, 20, 1-5.*

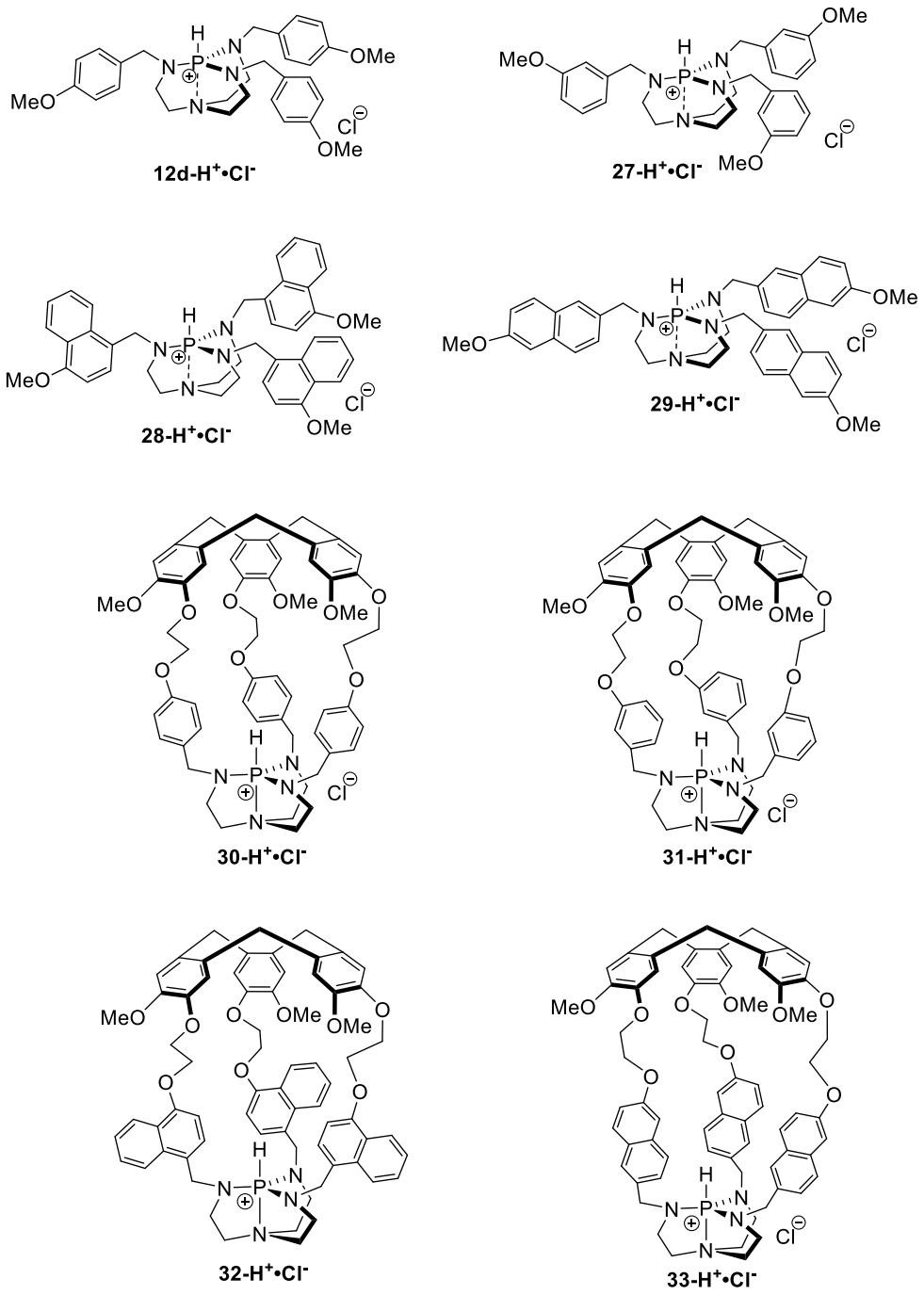

Figure 1.2.9 Azaphosphatranes **30**-$\mathbf{H^+ \cdot Cl^-}$, **31**-$\mathbf{H^+ \cdot Cl^-}$, **32**-$\mathbf{H^+ \cdot Cl^-}$, and **33**-$H^+ \cdot Cl^-$ with its open-faced corresponding analogues, **12d**-$\mathbf{H^+ \cdot Cl^-}$, **27**-$\mathbf{H^+ \cdot Cl^-}$, **28**-$\mathbf{H^+ \cdot Cl^-}$, and **29**-$\mathbf{H^+ \cdot Cl^-}$.

To study the effect of confinement on the catalytic activity of azaphosphatranes, the authors compared azaphosphatrane-hemicryptophanes **30**-$\mathbf{H^+ \cdot Cl^-}$, **31**-$\mathbf{H^+ \cdot Cl^-}$, **32**-$\mathbf{H^+ \cdot Cl^-}$, and **33**-$\mathbf{H^+ \cdot Cl^-}$ with their open-faced corresponding analogues, **12d**-$\mathbf{H^+ \cdot Cl^-}$, **27**-$\mathbf{H^+ \cdot Cl^-}$, **28**-$\mathbf{H^+ \cdot Cl^-}$, and

29-H$^+$·Cl$^-$ (Figure 1.2.9), which lack cavities.[20] The coupling of styrene oxide with carbon dioxide is chosen as a benchmark reaction (Figure 1.2.9), the reaction is carried out over 24 hours under mild conditions (1 bar, 100 ºC) with a catalyst loading of 1 mol%. The authors demonstrate that both the model and encaged azaphosphatranes catalysts give satisfactory results, with the yields of product being 73% and 82% for **30-H$^+$·Cl$^-$** and **12d-H$^+$·Cl$^-$**, 84% and 75% for **31- H$^+$·Cl$^-$** and **27-H$^+$·Cl$^-$**, 89% and 12% for **32-H$^+$·Cl$^-$** and **28-H$^+$·Cl$^-$**, respectively, however, only 3% and 77% for **33-H$^+$·Cl$^-$** and **29-H$^+$·Cl$^-$**. It is surprisingly that under the initial reaction conditions (1 mol% of catalyst, 24 hours, 100 ºC, 1 bar), model catalyst **29-H$^+$·Cl$^-$** is far more active than its encaged counterpart **33-H$^+$·Cl$^-$**, thus it is reasonable to clarify that the confinement space imposed by the hemicryptophane structure strongly affects the performance of the azaphosphatranes organocatalysts.

In a word, these specific tailor-made nanoreactors azaphosphatranes could be considered as basic structure of the corresponding hemicryptophane hosts, each defining a specific confined space around a catalytically active azaphosphatrane. Varying the shape of the space above the reactive center has allowed a unique study, which demonstrated how the nature of the nanospace of the molecular cavity can dramatically affect the stability and reactivity of the organocatalysts: the active site of the encaged azaphosphatranes not only increases the catalytic activity, but also prevents the degradation by protecting it from deactivation pathways. This study also brought to light new evidences concerning the previously proposed mechanism involving the simultaneous dual activation of the epoxide and carbon dioxide at a single azaphosphatrane molecule.

1.2.3 Azaphosphatranes in recognition properties

Self-assembly is an efficient tool for the construction of diverse functional architectures.[21] Azaphosphatranes, the conjugate acids of Verkade's superbases,[22] are attractive functional moieties for incorporation into the faces of tetrahedral capsules. Their polarized P-H$^+$ bonds enable them to be employed as catalysts for carbon dioxide activation and lactide ring-opening

[20] *a) P. Dimitrov-Raytchev, A. Martinez, H. Gornitzka, J.-P. Dutasta, J. Am. Chem. Soc. 2011, 133, 2157 – 2159. b) B. Chatelet, H. Gornitzka, V. Dufaud, E. Jeanneau, J.-P. Dutasta, A. Martinez, J. Am. Chem. Soc. 2013, 135, 18659-18664.*

[21] *a) Wang, W.; Wang, Y. X.; Yang, H. B. Chem. Soc. Rev. 2016, 45, 2656. b) Cook, T. R.; Stang, P. J. Chem. Rev. 2015, 115, 7001. c) Krieg, E.; Bastings, M.M. C.; Besenius, P.; Rybtchinski, B.Chem. Rev. 2016, 116, 2414. d) He, Z. F.; Jiang, W.; Schalley, C. A. Chem. Soc. Rev. 2015, 44, 779. e) Mauro, M.; Aliprandi, A.; Septiadi, D.; Kehr, N. S.; De Cola, L. Chem. Soc. Rev. 2014, 43, 4144. f) Yang, L. L.; Tan, X. X.; Wang, Z. Q.; Zhang, X. Chem. Rev. 2015, 115, 7196. g) Yu, G. C.; Jie, K. C.; Huang, F. H. Chem. Rev. 2015, 115, 7240.*

[22] *Lensink, C.; Xi, S. K.; Daniels, L. M.; Verkade, J. G. J. Am. Chem. Soc. 1989, 111, 3478.*

polymerization.[14, 21, 23] Both of these applications benefit from the hydrogen-bond donor ability of the P-H$^+$ group. Their use as anion receptors has been reported lately by D. Zhang and co-workers.[24] These cationic species can be rendered water-soluble via selection of a suitable counter ion, potentially allowing their as anion binders in water, this development has been recognized as a key challenge in supramolecular chemistry. In their research, the authors have shown anion-templated aqueous self-assembly results in the formation of an endohedrally functionalized $Fe^{II}_4L_4$ tetrahedron that based on azaphosphatrane subcomponents, this azaphosphatrane derivative is water-soluble, flexible and is able to encapsulate anions with volumes ranging from 35 Å to 219 Å through hydrogen bonding and electrostatic interactions, besides, its structure corresponds to the size and shape of the template anions, dynamically adopting a conformation of all four azaphosphatrane P-H$^+$ (vectors point inward, or one points outward and the other three inward).

A new azaphosphatrane-functionalized tetrahedron **36-H$^+$·X$^-$** (Figure 1.2.10) is assembled from triamine subcomponent **34-H$^+$·X$^-$** and **35;** The design of **36-H$^+$·X$^-$** is based on the following four principles: firstly, the cationic azaphosphatranes together with the metal ions provide an overall 12 positive charges, offering a strong electrostatic driving force for anion binding. Secondly, the cationic framework also inductively increases the affinity of the P-H$^+$ bond donor for anionic species.[25] Third, the sulfate counter ion was chosen to maximize the water solubility of **36-H$^+$·X$_{12}$$^-$**. Fourth, methylene groups between the phenyl rings and azaphosphatrane nitrogen atoms were introduced to enhance this flexibility, making the cavity fit a diverse array of anions.

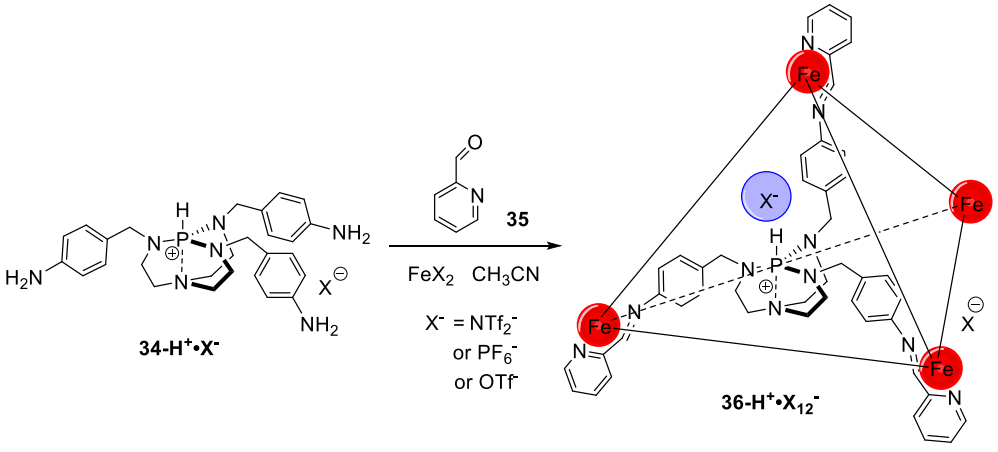

Figure 1.2.10 Subcomponent self-assembly of **36-H$^+$·X$^-$** in acetonitrile.

[23] *a) Chatelet, B.; Joucla, L.; Dutasta, J. P.; Martinez, A.; Szeto, K. C.; Dufaud, V. J. Am. Chem. Soc. 2013, 135, 5348. b) Zhang, D. W.; Jardel, D.; Peruch, F.; Calin, N.; Dufaud, V.; Dutasta, J. P.; Martinez, A.; Bibal, B. Eur. J. Org. Chem. 2016, 2016, 1619.*

[24] *D. Zhang, T. K. Ronson, J. Mosquera, A. Martinez, L. Guy, and J. R. Nitschke. J. Am. Chem. Soc. 2017, 139, 6574-6577.*

[25] *Ayme, J. F.; Beves, J. E.; Campbell, C. J.; Gil-Ramirez, G.; Leigh, D. A.; Stephens, A. J. J. Am. Chem. Soc. 2015, 137, 9812.*

36-H$^+$·X$^-$ were prepared as the bis(trifluoromethanesulfonyl)-imide (triflimide, NTf_2^-), hexafluorophosphate (PF_6^-), and trifluoromethanesulfonate (triflate, OTf^-) salts, all of them were soluble in acetonitrile (Figure 1.2.11). The chloride salt of subcomponent **34-H$^+$·X$^-$** was exchanged with NTf_2^-, PF_6^-, or OTf^- via anion metathesis directly, the subsequent reaction of **34-H$^+$·X$^-$** (4 equiv.) with the corresponding FeX_2 salt (NTf_2^-, PF_6^-, or OTf^-, 4 equiv.) and 2-formylpyridine **35** (12 equiv.) in acetonitrile gave a single product with one azaphosphatrane capping each face. The authors also attempted the preparation of a water-soluble **36-H$^+$·X$^-$** by introducing SO_4^{2-} counter ions.[26] The initial chloride salt of **34-H$^+$·Cl$^-$** was exchanged by SO_4^{2-} through the same procedure (Figure 1.2.11), however, the subsequent reaction of the sulfate salt of **34-H$^+$·SO$_4^-$** (4 equiv.) with $FeSO_4$ (4 equiv.) and 2-formylpyridine **35** (12 equiv.) in water failed to give the expected tetrahedron complex, perhaps the hydrophilic character of SO_4^{2-} prevents it from acting as a template for the formation of **36-H$^+$·X$^-$**.[27] Therefore, a series of other anions with different shapes and volumes (I^-, NO_3^-, BF_4^- ClO_4^- ReO_4^- $CB_{11}H_{12}^-$ listed in table 1.2.1) are tested to investigate their template effects in the aqueous reaction mixture (1 equiv. of anion was added in each case with regard to the final complex). All of the anions with volumes ranging from 35 Å^3 (I^-) to 219 Å^3 ($CB_{11}H_{12}^-$), were observed to serve as competent templates for **36-H$^+$·X$^-$** in water, indicating that its cavity can adapt readily to guests having different sizes and shapes.

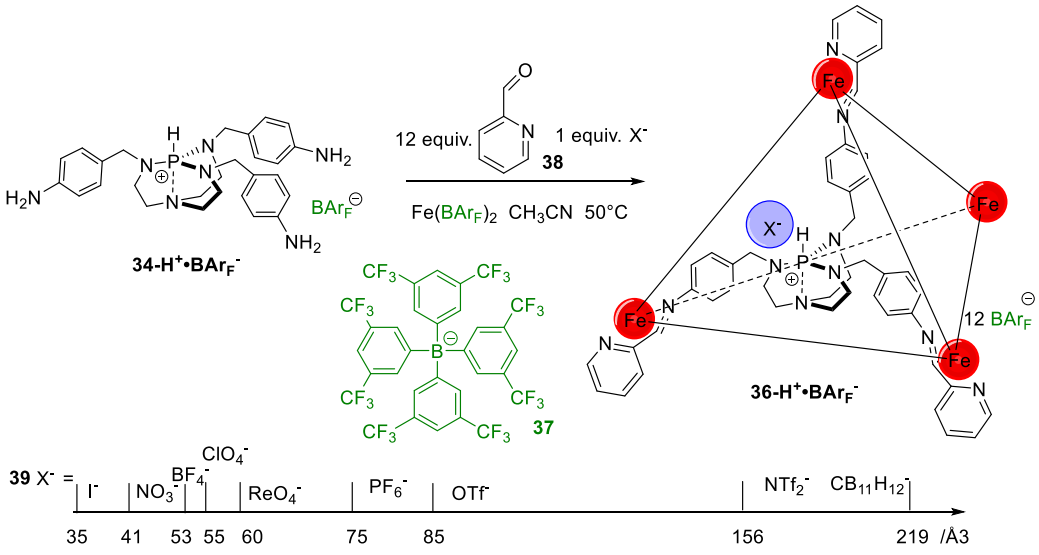

Figure 1.2.11 Subcomponent self-assembly of **36-H$^+$·BAr$^{F-}_{12}$** around 1 equiv. of template anion.

[26] *Bolliger, J. L.; Ronson, T. K.; Ogawa, M.; Nitschke, J. R. J. Am. Chem. Soc. 2014, 136, 14545.*

[27] *a) Custelcean, R. Chem. Commun. 2013, 49, 2173. b) Pandurangan, K.; Kitchen, J. A.; Blasco, S.; Boyle, E. M.; Fitzpatrick, B.; Feeney, M.; Kruger, P. E.; Gunnlaugsson, T. Angew. Chem., Int. Ed. 2015, 54, 4566*

Anion	NTf_2^-	$CB_{11}H_{12}^-$	ReO_4^-	OTf^-	PF_6^-	ClO_4^-	BF_4^-	I^-	NO_3^-
[a]	1	3.0×10^6	5.8×10^4	2.4×10^3	8.7×10^2	6.8	2.1×10^{-1}	-[b]	-[b]

Table 1.2.1 Relative binding constants of the different anions compared to NTf_2^- in CD_3NO_2. [a] Relative binding affinity; [b] Relative binding constant could not be calculated due to the new peaks having insufficient intensity during ^1H NMR titrations.

The authors have also reported that **36-H$^+$·BAr$^{F-}_{12}$** is able to extract, from water into nitromethane, an equimolar amount of ReO_4^-, a high value anion and a nonradioactive surrogate of TcO_4^-.[28] The salt **34-H$^+$·BAr$^{F-}_{12}$** is obtained by anion metathesis as was observed in water.[27] Non-coordinating tetrakis (3,5-bis(trifluoromethyl)phenyl)borate (BAr^{F-}) **37** was selected as the counter-anion based on its lipophilicity and bulk (Figure 1.2.12). The lipophilic nature of BAr^{F-} renders **36-H$^+$·BAr$^{F-}_{12}$** soluble in water-immiscible organic solvents such as nitromethane. Through competitive guest exchange, it is possible to measure the relative binding affinities of different anions X^- (**39**) in CD_3NO_2, the following hierarchy was observed by authors: $CB_{11}H_{12}^-$ > ReO_4^- > OTf^- > PF_6^- > ClO_4^- > NTf_2^- > BF_4^- > I^- > NO_3^- (Table 1.2.1). This ordering differs from the one observed in water: PF_6^- > ReO_4^- > OTf^- > ClO_4^- > $CB_{11}H_{12}^-$ > NTf_2^- > BF_4^- > I^- > NO_3^-,[27] especially as regards the binding affinity of $CB_{11}H_{12}^-$. To accommodate this largest anion, the **36-H$^+$** framework must expand; it was inferred that this larger conformation in water is unfavorable because it involves greater exposure of hydrophobic surface to water. In both solvents, ReO_4^- binds more strongly than other common anions, indicating potential for its selective extraction.

[28] *D. Zhang, T. K. Ronson, J. Mosquera, A. Martinez, J. R. Nitschke. Angew. Chem. 2018, 130, 3779-3712.*

1.3 Proazaphosphatranes

Since 1989, when the first proazaphosphatrane nonionic base was synthesized in professor Verkade's laboratory[29], a variety of proazaphosphatranes have been synthesized then, which proved to be the sublimable solids that could be isolated. Proazaphosphatranes have been used in an ever-growing list of organic transformations[30]; up to now, they have been considered to be efficient catalysts and promoters for many reactions, including the trimerization of isocyanates[31], the dehydrohalogenation of alkyl halides[32], the synthesis of α, β-unsaturated nitriles[33], β-hydroxy nitriles[34], and homoallylic alcohols[35], the transesterifcation of esters[36] and the deprotection of acylated alcohols[37]or silylated alcohols[38], the synthesis of β-nitroalkanols[39], the silylation of hindered alcohols[40], the synthesis of glutaronitriles[41]. Here, we will focus on more recent developments of the chemistry of proazaphosphatranes, namely their use in Frustrated Lewis pair systems and as ligands to transition metals.

1.3.1 Proazaphosphatranes as frustrated Lewis pair

As many FLPs examples were found and studied further, Suresh Mummadi and co-workers reported a new approach to intermolecular FLPs that connected available bulky organosuperbases to moderate weak boron-containing Lewis acid[42]. Their research mainly focused on isolation and structural characterization of phosphonium borohydride salts, besides, they proposed two FLPs that could be efficient catalysts in metal-free hydrogenation of N-benzylidenaniline. Firstly, six FLPs were tested to identify the moderate to weak Lewis acids. Form the calculated gas-phase hydride affinities of various organoboranes (Table 1.3.1), it

[29] *a) Schmidt, H.; Lensink, C.; Xi, S. K.; Verkade, J. G. Z. Anorg. Allg. Chem. 1989, 578. 75. 2. (b) Wroblewski, A.; Pinkas, J.; Verkade, J. G. Main Group Chem. 1995, 1. 69. 3. (c) D'Sa, B.; Verkade, J. G. Phosphorus, Sulfur Silicon 1997, 123. 301.*

[30] *Stambuli, J. P.; Buhl, M.; Hartwig, J. F. J. Am. Chem. Soc. 2002, 124, 9346.*

[31] *Tang, J.-S.; Verkade, J. G. J. Org. Chem. 1994, 59, 4931.*

[32] *Liu, X.; Verkade, J. G. J. Org. Chem. 1999, 64, 4840.*

[33] *D'Sa, B.; Kisanga, P.; Verkade, J. G. J. Org. Chem. 1998, 63, 3691.*

[34] *Kisanga, P.; McLeod, D.; D'Sa, B.; Verkade, J. G. J. Org. Chem. 1999, 64, 3090.*

[35] *Wang, Z.; Kisanga, P.; Verkade, J. G. J. Org. Chem. 1999, 64, 6559.*

[36] *Ilankumaran, P.; Verkade, J. G. J. Org. Chem. 1999, 64, 3086.*

[37] *Ilankumaran, P.; Verkade, J. G. J. Org. Chem. 1999, 64, 3086.*

[38] *Yu, Z.; Verkade, J. G. J. Org. Chem. 2000, 65, 2065.*

[39] *Kisanga, P.; Verkade, J. G. J. Org. Chem. 1999, 64, 4298.*

[40] *D'Sa, B.; Verkade, J. G. J. Org. Chem. 1996, 61, 2963.*

[41] *Kisanga, P.; D'Sa, B.; Verkade, J. G. J. Org. Chem. 1998, 63, 10057.*

[42] *Suresh Mummadi, Daniel K. Unruh, Jiyang Zhao, Shuhua Li and Clemens Krempner, J. Am. Chem. Soc. 2016, 138, 10, 3286-3289.*

appears that BPh_3 and $HBMes_2$ are significantly weaker hydride acceptors than their perfluorinated counterparts $B(C_6F_5)_3$ and $HB(C_6F_5)_2$. Moreover, 9-BBN and its readily accessible alkyl and aryl derivatives are weaker hydride acceptors than $HBMes_2$ and BPh_3 but still stronger than acyclic BEt_3.

Borane	ΔH_{HA}	Borane	ΔH_{HA}
$B(C_6F_5)_3$	−112.0[a]	9-Et-BBN	−65.2[c]
$HB(C_6F_5)_2$	−97.2[a]	9-Me-BBN	−62.4[c]
BPh_3	−74.4[b]	BEt_3	−58.5[b]
$HBMes_2$	−74.7[b]	9-MeO-BBN	−54.1[c]
9-BBN	−70.2[c]	9-H_2N-BBN	−39.9[c]
9-Ph-BBN	−69.0[c]	$B(OMe)_3$	−38.2[b]

Table 1.3.1 Calculated gas-phase hydride affinities, ΔH_{HA} (kcal/mol), of Selected Boranes. [a]Ref.[43] [b]Ref.[44] [c] This work.

Phosphazene **40** is a strong and bulky Brønsted base, whose pKa is 28.4 in acetonitrile. The moderate Lewis acids BPh_3 and $HBMes_2$ are tested by combining them with **40** (Figure 1.3.1), however, no Lewis acid-base adducts are obtained. Then, to their surprise, upon adding H_2 (2.5 atm) to hexane/benzene solutions of the FLPs **40**/BPh_3 and **40**/$HBMes_2$, respectively, instead of Lewis adducts being produced, zwitterionic compounds formed, which was confirmed by isolated crystalline solids and characterized by multinuclear NMR spectroscopy as the phosphazenium borates **41** and **42**. The cations of **41** and **42** (**40**-$\mathbf{H^+}$) exhibit resonances at 22 ppm in ^{31}P NMR spectrum. The anions of **41** and **42** ($HBPh_3^-$ and $H_2BMes_2^-$), give resonances at -9.1 and -23.0 ppm in ^{11}B NMR spectrum with scalar B-H coupling constants of 79 Hz (doublet) and 76 Hz (triplet).

[43] *Mendez, M.; Cedillo, A. Comput. Theor. Chem. 2013, 1011, 44.*

[44] *Li, H.; Aquino, A. J. A.; Cordes, D. B.; Hung-Low, F.; Hase, W. L.; Krempner, C. J. Am. Chem. Soc. 2013, 135, 16066.*

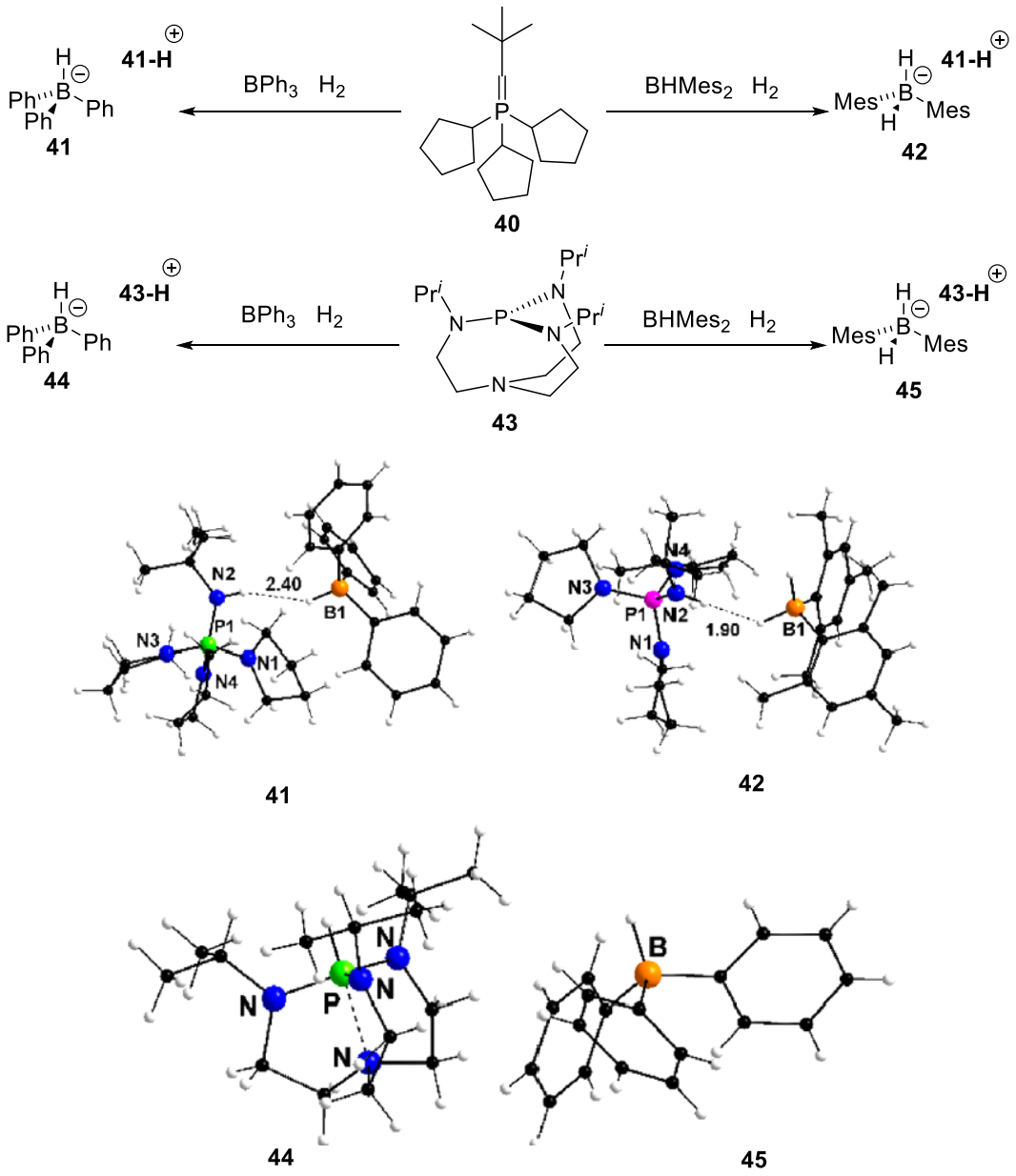

Figure 1.3.1 Formation of **41-42** and **44-45** (**40** and **43** as bases).

However, when weaker hydride acceptors 9-BBN and BEt_3 are tested in the presence of phosphazene **40**, they did not cleave H_2. An observation of insufficient Brønsted basicity is ascribed to this phenomenon, they assume that increasing basicity of the Brønsted bases may Account for this observation. Verkade's superbase **43**, whose pKa is 33.4 in acetonitrile,[45] is considered, and associated to the moderate weak hydride acceptors BEt_3 as well as BPh_3 and $BHMes_2$ (Figure 1.3.1). As in the previous cases, no Lewis acid-base adducts were obtained with this sterically demanding and exceptionally strong Brønsted base. Each FLP C_6D_6 solution was demonstrated stable even when prolonging the period of time. Hexane/benzene solutions

[45] *Venkat Reddy Chintareddy, Arkady Ellern and John G. Verkade. Org. Chem. 2010, 75, 7166.*

of BPh_3 or $BHMes_2$ and **43** reacted with H_2 directly, forming salts **44** and **45**, which were characterized by X-Ray analysis NMR spectra. In ^{31}P NMR spectrum, the cation of **44** and **45** resonances at 10 ppm, in ^{11}B NMR spectrum, **44** and **45** showed peaks at -9.1 and -23.0 ppm, respectively, which is similar to the ^{11}B NMR spectrum of **41** and **42**.

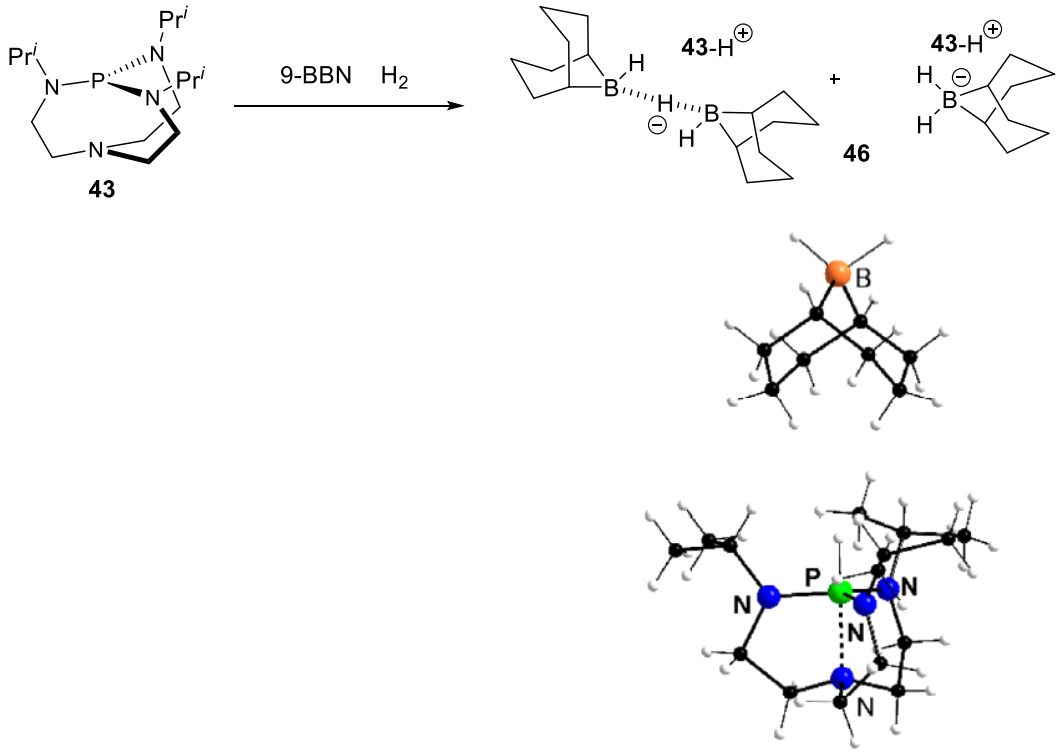

Figure 1.3.2 Formation of **46**(**43** as base).

Astonishingly, FLP 9-BBN/**43** exposed to H_2 (2.5 atm) reacted similarly, generating a crystalline solid (Figure 1.3.2), which was identified by multinuclear NMR spectroscopy and X-ray crystallography as **46**. The results of the X-ray data clearly showed a salt-type structure with $[9,9\text{-}H_2BBN]^-$ as the counter anion. In the ^{11}B NMR spectrum, **46** displays two signals, suggesting at least two anions present in solution; a sharp triplet at -16.5 ppm, due to the monomeric anion $9,9\text{-}H_2BBN^-$[46] and a broad singlet at around 4.0 ppm. The latter signal may be assigned to the anion, $[9\text{-H-BBN}\cdots\text{H}\cdots\text{BBN-H-9}]^-$, formed through bridging interactions between $[9,9\text{-}H_2BBN]^-$ and 9-BBN.

[46] *Brown, H. C.; Singaram, B.; Mathew, C. P. J. Org. Chem. 1981, 46, 2712.*

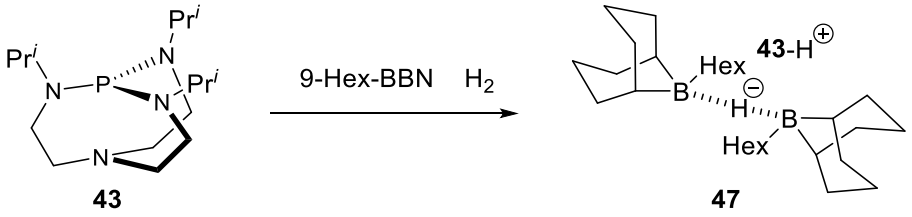

Figure 1.3.3 Formation of **47.**

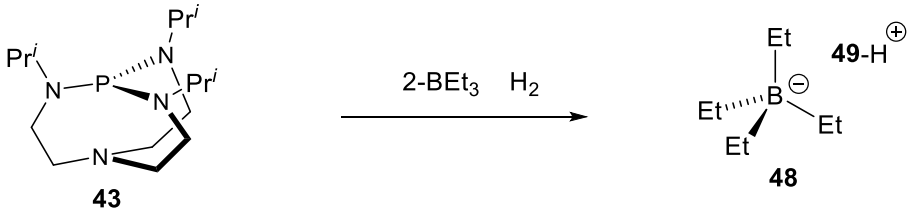

Figure 1.3.4 Formation of **48**.

The FLPs **43**/9-Hex-BBN readily reacted with H_2 (2.5 atm) to furnish a crystalline precipitate which was identified by ^{11}B NMR spectrum as **47** (Figure 1.3.3). Only one broad signal at -1 ppm was found (instead of the expected doublet at -13 ppm), perhaps it is due to the monomeric anion [9-Hex-9-H-BBN]$^-$.[47] The reaction of BEt_3/**43** with H_2 lead to a typical hydride-free salt **48** formed slowly as major product (Figure 1.3.4), they had achieved a better yield when adding 2-fold excess BEt_3.

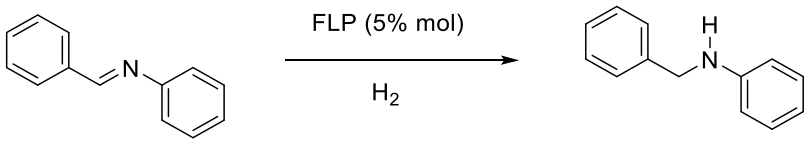

FLP	T (°C)	p(H^2) (bar)	Time (h)	Yield (%)
40/HBMes$_2$	60	50	16	3
40/BPh$_3$	60	50	40	32
40/BPh$_3$	80	100	40	>99
43/9-BBN	60	100	16	7
43/9-Hex-BBN	25	50	16	10
43/9-Hex-BBN	60	50	40	>99
43/9-BEt$_3$	25	100	16	5
43/9-BEt3	60	100	16	11

Table 1.3.2 Catalytic hydrogenation of *N*-Benzylidenaniline.[a a] Conditions (not optimized): 1.5 mL THF, 6.6 mmol substrate, 0.33 mmol FLP.

[47] *The monomeric anion, 9-Hex-9-H-BBN$^-$, derived from the reaction of KH with 9-Hex-BBN in THF, shows a doublet in the ^{11}B NMR at −13.2 ppm ($^1J_{B-H}$ = 70 Hz); Soderquist, J. A.; Rivera, I. Tetrahedron Lett. 1988, 29, 3195.*

Encouraged by the ability of designing "inverse" FLPs to activate hydrogen, catalytic hydrogenations using *N*-benzylidenaniline as the model substrate in THF were attempted (Table 1.3.2). FLPs **40**/BPh_3 and **43**/9-Hex-BBN at a catalytic amount of 5 mol % exhibit excellent activity, generating the quantitative formation of N-benzylaniline. For both systems, high temperatures are required, in agreement with the observation that the release of H_2 from their respective phosphonium borate salts **41**and **47** occurs more rapidly at elevated temperatures.[48]

Suresh Mummadi and co-workers also have reported the interaction of Verkade's superbase with strong Lewis acids,[49] they generated a series of Lewis acid-base complexes with the base **43**. Firstly, they measured the acidity strength of these Lewis acid by using the classic Gutmann-Beckett method (Table 1.3.3),[50] confirming that $AlCl_3$ is "harder" than $GaCl_3$ and that both are the strongest Lewis acids regardless of the donor applied, similar trends are noted for $Al(C_6F_5)_3$ and $Ga(C_6F_5)_3$, but these represent weaker Lewis acids.

Lewis acid	$OPEt_3$ $\delta^{31}P$	$\Delta\delta^a$	ANb	$SPEt_3$ $\delta^{31}P$	$\Delta\delta^a$
free	46.2	-	-	53.5	-
$AlCl_3$	82.2	36.0	91.4	62.7	9.2
$GaCl_3$	81.1	34.9	88.9	64.0	10.5
$BF_3{\cdot}SMe_2$	78.8	32.6	12.8	57.8	4.3
$BF_3{\cdot}OEt_2$	77.3	31.1	80.5	53.9	0.4
$Al(C_6F_5)_3$	76.0	29.8	77.6	61.2	6.7
$B(C_6F_5)_3$	76.0	29.8	77.6	58.0	4.5
$BH_3{\cdot}SMe_2$	75.7	29.5	76.9	53.5	0
$Ga(C_6F_5)_3$	73.1	26.9	71.2	61.3	7.8
BPh_3	72.0	25.8	68.7	53.5	0
$AlMe_3$	66.7	20.5	57.0	58.1	4.6
$AlEt_3$	65.9	19.7	55.2	58.3	4.8
BEt_3	53.7	7.5	28.2	53.5	0

Table 1.3.3 ^{31}P NMR chemical shifts (ppm) of $OPEt_3$ and $SPEt_3$ in C_6D_6 in the Presence of selected Lewis acids and Calculated Gutmann−Beckett Acceptor Numbers (ANs). [a] $\Delta\delta = \delta$ (Lewis acid) − δ(none). [b]AN =

[48] Berkessel, A.; Schubert, T. J. S.; Mueller, T. N. J. Am. Chem. Soc. 2002, 124, 8693.

[49] Kisanga, P. B.; Ilankumaran, P.; Fetterly, B. M.; Verkade, J. G. P(RNCH2CH2)3N: Efficient 1, 4- Addition Catalysts. J. Org. Chem. 2002, 67, 3555−3560.

[50] *a) Mayer, U.; Gutmann, V.; Gerger, W. Monatsh. Chem. 1975, 106, 1235−1257. b) Beckett, M. A.; Strickland, G. C.; Holland, J. R.; Sukumar Varma, K. Polymer 1996, 37, 4629−4631. c) Adamczyk-Wozniak, A.; Jakubczyk, M.; Sporzynski, A.; Zukowska, G. Inorg. Chem. Commun. 2011, 14, 1753−1755. d) Beckett, M. A.; Brassington, D. S.; Coles, S. J.; Hursthouse, M. B. Inorg. Chem. Commun. 2000, 3, 530−53.*

(δ31P − 41.0)[100/(86.1 − 41.0)].

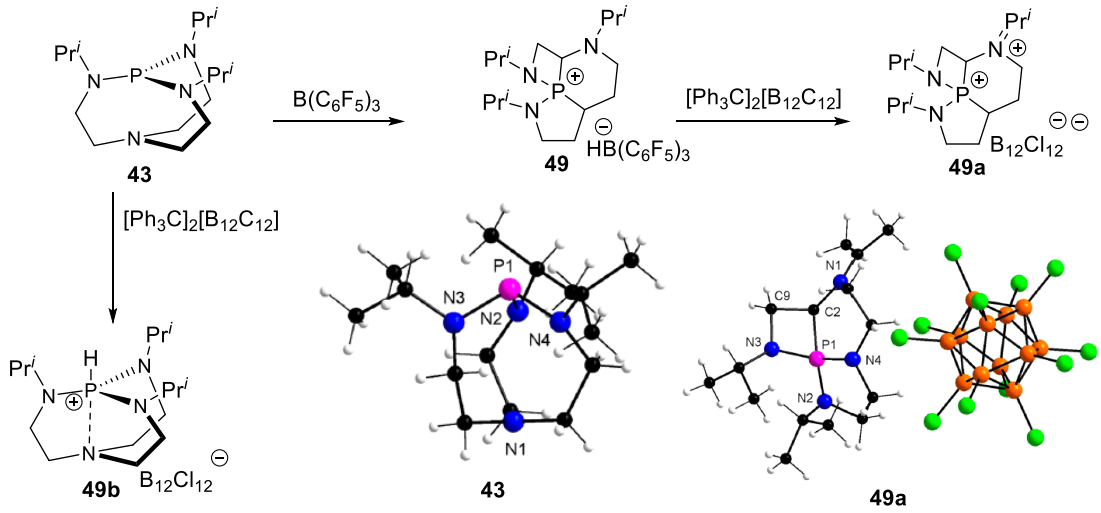

Figure 1.3.5 Reactions of Verkade's Base **43** with $B(C_6F_5)_3$ and $[Ph_3C]_2[B_{12}C_{12}]$

The reaction of **43** with $B(C_6F_5)_3$ gives liquid a phase (Figure 1.3.5)[51], it could be separated by decantation and purified by washing with hexanes. Analysis of this oily product was characterized by ^{31}P and ^{11}B NMR spectroscopy, which revealed a single phosphorus signal at 42 ppm and a doublet for boron at -26 ppm ($^1J_{B-H}$ = 94 Hz), suggesting the formation of a salt containing the anion $HB(C_6F_5)_3^-$. However, the ^1H and ^{13}C NMR data were not consistent with the formation of the expected iminium counter ion. So, the authors propose salt **49** to be generated most likely as a result of skeletal rearrangement (Figure 1.3.6), it is supported by the following experiment: when 1 equiv. of $[Ph_3C]_2[B_{12}C_{12}]$ was added to **49**, a crystalline product **49a** could be isolated and identified by multinuclear NMR spectroscopy, combustion analysis, and the results of X-ray analysis (Figure1.3.5). This unexpected cationic rearrangement can largely be attributed to the inability of mixtures of **43** and $B(C_6F_5)_3$, it forms a stable classical Lewis acid-base complex and the exceptionally high hydride affinity of both $B(C_6F_5)_3$ and the Ph_3C^+ cation. It should be noticed that the reaction of 1 equiv. of $[Ph_3C]_2[B_{12}C_{12}]$ and base **43** did not generate the same rearranged compound, a phosphonium salt **49b** was isolated in good yield.

The sterically more accessible tropylium tetrafluoroborate, on the other hand, was reacted with base **43** to generate the phosphonium salt **50** in 45% isolated yield as a crystalline material (Figure 1.3.6).

[51] *Erker, G. Tris(pentafluorophenyl)borane: a special boron Lewis acid for special reactions. Dalton Trans. 2005, 1812−1890.*

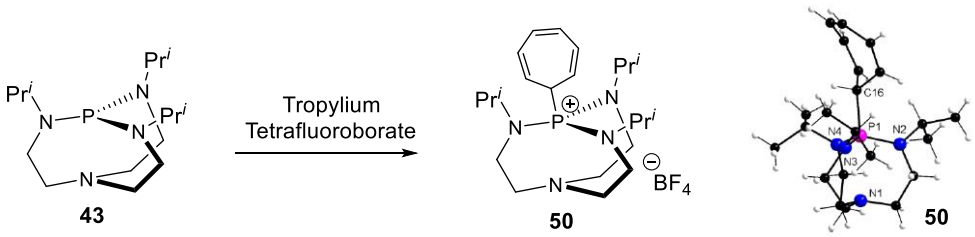

Figure 1.3.6 Reaction of Verkade's base **43** with Tropylium Tetrafluoroborate.

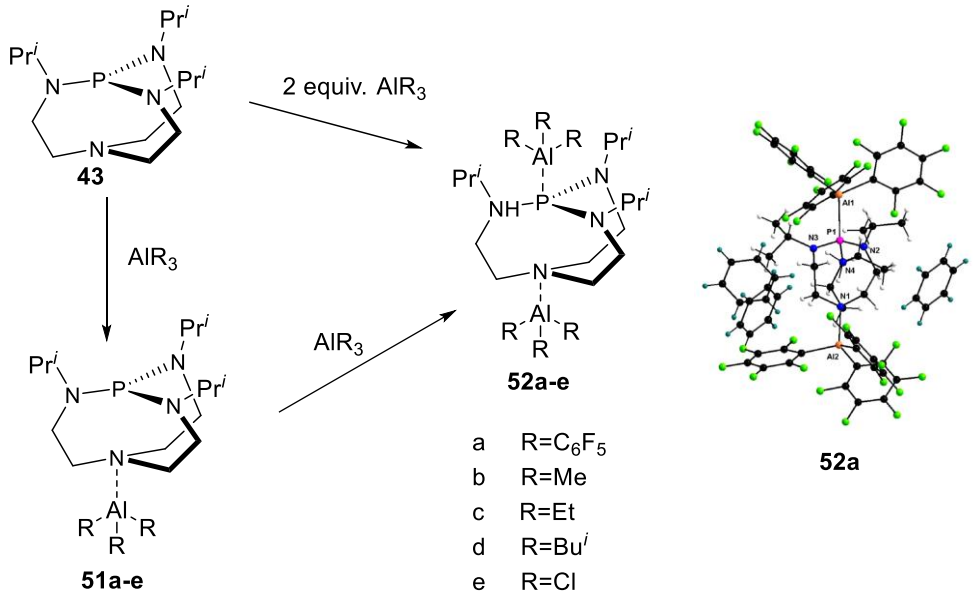

Figure 1.3.7 Formation of the Mono- and Binuclear LABCs **51a-e** and **52a-e.**

Then, they attempted to generate FLPs between strong Lewis acids AlR_3 and **43** (Figure 1.3.7). With 1 equiv. of AlR_3 and **43**, compound **51a-e** were formed, ^{31}P NMR displayed a new resonance at 103 ppm (**51a**), with 2 equiv. of AlR_3, compound **52a-e** could be observed, with a ^{31}P NMR chemical shift of 82 ppm (**52a**). This observation that "hard" aluminum Lewis acids preferentially bind to the "harder" nitrogen donor of **43** is in good agreement with Pearson's hard-soft concept.[52] Nonetheless, the softer phosphorus can be a good donor for hard Lewis acids as it is well reflected in the rapid and selective formation of the binuclear **52b**. Thus, in order to prove that a softer Lewis acid should bind to phosphorus prior to nitrogen, $BH_3{\cdot}SMe_2$ is treated with **43** to give the mononuclear borane (1 equiv. $BH_3{\cdot}SMe_2$ with **43**), with the boron linked to the phosphorus atom; adding 2 equiv. of $BH_3{\cdot}SMe_2$ (or even more) furnished the binuclear borane complex**.**

[52] *a) Pearson, R. G. Hard and soft acids and bases. J. Am. Chem. Soc. 1963, 85, 3533−3539. b) Pearson, R. G. Acids and bases. Science 1966, 151, 172−177.*

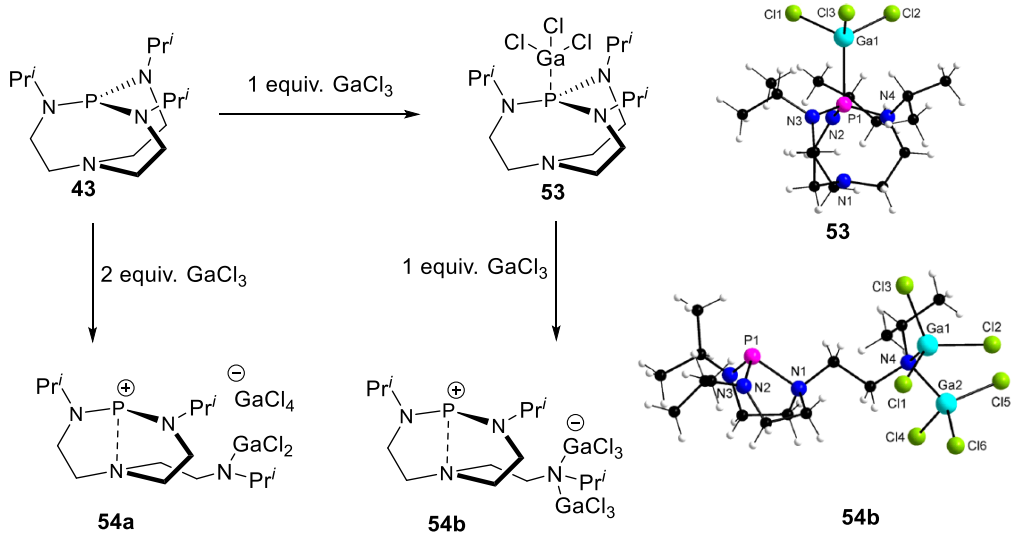

Figure 1.3.8 Formation of **53, 54a** and **54b.**

Furthermore, $GaCl_3$ is considered to form a more complicated binuclear compound (Figure 1.3.8), reaction of base **43** with 1 equiv. $GaCl_3$ gave compound **53** (^{31}P NMR spectrum displays a broad signal at 64 ppm), with 2 equiv. $GaCl_3$, compound **54a** and **54b** were obtained, the ^{31}P NMR spectrum revealed the formation of two isomers, **54a** and **54b**, which gave rise to single resonances at 161 ppm (sharp) and 162 ppm (broad), respectively. Interestingly, phosphorus or bottom nitrogen was no longer prior to give an expected binuclear formation, it was one of a P-N broken actually, and $GaCl_3$ linked to the nitrogen but not the phosphorus atom.

Timothy C. Johnstone and co-workers have further studied the reaction of proazaphosphatrane base **12** and $B(C_6F_5)$ (Figure 1.3.9).[53] Compound **55** is characterized by X-ray analysis and NMR spectrum: the ^{11}B NMR spectrum showed a doublet at -12.4 ppm with a coupling constant of 130 Hz; the ^{31}P NMR spectrum displayed an up field-shifted quartet at 80.0 ppm with a coupling constant of 130 Hz, and the ^{19}F NMR spectrum gave five signals with multiplicities and intensities consistent with two F_{ortho}, two F_{meta}, and one F_{para} signals.

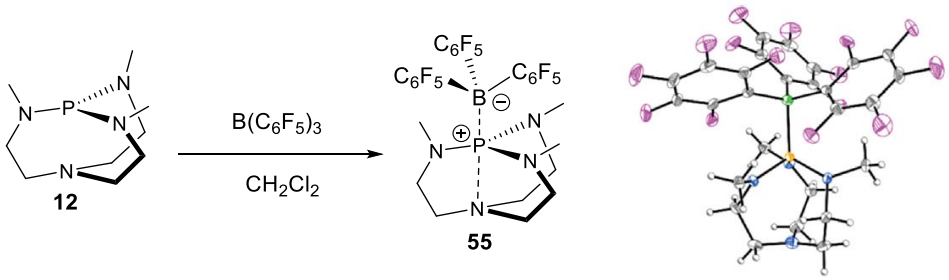

Figure 1.3.9 Synthesis of FLP **55**.

[53] *Timothy C. Johnstone, Gabriel N. J. H. Wee, and Douglas W. Stephan. Angewandte Chemie, International Edition 2018, 57(20), 5881-5884.*

The authors use natural bond orbital and electron density topology to acquire the perception of reactivity of **55**, and confirmed that both ways could prove that there was no bonding interaction between nitrogen and phosphorus, and be basically consistent with the crystalline structure. Property of **55** is between the electrophilic borane $B(C_6F_5)_3$ and proazaphosphatrane, even though its NMR spectrum did not show any evidence of dissociative liquid balance, still, it provided the products of FLP addition reactions with unsaturated substrates.

Although they did not display spectroscopic clue of **55** of dissociation into acid and base, they studied the products that came from frustrated Lewis pair addition reactions, with PhNCO, $PhCH_2N_3$, PhNSO, and CO_2 (Figure 1.3.10). According to the results, compound **55** have strong stability, tremendous reactivity and common applications in FLP chemistry field. The reaction of PhNCO and **55** formed a relatively pure and single compound **56** in 10 minutes, NMR and crystallographic characterization revealed it to be the product of 1,2-addition of **12** and $B(C_6F_5)_3$ across the C=O double bond of PhNCO. The formation of **56** corresponds to a formal FLP addition reaction, in the absence of $B(C_6F_5)_3$, **57** is that of 1, 2-addition across the C=O of CO_2, **58** is that of 1, 3-addition across the NSO functional group of PhNSO, **59** is the product of 1,3-addition across the N_3 group of $PhCH_2N_3$. The identities of **56-59** are confirmed spectroscopically and crystallographically. The authors concluded that the reactivity highlighted the importance of exploring obviously stable Lewis adducts for FLP chemistry and the possibility that many promising acid-base pairs would have been overlooked because they readily bound to form Lewis adducts.

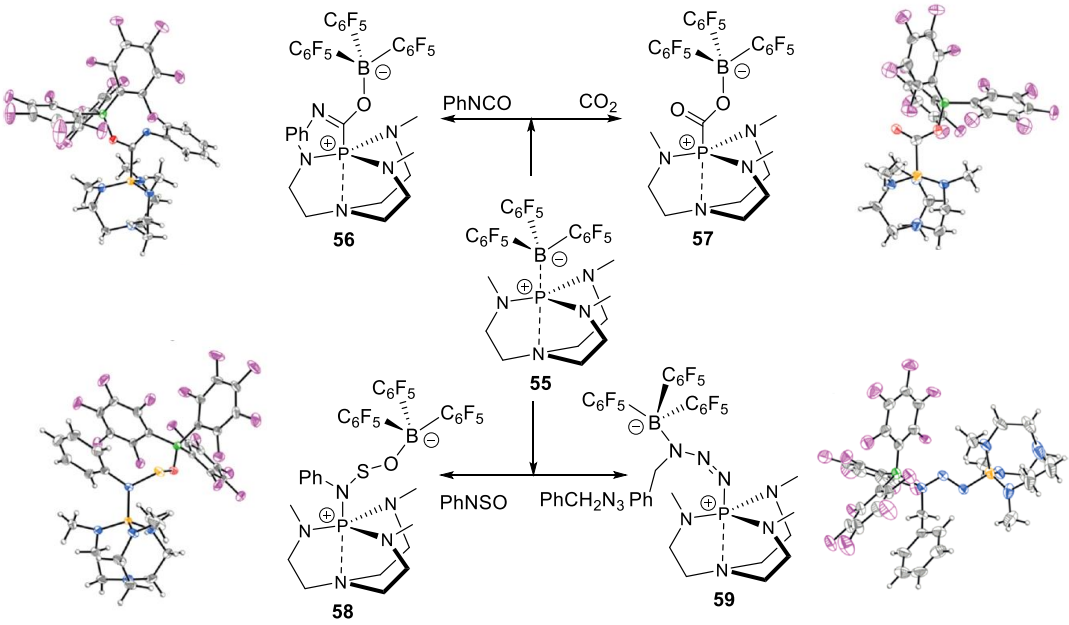

Figure 1.3.10 Formation of FLP addition products from **56-59**.

1.3.2 Proazaphosphatranes as superbases in confined space

Raymond and co-workers firstly reported the confined azaphosphatrane.[54] Based on their results, a Verkade's superbase has been covalently attached inside the host cavity of hemicryptophane, leading to a host superbase containing a preorganized cavity, this cavity is defined by the cyclotriveratrylene moiety above the strongly basic proazaphosphatrane. Chatelet and co-workers reported the synthesis of an encaged proazaphosphatrane superbase in a hemicryptophane-type structure, the thermodynamic and kinetic consequences of the encapsulation were investigated.[55]

It has been shown that the basicity of the proazaphosphatranes depend on the nature of the substituents on the nitrogen atoms.[56] Thus, to explore the effects of the environment and of the confinement on the activity of the phosphorus superbases, they synthesized the related model compounds **12d-H$^+$·Cl$^-$, 27-H$^+$·Cl$^-$, 29-H$^+$·Cl$^-$**, the azaphosphatranes **31-H$^+$·Cl$^-$, 32-H$^+$·Cl$^-$, 33-H$^+$·Cl$^-$**, and the encaged-azaphosphatranes **31**, **32**, and **33** which were deprotonated by *t*-BuOK (Figure 1.3.11). These model **12d-H$^+$·Cl$^-$**, base **31**, conjugated acids **32-H$^+$·Cl$^-$, 33-H$^+$·Cl$^-$** were characterized by X-Ray analysis, all compound were identified by NMR spectra. ^{31}P NMR spectra gave the resonances at -32 ppm, -32 ppm and -36 ppm for **31-H$^+$·Cl$^-$, 32-H$^+$·Cl$^-$, 33-H$^+$·Cl$^-$**, with a significant highfield shift of about 20 ppm compared to the model azaphosphatranes, resonances at 125 ppm 125 ppm 128 ppm for **31**, **32**, and **33**, respectively.

pKa values and rate constants for proton transfer of the azaphosphatrane conjugate acids were measured by competition experiments: addition of the azaphosphatrane to a solution of the Verkade's superbase **12a** (R = CH_3) in CD_3CN lead to an equilibrium mixture, it was then analyzed by ^{31}P and ^{1}H NMR spectroscopy. This afforded reproducible Ka values for the models and the supramolecular compounds (Table 1.3.4). Based on this table, the confinement in specific architectures affects the pKa values: more basic or less basic systems could be obtained, depending on the hemicryptophane structure. Moreover, the encapsulation of the phosphorus moiety strongly affects the rate of proton transfer when compared to that of the model molecules. The rate of proton transfer decreases when the cavity size of the host increases.

---

[54] *P. D. Raytchev, A. Martinez, H. Gornitzka, J.-P. Dutasta. J. Am. Chem. Soc. 2011, 133, 2157–2159.*

[55] *Chatelet, B., Gornitzka, H., Dufaud, V., Jeanneau, E., Dutasta, J., Martinez, A. (2013). J. Am. Chem. Soc., 2013, 135(49), 18659-64.*

[56] *a) Kisanga, P. B.; Verkade, J. G.; Schwesinger, R. J. Org. Chem. 2000, 65, 5431. b) Raders, M. R.; Verkade, J. G. J. Org. Chem. 2010, 75, 5308. c) Kisanga, P. B.; Verkade, J. G. Tetrahedron 2001, 57, 467.*

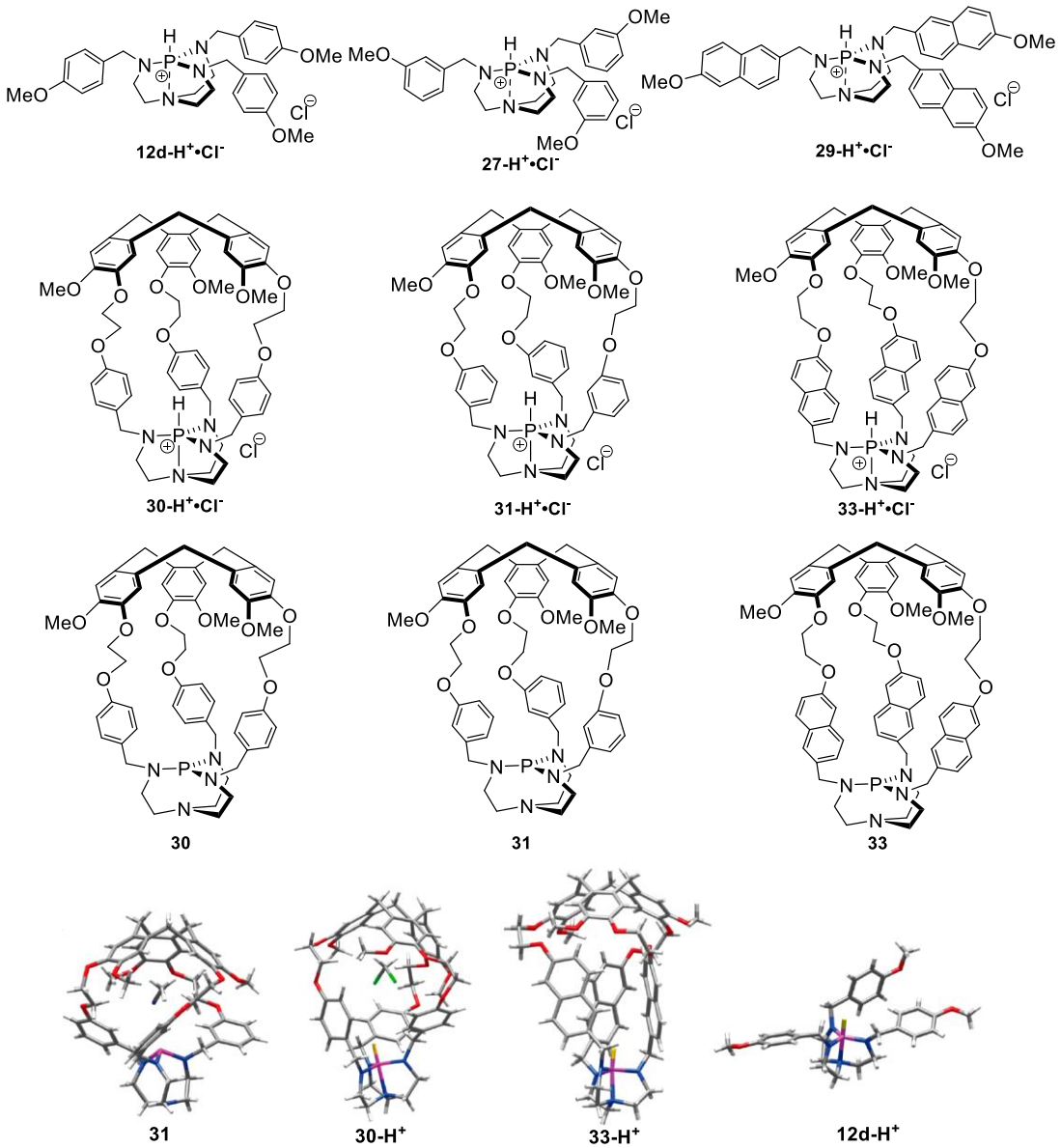

Figure 1.3.11 Formations of supramolecular proazaphosphatrane superbases.

	31	27	30	12d	33	29
pKa	31.35	32.90	32.98	32.14	>35	33.17
Ka	4.42×10^{-32}	1.26×10^{-33}	1.03×10^{-33}	7.25×10^{-33}	$<10^{-35}$	6.81×10^{-34}
k_1 (mol/L/s)	4.79×10^{-5}	-	1.88×10^{-6}	1.06×10^{-3}	1.76×10^{-7}	-
k_{-1}(mol/L/s)	6.77×10^{-6}	-	1.16×10^{-5}	0.93×10^{-3}	$<1.76 \times 10^{-9}$	-

Table 1.3.4 pKa values of conjugate acids of proazaphosphatrane bases and rate constants for proton transfer in acetonitrile (T = 298 K).

Encaged proazaphosphatrane **30** was tested as organocatalyst, and was reported by Chatelet and coworkers[57]. On the use of catalyst **30** and **12d** in base-catalyzed Diels-Alder reaction (Figure 1.3.12), high yields were obtained for two reactions: reaction between anthrone and *N*-methylmaleimide or dimethylfumarate in the presence of catalysts **30** or **12d** which gave the compound **60** (95% for catalyst **30** and 100% for catalyst **12d**) and **61** (100% for catalyst **30** and 95% for catalyst **12d**). Reaction of 3-hydroxy-2-pyrone with *N*-methylmaleimide or dimethylfumarate gave the compound **62** (100% for catalyst **30** and 99% for catalyst **12d**) and **63** (1% for catalyst **30** and 95% for catalyst **12d**). The catalytic activity in the confined space of **30** remains very close to that of the uncapped proazaphosphatrane **12d**. The diastereoselectivity of the Diels-Alder reaction could be improved by encaging the catalytic species.

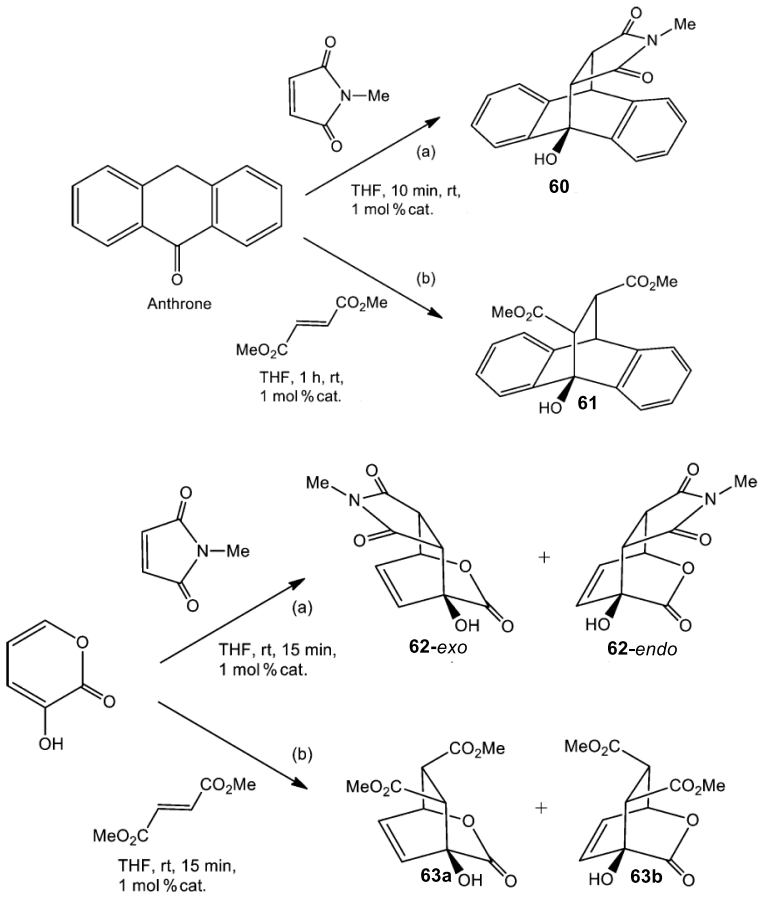

Figure 1.3.12 Diels−Alder Reaction of anthrone and 3-Hydroxy-2-pyrone with (a) N-methylmaleimide; (b) dimethylfumarate.

[57] *B. Chatelet, V. Dufaud, J.-P. Dutasta, A. Martinez. J. Org. Chem. 2014, 79, 8684−8688.*

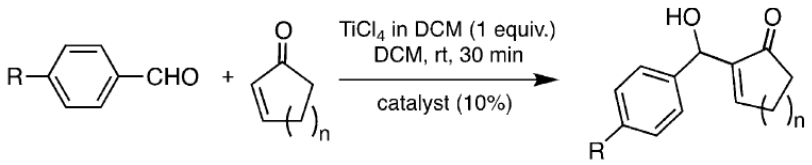

Figure 1.3.13 The Morita–Baylis–Hillman reaction catalyzed by **30** and **12d**.

A total FLP system (**30**/$TiCl_4$) that can catalyze the Morita–Baylis–Hillman reaction has been reported by Yang and coworkers (Figure 1.3.13).[58] They designed a FLP system, where the Lewis base partner is encapsulated in a cage structure. The confinement of the Verkade's superbase in the cavity of a hemicryptophane host **30** prevents the acid-base reaction with the Lewis acidic partner ($TiCl_4$) to take place, providing an effective system for the MBH reaction where both partners can act in concert without neutralizing each other (the improvement of the reaction rate is more than 200%, compared to the catalyst **30**, while base **12d** can react with $TiCl_4$ directly, losing the catalytic property. The key role of the cavity has been highlighted by a set of experiments, bringing evidence that the reaction does occur in the confined space of the molecular cavity.

1.3.3 Proazaphosphatranes as metal ligand in transition properties

In recent years new aspects of the proazaphosphatranes chemistry have been developed, and proazaphosphatranes, generally known as strong base, can act as a ligand for transition metal. Their coordination *via* the phosphorus atom to metal and their properties upon the metal complex formation have received attention. In 2015, the group of Yang reported the synthesis of TPAP and its coordination to Cobalt (II).[59] This tripyridyl ligand containing an apical phosphorus donor may be considered as an analog to tripyridylamine (TPA) (Figure 1.3.14).

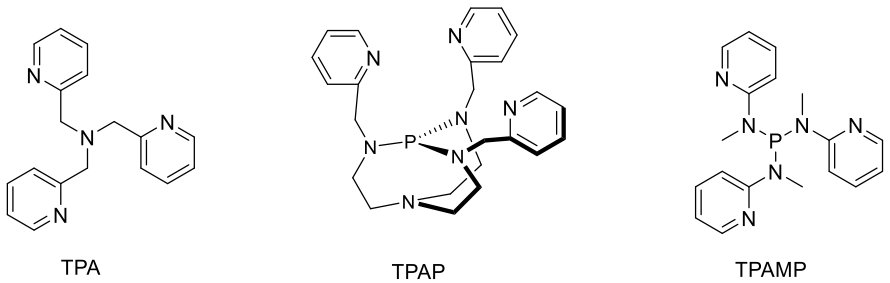

Figure 1.3.14 Structure of TPA, TPAP and TPAMP

[58] *J. Yang, B. Chatelet, V. Dufaud, D. Herault, S. Michaud-Chevallier, V. Robert, J.-P Dutasta, A. Martinez. Angew. Chem. Int. Ed. 2018, 57, 14212 - 14215.*

[59] *Thammavongsy, Z. ; Khosrowabadi Kotyk, J.F. ; Tsay, C. ; Yang, J.Y. Inorg. Chem.* ***2015****, 54, 11505-11510.*

They compared the coordination geometry of tri(N-methyl-pyridylamino)phosphine (TPAMP) **65** and TPAP **64** to Co(II) (Figure 1.3.15). TPAMP has one-atom spacer between the apical phosphorus and the pyridyl arms compared to two-atom spacer for TPAP. The crystal structure of the TPAMP cobalt complex showed only two pyridines and two phosphorus atoms which are coordinated, one pyridine is unbound to the metal ion. In contrast, according to the X-ray analysis of cobalt complex containing TPAP ligand, the $Co^{\cdots}N_{pyr}$ distance is similar for the three pyridines (1.997 Å, 2.035 Å, 2.094 Å) suggesting the coordination of all pyridines *via* a tetradentate coordination geometry. The determination of $Co\text{-}P_{apical}\text{-}N$ angle in **65** is in line with the $Co^{\cdots}N_{pyr}$ distance. In fact, the observed small angle (104.5°) prevents the coordination of the third pyridine to metal ion by steric hindrance. Therein the authors proved the great importance of ligand flexibility.

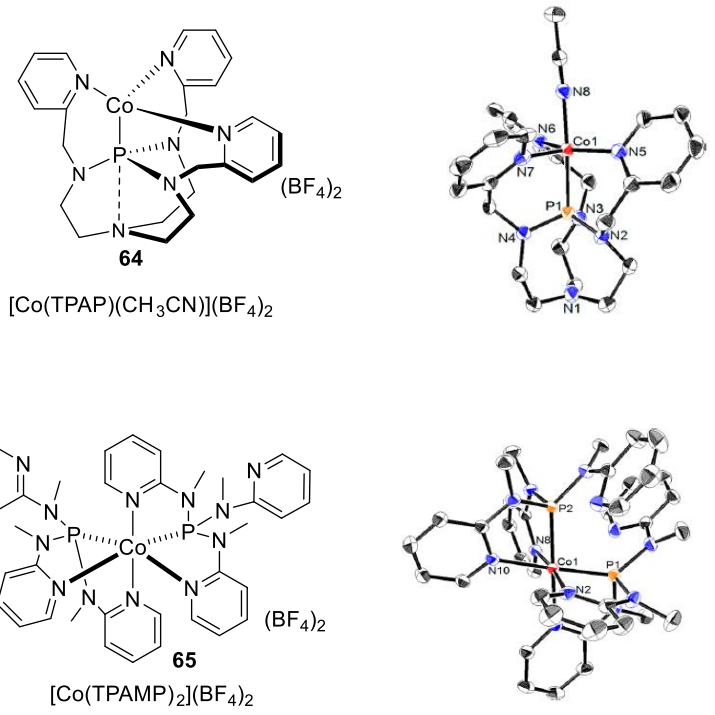

Figure 1.3.15 Structure of **64** and **65**.

The group of Verkade described for the first time the structure of the *trans*-$Cl_2Pt[P(NMeCH_2CH_2)_3N]$ and $Hg[(P(NMeCH_2CH_2)_3N)(Cl)_2]$ complexes in 1990.[60] Yang and co-workers later reported a more extensive analysis of the TPAP ligand properties using M(TPAP) complexes[61]. Upon the coordination to the metal, the flexible chelating ligand TPAP can adapt its phosphorus donor strength from the transannular bond between a tertiary nitrogen

[60] *Xi, S.K. ; Schmidt, H. ; Lensink, C. ; Kim, S. ; Wintergrass, D. ; Daniels, L.M. ; Jacobson, R.A. ; Verkade, J.G. Inorg. Chem.* ***1990****, 29, 2214-2220*

[61] *Thammavongsy, Z. ; Cunningham, D.W. ; Sutthirat, N. ; Eisenhart, R.J. ; Ziller, J.W. ; Yang, J.Y. Dalton Trans.* ***2018****, 47, 14101-14110.*

and phosphorus atom.[62] This transfer of electron density can change the environment and the reactivity of the metal. For evaluating the transannular interaction, Verkade and Yang determined the distance of P···N_{ax} upon the coordination to metal center. This distance was measured by X-ray crystallography and DFT calculations in **66-71** complexes (Figure 1.3.16).

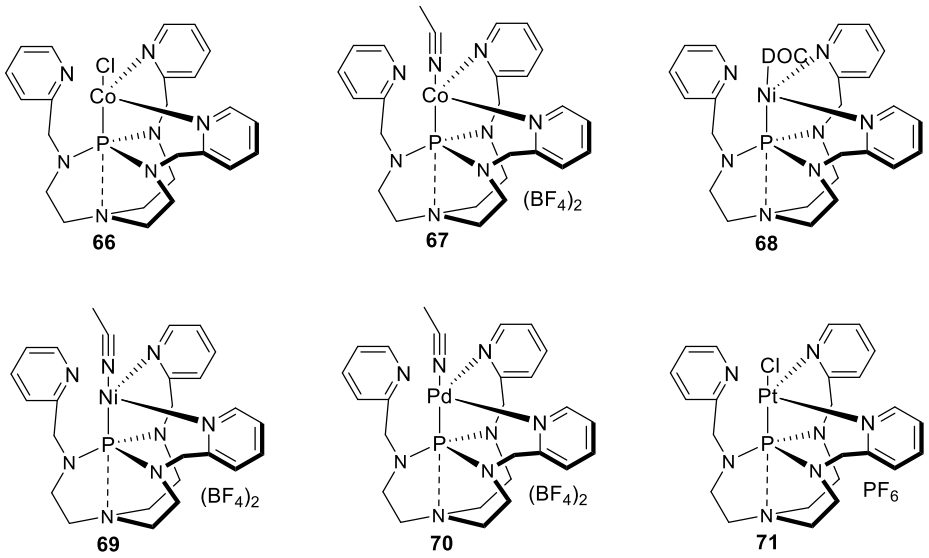

Figure 1.3.16 Structure of TPAP complexes **66-71**.

Lewis acids	**68**	**66**	**67**	**71**	**69**	**70**
P···N_{ax}/ Å	3.39	3.26	2.94	2.92	2.87	2.67
Acidity			⟶			

Table 1.3.5 Bond lengths (P···N_{ax}) of TPAP complexes **66-71.**

Verkade previously showed that the P···N_{ax} distance exceeds 3.2 Å in proazaphosphatrane whereas azaphosphatranes have P···N_{ax} under 2.0 Å, proof of the transannular interaction.[63] In this study, the distance of metal-TPAP ligand remains constant while the P···N_{ax} distance varies from 2.67 to 3.39 Å depending on the Lewis acidity of the metal center (Table 1.3.5). The P···Nax distance decreases with an increase of the Lewis acidity closely related to the oxidation state of the metal center. This information suggests that the ligand TPAP donates the electron density into the phosphorus atom leading to the stabilization of the more electron deficient metal ions.

[62] *Michael Meot-Ner. J. Am. Chem. Soc. 1992, 114, 3312-3322*

[63] *a) Xi, S.K. ; Schmidt, H. ; Lensink, C. ; Kim, S. ; Wintergrass, D. ; Daniels, L.M. ; Jacobson, R.A. ; Verkade, J.G. Inorg. Chem.* ***1990****, 29, 2214-2220 ; b) Tang, J.S. ; Laramay, M.A.H. ; Young, V. ; Ringrose, S. ; Jacobson, R.A. ; Verkade, J.G. J. Am. Chem. Soc.* ***1992****, 114, 3129-3131 ; c) Liu, X.D. ; Verkade, J.G. Inorg. Chem.* ***1998****, 37, 5189-5197.*

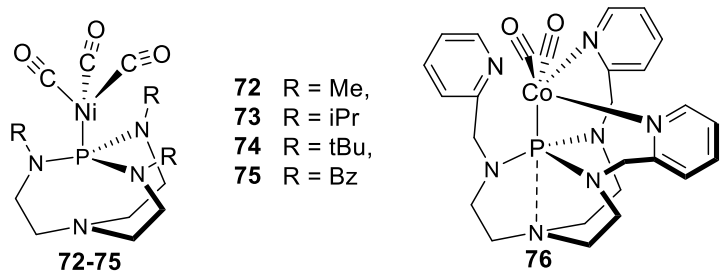

Figure 1.3.17 Structure of **72-76.**

	Complex	ν_{CO} A_1 (cm^{-1})	ν_{CO} E (cm^{-1})	Cone angle (°)
72	$Ni(CO)_3(L^{Me})$	2057.0	1977.7	152
73	$Ni(CO)_3(L^{iPr})$	2054.6	1974.7	179
74	$Ni(CO)_3(L^{tBu})$	2054.9	1975.3	200
75	$Ni(CO)_3(L^{Bz})$	2059.1	1981.1	207
76	$Ni(TPAP)(CO)_2$	-	-	-
-	$Ni(CO)_3(P(tBu)_3)$ [a]	2056.1	1971	182
-	$Ni(CO)_3(P(Me)_3)$ [a]	2064.1	1982	118

Table 1.3.6 CO vibrational frequencies in CH_2Cl_2 and cone angle of complexes and selected $Ni(CO)_3(PR_3)$ complexes. [a] TEP value taked from Tolman et al.[64]

The group led by Yang has analyzed the stereoelectronic effects of substituted proazaphosphatranes in $Ni(P(NRCH_2CH_2)_3N)(CO)_3$ complexes by the Tolman electronic parameters (TEP) and cone angles.[64] The TEP determined *via* CO stretching frequencies measurements allow the ranking of phosphorus ligand by their donor ability.[65] Based on the CO vibrational frequencies of the complexes **72-75** bearing various substituents (respectively Me, *i*Pr, *i*Bu, Bz), $Ni(TPAP)(CO)_2$ and $Ni(CO)_3(PR_3)$ where R = *t*Bu, Me, table 1.3.6 shows that the substituted proazaphosphatranes present donor strength of similar to that of the most donating phosphine $P(tBu)_3$ ligand (ν_{CO} 2056; mode A_1) (Figure 1.3.17). They noted a negligible effect of the substituents on the donor strength, while the cone angles depend on the steric bulk of the substituents on nitrogen atom. The proazaphosphatranes exhibit larger cone angles than the analogous trialkyl substituted phosphine impacting the reactivity of the metal center (i.e. : L^{tBu} = 200° *vs* $P(tBu)_3$ = 182°). Complex **76** (Figure 1.3.1) was synthesized in a similar fashion to that of complexes **72-75**. The solution infrared spectrum of **76** in CH_2Cl_2 displayed two CO vibrational stretches at 1981.7 and 1906.5 cm^{-1} supporting that TPAP binds to Ni(0) in a bidentate fashion, therefore, no direct comparison regarding the CO vibrational

[64] *Thammavongsy, Z. ; Kha, I.M. ; Ziller, J.W. ; Yang, J.Y. Dalton Trans.* ***2016****, 45, 9853-9859.*

[65] *Tolman, C.A. Chem. Rev. 1977, 77, 313-348.*

frequencies between **76** and **72-75** can be made.

In 2017, Martinez, Chatelet and co-workers reported the synthesis of Au(I) complexes bearing proazaphosphatranes as an alternative ligand to N-heterocyclic carbenes (NHCs).[66] In fact, protonated azaphosphatrane can be seen as an analogue of imidazolidium salts, the pre-ligand of NHCs.[67] According to their preliminary studies, they compared the donor strength of ligand azaphosphatrane with *N*-methyl substituents (L^{Me}) and NHC (I^{Mes}) in $[Ni(CO)_3(L)]$ and $[RhCl(CO)_2(L)]$ complexes by computing the CO vibrational frequencies. The results demonstrate the high electron-donating properties of the azaphosphatranes as ligand compared with I^{Mes} as NHC ligand (Table 1.3.7).

Complex	ν_{CO} A1 (cm^{-1})	ν_{CO} E (cm^{-1})	ν_{CO} cis (cm^{-1})	ν_{CO} trans (cm^{-1})
$Ni(CO)_3(L^{Me})$	2047	1993	---	---
$Ni(CO)_3(I^{Mes})$	2042	1985	---	---
$RhCl(CO)_2(L^{Me})$	---	---	1984	2066
$RhCl(CO)_2(I^{Mes})$	---	---	1982	2063

Table 1.3.7 Computed (TPSS/def2-TZVP) CO stretching frequencies (cm^{-1}) for metal carbonyl complexes.

After demonstrating their strong sigma-donating ability, they proposed the first synthesis of $AuCl[P(NRCH_2CH_2)_3N]$ with R = *i*Bu, PMB from $AuCl(S(CH_3)_2)$ and free superbase (Figure 1.3.18). They obtained the single crystals of the complex bearing L^{iPr} showing the linear coordination of the two ligands at the metal center (P-Au-Cl angle = 177°). The distance $P^{\cdots}N_{ax}$ is comparable to the one observed in proazaphosphatrane by Verkade *et al* ($P^{\cdots}N_{ax}$ = 3.127 Å in gold complex *vs* $P^{\cdots}N_{ax}$ = 3.2 Å in proazaphosphatrane) indicating a weak transannular interaction.

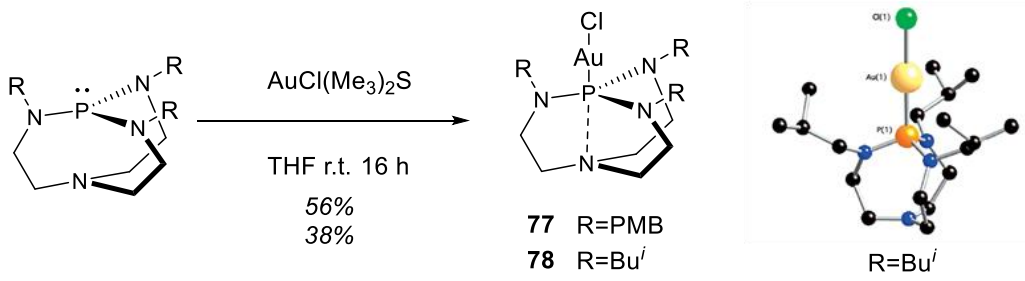

Figure 1.3.18 Preparation of complexes **77** and **78** from proazaphosphatranes

[66] *Chatelet, B. ; Nava, P. ; Clavier, C. ; Martinez, A. Eur. J. Inorg. Chem.* ***2017****, 4311-4316.*

[67] *Hanhn, F.E. ; Jahnke, M.C. Angew. Chem. Int. Ed.* ***2008****, 47, 3122-3172; Angew. Chem.* ***2008****, 120, 3166-3216.*

Inspired by the works of Lin and Nolan[68] showing the possibility to use the NHC-containing silver complexes as carbene transfer agents and the similar properties between azaphosphatranes and NHC, this research group introduced a new methodology to obtain the azaphosphatrane-containing gold complexes from the corresponding silver complex by transmetallation (Figure 1.3.19a). It must be noted that this method does not require strict and controlled handling conditions by using the air-, moisture-stable azaphosphatranes. The competition experiment of transmetallation between (proazaphosphatrane)-silver complex and (NHC)-silver complex with gold has been reported (Figure 1.3.19b). This experiment revealed that the proazaphosphatrane is more labile than NHC ligand, the proazaphosphatrane-gold complex is the only isolated complex. The lower calculated dissociation energy of the P···Ag bond in complex **77s** (45.7 kcal.mol^{-1}) than the C···Ag bond in complex **77** (54.3 kcal.mol^{-1}) confirm this enhanced lability.

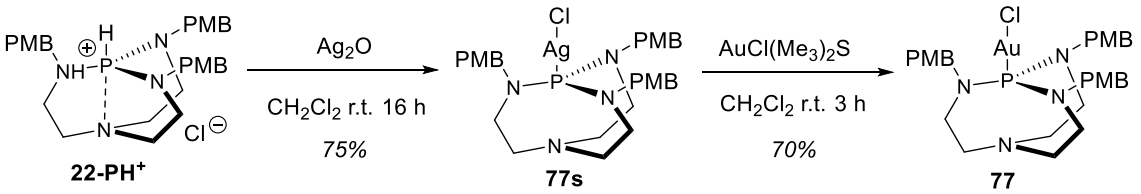

Figure 1.3.19a Synthesis of complexes **77** by formation of silver complexes **77s** from azaphosphatranes **22-PH**$^{+}$ and transmetallation.

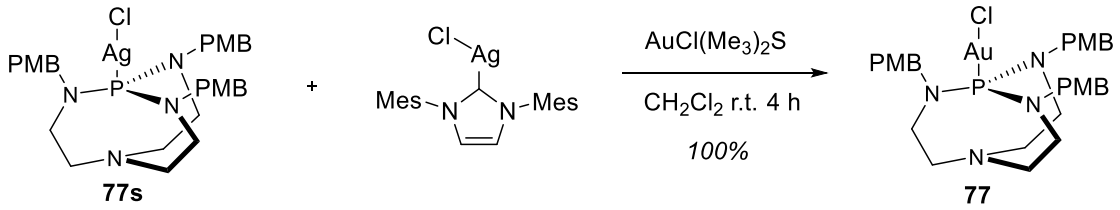

Figure 1.3.19b Competition experiment between proazaphosphatrane and NHC ligand.

Recently, Thammavongsy and co-workers[69] reported the synthesis of active site mimic of NiFe hydrogenase enzyme involving the tetradentate tripodal ligand TPAP. This model heterobimetallic NiFe(TPAP)(CO)$_5$ **79** was prepared from Ni(TPAP)(COD) **68** with Fe(CO)$_5$ and characterized (Figure 1.3.20). The main key structural moieties of the complex are the presence of terminal bond CO molecules on Fe(0) and TPAP coordinated to Ni(0) known both

[68] *a) Wang, H.M.J. ; Lin, I.J.B. Organometallics **1998**, 17, 972-975; b) De Frémont, P. Scott, N.M. ; Stevens, E.T. ; Nolan, S.P. Organometallics **2005**, 24, 2411-2418.*

[69] *Sutthirat, N. ; Ziller, J.W. ; Yang, J.Y. ; Thammavongsy, Z. Acta Cryst. **2019**, E75, 438-442.*

for the stabilization of the oxidation state of metal ions.[70] In addition, an arginine residue is conserved in NiFe hydrogenase enzyme and would play a role in the activation of H_2.[71] The use of TPAP with a proximal pendant base pyridine could mimic the vital arginine in the active site.

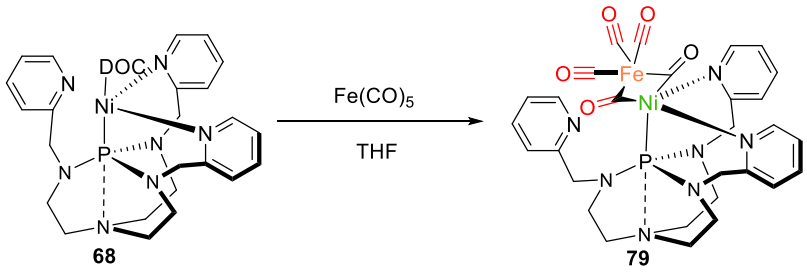

Figure 1.3.20 Structure of NiFe(TPAP)$(CO)_5$ **79**.

In line with the studies previously cited, proazaphosphatranes represent a unique class of ligands, especially by the flexibility of the transannular interaction which can be advantageous in cross-coupling reactions. In fact, the ligands could act as a good σ-donor during the oxidative addition step, but also could act as a good ligand during the reductive elimination step through the large cone angles. Palladium-catalyzed amination of aryl halides is one the most efficient tool for the formation of C-N bonds. This transformation is now known as the Buchwald-Hartwig amination (BHA).[72] In 2003, Verkade examined first the use of bulky proazaphosphatrane as ligand for the Pd-amination of aryl bromides and iodides (Figure 1.3.21).[73] This work revealed that the combination of $Pd(OAc)_2$ **83** with $P(N\textit{i}BuCH_2CH_2)_3N$ **12b** (ratio 1:2 respectively) was an effective catalyst for aryl amination with a large scope in good to excellent yields.

The mechanism and the putative intermediates for C-N cross-coupling reactions involving palladium bearing the ligand Verkade's superbase was further studied by the Johnson group in 2018. Thereby, they synthesized two catalytic intermediates supposed required in BHA: the catalyst $[Pd(0)]L_2$ (**A**) and the reactive intermediate [Pd(II)]L(Br)(Ar) (**B**) where L is tri-isobutylphosphatrane **12b**. The reaction was performed in the presence of catalysts **A** or **B** in similar yields demonstrating that these species represented key intermediates during the

[70] *Behnke, S.L. ; Shafaat, H.S. Comments Inorg. Chem.* ***2016****, 36, 123-140 ; Dalton Trans.* ***2018****, 47, 14101-14110 ; Inorg. Chem.* ***2015****, 54, 11505-11510.*

[71] *Evans, R.M. ; Brooke, E.J. ; Wehlin, S.A.M. ; Nomerotskaia, E. ; Sargent, F. ; Carr, S.B. ; Phillips, S.E.V. ; Armstrong, F.A. Nat. Chem. Biol.* ***2016****, 12, 46-50.*

[72] *Dorel, R. ; Grugel, C.P. ; Haydl, A.M. Angew. Chem. Int. Ed.* ***2019****, 58, 17118-17129.*

[73] *Urgaonkar, S. ; Nagarajan, M. ; Verkade, J.G. J. Org. Chem.* ***2003****, 68, 452-459.*

catalytic cycle (Figure 1.3.21). By X-ray cristallography, they determined the P---N_{ax} distance in the intermediates involving in C-N cross-coupling, Pd(0) bis(phosphine), Pd(II) aryl bromide and Pd(II) amide. Electron-poor complexes, Pd(II) aryl bromide and Pd(II) amide, exhibited shorter P---N_{ax} length than electron-rich Pd(0) bis(phosphine). These observations would explain the promotion of oxidative addition thanks to electron donation from ligand proazaphosphatrane to metal ion through transannulation. According to these results, they validated the beneficial flexibility effect of proazaphosphatrane in the stabilization of catalytic intermediates.

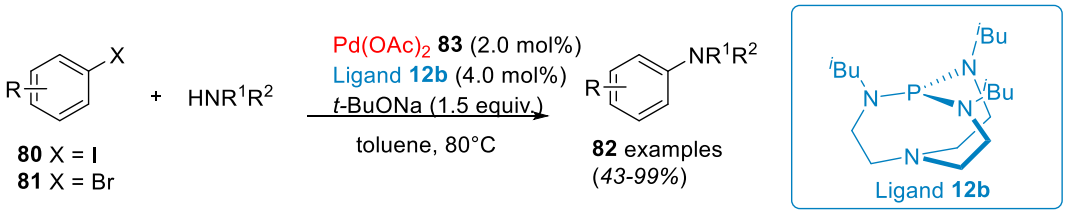

Figure 1.3.21 Proazaphosphatrane as ligand for aryl amination.

Chapter 2: Chloroazaphosphatranes: a new motif for halogen-bonding in solution

My special thanks to Dr. Anne-Doriane Manick.

Publications: Chunyang Li, Anne-Doriane Manick, Jian Yang, David Givaudan, Bohdan Biletskyi, Sabine Michaud-Chevalier, Jean-Pierre Dutasta, Damien Hérault, Xavier Bugaut*, Bastien Chatelet*, and Alexandre Martinez*. The Chloroazaphosphatrane Motif for Halogen Bonding in Solution. *Inorganic Chemistry*. DOI: 10.1021/acs.inorgchem.1c01005.

2.1 Introduction

Non-covalent bonds play a fundamental role in all sub-fields of chemistry, such as catalysis or supramolecular chemistry, but also, they are involved in the molecular interactions in biological processes. The most studied one is hydrogen bonding, which consists, mainly, in an attractive electrostatic interaction between an electron-poor hydrogen atom and a Lewis base (LB).

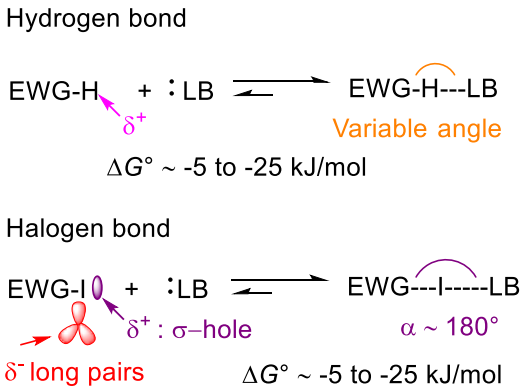

Figure 2.1.1 Comparison of hydrogen bond and halogen bond, EWG=C_nF_{2n+1}, C_nH_{5-n}.

Halogen bonding, is another emerging noncovalent interaction for constructing supramolecular assemblies. It refers to a related Lewis acid-base noncovalent stabilizing association that can exist between the electron-deficient region of a halogen atom, such as an iodine atom, linked to an electron-withdrawing group, which was called σ hole (Figure 2.1.1), and a Lewis base.[74] It results in a shortening of the distance between the two atoms below the sum of their van der Waals radii. Though similar to the more familiar hydrogen bonding, halogen bonds share some common features but they are notably longer, as the iodine atom has a much bigger van der Waals radius than the hydrogen atom (3.8 Å *vs* 2.5 Å).[75] Besides, there are four primary differences between these two interactions that make halogen bonding a unique tool for molecular recognition and the design of functional materials. Firstly, halogen bonds tend to be much more directional than single hydrogen bonds, since their existence requires a nearly perfect alignment between the three involved atoms, the σ hole is surrounded by a corolla of high electron density due to the three lone pairs of the halogen atom.[76] Secondly, the

[74] *a) R. S. Mulliken, J. Am. Chem. Soc.* ***1950****, 72, 600; b) O. Hassel, Science* ***1970****, 170, 497; c) P. Metrangolo, G. Resnati, Eds, Springer, Berlin,* ***2008****; d) M. Erdelyi, Chem. Soc. Rev.* ***2012****, 41, 3547; e) T. M. Beale, M. G. Chudzinski, M. G. Sarwar, M. S. Taylor, Chem. Soc. Rev.* ***2013****, 42, 1667; f) G. Cavallo, P. Metrangolo, T. Pilati, G. Resnati, M. Sansotera, G. Terraneo, Chem. Soc. Rev.* ***2013****, 39, 3772.*

[75] *S. Alvarez, Dalton Trans.* ***2013****, 42, 8617.*

[76] *S. M. Huber, J. D. Scanlon, E. Jimenez-Izal, J. M. Ugalde, I. Infante, Phys. Chem. Chem. Phys.* ***2013****, 15, 10350.*

interaction strength scales with the polarizability of the bond-donor atom, a feature that researchers can tune through single-atom mutation. In addition, halogen bonds are hydrophobic whereas hydrogen bonds are hydrophilic. Lastly, the size of the bond-donor atom of halogen is significantly larger than hydrogen. Despite its interesting features, which have been widely exploited in crystal engineering,[77] supramolecular chemistry,[78] polymer science,[79] medicinal chemistry,[80] or organocatalysis,[81] the applications of halogen bonding remain scarce because of the limited number of structural patterns that allow its existence: indeed, it generally requires a proper scaffold or a cationic heterocycle as substituent on the nitrogen atom. As a result, halogen bonding provides supramolecular chemists with design tools that cannot be easily met with other types of noncovalent interactions and opens up unprecedented possibilities in the design of smart functional materials.

Anions recognition plays a crucial role in medicine, biology, chemistry and environmental sciences.[82] Synthetic anion receptors have thus found various applications, ranging from sensors, organocatalysts or anion carriers in living systems to the remediation of toxic or radioactive anions from aqueous wastes.[83] As a consequence, the development of new motifs for anion binding arouses a considerable interest. Behind the traditional interactions often used for recognize anions, such as hydrogen-bonding, dispersion forces or electrostatic interactions, less common interactions, like anion-π interactions,[84] coordination with Lewis acid, such as metals or main group elements,[85] or σ-hole interactions,[86] have recently received a growing attention leading to the expansion of anion receptors and to the improvement of the selectivity and binding strength.

Among the σ-hole interactions, XB (halogen bonding) interaction appears as the most studied for anion recognition.[87] Indeed, its strength and strong directionality have led to its wide use in materials design and crystal engineering,[88] and has found more recently applications in

---

[77] *a) P. Metrangolo, G. Resnati, Crys. Growth Des.* ***2012****, 12, 5125; b) J.-Y. Le Questel, C. Laurence, J. Graton, CrystEngComm* ***2013****, 15, 3212.*

[78] *L. C. Gilday, S. W. Robinson, T. A. Barendt, M. J. Langton, B. R. Mullaney, P. D. Beer, Chem. Rev.* ***2015****, 115, 7118.*

[79] *G. Berger, J. Soubhye, F. Meyer, Polym. Chem.* ***2015****, 6, 3559.*

[80] *P. Auffinger, F. A. Hays, E. Westhof, P. S. Ho, Proc. Natl. Acad. Sci. U.S.A.* ***2004****, 101, 16789.*

[81] *D. Bulfield, S. M. Huber, Chem. Eur. J.* ***2016****, 22, 14434.*

[82] *Evans, N. H.; Beer, P. D. Angew. Chem. Int. Ed.* ***2014****, 53, 11716-11754.*

[83] *a) Gale, P. A.; Howe, E. N. W.; Wu, X. Anion receptor chemistry. Chem* ***2016****, 1, 351-422. b) Chen, L.; Berry, S. N.; Wu, X.; Howe, E.N.W.; Gale, P.A. Advances in anion receptor chemistry. Chem* ***2020****, 6, 61-141.*

[84] *a) Zhao, Y.; Cotelle, Y.; Liu, L.; López-Andarias, J.; Bornhof, A.-B.; Akamatsu, M.; Sakai, N.; Matile, S. Acc. Chem. Res.* ***2018****, 51, 2255-2263. b) Ballester, P. Acc. Chem. Res.* ***2013****, 46, 874-884.*

[85] *Wade, C. R.; Broomsgrove, A. E. J.; Aldridge, S.; Gabbaï, F. P. Chem. Rev.* ***2010****, 110, 3958-3984.*

[86] *Vogel, L.; Wonner, P.; Huber, S. M. Angew. Chem. Int. Ed.* ***2019****, 58, 1880-1891.*

[87] *Pancholi, J.; Beer, P. D. Coord. Chem. Rev.* ***2020****, 416, 213281.*

[88] *Metrangolo, P.; Resnati, G.; Pilati, T.; Biella, S.. Struct. Bond.* ***2008****, 126, 105-136. b) Fourmigué, M. Struct. Bond.* ***2008****, 126, 181-207. c)*

solution phase for anion recognition, transport and sensing, or organocatalysis.[89] Although the XB-anion receptors display a large range of various structures, from acyclic compounds to interlocked molecules,[90] the XB motifs used are still mainly limited to neutral or cationic hetero- or carbo-cycles, such as haloperfluoroarene, halotriazole, halotriazolium, haloimidazolium, and halopyridinium motifs. These XB donors are based on halogen atoms bounded to carbon atoms included in an aromatic cycle, inhibiting a possible nucleophilic substitution that could occur on aliphatic ones, in the presence of anions. Several requirements need to be fulfilled to build new XB donors: (i) the system must include a halogen atom linked to an electro-deficient unit, (ii) it must be stable in the presence of nucleophilic anions or other Lewis bases and (iii) ideally their synthesis should be easy and highly modulable.

In this chapter, haloazaphosphatranes appear as promising motif for XB.[91] Indeed, their non-halogenated derivatives, the proazaphosphatranes, also named Verkade's superbases,[92] are highly basic non-ionic organic compounds that have found a considerable range of applications for instance as catalysts or stoichiometric reagents.[93] This strong basicity related to the remarkable stability of their acidic counterparts, the azaphosphatranes is due to the formation, upon protonation, of a transannular bond between the apical nitrogen and the phosphorus atom, leading to the formation of three five-membered rings and the delocalization of the positive charge on the four nitrogen atoms.[94] We hypothesized that the strong stability of the azaphosphatranes might be retained to some extent in the haloazaphosphatranes, and that the electron-withdrawing effect of the positive phosphorus atom should allow XB formation. Moreover, the substituents on the nitrogen atom can be easily varied allowing a modulation of the stereo-electronic properties of the haloazaphosphatranes.

Hachem, H.; Jeannin, O.; Fourmigué, M.; Barrière, F.; Lorcy, D. CrystEngComm ***2020****, 22, 3579-3587.*

[89] *a) Cavallo, G.; Metrangolo, P.; Milani, R.; Pilati, T.; Priimagi, A.; Resnati, G.; Terraneo, G. The halogen bond. Chem. Rev.* ***2016****, 116, 2478-2601. b)Tepper, R.; Schubert, U. S. Halogen bonding in solution: anion recognition, templated self-assembly, and organocatalysis. Angew. Chem. Int. Ed.* ***2018****, 57, 6004-6016. c) Bulfield, D.; Huber, S. M. Halogen bonding in organic synthesis and organocatalysis. Chem. Eur. J.* ***2016****, 22, 14434-14450.*

[90] *a) Klein, H. A.; Kuhna, H.; Beer, P. D. Chem. Commun.* ***2019****, 55, 9975-9978. b) Bunchuay, T.; Docker, A.; Martinez-Martinez, A. J.; Beer, P. D. Angew. Chem. Int. Ed.* ***2019****, 58, 13823-13827. c) Borissov, A.; Marques, I.; Lim, J. Y. C.; Félix, V.; Smith, M. D.; Beer, P. D. J. Am. Chem. Soc.* ***2019****, 141, 4119-4129.*

[91] *Verkade, J. G. Coord. Chem. Rev.* ***1994****, 137, 233-295.*

[92] *Lensink, C.; Xi, S.-K.; Daniels, L. M.; Verkade, J. G. J. Am. Chem. Soc.* ***1989****, 111, 3478-3479. b) Laramay, M. A.; Verkade, J. G. J. Am. Chem. Soc.* ***1990****, 112, 9421-9422.*

[93] *Verkade, J. G.; Kisanga, P. B. Proazaphosphatranes: a synthesis methodology trip from their discovery to vitamin A. Tetrahedron* ***2003****, 59, 7819-7858. b) Thammavongsy, Z.; Khosrowabadi Kotyk, J. F.; Tsay, C.; Yang, J. Y. Inorg. Chem.* ***2015****, 54, 11505-11510. c) Thammavongsy, Z.; Kha, I. M.; Ziller, J. W.; Yang, J. Y. Dalton Trans.* ***2016****, 45, 9853-9859.*

[94] *Kisanga, P. B.; Verkade, J. G.; Schwesinger, R. pK_a Measurements of P(RNCH_2CH_3)$_3$N. J. Org. Chem.* ***2000****, 65, 5431-5432.*

Proazaphosphatrane **12** and its conjugated acid **12-H**$^+$ are shown in Figure 2.1.2. We attempted to synthesize haloazaphosphatranes **12-Br**$^+$ and **12-I**$^+$ firstly; however, it turned out that bromoazaphosphatranes and iodoazaphosphatranes are not stable enough even under argon, **12-H**$^+$ was always isolated instead of the expected products **12-X**$^+$. We assumed that perhaps it was due to the substituents group of NR in proazaphosphatrane, so azaphosphatranes bearing different NR substituents were considered to explore the halogenation, but we still had the same results (the **12-H**$^+$·**X**$^-$ was isolated). Herein, we focus on the synthesis and anion binding properties of the five chloroazaphosphatranes **12-Cl**$^+$·**Y**$^-$ (**Y** means different anions) bearing various substituents on the nitrogen atoms. NMR titrations led to the determination of the binding constants in the range of 50 M^{-1}, comparable with other "classic" monodentate motifs such as iodoperfluorobenzene or iodoimidazolium.[95]

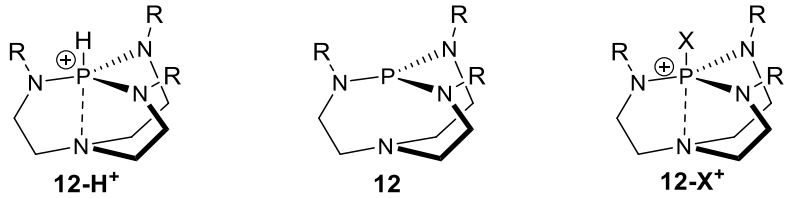

Figure 2.1.2 General structure of proazaphosphatrane (**12**), azaphosphatrane (**12-X**$^+$) and haloazaphosphatrane (**12-X**$^+$, with X = F, Cl, Br or I). Counterions are omitted for clarity.

[95] *Sarwar, M. G.; Dragisić, B.; Dimitrijević, E.; Taylor, M. S. Chem. Eur. J. 2013, 19, 2050-2058. b) Cametti, M.; Raatikainen, K.; Metrangolo, P.; Pilati, T.; Terraneoa, G.; Resnati, G. Org. Biomol. Chem. 2012, 10, 1329-1333.*

2.2 Results and discussion

2.2.1 Synthesis of [HP(RNCH$_2$CH$_2$)$_3$N][PF$_6$] (12-H$^+$·Cl$^-$)

Taking advantage of the versatility of their synthesis, the three known azaphosphatranes **(12b-d-H$^+$·Cl$^-$** and the new one **12e-H$^+$·Cl$^-$**, were synthesized in two steps (Figure 2.2.1), while **12a-H$^+$·Cl$^-$** was available from Sigma-Aldrich. **12-H$^+$·Cl$^-$** salts were characterized by ^{1}H, ^{13}C and ^{31}P NMR. In ^{31}P NMR, characteristic signal of **12a-H$^+$·Cl$^-$** (known product) shows at -10.56 ppm, signals of **12b-H$^+$·Cl$^-$**, **12c-H$^+$·Cl**, **12d-H$^+$·Cl$^-$**, and **12e-H$^+$·Cl$^-$** display at -7.91 ppm, -11.89 ppm, -12.68 ppm, and -11.74 ppm, respectively. We see that **12a-e-H$^+$·Cl$^-$** sharing the same part [P(NCH$_2$CH$_2$N)$_3$], but ^{31}P NMR showed some changed chemical shifts, which to some extent are consistent with their electron-rich substituents.

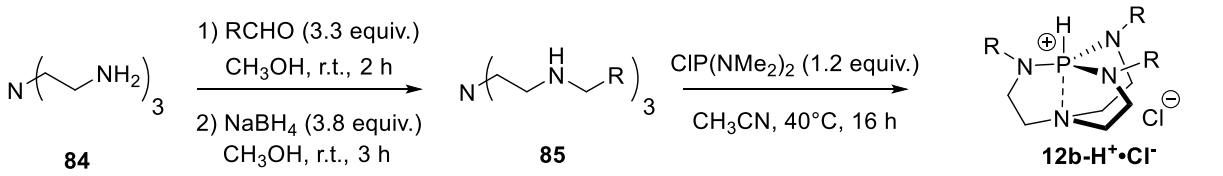

12a R=Me[a]
12b R=^{i}Bu (*84%*)
12c R=Bn (*56%*)
12d R=*p*-OMe-Bn (*85%*)
12e R=*p*-CF$_3$-Bn (*59%*)

12a-H$^+$•Cl$^-$ R=Me[a]
12b-H$^+$•Cl$^-$ R=^{i}Bu (*77%*)
12c-H$^+$•Cl$^-$ R=Bn (*81%*)
12d-H$^+$•Cl$^-$ R=*p*-OMe-Bn (*83%*)
12e-H$^+$•Cl$^-$ R=*p*-CF$_3$-Bn (*90%*)

Figure 2.2.1 Synthesis of **12-H$^+$·Cl$^-$** with different NR substituents, [a] commercially available.

2.2.2 Synthesis of [ClP(RNCH$_2$CH$_2$)$_3$N][Cl] (12-Cl$^+$·Cl$^-$)

The corresponding proazaphosphatranes **12a-e** were obtained by deprotonation of the azaphosphatranes by *t*-BuOK in CH_2Cl_2. The two previously reported chloroazaphosphatranes **12a-Cl$^+$·Cl$^-$** and **12b-Cl$^+$·Cl$^-$** and the three new ones **12c-Cl$^+$·Cl$^-$**, **12d-Cl$^+$·Cl$^-$** and **12e-Cl$^+$·Cl$^-$**, were obtained in good yields after the reaction of corresponding proazaphosphatranes with hexachloroethane (C_2Cl_6) for two hours at room temperature (Figure 2.2.2).[96]

[96] *Liu, X.-D.; Verkade, J. G. Inorg. Chem.* ***1998****, 37, 5189-5197. b) Matthews, A. D.; Prasad, S.; Schley, N. D.; Donald, K. J.; Johnson, M. W. Inorg. Chem.* ***2019****, 58, 15912-15992. c) Johnstone, T. C.; Briceno-Strocchia, A. I.; Stephan, D. W. Inorg. Chem.,* ***2018****, 57, 15299-15304.*

Characterizations by ^{31}P NMR of each proazaphosphatrane give resonance at δ =120.39 ppm (**12a**), δ = 130.29 ppm (**12b**), δ = 127.33 ppm (**12c**), δ = 126.80 ppm (**12d**), δ = 127.84 ppm (**12e**), which are highly down-fielded, compared to the **12a-e-H$^+$·Cl$^-$**. The chloroazaphosphatranes exhibit ^{31}P NMR signals at δ = -26.02 ppm (**12a-Cl$^+$·Cl$^-$**), δ = -13.81 ppm (**12b-Cl$^+$·Cl$^-$**), δ = -23.44 ppm (**12c-Cl$^+$·Cl$^-$**), δ = -23.38 ppm (**12d-Cl$^+$·Cl$^-$**), δ = -23.82 ppm (**12e-Cl$^+$·Cl$^-$**)$^-$, which are up-fielded, compared to the **12a-e-H$^+$·Cl$^-$**. This distinctness might be explained by the length of P-N_{axis} (central nitrogen atom). According to the previous studies, the distance of P-N_{axis} for proazaphosphatrane is 3.2 Å approximately (the distance of proazaphosphatranes bearing different substituents differs), which is only slightly below the sum of the van der Waals radius of 3.35 Å, while for azaphosphatrane, its bond length is around 2.0 Å approximately (the distance of azaphosphatranes baring different substituents differ).[97] It means proazaphosphatrane is less torsional than their conjugated acids azaphosphatrane, and it has high reactivity.

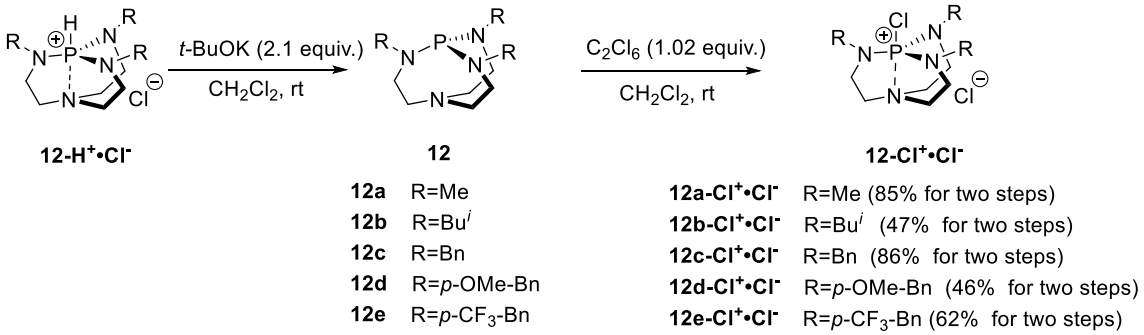

Figure 2.2.2 Synthesis of **12-Cl$^+$·Cl$^-$** with different NR substituents.

2.2.3 Synthesis of [ClP(RNCH$_2$CH$_2$)$_3$N][PF$_6$] (12-Cl$^+$·PF$_6^-$)

In order to remove the Lewis basic chloride anion of **12-Cl$^+$·Cl$^-$**, we managed to exchange the anions part from Cl^- to PF_6^- to give **12-Cl$^+$·PF$_6^-$** with a good yield (Figure 2.2.3). The subsequent anion exchanges revealed unsuccessful in the presence of water, but the use of acetonitrile as solvent allowed for the anion metathesis of the chloride anion by the PF_6^- one. ^{31}P NMR spectra revealed resonances at -21.34 ppm (**12a-Cl$^+$·PF$_6^-$**), -4.32 ppm (**12b-Cl$^+$·PF$_6^-$**), -20.07 ppm (**12c-Cl$^+$·PF$_6^-$**), -19.04 ppm (**12d-Cl$^+$·PF$_6^-$**), -22.65 ppm (**12e-Cl$^+$·PF$_6^-$**) were found, which have a little differences, compared to the **12a-e-Cl$^+$·Cl$^-$**. It is interesting that keeping the cation

[97] *a) Windus, T. L.; Schmidt, M. W.; Gordon, M. S. J. Am. Chem. Soc. 1994, 116, 11449−11455; b) M.A.H. Laramay and J.G. Verkade, J. Am. Chem. Soc., 112 (1990) 9421.*

part same, just changing the anions part, could have effect on the electron-rich region of NR substituents.

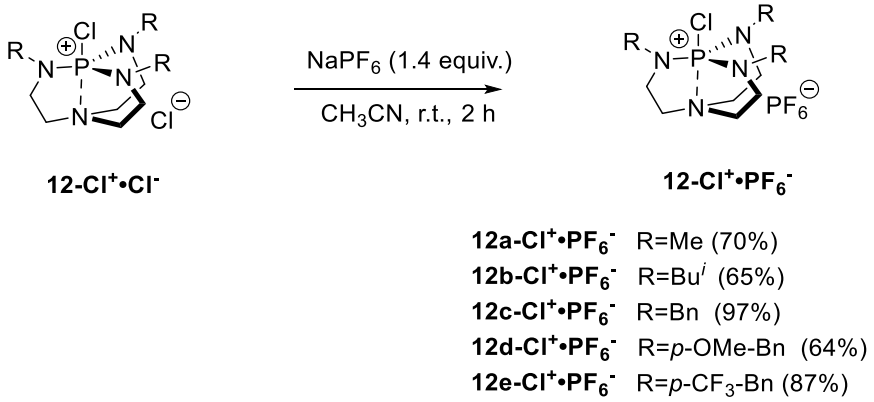

Figure 2.2.3 Synthesis of **12-Cl^{+}·PF$_6^{-}$** with different NR substituents.

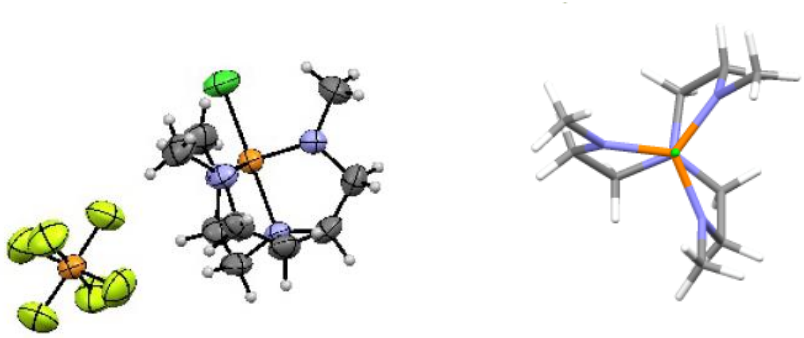

Figure 2.2.4 Crystallographically-derived molecular structure and helical arrangement of **12a-Cl^{+}·PF$_6^{-}$.**

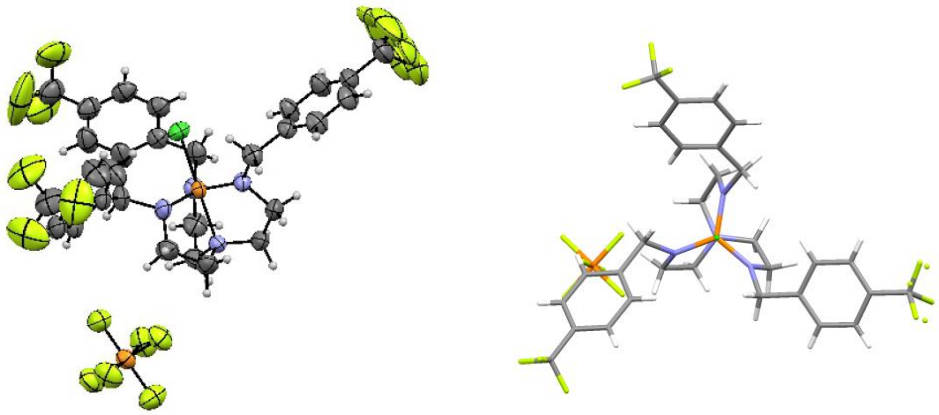

Figure 2.2.5 Crystallographically-derived molecular structure and helical arrangement of **12e-Cl^{+}·PF$_6^{-}$.**

In order to analyze the structure of **12-Cl^{+}·PF$_6^{-}$** further, crystals of **12a-Cl^{+}·PF$_6^{-}$** and **12e-Cl^{+}·PF$_6^{-}$** suitable for X-ray diffraction analysis were obtained by crystallization in a mixture

Et_2O/CH_3CN, and the resulting structures (Figure 2.2.4 and Figure 2.2.5) were compared with those reported of **12a-Cl$^+$·ClBPh$_3^-$** and **12b-Cl$^+$·PF$_6^-$** (Table 2.2.1).[98]

The structures of **12a-Cl$^+$·PF$_6^-$** and **12a-Cl$^+$·ClBPh$_3^-$** salts are almost similar, showing that these non-coordinating anions have little influence on the structure of the chloroazaphosphatrane cations in the solid state. The phosphorus atom adopts pseudo-trigonal pyramidal geometry and the apical nitrogen presents a pseudo-pyramidal one. Whereas the P-Cl bond lengths are similar in all these three structures (2.1 Å), the P-N_{axial} distances differ more strongly with 1.939 Å and 1.960 Å in **12a-Cl$^+$·PF$_6^-$** and **12e-Cl$^+$·PF$_6^-$**, respectively, and 2.128 Å in **12b-Cl$^+$·PF$_6^-$**. Moreover, the azatrane structures adopt a helical arrangement in **12a-Cl$^+$·PF$_6^-$** and **12e-Cl$^+$·PF$_6^-$**, while the five membered-rings in the azaphosphatrane **12b-Cl$^+$·PF$_6^-$** present eclipsed conformations (see dihedral angle C-N_{ax}-P-N_{eq} in Table 2.2.1 and Figures 2.2.4 and Figure 2.2.5). The steric hindrance of the isobutyl groups might account for the more elongated transannular distance and the specific conformation of the atrane structure in **12b-Cl$^+$·PF$_6^-$**. These structural features are also probably retained in solution, which could account for the peculiar ^{31}P NMR chemical shift observed for **12b-Cl$^+$·PF$_6^-$** (δ = -4.36 ppm).

	d_{PCl}/Å	d_{PNax}/Å	d_{PNeq}/Å	$\Sigma_{Neq\text{-}P\text{-}Neq}$ (deg)	$\Sigma_{C\text{-}Nax\text{-}C}$ (deg)	Dihedral angle C-N_{ax}-P-N_{eq} (deg)
12a-Cl$^+$[a]	2.101	1.928	1.663	359.1	336.0	29.4
12a-Cl$^+$[b]	2.123	1.939	1.656	358.8	339.3	35.6
12b-Cl$^+$[a]	2.109	2.128	1.643	354.2	340.9	1.1
12e-Cl$^+$[a]	2.112	1.960	1.662	358.3	339.6	32.8

Table 2.2.1. Selected crystallographic parameters for **12a-Cl$^+$**, **12b-Cl$^+$** and **12e-Cl$^+$** cations.

[a] PF_6^- as counterion; [b] $ClBPh_3^-$ as counterion obtained from literature.

2.2.4 Synthesis of [HP(*p*-CH_3O-$BnNCH_2CH_2)_3N$][PF_6] (12d-H$^+$·PF_6^-)

We also explored the anion exchange between **12d-H$^+$·Cl$^-$** and **12d-H$^+$·PF$_6^-$**, in the presence of H_2O and $NaPF_6$. The **12d-H$^+$·PF$_6^-$** salt was obtained with a very good yield (95%, Figure 2.2.6). As mentioned before, anion exchange between **12d-Cl$^+$·Cl$^-$** and **12d-Cl$^+$·PF$_6^-$** resulted in the different chemical shifts in ^{31}P NMR, but in this situation, we observed that the ^{31}P NMR resonance appears at -11.82 ppm (**12d-H$^+$·PF$_6^-$**), which is close to the chemical shift of **12d-H$^+$·Cl$^-$** (-12.68 ppm). It demonstrated that the NMR chemical shift of the cationic part **12d-H$^+$** is weakly sensitive to the nature of the counter ion.

[98] *a) Matthews, A. D.; Prasad, S.; Schley, N. D.; Donald, K. J.; Johnson, M. W. Inorg. Chem.* ***2019****, 58, 15912-15992. b) Johnstone, T. C.; Briceno-Strocchia, A. I.; Stephan, D. W. Inorg. Chem.,* ***2018****, 57, 15299-15304.*

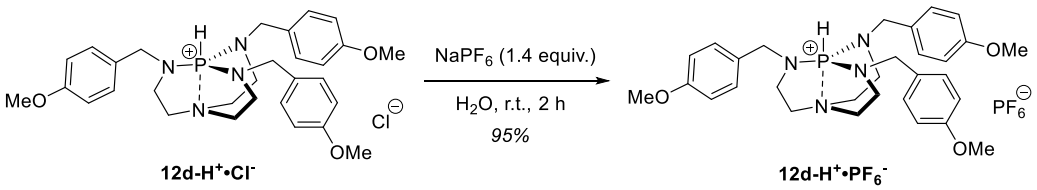

Figure 2.2.6 Synthesis of **12d-H$^+$·PF$_6^-$**

2.2.5 Synthesis of [ClP(*p*-CH$_3$O-BnNCH$_2$CH$_2$)$_3$N][BAr^F] (12d-Cl$^+$·BAr^{F-})

Anion metathesis of the chloride anion with BAr^{F-} was performed (Figure 2.2.7), leading to ^{31}P NMR spectrum resonances at δ = -17.43 ppm, δ = -23.38 ppm (**12d-Cl$^+$·Cl$^-$**) and -19.04 ppm (**12d-Cl$^+$·PF$_6^-$**) were described before, showing that **12-Cl$^+$·BAr^{F-}** might me the most stable ionic compound among them. Then, because of the potential interest of the bromo- and iodo- analogues, we attempted to isolate the **12-Br$^+$·BAr^{F-}** or **12-I$^+$·BAr^{F-}** compounds using the same sequence of reactions. However, we failed in these experiments, probably because of the higher sensitivity of these compounds event to the weak nucleophiles such as water or alcohols.

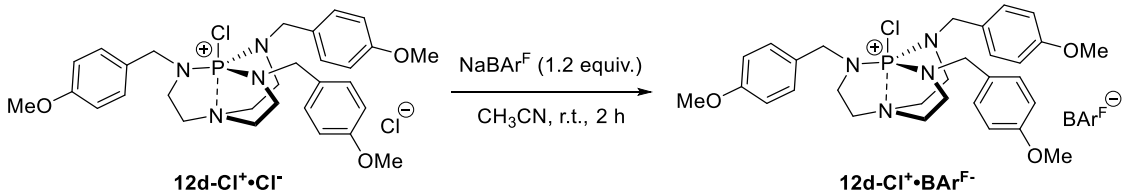

Figure 2.2.7 Synthesis of **12d-Cl$^+$·PF$_6^-$**

Thus, the desired compounds **12a-e-Cl$^+$·PF$_6^-$**, **12d-H$^+$·PF$_6^-$**and **12d-Cl$^+$·BAr^{F-}** were obtained in five steps from the commercial tris(2-aminoethyl)amine compound and the corresponding aldehydes in 20 to 38% yields.

2.2.6 Anions binding properties of haloazaphosphatranes [ClP(RNCH$_2$CH$_2$)$_3$N][PF$_6$] (12-Cl$^+$· PF$_6^-$)

The anion binding properties of the chloroazaphosphatranes were studied by ^{1}H NMR titration experiments at 298K, general reaction for titration experiments is shown in Figure 2.2.8. In these anion binding experiments, Cl$^-$, Br$^-$, I$^-$, AcO$^-$ and CN$^-$ were considered as anion guests (prepared as 50 mM solution in acetonitrile), they are titrated by host chloroazaphosphatranes

12-Cl^{+}·PF$_6^-$ (prepared as 5 mM solution in acetonitrile). The chloroazaphosphatranes revealed stable under the conditions that used during the titration experiments and no decomposition was observed. Figure 2.2.9b shows the typical changes that observed in the ^{1}H NMR spectrum of **12a-Cl^{+}·PF$_6^-$** upon progressive addition of tetrabutylammonium (TBA) chloride salt, the protons from tren (marked by red square and blue circle) part is getting down-fielded when more and more TBA solution was added. The chemical induced shifts Δδ of host's protons at 3.18 ppm were measured and plotted as a function of the [G]/[H] ratio, then curves fitted with the BindFit program (Figure 2.2.9a), the combination of TBACl with **12a-Cl^{+}·PF$_6^-$** reached to the maximum Δδ value, while TBAOAc binding with host gave a lowest Δδ among the five guests.

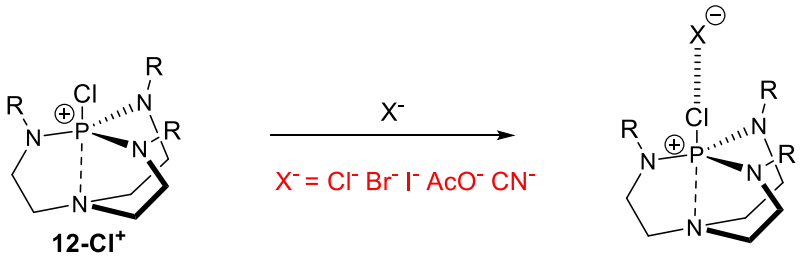

Figure 2.2.8 General reaction for titration experiments.

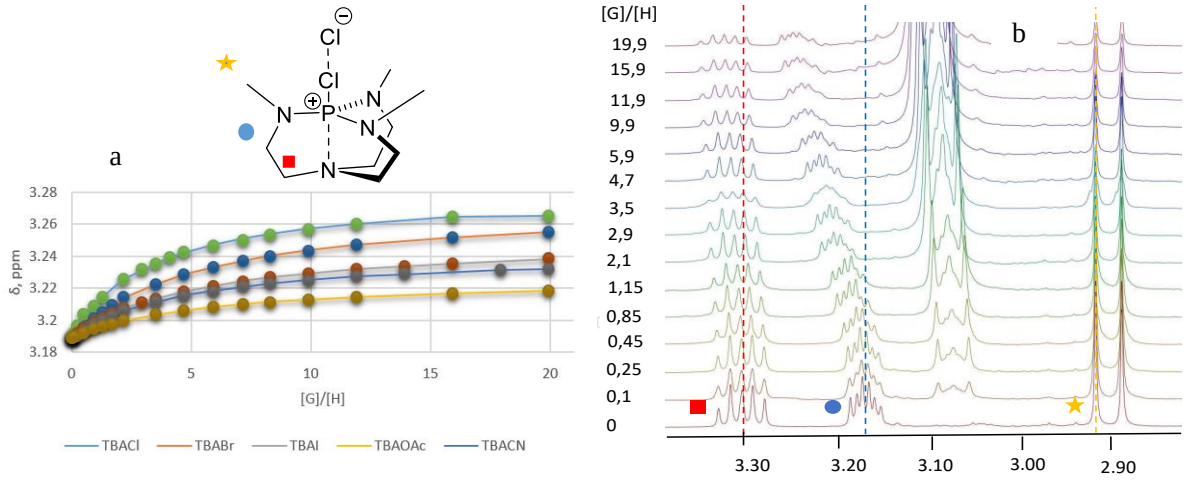

Figure 2.2.9 a) Titration curves of host **12a-Cl^{+}.PF$_6^-$** with TBAX salts and acetate salts in CD_3CN, the chemical induced shifts Δδ of host's protons at 3.18 ppm were measured and plotted as a function of the [G]/[H] ratio; b) Example of the ^{1}H NMR monitoring of the titration of host **12a-Cl^{+}·PF$_6^-$** (5mM) with Cl$^-$ (as a 50 mM solution of TBACl salt) in CD_3CN.

Following the same titration method, we obtained other curves for the combination of **12b-e-Cl^{+}·PF$_6^-$** with Cl$^-$, Br$^-$, I$^-$, AcO$^-$ and CN$^-$, which are shown in Figure 2.2.10. For each calculated curve, Cl$^-$ showed the best affinity among the five guests. Besides, compounds **12a-e-Cl^{+}·PF$_6^-$**

display only one set of signals during the titration experiments, showing that the XB process is in fast exchange on the NMR time scale. The titration experiment of CN^- and **12b-Cl$^+$·PF$_6^-$** failed as the formation of a precipitate was observed during the titration experiment.

For all chloroazaphosphatranes, the signals of the protons of the bridging methylenes clearly exhibit downfield shifts, whereas those of the R groups grafted on the equatorial nitrogen atoms displayed smaller NMR shifts. It suggests that these substituents are not directly involved in the recognition process (marked by yellow pentagon in Figure 2.2.9 for host **12a-Cl$^+$·PF$_6^-$**), but more probably only affect the electronic properties of the chloroazaphosphatranes. Thus, the interaction between anion and σ-hole might impact the trans-annular bond length, inducing changes in the chemical shifts of the methylene protons.

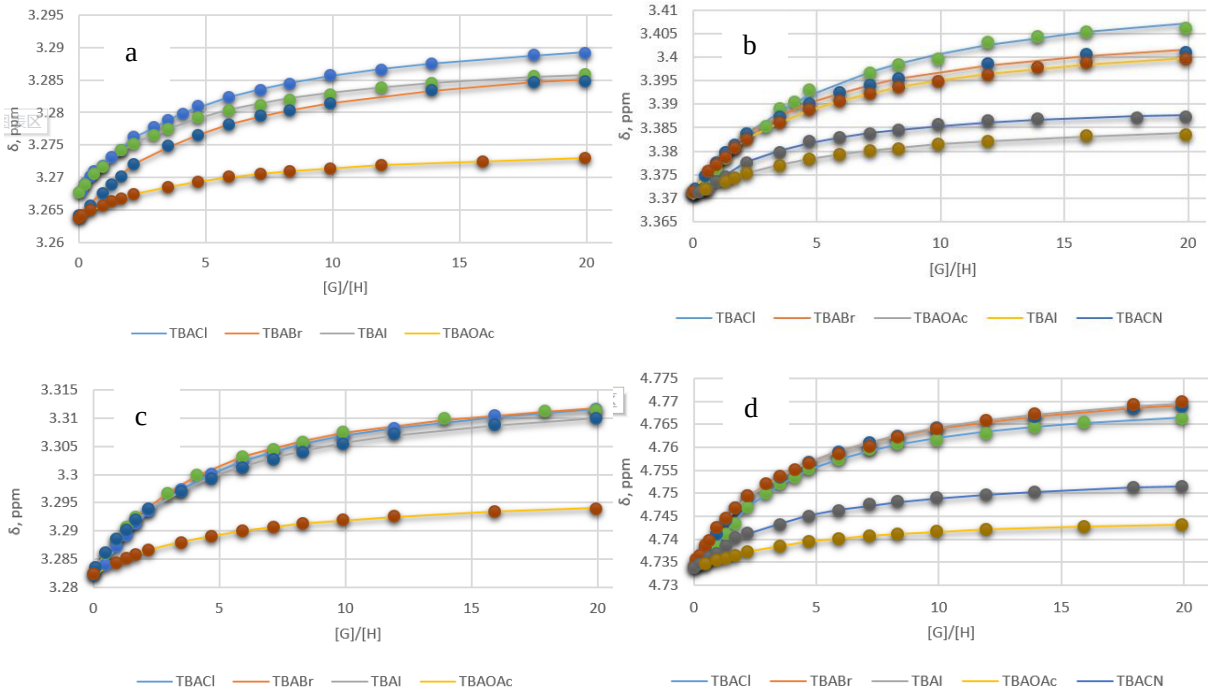

Figure 2.2.10 a) Titration curves of host **12b-Cl$^+$·PF$_6^-$** (Δδ=3.26 ppm), b) **12c-Cl$^+$·PF$_6^-$** (Δδ=3.37 ppm), c) **12d-Cl$^+$·PF$_6^-$** (Δδ=3.28 ppm), d) **12e-Cl$^+$·PF$_6^-$** (Δδ=4.73 ppm) with TBAX salts in CD_3CN.

The interaction between the **12d-Cl$^+$·PF$_6^-$** receptor and the iodide anion was also monitored by ^{31}P NMR spectrum, a change in the chemical shift of around 0.3 ppm was observed (Figure 2.2.11a). This is consistent with a close proximity of the phosphorus atom to the binding site. Furthermore, this experiment also supports that no direct reactivity between the nucleophilic anion and the electrophilic phosphorus atom occurs, since such reaction should lead to higher changes in the chemical shift. This lack of reactivity at the phosphorus is in agreement with the

unique stability of the azaphosphatrane structure described by J. G. Verkade.[99] Furthermore, to highlight the crucial role of the Lewis basicity of the anion and the negligible role played by the TBA cation, a titration experiment has been carried out with the **TBA^{+}·PF$_6^{-}$** salt (Figure 2.2.11b). No change in the ^{1}H NMR chemical shifts of the chloroazaphosphatrane **12d-Cl^{+}·PF$_6^{-}$** was observed during this experiment, evidencing the crucial role of halogen bonding in the recognition of anions by this class of receptor. Red dashed lines show that no chemical shift occurs for the benzylic and CH_2 protons, this evidences that no interaction takes place between the anion and the azaphosphatrane.

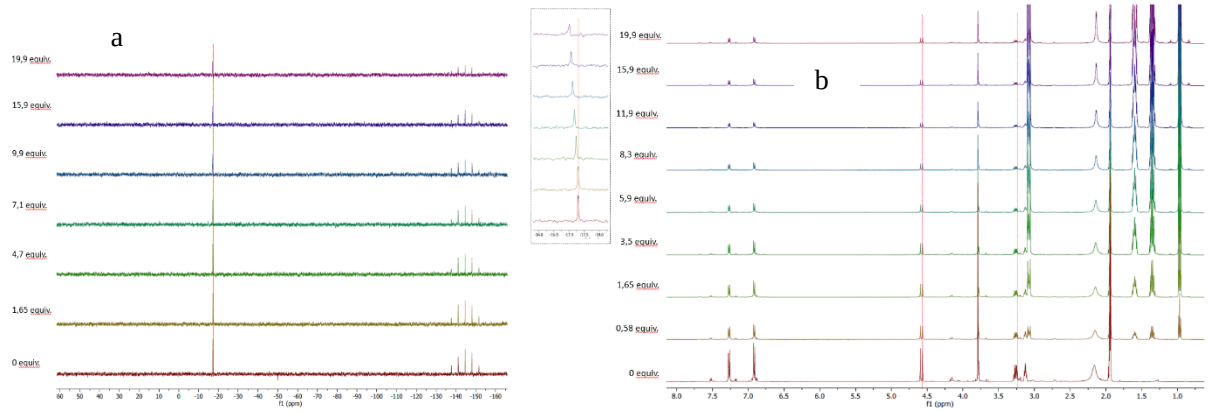

Figure 2.2.11 a) ^{31}P NMR spectra of **12d-Cl^{+}·PF$_6^{-}$** (5 mM) for several additions of a concentrated solution n-Bu$_4$N^{+} I^{-} (50 mM); b) ^{1}H NMR spectra of **12d-Cl^{+}·PF$_6^{-}$** (5 mM) for several additions of a concentrated solution n-Bu$_4$N^{+} PF$_6^{-}$ (5 mM).

Modelling of theses curves with the Bindfit program allowed for the determination of the binding constants, the 1:1 anion: receptor association provide the best fit, and give the binding constants K_a that reported in Table 2.2.2.[100] First of all, we note that the binding constants values are modest, from 20 to 50 M^{-1}, but importantly, they are in the same order of magnitude as those obtained with other "classical" monodentate XB receptors like iodoperfluorobenzene (C_6F_5I) or iodoimidazolium.[101]

[99] *a) Verkade, J. G. Coord. Chem. Rev.* ***1994****, 137, 233-295. b) Verkade, J. G.; Kisanga, P. B. Proazaphosphatranes: a synthesis methodology trip from their discovery to vitamin A. Tetrahedron* ***2003****, 59, 7819-7858.*

[100] *Hibbert, D. B.; Thordarson, P. Chem. Commun.* ***2016****, 52, 12792-12805; b) Thordarson, P. Chem. Soc. Rev.* ***2011****, 40, 1305-1323.*

[101] *Sarwar, M. G.; Dragisić, B.; Dimitrijević, E.; Taylor, M. S. Chem. Eur. J.* ***2013****, 19, 2050-2058. b) Cametti, M.; Raatikainen, K.; Metrangolo, P.; Pilati, T.; Terraneoa, G.; Resnati, G. Org. Biomol. Chem.* ***2012****, 10, 1329-1333.*

Entry	Receptor	Cl^-	Br^-	I^-	AcO^-	CN^-	p*Ka*
1	**12a-Cl^+.PF_6^-**	32 ± 0.5	26 ± 0.1	18 ± 0.1	22 ± 0.3	27 ± 0.4	32.90[102]
2	**12b-Cl^+.PF_6^-**	22 ± 0.2	21 ± 0.2	29 ± 0.3	24 ± 0.2	---[c]	33.53[29]
3	**12c-Cl^+.PF_6^-**	51 ± 0.4	26 ± 0.4	20 ± 0.3	20 ± 0.3	42 ± 1.2	31.80
4	**12d-Cl^+.PF_6^-**	43± 0.4[b]	31 ± 0.3	26 ± 0.3	23 ± 0.2	35 ± 1.3	32.14[103]
5	**12e-Cl^+.PF_6^-**	55 ± 0.7	39 ± 0.4	33 ± 0.4	26 ± 0.1	39 ± 0.6	29.80
6	**12d-Cl^+.BAr^F**	45 ± 1.3	---	---	---	---	---

Table 2.2.2 Binding constants *K*a (M^{-1}) for the 1:1 complexes formed between **(12a-e)-Cl^+** and anion guests in CD_3CN.[a]

[a] Ka were determined by fitting ^1H NMR titration curves (CD_3CN, 500 MHz, 298 K) of the methylene protons of the chloroazaphosphatranes with Bindfit program; estimated error 10%. [b] *K*a = 45 M^{-1} when BAr^{F-} was used as counterion instead of PF_6^-; [c] the formation of a precipitate was observed during the titration experiment.

This is all the more remarkable that these last two motifs (**12d-e-Cl^+·PF_6^-**) benefit from the high polarizability of the iodine atom to create an important electrophilic σ-hole whereas the low polarizability of the chlorine atom in the chloroazaphosphatranes is less suitable to induce halogen bonding. Here, although the chlorine atom is used as XB donor, association constants comparable with iodine based monodentate receptors are reached, underlining the great potentiality of this motif to build multidentate XB donors or to be combined with other interactions to design even more efficient receptors. Moreover, when BAr^{F-} was used as counterion instead of PF_6^-, no significant change in the value of the binding constant was observed: K_a of 43 M^{-1} and 45 M^{-1} were obtained for **12d-Cl^+·PF_6^-** and **12d-Cl^+·BAr^{F-},** respectively, with chloride as guest anion (Table 2.2.2, entry 4 and 6)**.**

Another feature that concerns the affinities of the five chloroazaphosphatranes for the chloride anion, is higher than for the bromide and iodide, as expected from the stronger basicity of the former. For instance, binding constants of 55, 39, and 33 M^{-1} were respectively obtained from Cl^-, Br^- and I^- anions when **12e-Cl^+·PF_6^-** was used as the halogen bond donor (entry 5, Table 2.2.2). We then examined if the binding constant could be related to the basicity of the corresponding Verkade's superbase. The pK_a of **12a**, **12b** and **12d** are known from the literature

[102] *Kisanga, P. B.; Verkade, J. G.; Schwesinger, R.* J. Org. Chem. *2000*, 65, *5431-5432.*

[103] *Dimitrov Raytchev, P.; Martinez, A.; Gornitzka, H.; Dutasta, J.-P.*. J. Am. Chem. Soc. *2011*, 133, *2157-2159.*

and those of **12c** and **12e** were estimated from competition experiments using our previously described procedure (Table 2.2.2; Figure 2.2.12; eq. 1).[104] It appears that the affinity of the chloroazaphosphatranes for the chloride anion decreases with the basicity of the pro-azaphosphatrane parents. This is consistent with the ability of the substituents to stabilize the positive charge on the phosphorus atom: the most basic proazaphosphatrane corresponds to the most stable azaphosphatrane, and thus probably to a less electrophilic σ-hole in the corresponding chloroazaphosphatrane.

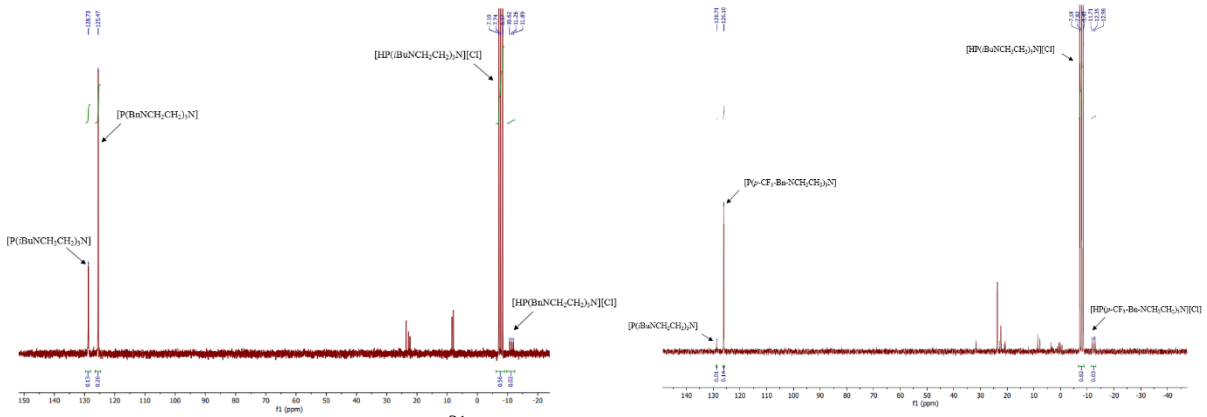

Figure 2.2.12 pK_a measure through ^{31}P NMR spectrum of the equilibrium between (a) **12c-H$^+$·Cl$^-$** [HP(BnNCH$_2$CH$_2$)$_3$N][Cl] and **12b** [P(iBuNCH$_2$CH$_2$)$_3$N]; (b) **12e-H$^+$·Cl$^-$** [HP(p-CF$_3$-Bn-NCH$_2$CH$_2$)$_3$N][Cl] and **12b** [P(iBuNCH$_2$CH$_2$)$_3$N].

$$K_a^{\mathbf{12\text{-}H^+}} = 10^{-33.53}\,\frac{[\mathbf{12}][\mathbf{12b\text{-}D^+}]}{[\mathbf{12\text{-}D^+}][\mathbf{12}]} \qquad (1)$$

For other anions, the binding constants are too close to allow for relevant comparisons. Nevertheless, the receptor **12e-Cl$^+$·PF$_6^-$**, associated to the less basic superbase **12e**, displays the better binding constant whatever the anion used, in agreement with the trend observed for chloride anion. HSO_4^- and $H_2PO_4^-$ were also tested as guests (TBA salts): whereas the former gives a low binding constant of 16 M^{-1} with **12d-Cl$^+$·PF$_6^-$** as XB donor, a solid precipitate was formed during the titration with the latter one, suggesting the formation of insoluble aggregates between chloroazaphosphatranes and dihydrogen phosphate anions.

[104] *Dimitrov Raytchev, P.; Martinez, A.; Gornitzka, H.; Dutasta, J.-P. J. Am. Chem. Soc.* ***2011****, 133, 2157-2159.*

2.2.7 Comparison of chloroazaphosphatranes with azaphosphatranes and fluroazaphosphatranes

Characterizing the real nature of non-covalent interactions is a thorny question, especially for XB donors. Titration experiments were also carried out by using the **12d-H$^+$·PF$_6^-$** and **12d-F$^+$·PF$_6^-$** salts as receptors in order to examine the role played by the XB interaction in the recognition process. When **12d-H$^+$·PF$_6^-$** was used as receptor, no change in the ^{1}H NMR spectrum was observed upon addition of tetrabutylammonium chloride (TBACl) salt (Figure 2.2.13). In particular, the chemical shift of the protons of the methylene bridge and of the P-H unit remain unchanged, showing that no hydrogen bond occurs and supporting that no interaction takes place between the **12d-H$^+$** cation and the chloride anion.

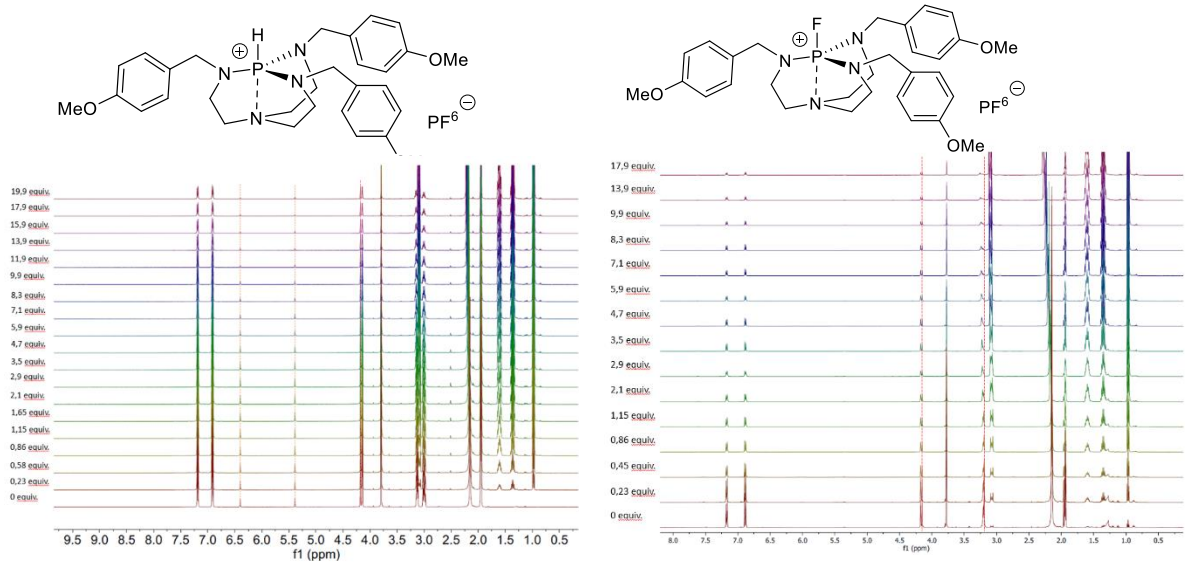

Figure 2.2.13 ^{1}H NMR spectra of **12d-H$^+$·PF$_6^-$** (5 mM) and **12d-F$^+$·PF$_6^-$** (5 mM) for several additions of a concentrated solution *n*-Bu$_4$N$^+$ Cl$^-$ (50 mM).

During the ^{1}H NMR titration experiment of **12d-F$^+$·PF$_6^-$**, the N-CH$_2$-Ar signal shows no modification and the methylene bridges resonances evidence only extremely small changes preventing establishing and modelling any titration curve (Figure 2.2.13). This is in sharp contrast with the notable changes of the chemical shifts of these protons when **12d-Cl$^+$·PF$_6^-$** is used as receptor, ruling out non-directional electrostatic interactions, which should have been stronger in the fluorinated analogue, as the main contribution to the observed association. Moreover, this also supports that no direct reaction between the electrophilic phosphorus atom and the nucleophilic anion occurs, as suggested by the ^{31}P NMR study. Indeed, such reaction should be favored when the chlorine is replaced by a fluorine atom: the higher electron-

withdrawing properties of this latter probably increases the potential electrophilicity of the phosphorus atom. Thus, neither the **12d-H$^+$·PF$_6^-$** nor the **12d-F$^+$·PF$_6^-$** salts are able to clearly interact with the chloride anion. This indicates that the XB donors is crucial in this recognition process.

2.2.8 Comparison of chloroazaphosphatranes with other XB donors

As for other Lewis acid-base interactions, comparing the properties of XB donors in solution is a daunting challenge as the strength of halogen bonding depends on the nature of the Lewis base and the conditions that used for titration (method, solvent, concentration).[105] Guttmann and Beckett have reported the use of triethylphosphine oxide (TEPO) as probe to measure the Lewis acidity by ^{31}P NMR spectrum.[106] Recently, Franz described a unified and easily reproducible procedure to quantify the halogen bonding abilities of different neutral and cationic halogen bond donor motifs, by comparing the ^{31}P NMR shifts of a solution of TEPO in CD_2Cl_2, in the absence and presence of the XB donors.[107]

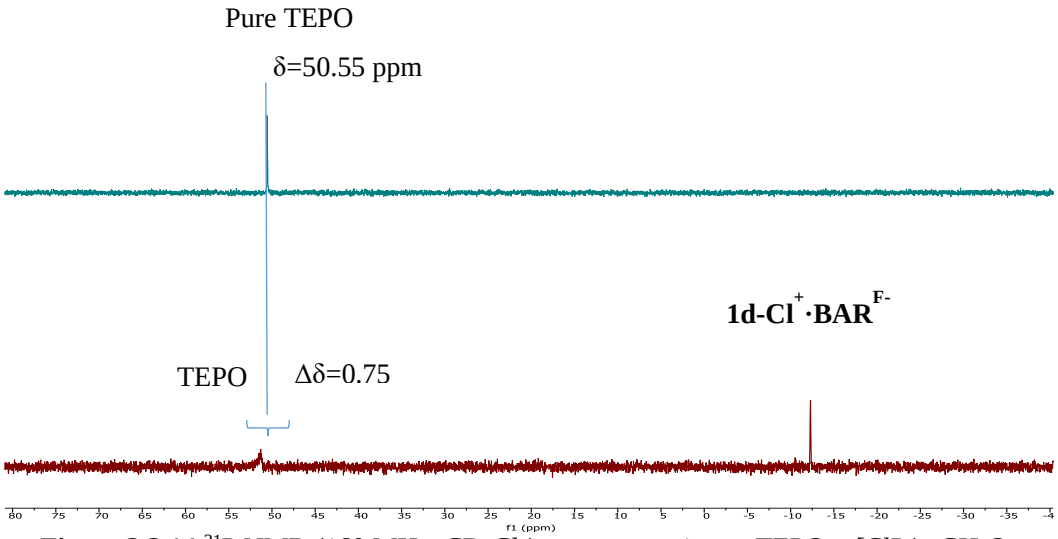

Figure 2.2.14 ^{31}P NMR (160 MHz, CD_2Cl_2) spectrum: mixture TEPO + [ClP(*p*-CH_3O-BnNCH_2CH_2)$_3$N][BAr^F]

[105] *a) Laurence, C.; Graton, J.; Berthelot, M.; El Ghomari, M. J. Chem. Eur. J.* ***2011****, 17, 10431-10444. b) Ostras', A. S.; Ivanov, D. M.;. Novikov, A. S.; Tolstoy P. M. Molecules* ***2020****, 25, 1406-1423.*

[106] *a) Mayer, U.; Gutmann, V.; Gerger, W. Monatsh. Chem.* ***1975****, 106, 1235–1257. b) Beckett, M. A.; Strickland, G.C.; Holland, J.R.; Varma, K.S. Polymer* ***1996****, 37, 4629–4631.*

[107] *Chang, Y.-P.; Tang, T.; Jagannathan, J. R.; Hirbawi, N.; Sun, S.; Brown, J.; Franz, A. K. Org. Lett.* ***2020****, 22, 6647-6652.*

With **12d-Cl^{+}·BAr^{F-}** a $\Delta\delta$ (^{31}P) of 0.75 ppm was measured (Figure 2.2.14),[108] although modest, this value is higher than the one reported for pentafluoroiodobenzene **86** (0.21 ppm) and comparable to those of iodoimidazole **87** (0.89 ppm) and chloroimidazolium **88** (1.21 ppm) (Figure 2.2.15a). This result gives insight into the relative strength of chloroazaphosphatranes compared to other XB donors to induce X-bonding with a Lewis base. To complement this result, a competition experiment was also carried out by mixing proazaphosphatrane **12d** and chloroimidazolium chloride **89** (Figure 2.2.15b). ^{31}P NMR show resonance at -22.04 ppm for P-Cl, this study of the reaction mixture revealed the transfer of the chlorine atom from the carbon atom of **89** to the phosphorus atom to afford **12d-Cl^{+}·Cl^{-}** along with the protonation product **12d-H^{+}·Cl^{-}**. This observation is in agreement with the slightly higher XB-donor potency of chloroimidazolium salts compared to chloroazaphosphatranes and the stronger reported basicity of phosphatranes compared to imidazolylidene N-heterocyclic carbenes (NHCs).

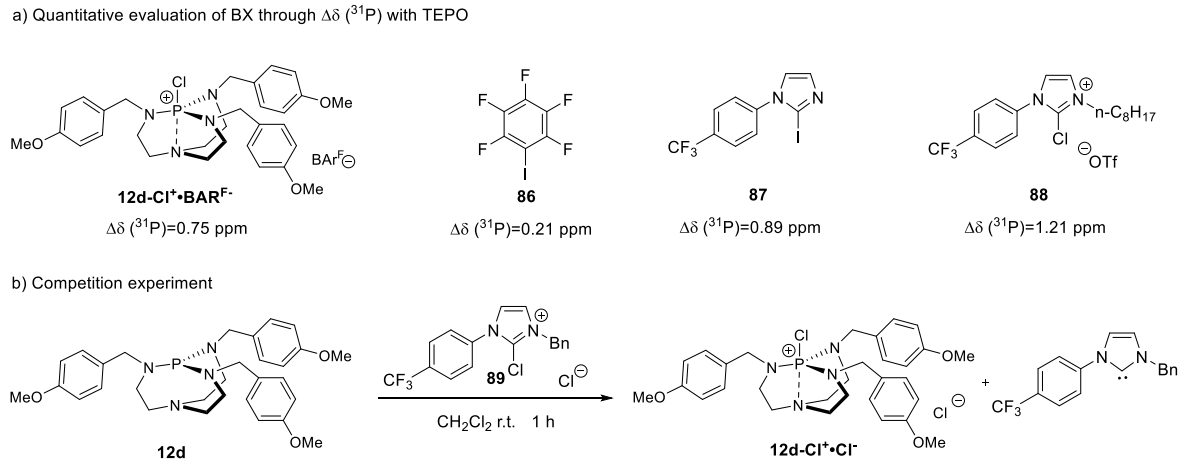

Figure 2.2.15 Comparing chloroazaphosphatranes with other XB donors.

2.2.9 Chloroazaphosphatranes as XB donors in catalysis

Since the first XBs in organocatalysis was reported in 2008 by Bolm,[109] XBs revealed efficient to catalyze various reactions like Diels-Alder reaction,[110] halogen abstraction,[111] or Michael

[108] *M. S. Taylor. Anion recognition based on halogen, chalcogen, pnictogen and tetrel bonding. Coord. Chem. Rev.* ***2020****, 413, 213270.*

[109] *Bruckmann, H. A.; Pena, M. A.; Bolm, C. Synlett*. ***2008****, 2008, 900−902.*

[110] *a) Haraguchi, R.; Hoshino, S.; Sakai, M.; Tanazawa, S.; Morita, Y.; Komatsu, T.; Fukuzawa, S. Chem. Commun.* ***2018****, 54, 10320−10323. b) Kaasik, M.; Metsala, A.; Kaabel, S.; Kriis, K.; Järving, I.; Kanger T. J. Org. Chem.* ***2019****, 84, 4294−4303; c) Jungbauer, S. H.; Walter, S. M.; Schindler, S.; Rout, L.; Kniep, F.; Huber, S. M. Chem. Commun. 2014, 50, 6281−6284. d) Takeda, Y.; Hisakuni, D.; Lin, C.-H.;Minakata, S. Org. Lett.* ***2015****, 17, 318−321.*

[111] *a) Benz, S.; Poblador-Bahamonde, A. I.; Low-Ders, N.; Matile, S. Angew. Chem. Int. Ed.* ***2018****, 57, 5408−5412. b) Jungbauer, S. H.; Huber, S. M.*

addition.[112] We therefore decide to evaluate the ability of chloroazaphosphatranes to act as catalyst using an aza Diels-Alder between the imine **90** and the Danishefsky diene a benchmark reaction. Imine **90** and diene **91** were mixed in the presence of 0.1 equiv. of chloroazaphosphatrane **12d-Cl^{+}·PF$_6^-$** in CH_2Cl_2 at room temperature (Figure 2.2.16). **92** was generated in yield of 46%, whereas no other product was obtained in the absence of chloroazaphosphatrane. Thus, chloroazaphosphatranes appear as a promising class of XB-donor catalysts.

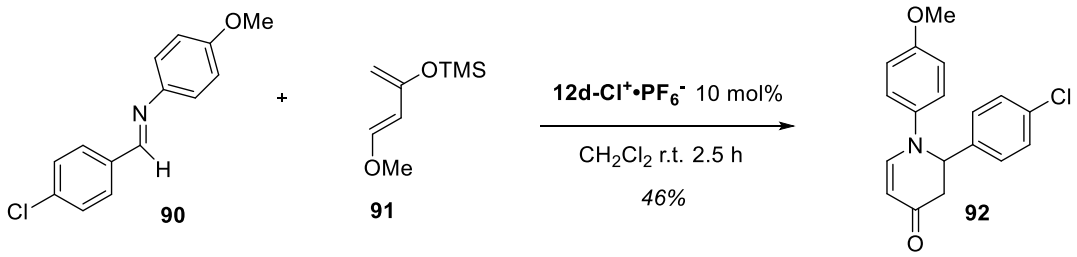

Figure 2.2.15 Chloroazaphosphatrane **12d-Cl^{+}·PF$_6^-$** as catalyst for an aza Diels-Alder reaction.

J. Am. Chem. Soc. ***2015****, 137, 12110−12120. c) Dreger, A.; Engelage, E.; Mallick, B.; Beer, P. D.; Huber, S. M. Chem. Commun.* ***2018****, 54, 4013−4016. d) Kniep, F.; Walter, S. M.; Herdtweck, E.; Huber, S. M. Chem. Eur. J.* ***2012****, 18, 1306−1310. e) Walter, S. M.; Kniep, F.; Herdtweck, E.; Huber, S. M. Angew. Chem., Int. Ed.* ***2011****, 50, 7187−7191. f) Kniep, F.; Rout, L.; Walter, S. M.; Bensch, H. K. V.; Jungbauer, S. H.; Herdtweck, E.; Huber, S. M. Chem. Commun.* ***2012****,* ***48****, 9299−9301.*

[112] *a) Gliese, J.-P.; Jungbauer, S. H.; Huber, S. M. Chem. Commun.* ***2017****, 53, 12052−12055. b) von der Heiden, D.; Detmar, E.; Kuchta, R.; Breugst, M. Synlett* ***2018****, 29, 1307−1313.*

2.3 Conclusion

In this work, we have reported the synthesis of five different chloroazaphosphatranes with PF_6^- as counterion. NMR titration experiments were performed showing that the chloroazaphosphatranes can bind anions with association constants from 20 to 50 M^{-1} whereas no interaction was detected with both the protonated counterpart azaphosphatranes and the fluroazaphosphatranes. The substituents on the equatorial nitrogen atoms probably do not interact directly with the anion, but modulate the electrophilicity of the σ-hole on the chlorine atom. These results highlight the crucial role of XB in the recognition of anions by chloroazaphosphatranes and make them a new class of relevant motifs for X-bonding with the following features: (i) the XB donor is not a halogen linked to an aromatic carbon, in contrast with most the classical motif reported today, (ii) the interaction with anion is comparable to that reached with iodoperfluorobenzene or iodo-imidazolium, although a chlorine atom is involved instead of a much more polarizable iodine atom, and (iii) the electronic properties of the R groups on the equatorial nitrogens can tune the XB properties of the chloroazaphosphatrane. Experiments are in progress in our laboratory in order to design anion receptors combining two or more chloroazaphosphatrane units or by associating them with other motifs for a more selective and efficient anion recognition.

Chapter 3: Enantiopure hemicryptophanes presenting unusual C_1 Conformations in solution: Reactivity Outcome.

Publication: Chunyang Li, Anne-Doriane Manick, Marion Jean, Muriel Albalat, Nicolas Vanthuyne, Jean-Pierre Dutasta, Xavier Bugaut,* Bastien Chatelet,* Alexandre Martinez*. Hemicryptophane Cages with a C_1-Symmetric Cyclotriveratrylene Unit. *Organic chemistry*. https://doi.org/10.1021/acs.joc.1c01731

3.1 Introduction

Cyclotriveratrylenes (CTVs) are bowl-shaped molecules whose symmetry is related to the cone conformation and the arrangement of the six peripheral substituents (Figure 3.1.1a).[113] When R_1 is different from R_2 CTVs become chiral,[114] and present most of time a C_3 symmetry although some chiral CTV with C_1 symmetry have been reported.[115] Connecting two CTV units leads to cryptophane host molecules first synthesized by A. Collet in 1981 (Figure 3.1.1b).[116] Cryptophanes have been widely used for their remarkable binding properties, with special emphasize for the enantiopure molecules that display interesting enantioselectivity in recognition and detection of chiral analyses such as epoxides or bromofluoroiodomethane.[117] Cryptophanes were also used for the design of various covalent or self-assembled supramolecular architectures.[118] Hemicryptophanes constitute another class of covalent cages based on the CTV unit bonded to a different entity making it possible to introduce functionalities at the molecular cavity (Figure 3.1.1c). Hemicryptophanes have found a wide range of applications from molecular switches to enantioselective receptors and supramolecular catalysts.[119] The C_3 symmetrical CTV unit of the hemicryptophane structure can be connected to a moiety of C_3- or C_1-symmetry to vary the size and shape of the cavity.[120] However, no hemicryptophane cages built from a C_3 asymmetrical CTV have been reported. To access to such dissymmetric cages presents an increasing interest as they can exhibit

---

[113] *a) Hardie, M. J. Chem. Soc. Rev.* ***2010****, 39, 516–527. b) Collet, A. Tetrahedron* ***1987****, 43, 5725–5759.*

[114] *a) Long, A.; Colomban, C.; Jean, M.; Albalat, M.; Vanthuyne, N.; Giorgi, M.; Di Bari, L.; Górecki, M.; Dutasta, J.-P.; Martinez A. Org. Lett.* ***2019****, 21, 160-165; b) Lefevre, S.; Héloin, A.; Pitrat, D.; Mulatier, J.-C.; Vanthuyne, N.; Jean, M.; Dutasta, J.-P.; Guy, L.; Martinez, A. J. Org. Chem.* ***2016****, 81, 3199–3205.*

[115] *a) Song, J.-R.; Huang, Z.-T.; Zheng, Q.-Y. Tetrahedron* ***2013****, 69, 7308–7313. b) Chakrabarti, A.; Chawla, H. M.; Hundal, G.; Pant, N. Tetrahedron* ***2005****, 61, 12323–12329. c) Milanole, G.; Gao, B.; Mari, E.; Berthault, P.; Pieters, G.; Rousseau, B. Eur. J. Org. Chem.* ***2017****, 2017, 7091–7100. d) Lutz, M. R.; Ernst, E.; Zeller, M.; Dudzinski, J.; Thoresen, P.; Becker, D. P. Eur. J. Org. Chem.* ***2018****, 2018, 4639–4645. e) El Ayle G. G., PhD Thesis, Georgetown University, Washington D.C. (USA),* ***2017***

[116] *a) Brotin, T.; Dutasta, J.-P. Chem. Rev.* ***2009****, 109, 88–130; b) Hardie, M. J. Chem. Lett.* ***2016****, 45, 1336–1346.*

[117] *a) Bouchet, A.; Brotin, T.; Linares, M.; Ågren, H.; Cavagnat, D.; Buffeteau, T. J. Org. Chem.* ***2011****, 76, 4178–4181. b) Garel, L.; Dutasta, J.-P.; Collet, A. Angew. Chem. Int. Ed.* ***1993****, 22, 1169–1171. c) De Rycke, N.; Jean, M.; Vanthuyne, N.; Buffeteau, T.; Brotin, T. Eur. J. Org. Chem.,* ***2018,*** *1601-1607.*

118 a) Oldknow, S.; Martir, D. R.; Pritchard, V. E.; Blitz, M. A.; Fishwick, C. W. G.; Zysman-Colman, E.; Hardie, M. J. Chem. Sci. 2018, 9, 8150-8159. b) Kai, S.; Kojima, T.; Thorp-Greenwood, F. L.; Hardie, M. J.; Hiraoka, S. Chem. Sci. 2018, 9, 4104–4108. c) Cookson, N. J.; Fowler, J. M.; Martin, D. P.; Fisher, J.; Henkelis, J. J.; Ronson, T. K.; Thorp-Greenwood, F. L.; Willans, C. E.; Hardie, M. J. Supramol. Chem. 2018, 30, 255–266.

[119] *a) Canceill, J.; Collet, A.; Gabard, J.; Kotzyba-Hibert, F.; Lehn, J.-M. Speleands. Helv. Chim. Acta* ***1982****, 65, 1894–1897. b) Zhang, D.; Martinez, A.; Dutasta, J.-P. Chem. Rev.* ***2017****, 117, 4900–4942.*

[120] *a) Martinez, A.; Robert, V.; Gornitzka H.; Dutasta J.-P. Chem. Eur. J.,* ***2010****, 16, 520-527. b) Chatelet, B.****;*** *Payet, E.; Perraud, O.; Dimitrov-Raytchev, P.; Chapellet, L.-C.; Dufaud, V.; Martinez, A.; Dutasta, J.-P. Org. Lett.* ***2011****, 13, 3706-3709. c) Zhang, D.; Cochrane, J. R.; Di Pietro, S.; Gornitzka, H.; Guy, L.; Dutasta, J-P.; Martinez, A. Chem. Eur. J.* ***2017****, 23, 6495-6498; d) Yang, J.; Chatelet, B.; Dufaud, V.; Hérault, D.; Jean, M.; Vanthuyne, N.; Mulatier, J.-C.; Pitrat, D.; Guy, L.; Dutasta, J.-P.; Martinez, A. Org. Lett.* ***2020****, 22, 8984-8988. e) Qiu, G.; Nava, P.; Martinez, A.; Colomban C. Chem. Commun.* ***2021****, 57, 2281-2284.*

remarkable properties for different issues in terms of molecular recognition, asymmetric catalysis or chiroptical spectroscopy.[121]

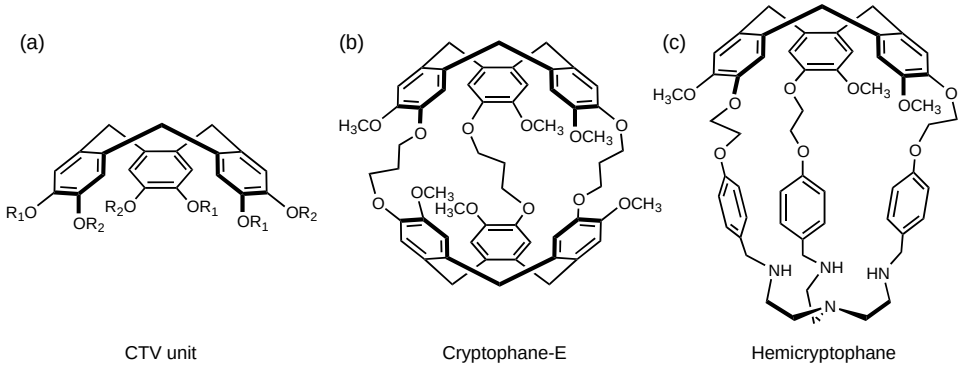

Figure 3.1.1 General structures of cyclotriveratrylene derivatives (a), cryptophane (b) and hemicryptophane (c).

Here, in this chapter, we report on the synthesis of two chiral hemicryptophane cages that combines a CTV unit linked either to an amino-trisamide moiety **93** or to a tris-(2-aminoethyl)amine (tren) one **94**. These two hemicryptophanes present an unexpected C_1 arrangement of the substituents of the CTV unit as evidenced by NMR analyses and X-ray molecular structure of **94**. Compound **93** was optically resolved by chiral HPLC to give the two enantiomers with ee > 99%, and their absolute configurations were determined from ECD spectra and TD-DFT calculations. As a consequence, the reaction of tren-based cage with $PCl(NMe_2)_3$ doesn't lead to the expected azaphosphatrane, but to the enantiopure secondary phosphine oxide, highlighting how the specific conformation of the tren unit, imposed by the CTV one, can change its reactivity.

3.2 Result and discussion

3.2.1 Synthesis of hemicryptophanes 93

We envisaged the synthesis of the enantiopure small hemicryptophane cages **93** and **94** (Figure

121 a) Sun, Q.-F.; Sato, S.; Fujita, M. Angew. Chem. Int. Ed. *2014,* 53, *13510 –13513. b) Johnson, A. M.; Hooley, R. J.* Inorg. Chem. *2011,* 50, *4671-4673. c) Preston, D.; Barnsley, J. E.; Gordon, K. C.; Crowley, J. D.* J. Am. Chem. Soc. *2016,* 138, *10578–10585. d) Bloch, W. M.; Holstein, J. J.; Hiller, W.; Clever, G. H.* Angew. Chem. Int. Ed. *2017*, 56, *8285–8289. e) Sudan, S.; Li, R.-J.; Jansze, S. M.; Platzek, A.; Rudolf, R.; Clever, G. H.; Fadaei-Tirani, F.; Scopelliti, R.; Severin, K.* J. Am. Chem. Soc. *2021*, 143, *1773–1778. f) Bloch, W. M.; Abe, Y.; Holstein, J. J.; Wandtke, C. M.; Dittrich, B.; Clever, G. H.* J. Am. Chem. Soc. *2016*, 138, *13750–13755.*

3.2.1), then it could be used either to complex small enantiopure cations or zwitterions like amino-acids or to encage azaphosphatranes to give chiral enantiopure Verkade's superbase in confined space.[122] Figure 3.2.1 shows the synthetic pathway to obtain hemicryptophanes **93**. The reaction between vanillyl and 1, 3-dibromopropane was the first step, it was a nucleophilic substituent reaction in ethanol, then compound **95** was isolated in 72% yield. In order to avoid the reactivity of alcohol group $Br(CH_2)_3$-O-Ph-CH_2-OH, a THP group was introduced to protect it and generated the compound **96** in the second step with catalytic amount of PPTS involved, with a yield was achieved to 98%, in this step, we found that using different solvent resulted in different yields for the same reaction: when this reaction was carried out in tetrahydrofuran or chloroform, the protection was less efficient, compared to the dichloromethane solvent, with yields of 87%, 89%, and 98%, respectively. In third step, a subsequent nucleophilic substitution with sodium azide was performed in *N*,*N*-dimethylformamide to give **97**, no further purification was needed in this step. Then, **97** was reduced under the Staudinger condition to give **98** in 92% yield. Because of the fast reactivity, the triphenylphosphine was added at 0 °C, then the reaction mixture was slowly warmed up to room temperature. Compound **98** was very polar and was difficult to purify by getting precipitate or column chromatography. Thus, we also followed Gabriel reaction to get **98** from **96**. However, low yields were obtained under these conditions. In the fifth step, in the presence of DCC/HOBT as coupling agent, nitrilotriacetic acid was introduced and reacted with amine **98** in tetrahydrofuran. The coupling agent was added at 0 °C, the reaction was slowly warmed up to room temperature then heated at 50 °C, the byproduct *N*, *N*′-dicyclohexylurea was not soluble in tetrahydrofuran, it can be very easy to remove just by filtering it for several times. Then the rest impurities were removed through aqueous workup, leading to triamidoamine **99** in high yield (97%) with the desired purity. At the same time, we tried to obtain **99** by introducing pyridine as the base and solvent directly, and triphenyl phosphite, but this reaction easily gave byproduct such as triphenyl phosphate, and pyridine salt, instead of expecting product (we observed low yield for it).

[122] *Raytchev P. D., Martinez A, Gornitzka H, Dutasta J.P. J Am Chem Soc. 2011;133(7):2157-2159*

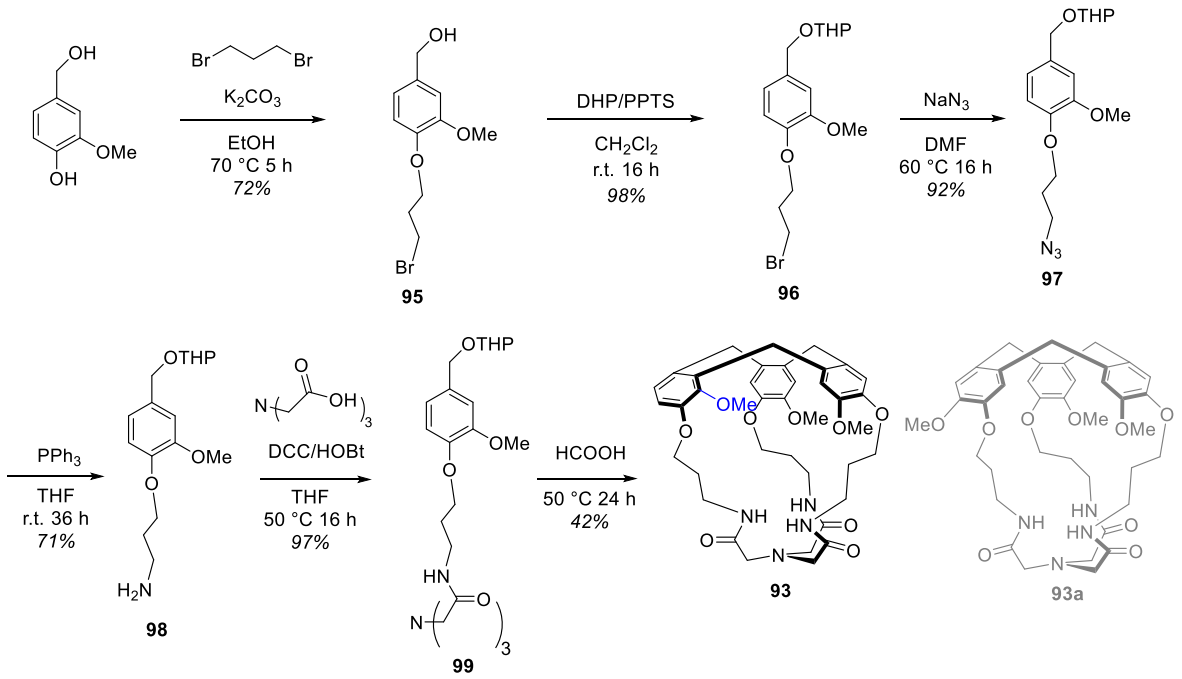

Figure 3.2.1 Synthetic pathway follows for the synthesis of hemicryptophanes **93**.

In the sixth step, we aimed to synthesize the hemicryptophane **93** by cyclizing the CTV part in formic acid. The room temperature was unable to provide enough energy to finish the whole cyclization process even we let this reaction going for 3 days. Thus, this reaction was heated at 50°C for one day and hemicryptophane **93** was isolated with a moderate yield of 42 %. It is remarkable and important to note that the expected C_3-symmetrical hemicryptophane **93a** was not detected, one Friedel-Crafts reaction did not occur on the expected position for one aromatic ring, three arms are not symmetry as one methoxy group (Ph-O-Me) substituent has changed its position (in blue in Figure 3.2.1).

3.2.2 Synthesis of hemicryptophane 94

The reduction reaction of **93** was not easy, reductant such as $Zn(OAc)_2$ was used according to the report,[123] but there was no reactivity, so borane dimethyl sulfide was considered. A solution of borane dimethyl sulfide in tetrahydrofuran was introduced to a solution of **93** in THF. Then after seven days, methanol and 1 M solution of hydrogen chloride in water were added twice to quench the reaction. However, the hemicryptophane **94** carrying amine groups was too polar, thus it was difficult to purify directly. Indeed, a pure precipitate was hard to obtain because some byproducts that contained boron were always obtained together with hemicryptophane

[123] *E. L. Stoll, T. Tongue, K. G. Andrews, D. Valette, D. J. Hirst and R. M. Denton. Chem. Sci., 2020, **11**, 9494-9500*

94. So, we had to use di-tert-butyl dicarbonate to protect the amine groups of crude hemicryptophane **94** firstly. This makes hemicryptophane **94-Boc** less polar (yield 97%), hence easier to purify. With the pure hemicryptophane **94-Boc** in hands**,** trifluoroacetic acid was then used to remove the protective groups directly, leading to compound **94** without further purification (yield 71%, Figure 3.2.2).

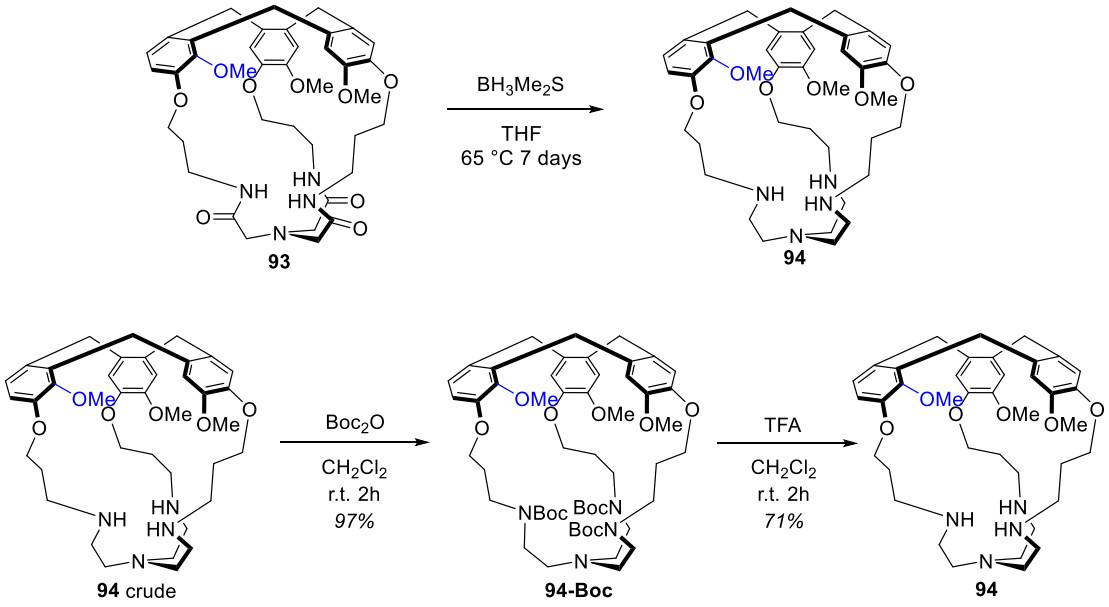

Figure 3.2.2 Synthetic pathway follows for the synthesis of hemicryptophanes **94**.

3.2.3 Characterization and molecular structure for hemicryptophane 93 and 94

Because of the unexpected outcome of this synthesis pathway, characterizations of the new hemicryptophanes were cautiously done by mass measurements and NMR analyses. While hemicryptophane **93** displays the expected exact mass (m/z = 716.3312), its ^{1}H NMR spectrum does not present the C_3 symmetry that usually observed for hemicryptophanes in solution (Figure 3.2.3). Hemicryptophane **93** exhibits the characteristic signals of a CTV moiety but with a lack of the usual C_3 symmetry: three different AB systems for the diastereotopic H_a and H_e $ArCH_2Ar$ protons (4.76, 4.72, 4.30 ppm and 4.12, 3.56, 3.51 ppm were observed, respectively). Three singlets for the methoxy groups at 3.93, 3.80 and 3.79 ppm were found. Four singlets (7.55, 6.91, 6.88 and 6.12 ppm) and two AB doublets (7.02 and 6.72 ppm; J_{AB} =

8.5 Hz) were assigned that there are no equivalent aromatic protons. The $OCH_2CH_2CH_2N$ methylene protons of the linkers give a complex pattern between 3.6-4.5 and 1.5-2.3 ppm. The CH_2 protons of the amino-trisamide core also reveal as diastereotopic leading to multiplets between 1.7 and 2.8 ppm. Finally, three different signals can be observed for the NH at 5.77, 6.48 and 7.13 ppm. The ^{13}C NMR spectrum also confirms the absence of C_3 symmetry for **93**, for instance three peaks for the C_{amide} at 169.5, 169.4, and 169.20 ppm were found.

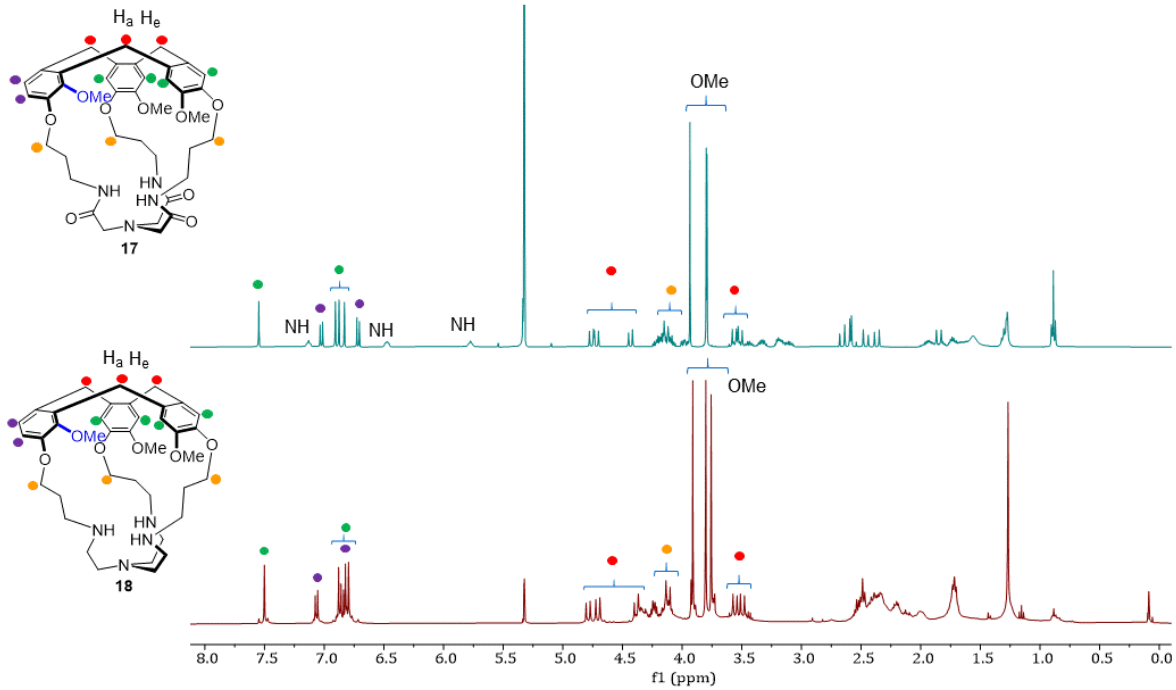

Figure 3.2.3 ^1H NMR spectra (400 MHz, CD_2Cl_2, 298 K) of hemicryptophanes **93** and **94**.

The presence of six different aromatic protons for the CTV unit, including one AB system between protons of one aromatic ring, and the splitting of other sets of signals are consistent with the observed C_1 symmetry. This is a different situation compared to the loss of the C_3-symmetry due to intramolecular hydrogen bonding between the amide functions as previously observed in the solid state for other hemicryptophane parents, where one linker was oriented inside the molecular cavity, breaking the C_3 symmetrical conformation that observed in solid state but not in solution.[13]. In order to rule out this possibility, the ^1H NMR spectrum of **93** has been also performed in DMSO-d_6 to break any intramolecular hydrogen bonds: the C_1 symmetry is again retained.

A decisive argument is brought by studying the hemicryptophane-tren **94** that obtained from hemicryptophane-amide **93**. The ^1H and ^{13}C NMR spectra of hemicryptophane **94** show similar patterns to those observed for **93** (Figure 3.2.3), proofing the C_1 symmetry of hemicryptophane-

tren **94** in solution. In particular, the aromatic protons of the CTV unit of **94** appear as four singlets and two AB doublets. Main differences are in the resonances of the protons of the tren unit (between 2 and 2.7 ppm compared to the amino-trisamide core (between 1.7 and 2.8 ppm). We hypothesize that these C_1-symmetrical hosts result from an unusual regioselectivity of the last Friedel-Crafts reaction during the cyclization step from precursor **99** to afford host hemicryptophane **93**. Although this regioselectivity has never been observed for CTVs, cryptophanes or hemicryptophanes, this new structure could arise from a specific arrangement of the amino-trisamide unit under acidic conditions that control the relative position and orientation of the vanillyl aromatic rings.

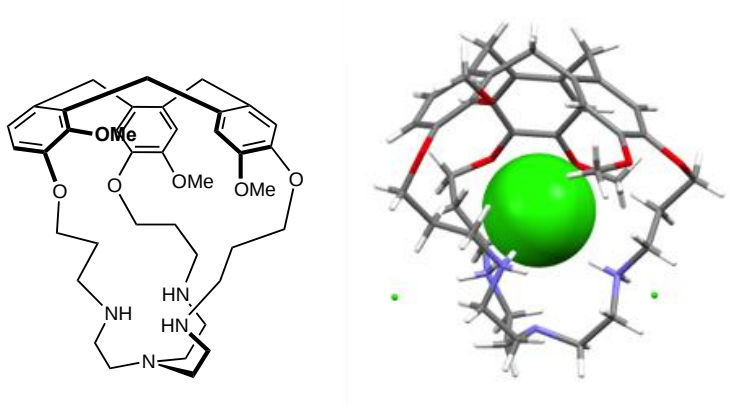

Figure 3.2.4 Hemicryptophane **94** and X-ray structure of **94**·[4H$^+$Cl$^-$].

A molecular structure of the protonated cage **94**·4[H$^+$Cl$^-$] was determined by X-ray diffraction on crystals obtained by slow evaporation from a $CHCl_3$ solution (Figure 3.2.4). Protonation of the cage probably occurs during the crystallization because of traces of HCl usually found in chloroform. This solid-state structure is consistent with the structure of **94** characterized by NMR, with a CTV unit presenting a C_1 symmetry induced by an unprecedented arrangement of the substituents on one of the aromatic rings. Indeed, two arms exhibit the expected position for their OMe group, whereas for the last one, the OMe group lies between the -$OCH_2CH_2CH_2N$- linker and the methylene bridge. Hemicryptophane **94** presents a well-defined cavity, with a chloride anion trapped inside. Hydrogen bonding between the three secondary ammonium functions of the linkers and the chloride anion (average distance $d_{N\ldots Cl}$ = 2.247 Å), can account for the formation of this host-guest complex. This constitutes the example of an X-ray structure of a hemicryptophane complex with an anion inside, confirming the ability of this class of hosts to complex ions both in solution and in solid state.

3.2.4 Optical resolution of hemicryptophane 93 and 94-Boc

Resolution of the racemic mixture of **93** was then performed by chiral high-performance liquid chromatography (HPLC), using a mixture solution of heptane/ethanol/triethylamine as the eluent. The two enantiomers were obtained with high purity (ee>99%). The electronic circular dichroism (ECD) spectra of the two enantiomers were recorded in order to assign their absolute configuration. Indeed, Collet and co-workers have shown that the sign of exciton pattern center on ^1L_a (~240 nm) transition is weakly sensitive to the substituents that grafted on the CTV unit.[124] Thus, a direct comparison of this sign for one enantiomer with one of the CTV of known absolute configuration allow for a direct assignment of its absolute configuration, the (+)-*M*-**93** and (–)-*P*-**93** configurations were assigned to the first and second eluted enantiomers respectively (Figure 3.2.5). As the spatial arrangement of the CTV substituents in **93** differs from that of usual C_3-symmetry derivatives, the simple comparison of the ECD spectra of enantiomers (+)-**93** and (–)-**93** with those of other C_3 CTV of known configuration might be not relevant. Therefore, to support our previous proposed stereochemical assignment, the ECD spectrum of *P*-**93** (second eluted) was calculated using the TD-DFT method. In order to guarantee the quality of the obtained data, two hybrid functionals (CAM-B3LYP, ωB97X-D) with the SVP basis set and PCM model for MeCN were tested. The results confirm our initial assignment: the first eluted peak corresponds to a CTV with an *M* configuration, while the second one is *P*-**93.**

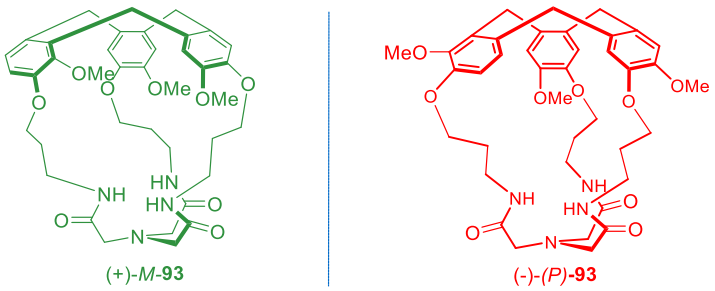

[124] *Canceill, J.; Collet, A.; Gabard, J.; Gottarelli, G.; Spada, G. P. J. Am. Chem. Soc.* ***1985****, 107, 1299–1308.*

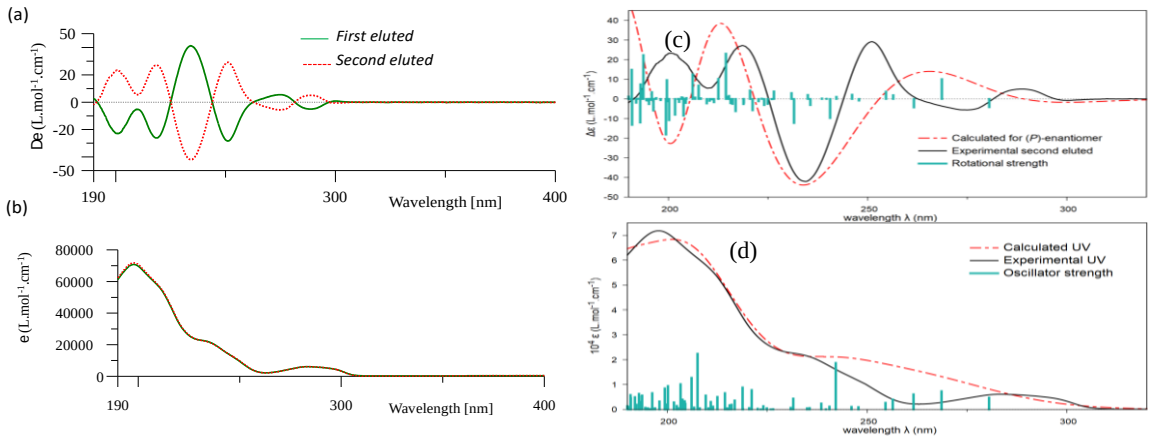

Figure 3.2.5 (a) Experimental ECD spectra of the enantiomers of **93**: the first eluted enantiomer is represented with a green solid line (0.165 mmol.L^{-1} in CH_3CN) and the second one by a red dotted line (0.166 mmol.L^{-1} in CH_3CN). (b) The experimental UV spectra of **93**. Comparison of ECD (c) and UV (d) experimental spectra in acetonitrile for the second eluted enantiomer on Chiralpak IF and TD-DFT calculated spectra (σ = 0.35 eV, shifted by 5 nm). Vertical bars are oscillator and rotational strengths calculated for the two conformers with arbitrary unit.

The racemic mixture of **94-Boc,** was also resolved by Chiral HPLC, leading the enantiopure hemicryptophane **94-Boc**. The (+)-*M*-**94-Boc** and (–)-*P*-**94-Boc** configurations were assigned to the first and second eluted enantiomers respectively (Figure 3.2.6).

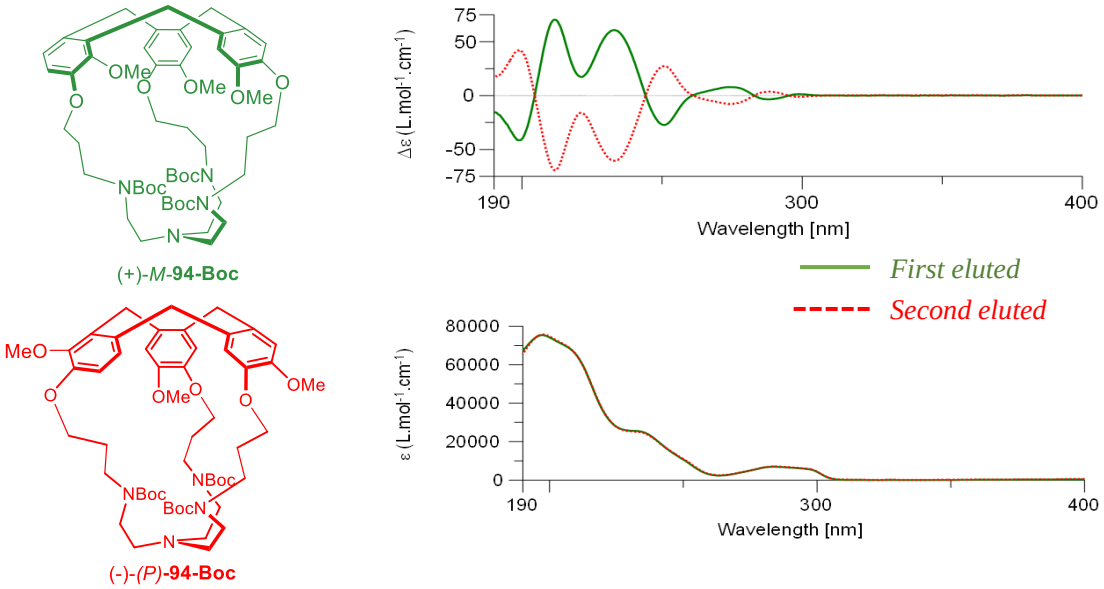

Figure 3.2.6 Experimental ECD spectra of the enantiomers of **94-Boc**: the first eluted enantiomer is represented with a green solid line (0.22 mmol.L^{-1} in CH_3CN) and the second one by a red dotted line (0.22 mmol.L^{-1} in CH_3CN). (b) The experimental UV spectra of **94-Boc.**

3.2.5 Discussion and potential application of *C*$_1$ hemicryptophanes 93 and 94

We then wonder if the *C*$_1$ hemicryptophane **94** could be used to complex a phosphorus atom inside the tren unit to give encaged azaphosphatranes **94-PH$^+$·Cl$^-$**. As we described in **3.3.2**, hemicryptophane **94** was too polar to separate directly, so we synthesized **94-Boc** first under mild condition. After purification, the protective group was removed by a few drops of trifluoroacetic acid. In this case, it was impotent to calculate the exact amount of trifluoroacetic acid, because too much of it (more than 120 equiv.) would break the CTV structure to give the CTV-opened **94** (we don't know which bonds break)**,** while less than 80 equiv. of it would not remove all of protective group -Boc (one arm of **94** was still attached by the -Boc group). Then, the $PCl(NMe_2)_3$ reactant was introduced to a solution of hemicryptophane **94** in dichloromethane, the expected azaphosphatrane **94-PH$^+$·Cl$^-$** was not detected neither in the ^{31}P and ^{1}H NMR spectra nor in the mass spectrum. However, when we used CTV-opened **94** (more than 120 equiv. of TFA was added, we suspect the bond were broken as the scheme showed, in Figure 3.2.7), we did observe the corresponding signal of **94-PH$^+$·Cl$^-$** both in ^{31}P NMR and mass spectra, signal of ^{31}P NMR spectrum resonances at around -12 ppm, the mass was confirmed at *m/z* = 707.4. We deprotonated the CTV-opened **94-PH$^+$·Cl$^-$**, the chemical shift of the ^{31}P NMR spectrum resonance at 120 ppm was observed. But, we never observed the similar signal of ^{31}P NMR that resonances at around -12 ppm when same experiments were performed with pure hemicryptophane **94** and $PCl(NMe_2)_3$, only the secondary phosphine oxide **94-PH=O** was isolated. In the ^{31}P NMR spectrum, the signal show resonances at 20.7 ppm and characteristic P-H coupling of 391 Hz, the mass was confirmed by *m/z* = 721.3727 (plus one proton).

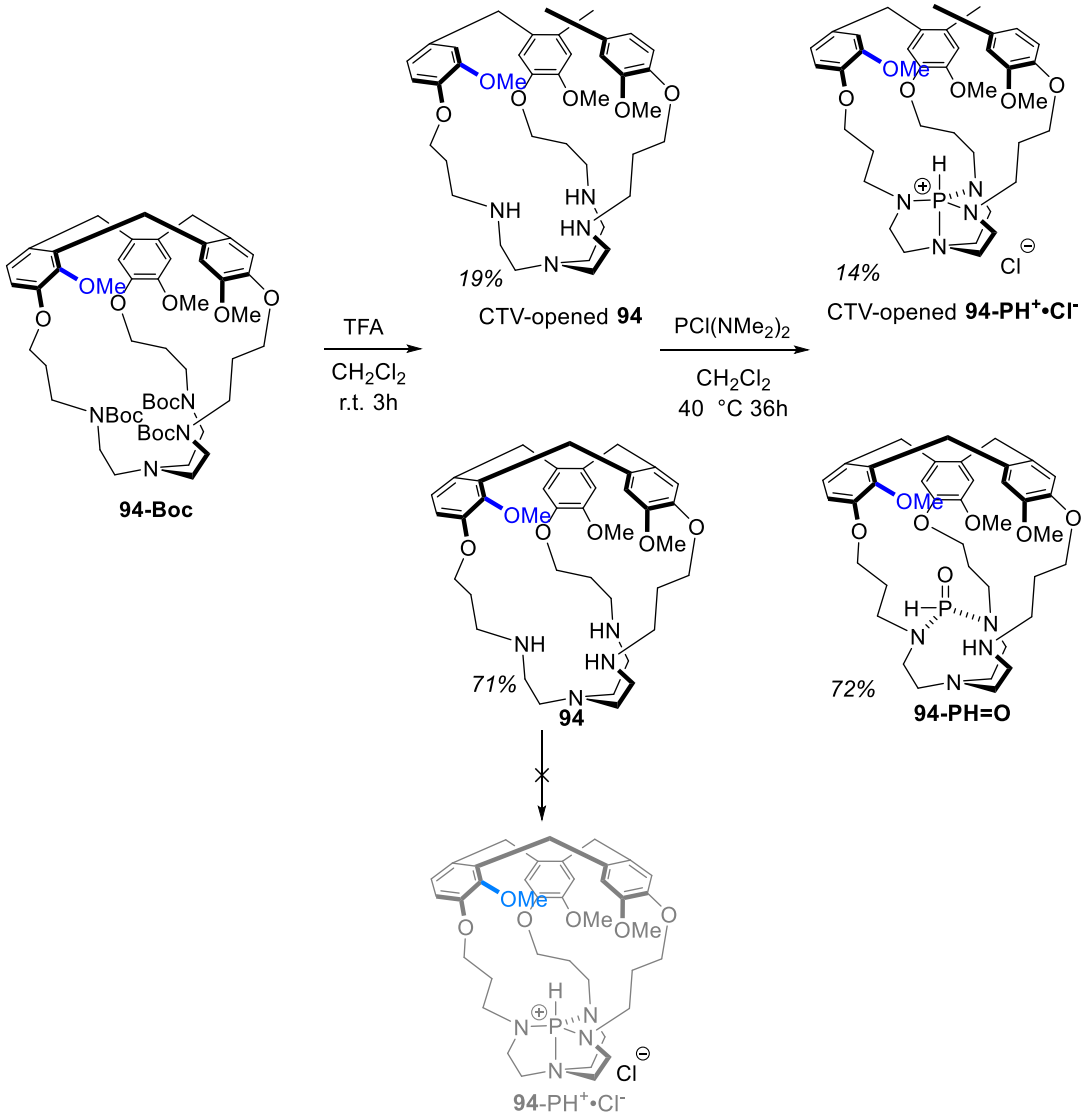

Figure 3.2.7 Attempts to synthesize the azaphosphatrane **94-PH^{+}·Cl^{-}**.

The formation of crude **94-PH=O** leads to six different signals for the methoxy protons in the ^{1}H NMR spectrum. A much more complex patterns both in the aromatic or Ha/He areas were observed. So, in order to identify the structure, **94-PH=O** was dissolved in mobile phase, a mixture solution of ethanol+ tea 0.5% / dichloromethane (30/70), separated by Column Chiralpak IB (250 x 10 mm), finally two diastereomers were obtained. The formation of two diastereomers upon phosphorus complexation can account for this experimental result: once linked to one nitrogen of one arm, the phosphorus can connect to one or the other linker (there are three possibilities for phosphorus to grab two nitrogen), leading to two diastereomeric compounds. While the ^{1}H NMR spectra of **94-PH=O** (first fraction of **94-PH=O** that separated by HPLC) presents a clear C_1 symmetry in solution (Figure 3.2.8) just like **93** and **94**.

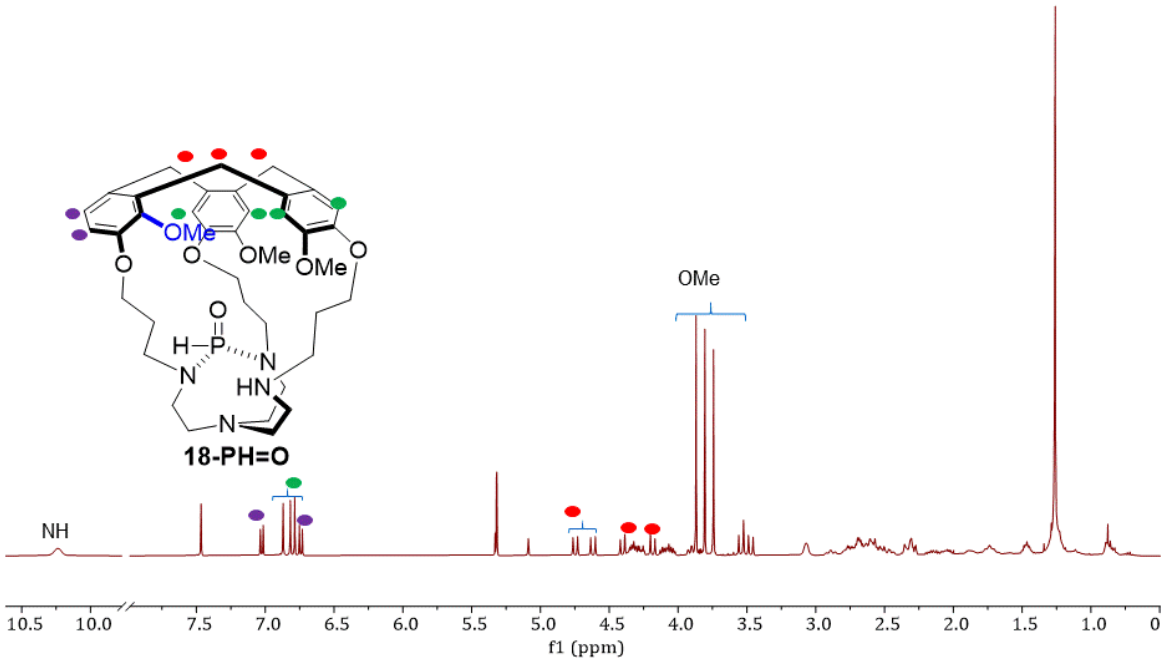

Figure 3.2.8 ^{1}H NMR (400 MHz, CD_2Cl_2, 298 K) spectra of hemicryptophane **94-PH=O**.

A broad signal for NH was observed at 10.23 ppm, four singlets (7.47 ppm, 6.87 ppm, 6.82 ppm, 6.79 ppm, blue) and two AB doublets (7.02 ppm, J = 8.4 Hz, 6.74 ppm, J = 8.3 Hz, red) are assigned to aromatic protons, three different AE $_{OMe}$ s for the diastereotopic H_a and H_e $ArCH_2Ar$ protons at 4.75 ppm, 4.62 ppm, 4.40 ppm, 4.18 ppm, 3.54 ppm, and 3.47 ppm (J = 13.6 Hz, black), three singlets for methoxy group at 3.87 ppm, 3.81 ppm, 3.74 ppm, while $OCH_2CH_2CH_2N$ methylene protons of the linkers give a complex pattern between 4.06 – 4.32 ppm and 1.47-2.31 ppm, the protons of the tren unit present resonances at 2.50-2.78 ppm, which differentiate from hemicryptophane **93** (between 2 and 2.7 ppm) and **94** (between 1.7 and 2.8 ppm). This result shows that the conformation of the tren unit, imposed by the CTV moiety, strongly ^{NH}ects its reactivity properties. The formation of the azaphosphatranes structure **94-PH^{+}·Cl^{-}** is not possible probably because the specific arrangement of one arm prevents the nucleophilic attack of the third nitrogen to the electrophilic phosphorus atom. Only two nitrogen atoms of **94** can bind to the phosphorus and the subsequent hydrolysis provides the **94-PH=O**. Thus, this unusual control of the reactivity of the tren moiety lead to an unexpected enantiopure SPO compounds. The ^{1}H NMR spectrum of second fraction (**94-PH=O**) is very similar to the first fraction, except one signal of O-Me is high-fielded a little (3.74 ppm to 3.6 ppm).

3.3 Conclusion

The synthesis of chiral covalent molecular cages still constitutes a challenging and key issue in supramolecular chemistry.[15] Herein we have reported an unexpected alternative to hemicryptophanes of low symmetry using conventional synthetic pathway. The usual Friedel-Crafts cyclization in formic acid of an adequately tris-substituted nitrilo-trisamide precursor **99** afforded C_1-symmetric hemicryptophane **93**; it was then reduced to give the *tren* derivative **94**. The racemic mixture (±)-**93** was resolved by chiral HPLC. The absolute configuration of the resulting enantiomers was determined from their ECD spectra and corroborated by TD-DFT calculations. The hemicryptophane cages **93** and **94** display an unprecedented C_1 symmetry in solution, evidenced by the NMR analyses, and supported by the X-ray structure of the tetra-ammonium derivative **94**·4[$H^+ \cdot Cl^-$]. This compound, displays an unprecedented C_1 symmetry in solution. The reduction of the amide function doesn't allow restoring the C_3 symmetry. Theses C_1 symmetry are due to the unusual arrangement of the substituent of CTV moiety, leading to original hemicryptophane cages. Attempts to introduce an azaphosphatrane function in the south part failed: an unexpected reactivity was observed since the only two nitrogen atoms can link to the phosphorous one, providing an enantiopure product after hydrolysis. These results open the way for the synthesis of cages presenting a CTV unit with lower symmetry for more tunable and specific properties. This approach is currently being carried out in our laboratory for applications in supramolecular catalysis and molecular recognition.

Chapter 4: New hemicryptophanes cages: applications in recognition, catalysis and consequences on thermodynamics and kinetic proton transfer

Publication: Chunyang Li, Anne-Doriane Manick, Jean-Pierre Dutasta, Xavier Bugaut, Bastien Chatelet, Alexandre Martinez. Cavity Control of Frustrated Lewis/Bronsted Pairs Behavior. In preparation.

4.1 Introduction

The design of various molecular containers have been reported widely, especially being receptors that contain a reactive site is very attractive, because they can act as supramolecular catalysts and can mimic biological entities such as enzymes.[125] Chemists have already found that there are some changes in the confined space of enzymes in the reactivity, which impel them to explore and reproduce these by some ideas such as the formation of supramolecular structures.[126] Thus the different host molecules have been synthesized to illustrate the special tailored functional groups inside the cavity.[127] In particularly, endohedral functionalized reactive species in such artificially protected and confined spaces has exhibited the great potential.[128] Artificial cages have found a wide range of applications in guests binding,[129] transport,[130] drug delivery,[131] gas adsorption,[132] chemical purification,[133] stabilization of reactive species[134] and catalysis.[135] Such complex structures have been obtained either by self-assembly or covalent strategies.[136] When use as supramolecular catalysts, the nano-confinement of the reactants and/or the catalytic site, can lead (i) to an increase of the reaction rate by, for instance, controlling the conformation of the substrate or stabilizing transition states,[137] (ii) to an improvement or change of the selectivity by substrate size selectivity, by controlling the second coordination sphere or the folding of the substrate,[138] or by masking

[125] *Yoshizawa, M.; Klosterman, J. K.; Fujita, M. Angew. Chem., Int. Ed. 2009, 48, 3418–3438. (e) Rebek, J., Jr. Acc. Chem. Res. 2009, 42, 1660–1668.*

[126] *Engeldinger, E.; Armspach, D.; Matt, D. Chem. Rev. 2003, 103, 4147–4173. (e) Homden, D. M.; Redshaw, C. Chem. Rev. 2008, 108, 5086–5130.*

[127] *Koblenz, T. S.; Wassenaar, J.; Reek, J. N. H. Chem. Soc. Rev. 2008, 37, 247–262.*

[128] *Deutman, A. B. C.; Monnereau, C.; Elemans, J. A. A. W.; Ercolani, G.; Nolte, R. J. M.; Rowan, A. E. Science 2008, 322, 1668–1671.*

[129] *a) Jie, Y. Zhou, E. Li, F. Huang, Acc. Chem. Res. 2018, 51, 2064 – 2072; b) P. Howlader, E. Zangrando, P. S. Mukherjee, J. Am. Chem. Soc. 2020, 142, 9070 – 9078; c) M. Yamashina, Y. Tanaka, R. Lavendomme, T. K. Ronson, M. Pittelkow, J. R. Nitschke, Nature 2019, 574, 511 – 515.*

[130] *Gale, P. A.; Davis, J. T.; Quesada, R. Chem. Soc. Rev. 2017, 46, 2497−2519.*

[131] *a) M. J. Webber, R. Langer, Chem. Soc. Rev. 2017, 46, 6600 – 6620; b) X. Ma, Y. Zhao, Chem. Rev. 2015, 115, 7794 – 7129.*

[132] *a) G. Zhang, M. Mastalerz, Chem. Soc. Rev. 2014, 43, 1934 – 1947; b) I. A. Riddell, M. M. J. Smulders, J. K. Clegg, J. R. Nitschke, Chem. Commun. 2011, 47, 457 – 459; c) D. Yang, J. Zhao, Y. Zhao, Y. Lei, L. Cao, X.-J. Yang, M. Davi, C. Janiak, Z. Zhang, Y.-Y. Wang, B. Wu, Angew. Chem. Int. Ed. 2015, 54, 8658 – 8661; Angew. Chem. 2015, 127, 8782 – 8785.*

[133] *Zhang, D.; Ronson, T. K.; Lavendomme, R.; Nitschke, J. R. J. Am. Chem. Soc. 2019, 141, 18949−18953.*

[134] *a) R. Warmuth, M. A. Marvel, Angew. Chem. Int. Ed.* ***2000****, 39, 1117; b) Y. C. Horng, P. S. Huang, C. C. Hsieh, C. H. Kuo, T. S. Kuo, Chem. Commun.* ***2012****, 48, 8844; c) M. Fujita, D. Oguro, M. Miyazawa, H. Oka, K. Yamaguchi, K. Ogura, K. Nature,* ***1995****, 378, 469.*

[135] *a) M. Yoshizawa, J. K. Klosterman, M. Fujita, Angew. Chem. Int. Ed. 2009, 48, 3418 – 3438; Angew. Chem. 2009, 121, 3470 – 3490; b) S. Zarra, D. M. Wood, D. A. Roberts, J. R. Nitschke, Chem. Soc. Rev. 2015, 44, 419 – 432; c) C. J. Brown, F. D. Toste, R. G.Bergman, K. N. Raymond, Chem. Rev. 2015, 115, 3012 – 3035; d) Q. Zhang, K. Tiefenbacher, Nat. Chem. 2015, 7, 197 – 202.*

[136] *S. Pullen, J. Tessarolo, G. H. Clever. Chem. Sci., 2021, 12, 7269. b) T. Brotin, J.-P. Dutasta Chem. Rev. 2009, 109, 1, 88–130.*

[137] *a) N.-W. Wu, I. D. Petsalakis, G. Theodorakopoulos, Y. Yu and J. Rebek Jr, Angew. Chem., Int. Ed., 2018, 57, 15091–15095. b) C. M. Hong, M. Morimoto, E. A. Kapustin, N. Alzakhem, R. G. Bergman, K. N. Raymond and F. D. Toste, J. Am. Chem. Soc., 2018, 140, 6591–6595.*

[138] *a) A. Cavarzan, J. N. H. Reek, F. Trentin, A. Scarso and G. Strukul, Catal. Sci. Technol., 2013, 3, 2898–2901. b) P. Zhang, J. Meijide SuaÅLrez, T. Driant, E. Derat, Y. Zhang, M. MeÅLnand, S. Roland and M. Sollogoub, Angew. Chem., Int. Ed., 2017, 56, 10821–10825. c) H. Takezawa, T. Kanda, H. Nanjo, M. Fujita J. Am. Chem. Soc. 2019, 141, 5112−5115.*

with a supramolecular shadow some specific reactive sites[139] and (iii) to a protection of the catalytic site, allowing for example to improve the stability of the catalyst or to perform sequential catalysis with incompatible systems.[140] Our group recently reported that endohedral functionalization of the inner space of cages can provide frustrated Lewis pairs system: the encapsulation of the Lewis base partner prevents its interaction with the Lewis acid, leading to FLP system active in catalysis.[141] Given the great interest aroused by FLP systems, it can activate for instance C-H or C-F bonds,[142] and small molecules like H_2, N_2, or CO_2,[143] and lead to new and original reactive systems for catalysis,[144] several strategies have been reported to modulate the FLP properties by changing either the electronic and steric properties of the units linked to the acid or Lewis sites,[145] or the nature of the Lewis acid or basic atoms.[146] Hence, new and original systems, like "reverse FLP", have emerged from these studies.

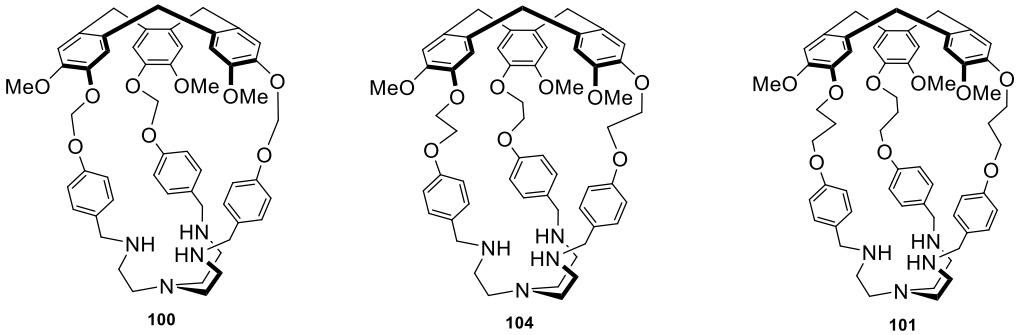

Figure 4.1.1 Comparison of three hemicryptophanes.

In this context, two new hemicryptophanes **100** and **101** that contain different size cavities were synthesized, it is interesting because it allows for investigating the effect of the flexibility on the selectivity of recognition processes. Thus, a comparison of the recognition properties of these two new cages **100** and **101** with the classic hemicryptophane **104** that was synthesized previously in our group will be presented (Figure 4.1.1).[147] In previous studies, S. Lefevre and her colleagues synthesized the enantiopure hemicryptophane **104**, and used it as receptor to

[139] *a) H. Takezawa, T. Kanda, H. Nanjo and M. Fujita, J. Am. Chem. Soc., 2019, 141, 5112–5115 (b) C. Fuertes-Espinosa, C. Garcı´a-Simo´n, M. Pujals, M. Garcia-Borra`s, L. Go´mez, T. Parella, J. Juanhuix, I. Imaz, D. Maspoch, M. Costas and X. Ribas, Chem, 2020, 6, 169–186.*

[140] *Y. Ueda, H. Ito, D. Fujita and M. Fujita, J. Am. Chem. Soc., 2017, 139, 6090–6093.*

[141] *J. Yang, B. Chatelet, V. Dufaud, D. Hérault, S. Michaud-Chevallier, V. Robert, J.-P. Dutasta, A. Martinez, Angew. Chem. Int. Ed. 2018, 57, 14212.*

[142] *M. A. Légaré, M. Courtemanche, E. Rochette, F. G. Fontaine, Science 2015 349, 513.*

[143] *Jolie Lam, Kevin M. Szkop, Eliar Mosaferi and Douglas W. Stephan Chem. Soc. Rev., 2019, 48, 3592.*

[144] *Douglas W. Stephan, Chem, 2020.*

[145] *Qiang Liu, Liu Yang, Chenfei Yao, Jiao Geng,* Youting Wu,* and Xingbang Hu* Org. Lett. 2021, 23, 3685−3690.*

[146] *J. Backs, M. Lange, J. Possart, A. Wollschl, C. Mgck-Lichtenfeld. Angew. Chem. Int. Ed. 2017, 56, 3094 –3097.*

[147] *Sarah. Lefevre, et al. Chemistry–A European Journal. 2016, 2068-2074.*

combine small molecules, such as norephedrine as guest to give the binding constants (5.1×10^6 for *P*-**104** and 4.9×10^7 for *M*-**104**), the ratio of enantioselectivity is 9:91.

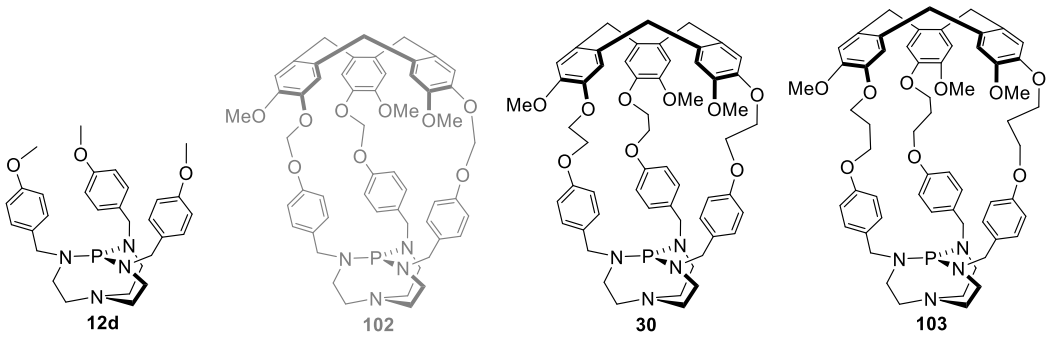

Figure 4.1.2 Structures of the model and confined Verkade's superbases.

We also envisioned that endohedrally functionalized molecular cages could be exploited as a tool for tuning the degree of frustration of such systems by modulating the cavity size and shape. This chapter will describe the properties of encaged Verkade's superbases in three different cavities,[148] varying only by one methylene in each linker (Figure 4.1.2). **12d** is considered as the model to reveal that bases without cavities cannot act as hindered FLPs. The small change in the cage structures affects strongly their reactivity when used in FLP systems: whereas the system involving the medium cage **30** behave as a classical FLP one, the larger one **103** presents only a partial frustration behavior since the reaction between the encaged Lewis base and the Lewis acid takes place to some extent, and the smallest one **102** is so frustrated than even the transfer of proton is not possible leading to frustrated Bronsted pairs. It highlights how a small change in the cavity size strongly affect the FLP behavior.

[148] *a) G. Verkade, P. Kisanga, Tetrahedron 2003, 59, 7819; b) P. Kisanga, J. G. Verkade, R. J. Schwesinger, R. J. Org. Chem. 2000, 65, 5431; c) M. A. H. Laramay, J. G. Verkade, J. Am. Chem. Soc. 1990, 112, 9421.*

4.2 Results and discussion

4.2.1 Synthesis of two new hemicryptophanes 100 and 101

4.2.1.1 Synthesis of hemicryptophane 100

The synthesis of hemicryptophanes **100** was a little tricky, we could not use the classic pathway to obtain it: when vanillyl alcohol or hydroxybenzaldehyde are used as starting materials together with 1, 2-dichloromethane, or 1, 2-dibromomethane, or dichloromethane, only dimers were isolated with good yields of more than 90% (Figure 4.2.1), instead of expected compound **106** or **106a**. Thus, in order to get the compound **106**, we have to find another synthesized route.

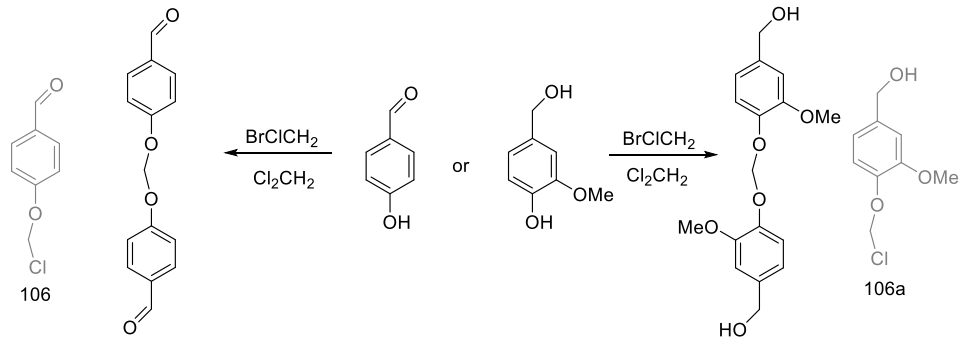

Figure 4.2.1 Attempts to get compound **106**.

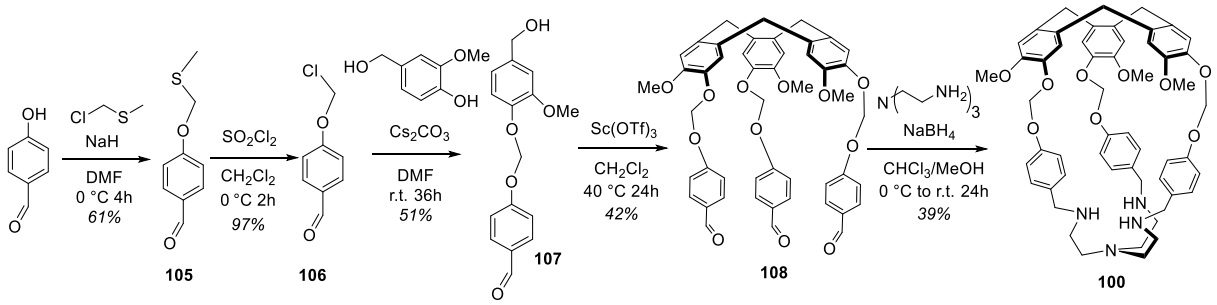

Figure 4.2.2 Synthesis of hemicryptophane **100.**

We found that it was possible to obtain compound **106** by the two-step procedure shows in Figure 4.2.2. Firstly, vanillyl alcohol is taken as the starting material to react with chloromethyl methyl sulfide, but, the base sodium hydride is too strong, it can deprotonate the proton of benzyl alcohol leading to a mixture of product. Hydroxybenzaldehyde, was thus used as it contained only one -OH; so compound **105** was isolated successfully with good yield (61%)

based on the reported procedure,[149] it is a substitution reaction, and sodium hydride deprotonated the proton of phenol in ethanol to give phenolate. In the second step, sulfuryl chloride was used as chlorinating reagent to remove the sulfur methyl part in dry dichloromethane and to give the compound **106**. **106** is very sensitive, we could only perform this experiment under strict argon condition.

In the third step, in the presence of base cesium carbonate, vanillyl alcohol was deprotonated in dry *N, N*-dimethylformamide to give the corresponding phenolate, then reacts with compound **106** to provide compound **107** in 51% yield. In the fourth step, it was the cyclization leading to the CTV unit: **107** was treated with a catalytic amount of scandium (III) trifluoromethanesulfonate in dichloromethane to give the hemicryptophane precursor **108**. In the last step, an reductive amination was performed by mixing compound **108**, tris(2-aminoethyl)amine (tren) and the subsequent addition of the reducing reagent sodium borohydride, giving the hemicryptophane **100.**

4.2.1.2 Synthesis of hemicryptophane 101

The syntheses of hemicryptophane **101** was not so difficult compared to the synthesis of hemicryptophane **101**, as the classic synthesis strategy revealed successfully. The four-step synthesis procedure is depicted in Figure 4.2.3. For the first step, it was the substitution reaction, we used vanillyl alcohol as the starting material, potassium carbonate as the base, 1,3-dibromopropane as the linker in ethanol to obtain compound **109** in 72% yield. In the second step, we used catalytic amount of scandium (III) trifluoromethanesulfonate in acetonitrile to build the CTV unit of compound **110**. In the third step, we used hydroxybenzaldehyde to prolong the linkers, the reaction was performed in *N, N*-dimethylformamide, and cesium carbonate was used as the base to give the compound **111** in 87% yield. In the last step, we used tris(2-aminoethyl)amine (tren) as the C_3-symmetric ligand to construct the hemicryptophane **101** (43% yield), by using a similar reductive amination .

As we described, we managed to synthesize two new hemicryptophanes **100** and **101**. Interestingly, we could make a comparison with hemicryptophane **104** (contain two CH_2 Figure 4.1.2), for example, these three hemicryptophanes have similar structures, but hemicryptophane **100** presents a more rigid cavity, only containing one CH_2, **104** is the medium one (two CH_2 in each linker), and hemicryptophane **101** with three CH_2 in each liker is probably

[149] *T. Iwasaki, Y. Miyata, R Akimoto, Y. Fujii. J. Am. Chem. Soc. 2014, 136, 26, 9260–9263.*

the more flexible one. It is interesting that each hemicryptophane is special and we could explore its enantioselectivity recognition property, besides, we could find some interesting catalytic applications and relationship between flexibility and catalytic activity or between flexibility and recognition properties.

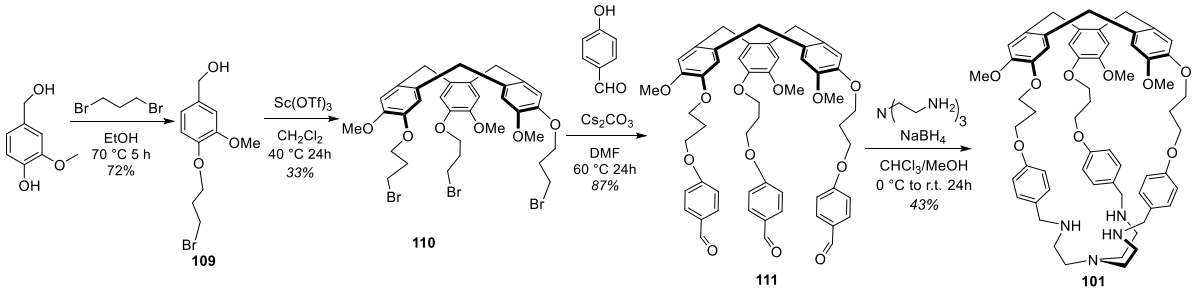

Figure 4.2.3 Synthesis of hemicryptophane **101.**

4.2.2 Resolution of the racemic mixtures and assignment of absolute configuration of the resulting enantiopures hemicryptophanes

Normally, a convenient way based on determination of X-ray structure analysis could be considered to know the absolute configuration of enantiopure hemicryptophane, but sometimes it was difficult to get the expecting crystals.[150] Electronic circular dichroism (ECD) spectra, on the other hand, has been widely considered in the literature as the essential and suitable way to determine the absolute configuration of hemicryptophane bearing CTV unit. Indeed, the spectra can be interpreted as the result of the excitonic coupling of the three aromatic rings of the CTV unit, which gives a specific ECD signature.[151]

4.2.2.1 Assignment of absolute configuration of hemicryptophanes 100

In order to determine the absolute configuration of enantiopure hemicryptophanes, we firstly turned our attention on the resolution of the racemic mixture **108,** and the assignment of the absolute configuration of enantiopure **108**. The racemic mixture **108** was resolved by semi preparative chiral HPLC on Chiralpak IG column (250*10 mm), Hexane/EtOH/CH_2Cl_2 (40/30/30) was used as mobile phase. Finally, we obtained the two enantiomers *(P)*-**108** / *(M)*-**108** (ee is more than 99% for each enantiomer). Then, ECD and UV spectra of two enantiomers were recorded, as depicted in Figure 4.2.4. Optical rotation calculations have been measured

[150] *Zhang, W. Z. et etc. Eur. J. Org. Chem. 2015, 2015, 765−774.*

[151] *Canceill, J. et etc. J. Am. Chem. Soc. 1985, 107, 1299−1308, Freedman, T. B.; Chirality 2003, 15, 743−758.*

on a 241nm Perkin-Elmer polarimeter with a mercury lamp (589, 578, 546, 436, 405 and 365 nm), as table 4.2.1, The absolute configuration of the *(P)*-**108** / *(M)*-**108** was assigned by comparing the sign of the bands of the experimental ECD spectrum around the ^1L_A transition with those of the calculated ECD spectrum, because these signs are poorly sensitive to the substituent effect in the ^1L_A transition area, they are usually compared with the calculated ECD spectra of a reference CTV, previously obtained by Collet and co-workers.[151]

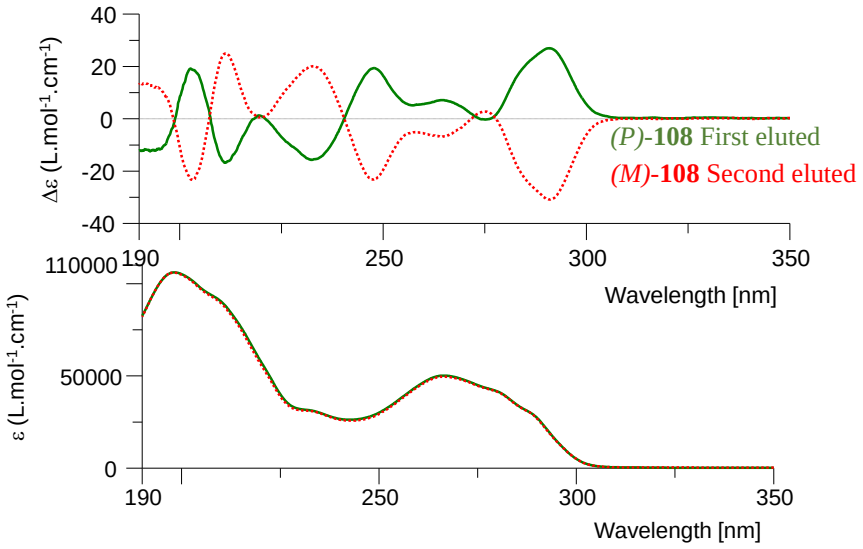

Figure 4.2.4 Experiment EDC and UV spectra in CH_3CN at 25 ^{0}C of *(P)*-**108** / *(M)*-**108**; Green: first eluted enantiomer *(P)*-**108** (c=0.17 mmol·L^{-1}); Red: second eluted enantiomer *(M)*-**108** (0.17 mmol·L^{-1})

Based on these previous works, it is clear that two enantiomers have two characteristic sequent negative-positive signals from higher to lower energies,[152] then a *P*-configuration is assigned, otherwise a *M*-configuration. In our case, the first eluted enantiomer corresponds to the (*P*)-configuration (*P*-**108**), the second eluted enantiomer corresponds to the (*M*)-configuration (*M*-**108**).

λ(nm)	**first eluted on Chiralpak IG** $[a]_\lambda^{25}$ **(CH_2Cl_2, c =0.18)**	**second eluted on Chiralpak IG** $[a]_\lambda^{25}$ **(CH_2Cl_2, c =0.23)**
589	+ 161	- 161
578	+ 170	- 170
546	+ 200	- 200
436	+ 400	- 400
405	+ 550	- 550
365	+ 925	- 925

Table 4.2.1 Optical rotations measured on a 241 Perkin-Elmer polarimeter with a mercury lamp.

[152] *J. Canceill, A. Collet, G. J. Am. Chem. Soc. 1987, 109, 6454.*

Enantiopure hemicryptophane **100** was obtained by next experiment (Figure 4.2.5): the ligand tren was introduced in a solution of *(P)*-**108** or *(M)*-**108** in MeOH/$CHCl_3$, respectively, sodium borohydride was added at 0 ºC, after four hours, the *(P)*-**100** / *(M)*-**100** were isolated by column chromatography (yield: 39% for each enantiopure hemicryptophane **100**).

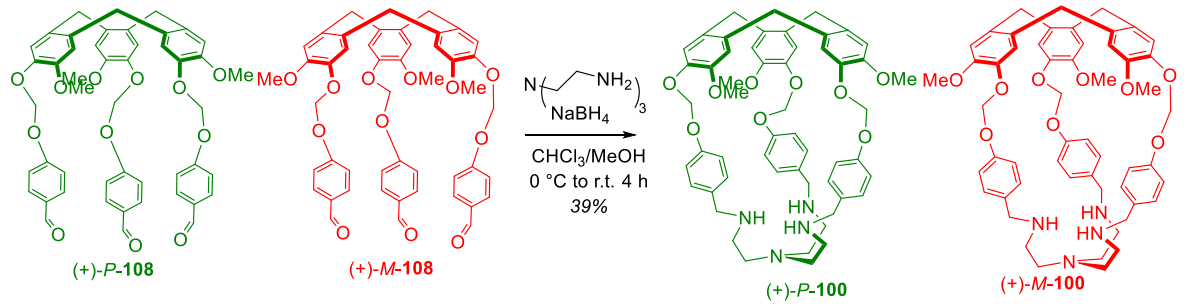

Figure 4.2.5 Synthesis of enantiopure hemicryptophane **100**.

4.2.2.2 Assignment of absolute configuration of hemicryptophanes 101

Two enantiomers of CTV-**111** were obtained by the same way: racemic compound was dissolved in a mixture solution of dichloromethane and ethanol, separated by Chiralpak IF (250 x 10 mm) column, two enantiomers *(P)*-**111** / *(M)*-**111** were isolated as first or second eluted fraction. ECD and UV spectra are showed in Figure 4.2.6, table 4.2.2 shows the optical rotations measured on a 241 nm Perkin-Elmer polarimeter with a mercury lamp (589, 578, 546, 436, 405 and 365 nm). After compared with the known absolute configuration of CTV, the first eluted enantiomer is assigned for (*P*)-**111** (ee is more than 99%) the second eluted enantiomer is assigned for (*M*)-**111** (ee is more than 99%).

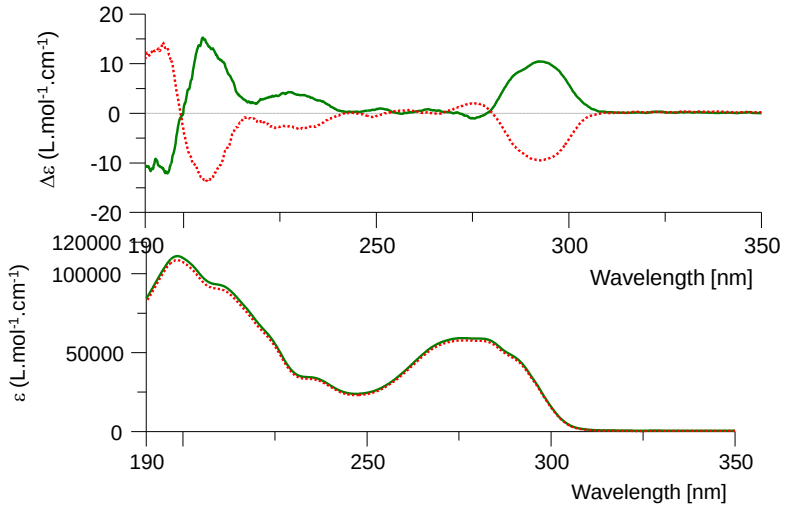

Figure 4.2.6 Experiment EDC and UV spectra in CH_3CN at 25 ^{0}C of 3; Green: first eluted enantiomer ***P*-111** (c=0.17 mmol.L^{-1}); Red: second eluted enantiomer ***M*-111** (0.17 mmol.L^{-1})

λ (nm)	first eluted on Chiralpak IF [a]λ_{25} (CH_2Cl_2, c =0.16)	second eluted on Chiralpak IF [a]λ_{25} (CH_2Cl_2, c =0.18)
589	+ 45	- 45
578	+ 48	- 48
546	+ 58	- 58
436	+ 109	- 109
405	+ 147	- 147
365	+ 250	- 250

Table 4.2.2 Optical rotations measured on a 241 Perkin-Elmer polarimeter with a mercury lamp.

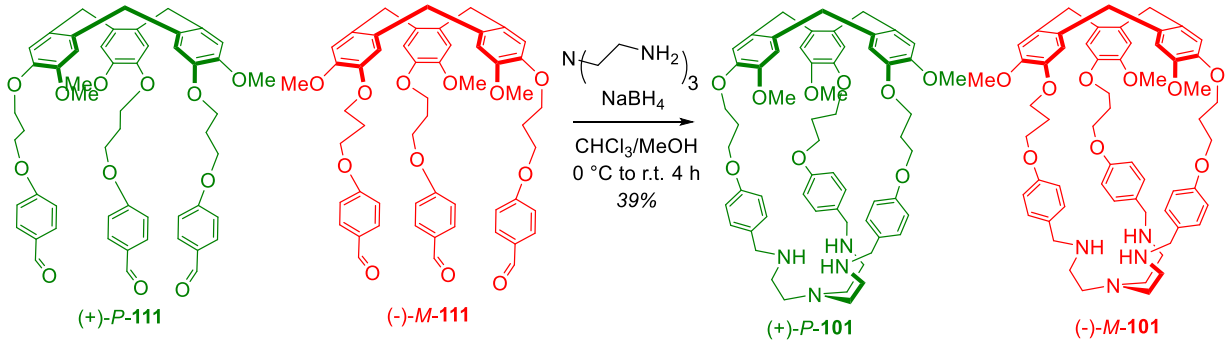

Figure 4.2.7 Synthesis of enantiopure hemicryptophane **101**.

We could isolate the enantiopure hemicryptophane **101** by carefully treated the experiment (same procedure with **100**): the reaction of tren and enantiomers *(P)*-**111** / *(M)*-**111**. The synthesis of enantiopure hemicryptophane **101** is shown in Figure 4.2.7.

4.2.3 Enantioselective recognition properties of hemicryptophanes 100 and 101

The C_3-symmetrical hemicryptophanes bearing a tris (2-aminoethyl) amine (tren) ligand exhibit substrate-, diastereo-, and enantioselective recognition properties toward neurotransmitters and carbohydrates.[153] Moreover, encaged azatrane structures can be formed when a metal or heteroelement is introduced into the tren unit. For instance, the cupric complex is shown to display remarkable properties in C-H oxidation.[154] In our cases, we did not explore metal complex part, instead, inspired by the enantiopure properties of hemicryptophanes, we focused on the enantioselectivity of neurotransmitters, such as norephedrine and ephedrine,

[153] *A. Schmitt, et etc. Org. Lett. 2014, 16, 2374. / D. Zhang, et etc. Chem. Commun. 2015, 51, 2679.*

[154] *O. Perraud, et etc. Chem. Commun. 2013, 49, 1288.*

they are seen as guests, and the enantiopure hemicryptophanes **100** and **111** are as hosts. Thus, we investigated their stereoselective recognition properties.

Hemicryptophane *(P)*-**100** / *(M)*-**100** and *(P)*-**101** / *(M)*-**101** remains enantiopure, because the energy barrier for the interconversion process of the CTV was evaluated from kinetics of racemization by S. Lefevre and coworkers.[24] They found an energy barrier of 112.7 kJ/mol at 78 ºC in ethanol, this value is consistent with those previously reported for other CTV derivatives.[155] In the much less polar solvent chloroform, a similar energy barrier of 112.5 kJ/mol was measured. It reveals that the polarity of the solvent has little effect on energy barrier. Subsequent reactions have to be performed at room temperature to avoid racemization. Figure 4.2.5 and Figure 4.2.7 show the synthesis of hemicryptophane *(P)*-**100** / *(M)*-**100** and *(P)*-**101** / *(M)*-**101**, the reaction condition is consistent with the results that have been reported by S. Lefevre and coworkers.

We prepared the picrate salts solution of norephedrine and ephedrine in chloroform/menthol (95:5), the concentration was 0.5 mM, then we prepared a solution of hemicryptophane *(P)*-**100** / *(M)*-**100** and *(P)*-**101** / *(M)*-**101** in chloroform/menthol (95:5), respectively, the concentration was 5 mM. In order to make the all products totally dissolved, we added 5% methanol into the solution. The recognition properties of hemicryptophane *(P)*-**100** / *(M)*-**100** and *(P)*-**101** / *(M)*-**101** toward norephedrine and ephedrine were studied by ^{1}H NMR titration experiments. In all cases, three set of signals (protons from guests) are observed for the complex and receptor, which indicates fast exchange on the ^{1}H NMR spectroscopy timescale. Three set of signals (proton from guests) were up-fielded upon progressive addition of the host. Shielding induced by the aromatic units of the host upon encapsulation could account for this experimental result. Complexation-induced shifts of the aliphatic protons (-CH_3) of norephedrine and ephedrine were plotted as a function of the guest/host ratio, and the resulting curves were fitted with the Bindfit software by using a 1:1 host/guest model. The binding constants, K_a, were determined by fitting ^{1}H NMR titration curves of the Ha protons of the norephedrine and ephedrine (δ = at 1.0659 and 1.0631 ppm for the two free guest) with Bindfit program, estimated error less than 6% (table 4.2.3).

[155] *J. Canceill, A. Collet, G. Gottarelli, J. Am. Chem. Soc. 1984, 106, 5997.*

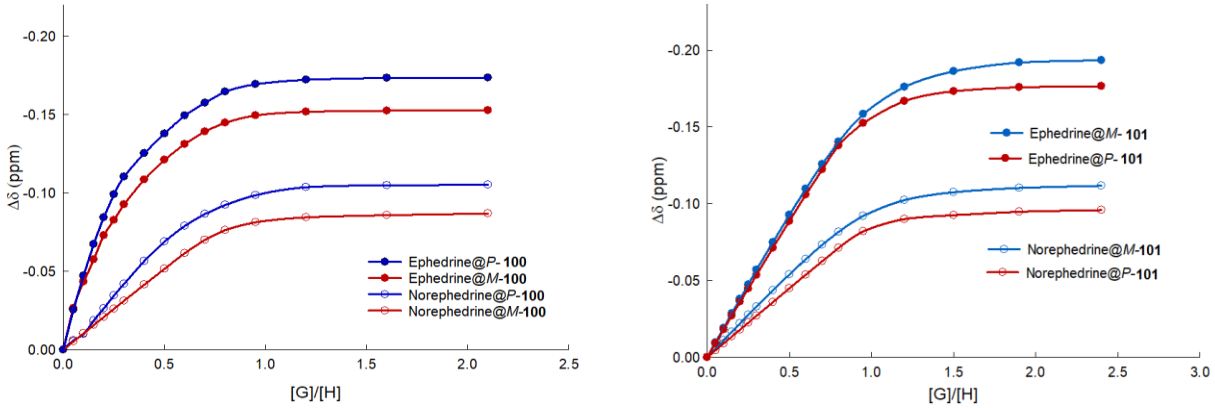

Figure 4.2.8 Titration curves of host *(P)*-**100** / *(M)*-**100** (left) and *(P)*-**101** / *(M)*-**101** (right) (5 mM in $CDCl_3$/MeOH 95:5) to norephedrine and ephedrine (as picrate salts solution of 0.5 mM in $CDCl_3$/MeOH 95:5). The chemical induced shifts Δδ of host's protons were measured and plotted as a function of the [G]/[H] ratio.

As showed in Figure 4.2.8 and Table 4.2.3, the binding constants were very different. The reference binding constants of hemicryptophane **104** toward norephedrine was obtained by HypNMR2008 software, which gave a very high binding constants of 5.1×10^6 and 4.9×10^7 for *(P)*-**104** and *(M)*-**104,** while hemicryptophane (*M*)-**100** and (*M*)-**101** toward norephedrine and ephedrine gave low binding constants (58.15 M^{-1}, 60.71 M^{-1}, and 143.25 M^{-1}), except for (*M*)-**101** toward ephedrine (2714.58 M^{-1}) (obtained by BindFit software). To control if this difference was related to the software (Bindfit or HypNMR2008), the data that obtained from the model titration curves (hemicryptophane **104**) have been also fitted with the Bindfit software, and similar values to those obtained with HypNMR2008 were calculated. Hemicryptophane (*P*)-**100** gave binding constants 897.02 M^{-1} and 194.86 M^{-1} (toward norephedrine and ephedrine), respectively, whereas (*P*)-**101**, gave binding constants 1093.53 M^{-1} and 1338.18 M^{-1}(toward norephedrine and ephedrine) respectively.

	Norephedrine	Enantioselectivity[c]	Host/Guest	Ephedrine	Enantioselectivity
(P)-**104**[a]	5.1×10^6	0.1:1	1:2	–	–
(M)-**104**[a]	4.9×10^7		1:2	–	
(P)-**100**[b]	897.02	15.5:1	1:1	194.86	3.2:1
(M)-**100**[b]	58.15		1:1	60.71	
(P)-**101**[b]	1093.53	7.6:1	1:1	1338.18	0.5:1
(M)-**101**[b]	143.25		1:1	2714.58	

Table 4.2.3 Binding constants of the hemicryptophane *P/M*-**100** and *P/M*-**101** toward norephedrine and

ephedrine. [a] Reference binding constants were obtained with HypNMR2008 software; unit [M^{-2}]; estimated error 10%. [b] host/guest =1:1; [c] Ratio of two enantiomer hemicryptophanes (*P/M*).

It is difficult to compare hosts **104**, **100** and **101**, because the host/guest stoichiometry of the recognition processes is 1:2 for the former and 1:1 for the latters. **100** displays higher enantioselectivity than host **101**, for example, the enantioselectivity of (*P*)-**100** and (*M*)-**100** toward norephedrine is 15.5:1, while the enantioselectivity of (*P*)-**101** and (*M*)-**101** toward norephedrine is 7.6:1. Perhaps it is due to higher flexibility of hemicryptophane **101,** the more rigid cage **100** leading to more selective host-guest interactions.

4.2.4 Synthesis and discussion of Verkade's superbase in confined space

Since 2011, the synthesis of first Verkade's superbase encapsulated in a covalent hemicryptophane was achieved, so far, its basicity, catalytic activity, and recognition of chiral azides were studied. Confined azaphosphatranes, the conjugated acid of verkade's superbase, were also reported. In our cases, we regarded hemicryptophane **100** and hemicryptophane **101** as receptors to provide encaged azaphosphatrane **102-H$^+$·Cl$^-$** and **103-H$^+$·Cl$^-$** and proazaphosphatrane **102** and **103**.

4.2.4.1 Synthesis and discussion of encaged Verkade's superbase 102-H$^+$

Hemicryptophane **100** was added to a solution of bis(dimethylamino)chlorophosphine in anhydrous dichloromethane, the procedure is shown in Figure 4.2.9, and leads to the expected compound **102-H$^+$** in a very high yield. The ^{31}P NMR spectrum displays a signal at around -32 ppm, while the ^{31}P CPD NMR spectrum gives a doublet signal of P-H, because of the coupling between P-H. Normally, as we did for the azaphosphatranes **12-H$^+$**, (see **Chapter 2**), the subsequent deprotonation using potassium *tert*-butoxide as a base would generate the proazaphosphatranes directly. In this case, the confined superbase **102** should have been obtained. However, after numerous attempts, for instance by increasing times (from hours to weeks), temperature (from r.t. to reflux), we were unable to deprotonate this encaged azaphosphatrane. Makita and coworkers have already reported an encaged proazaphosphatrane in a hemicryptophane even smaller than **102**,[156] and they were also unable to deprotonate it. So we think that isolating the corresponding proazaphosphatrane **102** is very challenging, even

[156] *Y. Makita, et etc. Ogawa, Tetrahedron Lett. 2011, 52, 4129–4131.*

impossible, probably because of the shielding effects of the aromatic linkers and the small size of cavity; based on the ^{31}P NMR, as we described before, the chemical shift was around -32 ppm, it is high-fielded, compared to the normal phosphorus chemical shift of azaphosphatranes, for example, **12-H$^+$**, (n=a, b. c, d, e, in **chapter 2**), their ^{31}P NMR resonances show at around -12 ppm, even the hemicryptophane **30-H$^+$** (the classical hemicryptophane), the ^{31}P NMR resonance at around -26 ppm in CD_2Cl_2, these chemical shifts, to some extent, could account for this unusual situation.

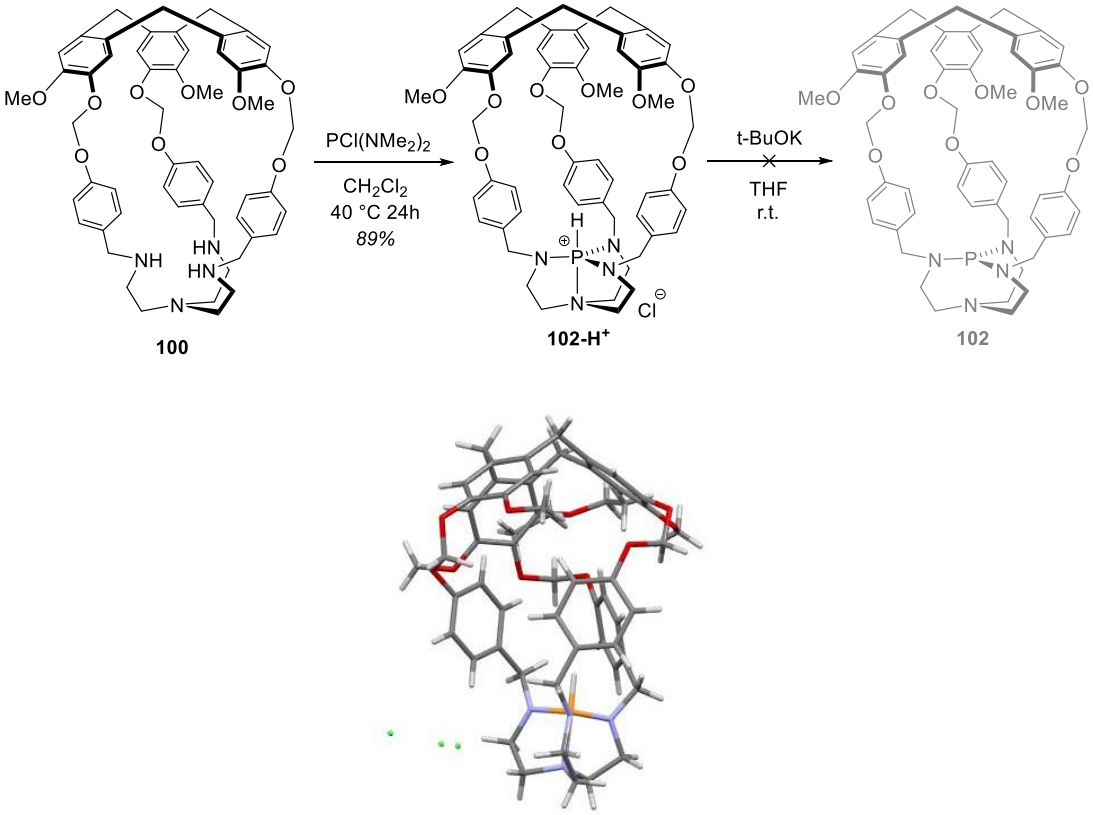

Figure 4.2.9 Synthesis of encaged azaphosphatrane **102-H$^+$** and its solid state.

Despite the failure in the deprotonation step, **102-H$^+$** is still the conjugated acid of the superbase base **102**. The solid structure of it was well defined, presenting a perfect C_3 symmetry (Figure 4.2.9). We find one interesting application for this azaphosphatrane, **102-H$^+$** (10 mol%, Figure 4.2.10) was used as a catalyst to get the formation of cyclic carbonates from CO_2 and epoxides, it was found to be the efficient catalyst, leading to the yield of around 90%. We haven't explored more on this part, but there is no doubt that a catalytic amount of **102-H$^+$** could be as an excellent catalyst in carbon dioxide conversion experiment.

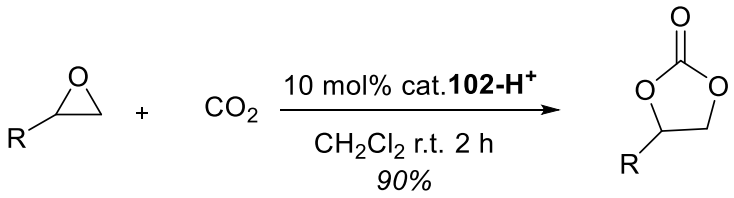

Figure 4.2.10 Conversion of carbon dioxide into cyclic carbonates catalyzed by **102-H**$^+$.

4.2.4.2 Synthesis and discussion of encaged Verkade's superbase 103

The synthesis of confined space hemicryptophane **103-H**$^+$ was a little complicated compared to the **102-H**$^+$, because the reaction in acetonitrile yielded one byproduct **103-PH=O**, while in dichloromethane, only **103-H**$^+$ was isolated. The procedure is shown in Figure 4.2.11: to a solution of bis(dimethylamino)chlorophosphine in acetonitrile was added a solution of hemicryptophane **101** in acetonitrile under argon condition in a dry flask, byproduct **103-PH=O**, which is devoided of C_3 symmetry, like we described in **Chapter 2** for the hemicryptophane **94-PH=O**, was isolated (yield 39%). We assumed that there was some moisture inside the dry acetonitrile, who gave this compound. When we changed the solvent to dry dichloromethane, we did not observe the similar structure, only **103-PH**$^+$ was isolated (yield 84%).

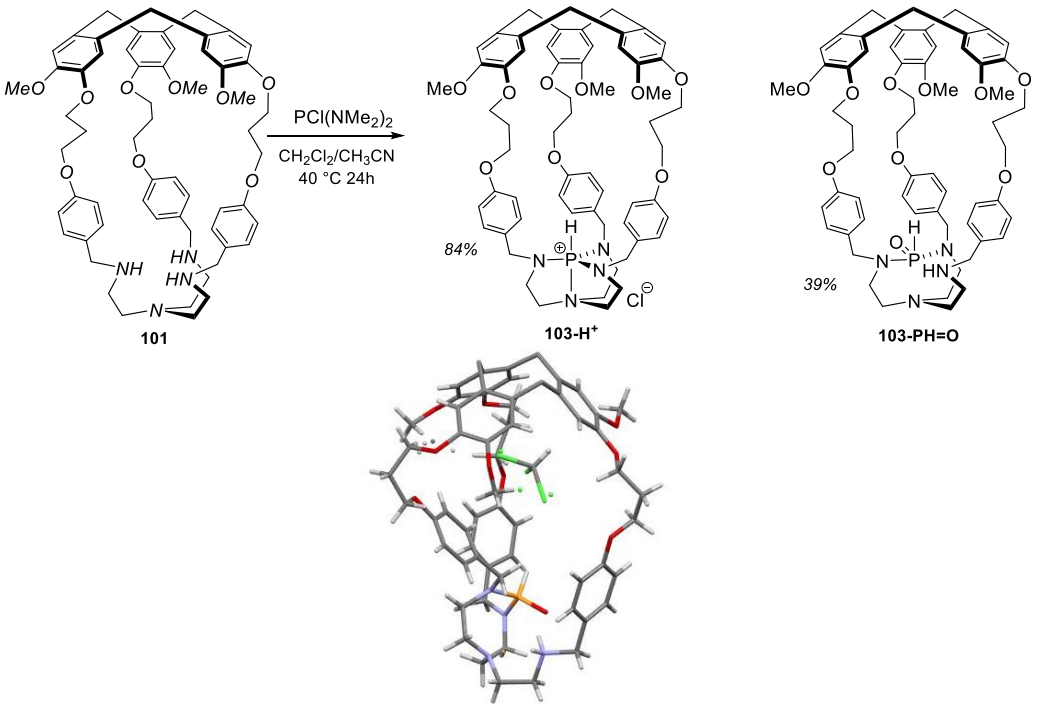

Figure 4.2.11 Synthesis of encaged azaphosphatrane **103-H**$^+$; solid state of **103-PH=O**.

In our previous works dealing with hemicryptophanes including aromatic rings in their linkers,[157] we never observed encaged compound like **103-PH=O**. Based on the ^{31}P CPD NMR spectrum, the chemical shift was around 15 ppm, and a doublet pick (coupling with hydrogen) in $CDCl_3$. The solid state of **103-PH=O** is showed in Figure 4.2.11, phosphorus is getting inside the cavity of **103**, but grabbed only two nitrogen, perhaps it is the reason why **103-PH=O** presents C_3 asymmetry.

Due to the inherent chirality of CTV-**111,** hemicryptophane **103-PH=O** still remains chiral, probably, it will be of potential interest in the asymmetric allylic alkylation of allylic carbon, we found the similar model (S,R_P)-DIAPHOXs **105**,[158] the procedure is shown in figure 4.2.12. We have not explored this part yet, but it will be our next goal to test this reaction, as it is promising to give enantiopure products (s)-**106** and **107** in the presence of catalyst **103-PH=O** as chiral ligand.

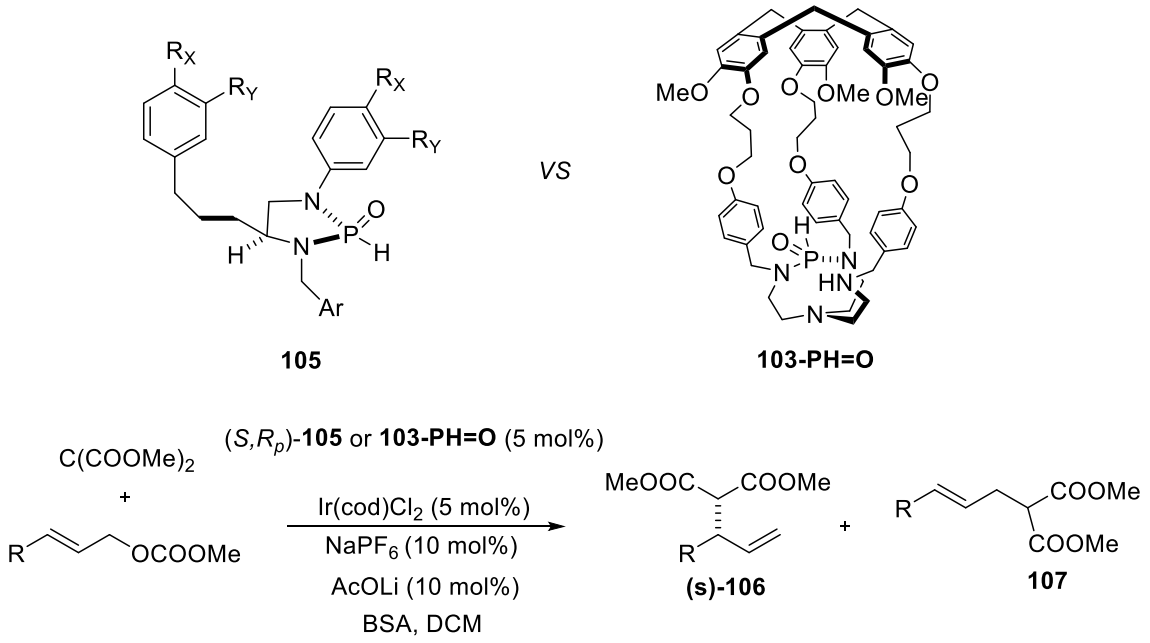

Figure 4.2.12 Attempts to perform the asymmetric allylic alkylation of allylic carbon by using **103-PH=O** as catalyst**.**

For **103-H**$^+$, in the ^{31}P NMR and ^{31}P CPD NMR spectra, a signal at around -23 ppm and a doublet pick appear in $CDCl_3$. When we used potassium *tert*-butoxide to deprotonate the **103-H**$^+$ in a mild condition (Figure 4.2.13), it was working well. We obtained **103** with a good yield (85%), the chemical shift was around 115 ppm in the ^{31}P NMR spectra in toluene-d_8. The results

[157] *Chatelet, Bastien et al.J. Am. Chem. Soc. 135 49 (2013): 18659-64.*

[158] *Nemoto, T. et etc. Tetrahedron Lett. 2007, 48, 4977-4981.*

of thermodynamic and kinetic experiments related to proton transfer demonstrated the pK_a of **103** is 32.32 (see in table 4.2.4), which corresponds to a very basic system.

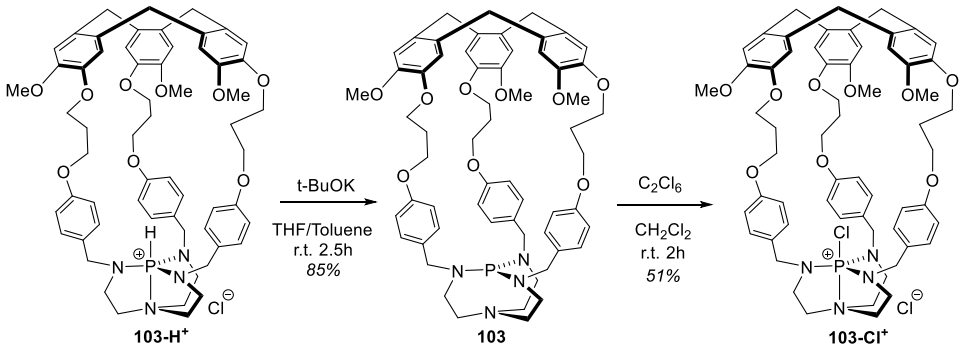

Figure 4.2.13 Synthesis of Verkade's superbase **103**.

Haloazaphosphatrane in confined space, as mentioned in **Chapter 2**, was also explored in this chapter (Figure 4.2.13). We would like to use hemicryptophane **102** to study **102-Cl**$^+$ as halogen bonding system, but as we described, hemicryptophane **102-H**$^+$ was too difficult to deprotonate by potassium *tert*-butoxide, so we could not study further on it. Encaged proazaphosphatrane **103** was considered to be a motif to expand the knowledge of XB. Br_2 and I_2 were introduced in the solution of **103** in ether or dichloromethane, respectively, but only **103-H**$^+$ was isolated. Following the classical procedure for the synthesis of chloroazaphosphatranes (as present in **chapter 2**), using hexachloroethane as the chloro-resource in mild condition, **103-Cl**$^+$ was generated with a good yield (51%). The studies of its recognition and catalytic properties will be one of our next goals.

Previous works have been done in our group, showing that encaged proazaphosphatrane **30** is an endohedrally functionalized tool to create Frustrated Lewis Pairs.[159] Lewis base was entrapped in the cage structure, the confinement of the Verkade's superbase in the cavity of an encaged proazaphosphatrane **30** host prevent the Lewis acid-base reaction with the titanium chloride to take place. Thus, an efficient system for the Morita-Baylis-Hillman reaction was provided where both partners (Verkade's superbase and titanium chloride) could act in concert without neutralizing each other.

[159] *J. Yang et etc. Angew. Chem. Int. Ed. 2018, 57, 14212 –14215.*

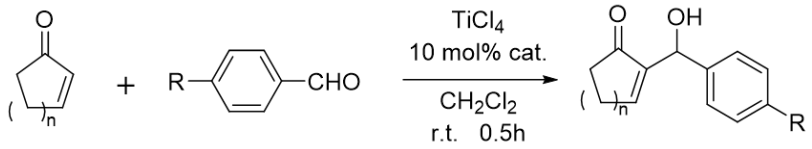

Figure 4.2.14 The Morita Baylis Hillman reaction catalyzed by different systems.

Entry	n	R	Superbase	Yield (%)[b]
1	1	Cl	**12d**	15[a]
2	1	Cl	**30**	75[a]
3	1	Cl	**103**	72
4	2	Cl	**12d**	8[a]
5	2	Cl	**30**	63[a]
6	2	Cl	**103**	71
7	1	CH_3	**12d**	11[a]
8	1	CH_3	**30**	44[a]
9	1	CH_3	**103**	51
10	2	CH_3	**12d**	11[a]
11	2	CH_3	**30**	48[a]
12	2	CH_3	**103**	66
13	1	NO_2	**12d**	10[a]
14	1	NO_2	**30**	55[a]
15	1	NO_2	**103**	55
16	2	NO_2	**12d**	29[a]
17	2	NO_2	**30**	81[a]
18	2	NO_2	**103**	86

Table 4.2.4 Reaction conditions: Aldehyde (0.3 mmol), enone (0.9 mmol), catalyst (0.03 mmol, 10 mol%), $TiCl_4$ (1M in DCM, 0.3 mmol), CH_2Cl_2 (1.0 mL), 30 min under an atmosphere of argon. [a] obtain from reference; [b] Isolated yield.

In our case, encaged proazaphosphatrane **103** was more flexible compared to the encaged proazaphosphatrane **30** (Figure 4.1.2). We compared the ability of **103** and **30** to behave as FLP systems: the catalytic properties of the FLP system **103**/$TiCl_4$ and **30**/$TiCl_4$ in the MBH reaction between cyclohexenone and *p*-chlorobenzaldehyde (Figure 4.2.14). Indeed, we have

previously demonstrated that very low yield is obtained with the model **12d**/$TiCl_4$ system: an interaction followed by a reaction between the two Lewis acid/base partners and lead to the chloroazaphosphatrane that is devoid of any catalytic activity. This reaction is prevented with the **30**/$TiCl_4$ system, allowing for restoring catalytic activities. Thus, we decided to use this reaction as a probe to test if the pair **103**/$TiCl_4$ also behaves as a FLP system. Surprisingly, the **103**/$TiCl_4$ pair presents a catalytic activity much higher than that of the **12d**/$TiCl_4$ system and, more interestingly, better than the **30**/$TiCl_4$ one : yields of 77%, 8% and 63 % were reached respectively with **103**/$TiCl_4$, **12d**/$TiCl_4$, **30**/$TiCl_4$ and *p*-chloro-benzaldehyde as reactant (entries 2, 3, 4), and yields of 11%, 48% and 66% were achieved with **12d**/$TiCl_4$, **30**$TiCl_4$, **103**/$TiCl_4$ respectively using *p*-methyl-benzaldehyde as an electrophile.

However, a ^{31}P NMR spectrum of the crude mixture of the MBH reaction evidenced the formation of some **103-Cl**$^+$ compound (^{31}P NMR spectra at -18.89 ppm). It can be noticed that such compound was not detected when **30** was tested under the same conditions. This demonstrates that the **30**/$TiCl_4$ pair constitutes a "true" FLP system, whereas the **103**/$TiCl_4$ one is not fully frustrated, since some reactions between the Lewis acid-base partners occur giving the chloroazaphosphatrane derivative. However, this latter is the more efficient Lewis acid/base pair in the MBH reaction, probably because it presents the right balance between (i) the flexibility that allows for accommodating more easily the substrates and (ii) the frustrated behavior to prevent in part the Lewis acid-base interaction. Thus, although the **103**/$TiCl_4$ system is not as frustrated as the **30**/$TiCl_4$ one, it presents a better catalytic activity, since its flexibility favored more the interaction and subsequent reaction with the MBH substrates than with $TiCl_4$.

4.2.5 Thermodynamic and kinetic studies on hemicryptophanes

As we described, we attempted to deprotonate the encaged azaphosphatranes in order to obtain the enclosed superbases **102** and **103** and to measure the pK_a values. **103** was easily deprotonated with potassium *tert*-butoxide in THF, according to the classical procedure that described by Verkade, a signal at +115 ppm was observed in the ^{31}P NMR spectrum as expected for proazaphosphatrane derivatives. The pK_a value was estimated using previous published procedure: addition of the **103** to a solution of the model Verkade's superbase **12a** in CD_3CN, once the thermodynamic equilibrium was reached, a pK_a value of 32.32 was calculated by the data that were from the ^{31}P NMR spectra (Figure 4.2.15, eq. 1), lower than that of cage **30** (pKa = 32.99, classical cage) and slightly higher than that of its model parent **12d** (pKa = 32.14,

Table 4.2.4). The more important flexibility of **103** could account for this less marked effect of the confinement on the basic properties of the encapsulated Verkade's superbase. Indeed, the higher basicity of **30**, when compared to its model parents **12d,** was attributed to the stabilization of its conjugated acid **30-H**$^+$ via cation-π interactions between the aromatic rings of the linkers and the cationic azaphosphatrane unit. Such interactions are probably less favored with this larger and more flexible cage **103**.

$$\frac{K_a^{\mathbf{103\text{-}H^+}}}{K_a^{\mathbf{12a\text{-}H^+}}} = \frac{[\mathbf{103}][\mathbf{12a\text{-}D^+}]}{[\mathbf{103\text{-}D^+}][\mathbf{12a}]} = \frac{1\times 1.8953}{0.1586\times 3.1581} = 3.78 \quad (1)$$

$$with \quad K_a^{\mathbf{12a\text{-}H^+}} = 1.26\times 10^{-33}$$

$$K_a^{\mathbf{103\text{-}H^+}} = 4.77\times 10^{-33}$$

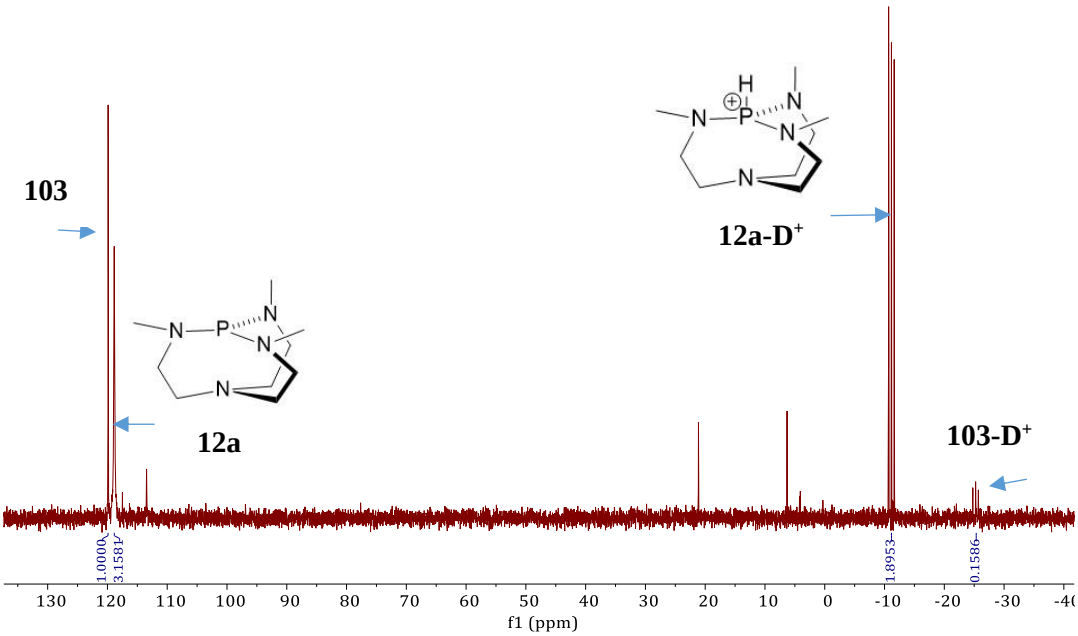

Figure 4.2.15 pKa measure of **103** in ^{31}P NMR spectrum.

The rate of proton transfer was measured (Table 4.2.5 and eq. 2 ad 3). As in the case of **30**, the deprotonation/protonation is much slower with **103** than with its model counterpart **12d**, confirming that the cavity strongly affects the rates of these reactions. The rate constants of deprotonation/protonation of **30** and **103** are in the same order of magnitude, supporting that the phosphorus atom is not easily accessible in **103**. This is also in agreement with the fact that

a FLP system has been obtained with **103** once associated with a Lewis acid, the *K*a of **103** was calculated according to the integrals (Figure 4.2.15) and the eq.1.

As described previously, the same sets of experiments were then carried out with **102·H$^+$**. However, no reaction occurs when potassium *t*-butoxide was mixed with **102·H$^+$** in THF. Increasing the number of equivalents of potassium *t*-butoxide or the temperature let the reaction medium unchanged. We hypothesis that potassium *t*-butoxide is too big to enter inside this smaller cavity, thus we decided to perform this deprotonation using smaller and planar $^-CD_2CN$ anion. **102·H$^+$** and the model compound **12d** were solubilized in CD_3CN in an NMR sealed tube, and the reaction mixture was left standing for several weeks, but no reaction took place even after heating for days. Thus, a slight shortening of the cavity size obtained by removing only one methylene in each linker, prevented the acid-base reaction, providing Frustrated Bronsted pairs. This highlights how a simple tuning of the cavity size can strongly affect the reactivity properties of the encaged Bronsted bases.

Base	pK_a	K_a	k_1 (L mol^{-1} s^{-1})	k_{-1} (L mol^{-1} s^{-1})
12a	32.90[a]	1.26 × 10^{-33}	-	-
12e	32.14[a]	7.25 x 10^{-33}	1.06 x 10^{-3}	0.93 x 10^{-3}
102	-	-	-	-
30	32.99[a]	1.03 x 10^{-33}	1.88 x 10^{-6}	1.16 x 10^{-5}
103	32.32	4.77 x 10^{-33}	1.04 x 10^{-6}	1.37 x 10^{-6}

Table 4.2.5 pKa values of conjugate acids of proazaphosphatrane bases in CH_3CN and rate constants values for proton transfers (T = 298 K). [a] known binding constants.

Rate constants of proton exchange of 103-H$^+$

$$\mathbf{103\text{-}H^+} + CNCD_2^- \overset{k_1/k_{-1}}{\Longleftrightarrow} \mathbf{103} + CNCHD_2 \qquad (2)$$

$$\mathbf{103} + CNCD_3 \overset{k_2/k_{-2}}{\Longleftrightarrow} \mathbf{103\text{-}D^+} + CNCD_2^- \qquad (3)$$

$$-\frac{d([\mathbf{103\text{-}H^+}])}{dt} = k_1[\mathbf{103\text{-}H^+}][CD_2CN^-] = +\frac{d([\mathbf{103}])}{dt}$$

$$\frac{d\left(\frac{[\mathbf{103}]}{[\mathbf{103}\text{-}H^+]}\right)}{dt} = \frac{\frac{d[\mathbf{103}]}{dt}[\mathbf{103\text{-}H^+}] - \frac{d[\mathbf{103\text{-}H^+}]}{dt}[\mathbf{103}]}{([\mathbf{103\text{-}H^+}])^2}$$

$$= k_1[\mathrm{CD_2CN^-}] + \frac{k_1[\mathrm{CD_2CN^-}][\mathbf{103}]}{[\mathbf{103\text{-}H^+}]}$$

$$= k_1[\mathrm{CD_2CN^-}]\left(1 + \frac{[\mathbf{103}]}{[\mathbf{103\text{-}H^+}]}\right)$$

$$\textit{with} \quad [CD_2CN^-] = \frac{\mathrm{K_e}}{\mathrm{K_a^{12a\text{-}H^+}}} \frac{[\mathbf{12a}]}{[\mathbf{12a\text{-}H^+}]}$$

$$\rightarrow \frac{\mathrm{d}\left(\frac{[\mathbf{103}]}{[\mathbf{103\text{-}H^+}]}\right)}{\mathrm{dt}} = \frac{k_1 \mathrm{K_e}}{\mathrm{K_a^{12a\text{-}H^+}}} \times \frac{[\mathbf{12a}](1 + [\mathbf{103}]/[\mathbf{103\text{-}H^+}])}{[\mathbf{12a\text{-}H^+}]}$$

$$\textit{and} \qquad k_{-1} = \frac{\mathrm{K_e} k_1}{\mathrm{K_a^{103\text{-}H^+}}}$$

4.3 Conclusion

In this chapter, we synthesized two new hemicryptophanes, their resolution was performed and recognition properties were studied. Then the thermodynamic and kinetic of the proton transfer of the corresponding encaged azaphosphatrane was studied. A strong encaged Verkade' super base (**103**) and a frustrated Bronsted pair (**102-H$^+$/t-BuOK**) was obtained. The ability of endohedrally functionalized cages to control the frustration level of acid/base couples has been investigated. A simple change of one methylene group in the linkers allows for controlling the reactivity of the encaged basic unit. Indeed, the smaller cage lead to an extremely frustrated system that even prevents its deprotonation, giving fully frustrated Bronsted pairs **102-H$^+$**/*t*-BuOK and **102-H$^+$**/$^-$$CD_2CN$. In contrast, the medium and large cages can be easily deprotonated under the same conditions. In presence of $TiCl_4$ Lewis acid, both the medium and large cages **30** and **103** lead to FLP. Nevertheless, the **103**/ $TiCl_4$ system provides a better yield in the MBH reaction, underling that if rigidity is key to prevent the Lewis acid/base interaction, some flexibility has to be retained to induce an improvement of the reactivity. Thus, the confinement in well-defined molecular cages appears as an efficient tool to control the degree of frustration of the acid and the base, opening the way to a wider use of this strategy to modulate FLP systems.

General Conclusion

In this manuscript, we introduced some interesting applications for proazaphosphatranes and azaphosphatranes, we synthesized some derivatives to complement the system of proazaphosphatranes and azaphosphatranes, and we expanded the concept of halogen bonding into proazaphosphatrane and confined proazaphosphatranes.

Firstly we synthesized chloroazaphosphatranes as another halogen bond donors, we explored the anion binding properties by using five chloroazaphosphatranes as anion receptors and tetrabutylammonium salts as guests. We determined the pK_a of news proazaphosphatranes and calculated the binding constants through the titration experiments, even the values are modest, we still inspired by these halogenazaphosphatranes, we may use other guests to explore the anion binding properties with different solvent, also we could focus on the catalysis of these chloroazaphosphatranes, such as in Diels-Alder reaction, halogen abstraction and Michael addition.

Secondly, in order to maintain the stable chloroazaphosphatranes, we designed the encaged chloroazaphosphatranes, but to our surprise, we obtained the unusual hemicryptophanes presenting C_1 symmetry structure, this is the first time that C_1 symmetry hemicryptophanes are reported, it gave us the inspiration that how to synthesize C_1 symmetry hemicryptophanes. Beside, we fond other ways to synthesize C_3 symmetry hemicryptophanes, thus in this part, we will continue to work on, for example, the recognition properties of C_1 and C_3 symmetry hemicryptophanes, it is interesting to compare given their different cavities.

Finally, we perfect the system of endohedrals functionalized cages by synthesized other two hemicryptophanes, we just increased or decreased one methylene on the linkers, we found that the steric hindrances of hemicryptophanes can strongly effect on their properties, when decreased on methylene, the Bronsted acid is isolated and it is impossible to make the deprotonation, we never observed the corresponding encaged proazaphosphatranes. Instead, when increased one methylene, the cage is more flexible, it is shown as an efficient organocatalyst in MBH reaction in the presence of $TiCl_4$.

Experimental section

General information

All reactions were performed under inert atmosphere of dry argon if necessary. ^{1}H and ^{13}C NMR spectra were recorded on a Brucker AC 400 (400 MHz for 1H NMR, 100 MHz for 13C NMR), Brucker AC 300 (300 MHz for 1H NMR, 75 MHz for 13C NMR), Bruker 500 MHz HD (500 MHz for 1H NMR) and Bruker Avance III – 600 MHz (600 MHz for 1H NMR) spectrometers. Chemical shifts were reported in ppm on the δ scale relative to residual $CHCl_3$ (δ = 7.26 for ^{1}H NMR and δ = 77.16 for ^{13}C NMR) and CH_3CN (δ = 1.94 for ^{1}H NMR and δ = 1.32 and 118.26 for ^{13}C NMR) as the internal references. Coupling constant (J) are reported in Hertz unit (Hz). Multiplicities are described with standard following abbreviations: s = singlet, br = broad, d = doublet, t = triplet, q = quadruplet, m = multiplet. Column chromatographies were performed with gel 60 (Macherey-Nagel® Si 60, 0.040-0.063 mm). Analytical thin layer chromatography (TLCs) were carried out on Merck®Kieselgel 60 F254 plates and achieved under a 254 nM UV light, visualized with a KMnO4 solution. High-resolution mass spectra (HRMS) were performed on a SYNAPT G2 HDMS (Waters) spectrometer equipped with atmospheric pression ionization source (API) pneumatically assisted. Infrared spectra were recorded on a Bruker TENSOR 27 FourierTransform infrared spectrometer equipped with a single reflection diamond Attenuated Total Reflexion accessory (Bruker A222). Melting points were measured on Büchi Melting Point B-540. Anhydrous dichloromethane and toluene were obtained from the Solvent Purification System BRAUN MB-SPS800. Dry acetonitrile was purchased from chemical suppliers.

Synthesis of the compounds

General procedure for synthesis 12a-e-H$^+$ The reductive amination between the tris (2-aminoethyl) amine (tren) unit **84** and chosen aldehydes **85b-e** followed by a reaction with $PCl(NMe_2)_2$ that provided the azaphosphatranes bearing various substituents on the nitrogen atoms. The compound tris (alkyl or aryl) tren **85** was prepared following a known procedure with modification. To a flame dried round bottom flask were added tris(2-aminoethyl)amine (tren) **84** (1.0 equiv.), the corresponding aldehyde (3.3 equiv.) and MeOH (C = 1.0 mol/L). The reaction was stirred at room temperature for 2 h. Then the reaction was allowed to cool at 0 °C, $NaBH_4$ (3.8 equiv.) was added slowly over a period of one hour. The reaction was allowed to warm to room temperature and stirred for another 2 h. To the crude mixture was added water and extracted three times by Et_2O. The combined organic extracts were washed twice with aqueous HCl (1M). The combined aqueous layers were extracted with Et_2O, and then made basic with solid K_2CO_3 to a pH > 10. The basic aqueous layer was extracted with Et_2O, and the combined organic layers were dried over anhydrous $MgSO_4$, filtered, and concentrated under vacuum to give crude product **85**. The crude product was directly used for the following step. In an ice-bath cooled round bottom flask equipped with a stirring bar, bis(dimethylamino)chlorophosphine (1.2 equiv.) was dissolved in dry acetonitrile (C = 0.48 mol/L), and a solution of **85** (1.0 equiv.) in acetonitrile (C = 1.15 mol/L) was added dropwise. The reaction mixture was stirred at 0 °C under an argon atmosphere for 30 minutes. And then the reaction was heated to 40 °C and stirred overnight. The solvent was removed under reduced pressure to give the crude product, which was purified on silica gel by column chromatography (CH_2Cl_2/MeOH, 90/10) to obtain **12-H$^+$·Cl$^-$**.

N^1-(4-(trifluoromethyl)benzyl)-N^2,N^2-bis(2-((4(trifluoromethyl)benzyl)amino)ethyl)ethane-1,2-diamine **(85e)** Colorless paste; yield: 59% (1.26 g).

^{1}H NMR ($CDCl_3$, 300 MHz) δ = 7.51 (d, *J* = 6.0 Hz, 6H), 7.38 (d, *J* = 9.0 Hz, 6H), 3.80 (s, 6H), 2.82 (br s, 3H), 2.75-2.67 (m, 6H), 2.67-2.58 (m, 6H).

^{13}C NMR ($CDCl_3$, 75 MHz) δ = 143.6, 130.5 (d, J_{FC} = 97.5 Hz), 129.6 (d, J_{FC} = 33.0 Hz), 128.5, 125.5 (q, J_{FC} = 4.5 Hz), 124.2 (d, J_{FC} = 270.0 Hz), 54.0, 53.3, 47.0. ^{19}F NMR ($CDCl_3$, 282 MHz) δ = -62.15.

HRMS (ESI) : *m/z* $[M+H]^+$ calcd for $C_{30}H_{34}N_4F_9$ 621.2634; found : 621.2634.

IR cm^{-1} 3745, 2915, 2859, 1612, 1616, 1458, 1321, 1239, 1208, 1094, 1061, 937, 871, 637, 518.

[*HP(iBuNCH$_2$CH$_2$)$_3$N*][*Cl*] (12b-H$^+$·Cl$^-$) White solid; yield: 77% (2.3 g).

^{1}H NMR ($CDCl_3$, 300 MHz) δ = 5.13 (d, *J* = 501 Hz, 1H), 3.61 (q, *J* = 6.0 Hz, 6H), 3.05 (dt, *J* = 6.0 Hz, 9.0 Hz, 6H), 2.64 (dd, *J* = 6.0 Hz, 18.0 Hz, 6H), 1.80 (sept., *J* = 9.0 Hz, 3H), 0.84 (d, *J* = 6.0 Hz, 18H).

^{13}C NMR ($CDCl_3$, 100 MHz) δ = 55.9 (d, *J* = 13.0 Hz), 47.1 (d, *J* = 7.0 Hz), 39.7 (d, *J* = 6.0 Hz), 27.0 (d, *J* = 4.0 Hz), 19.97.

^{31}P NMR ($CDCl_3$, 120 MHz) δ = -7.91.

[*HP(BnNCH$_2$CH$_2$)$_3$N*][*Cl*] (12c-H$^+$·Cl$^-$) White solid; yield: 81% (748 mg).

^{1}H NMR ($CDCl_3$, 300 MHz) δ = 7.40-7.28 (m, 9H), 7.21-7.12 (m, 6H), 5.79 (d, *J* = 496.6 Hz, 1H), 4.15 (d, *J* = 17.25 Hz, 6H), 3.68 (q, *J* = 5.85 Hz, 6H), 3.11 (dt, *J* = 6.21 Hz, 10.11 Hz, 6H).

^{13}C NMR ($CDCl_3$, 75 MHz) δ = 137.2 (d, *J* = 5.6 Hz), 129.2, 128.2, 127.4, 51.5 (d, *J* = 15.8 Hz), 47.2 (d, *J* = 7.1 Hz), 39.5 (d, *J* = 6.5 Hz).

^{31}P NMR ($CDCl_3$, 120 MHz) δ = -11.89.

[*HP(p-OMe-BnNCH$_2$CH$_2$)$_3$N*][*Cl*] (12d-H$^+$·Cl$^-$) White solid; yield: 12% (4.54 g).

^{1}H NMR ($CDCl_3$, 300 MHz) δ = 7.06 (dt, *J* = 8.6 Hz, 6H), 6.85 (dt, *J* = 8.6 Hz, 6H), 5.78 (d, *J* = 495.7 Hz, 1H), 4.08 (d, *J* = 17.1 Hz, 6H), 3.81 (s, 9H), 3.62 (q, *J* = 5.85 Hz, 6H), 3.04 (dt, *J* = 6.06 Hz, 10.29 Hz, 6H).

^{13}C NMR ($CDCl_3$, 100 MHz) δ = 159.5, 129.1 (d, *J* = 5.0 Hz), 128.8, 114.4, 55.5, 51.0 (d, *J* = 16.0 Hz), 47.1 (d, *J* = 8.0 Hz), 39.3 (d, *J* = 7.0 Hz).

^{31}P NMR ($CDCl_3$, 121 MHz) δ = -12.68.

[*HP(p-CF$_3$-BnNCH$_2$CH$_2$)$_3$N*][*Cl*] (12e-H$^+$·Cl$^-$) White solid; yield: 90% (1.98 g) ; mp 235°C. IR cm^{-1} 3648, 2957, 2859, 2333, 1652, 1489, 1417, 1358, 1221, 1162, 1042, 975, 909, 856, 819, 758, 651, 594, 528.

^{1}H NMR ($CDCl_3$, 300 MHz) δ = 7.61 (d, *J* = 6.0 Hz, 6H), 7.30 (d, *J* = 6.0 Hz, 6H), 5.66 (d, *J* = 495.0 Hz, 1H), 4.25 (d, *J* = 18.0 Hz, 6H), 3.74 (q, *J* = 6.0 Hz, 6H), 3.23 (dt, *J* = 6.0 Hz, 12.0 Hz, 6H).

^{13}C NMR ($CDCl_3$, 75 MHz) δ = 141.2 (d, J_{FC} = 5.2 Hz), 130.6 (d, J_{FC} = 33.0 Hz), 127.6, 126.2 (q, J_{FC} = 3.7 Hz), 124.0 (d, J_{FC} = 270.0 Hz), 50.9 (d, J_{PC} = 16.5 Hz), 47.6 (d, J_{PC} = 6.7 Hz), 39.7 (d, J_{PC} = 6.0 Hz).

^{31}P NMR ($CDCl_3$, 120 MHz) δ = -11.74.

^{19}F NMR ($CDCl_3$, 282 MHz) δ = -62.64.

HRMS (ESI) : *m/z* $[M]^+$ calcd for $C_{30}H_{31}N_4F_9P^+$ 649.2137; found : 649.2136.

General procedure for 12 and 12-Cl$^{+\cdot}$Cl^{-} Under an atmosphere of argon, in a flame-dried Schlenk flask, azaphosphatrane **12-H^{+}.Cl^{-}** (1.0 equiv.) was dissolved in dried CH_2Cl_2 (C = 0.16 mol.L^{-1}), *t*-BuOK (2.1 equiv.) was added, and the reaction mixture was stirred at room temperature for 2 h. Then the solvent was removed under vacuum, and anhydrous toluene (C = 0.075 mol.L^{-1}) was added. The reaction mixture was stirred for another 0.5 h, and then the suspension was filtered under argon through a two-necked fritted glass funnel, then the solvent was removed under vacuum to give pure proazaphosphatrane **12**. The product was directly used for the following step. To a flame-dried Schlenk tube was added freshly prepared proazaphosphatrane 1 (1.0 equiv.), dried CH_2Cl_2 (C = 0.33 mol.L^{-1}), and hexachloroethane (1.02 equiv.); the mixture was stirred under argon at room temperature for 2 h. The solvent was evaporated under vacuum and the residual was washed three times by Et_2O to give the desired product **12-Cl$^{+\cdot}$Cl^{-}**.

[*P(MeNCH$_2$CH$_2$)$_3$N*] (12a) Colorless oil ; the product was directly used for the following step.
^{1}H NMR (toluene-d_8, 400 MHz) δ = 2.68-2.58 (m, 12H), 2.62 (d, *J* = 16.0 Hz, 9H).
^{31}P NMR (toluene-d_8, 160 MHz) δ = 120.39.

[*P(iBuNCH$_2$CH$_2$)$_3$N*] (12b) Colorless oil ; the product was directly used for the following step.
^{1}H NMR (toluene-d_8, 300 MHz) δ = 2.76-2.68 (m, 12H), 2.74 (dd, *J* = 9.0 Hz, 12.0 Hz, 6H), 1.82 (sept, *J* = 6.0 Hz, 3H), 0.93 (dd, *J* = 0.72 Hz, 6.0 Hz, 18H).
^{31}P NMR (toluene-d_8, 120 MHz) δ = 130.29.

[*P(BnNCH$_2$CH$_2$)$_3$N*] (12c) Colorless oil ; the product was directly used for the following step.
^{1}H NMR (toluene-d_8, 400 MHz) δ = 7.37-7.30 (m, 6H), 7.23-7.16 (m, 6H), 7.12-7.08 (m, 3H), 4.13 (d, *J* = 9.32 Hz, 6H), 2.70-2.64 (m, 6H), 2.60 (dd, *J* = 4.16 Hz, 7.28 Hz, 6H).
^{31}P NMR (toluene-d_8, 160 MHz) δ = 127.33.

[*P(p-OMe-BnNCH$_2$CH$_2$)$_3$N*] (12d) Yellow oil ; the product was directly used for the following step.^{1}H NMR (toluene-d_8, 400 MHz) δ = 7.29 (dt, *J* = 2.92 Hz, 8.56 Hz, 6H), 6.79 (dt, *J* = 1.96 Hz, 8.60 Hz, 6H), 4.16 (d, *J* = 9.32 Hz, 6H), 3.36 (s, 9H), 2.79-2.71 (m, 6H), 2.70-2.63 (m, 6H).
^{31}P NMR (toluene-d_8, 160 MHz) δ = 126.80.

[*P(p-CF$_3$-BnNCH$_2$CH$_2$)$_3$N*] (12e). Yellow oil ; the product was directly used for the following step.^{1}H NMR (toluene-d_8, 300 MHz) δ = 7.41 (d, *J* = 7.68 Hz, 6H), 7.16 (d, *J* = 7.92 Hz, 6H), 3.97 (d, *J* = 9.69 Hz, 6H), 2.60-2.53 (m, 6H), 2.53-2.45 (m, 6H).
^{31}P NMR (toluene-d_8, 160 MHz) δ = 127.84. ^{19}F NMR (toluene-d_8, 376 MHz) δ = -62.10.

ClP(MeNCH$_2$CH$_2$)$_3$N][Cl] **12a-Cl$^{+\cdot}$Cl^{-}** Beige solid; yield: 85% (562 mg); mp 65-66°C.
IR cm^{-1}: 3565, 2960, 2727, 2517, 1647, 1465, 1229, 1142, 984, 884, 764, 723, 642.

^{1}H NMR ($CDCl_3$, 300 MHz) δ = 3.74 (td, J = 3.0 Hz, 6.0 Hz, 6H), 3.39 (dt, J = 6.0 Hz, 12.0 Hz, 6H), 2.95 (d, J = 15.0 Hz, 9H).

^{13}C NMR ($CDCl_3$, 75 MHz) δ = 46.4 (d, J = 9.7 Hz), 45.1 (d, J = 9.0 Hz), 39.8 (d, J = 6.0 Hz).

^{31}P NMR ($CDCl_3$, 120 MHz) δ = –26.02. HRMS (ESI) : *m/z* $[M]^+$ calcd for $C_9H_{21}N_4ClP^+$ 251.1187; found: 251.1186.

ClP(iBuNCH₂CH₂)₃N][Cl] **(12b-Cl⁺·Cl⁻)** White solid; yield: 47% (206 mg); mp 125-127°C. IR cm^{-1}: 3379, 2958, 2827, 1668, 1651, 1466, 1388, 1282, 1111, 1077, 1057, 869, 774, 573.

^{1}H NMR ($CDCl_3$, 300 MHz) δ = 3.63 (td, J = 3.0 Hz, 6.0 Hz, 6H), 3.34 (dt, J = 6.0 Hz, 12.0 Hz, 6H), 3.12 (dd, J = 6.0 Hz, 15.0 Hz, 6H), 2.01 (sept, J = 6.0 Hz, 3H), 0.93 (d, J = 6.0 Hz, 3H).

^{13}C NMR ($CDCl_3$, 75 MHz) δ = 59.6 (d, J = 2.2 Hz), 46.1 (d, J = 9.0 Hz), 45.7 (d, J = 7.5 Hz), 28.5 (d, J = 4.5 Hz), 20.3.

^{31}P NMR ($CDCl_3$, 120 MHz) δ = –13.81. HRMS (ESI) : *m/z* $[M]^+$ calcd for $C_{18}H_{39}N_4PCl^+$ 377.2595; found: 377.2593.

[ClP(BnNCH₂CH₂)₃N][Cl] **(12c-Cl⁺·Cl⁻)** White solid; yield: 86% (261 mg); mp 145 °C. IR cm^{-1}: 3364, 3060, 2925, 2884, 1635, 1604, 1493, 1384, 1299, 1261, 1142, 1071, 1024, 971, 920, 865, 766, 696, 590, 510.

^{1}H NMR ($CDCl_3$, 300 MHz) δ = 7.40-7.24 (m, 15H), 4.68 (d, J = 14.7 Hz, 6H), 3.65 (td, J = 6.8, 4.3 Hz, 6H), 3.32 (dt, J = 12.0, 6.7 Hz, 6H).

^{13}C NMR ($CDCl_3$, 75 MHz) δ = 136.9 (d, J = 5.25 Hz), 129.1, 128.2, 127.7, 55.7 (d, J = 4.5 Hz), 44.5 (d, J = 9.75 Hz), 44.2 (d, J = 9.0 Hz).

^{31}P NMR ($CDCl_3$, 120 MHz) δ = –23.44. HRMS (ESI): *m/z* $[M]^+$ calcd for $C_{27}H_{33}ClN_4P^+$ 479.2126, found: 479.2126.

[ClP(p-OMe-BnNCH₂CH₂)₃N][Cl] **(12d-Cl⁺·Cl⁻)** White solid; yield: 46% (226 mg); mp 205°C. IR/cm^{-1}: 3744, 3648, 3367, 2946, 2123, 2787, 2362, 1652, 1584, 1541, 1509, 1389, 1419, 1354, 1274, 1172, 1098, 945, 869, 816, 761, 657, 602, 572.

^{1}H NMR ($CDCl_3$, 300 MHz) δ = 7.21 (d, J = 8.7 Hz, 6H), 6.86 (d, J = 8.6 Hz, 6H), 4.59 (d, J = 14.7 Hz, 1H), 3.53 (td, J = 6.8, 4.5 Hz, 6H), 3.23 (dt, J = 13.0 Hz, 6.7 Hz, 6H).

^{13}C NMR ($CDCl_3$, 100 MHz) δ = 159.5, 129.3, 128.8 (d, J = 4.65 Hz), 114.3, 55.4, 54.9 (d, J = 4.14 Hz), 44.4 (d, J = 9.9 Hz), 43.9 (d, J = 9.59 Hz).

^{31}P NMR ($CDCl_3$, 120 MHz) δ = –23.38. HRMS (ESI): *m/z* $[M]^+$ calcd for $C_{30}H_{39}ClN_4O_3P^+$ 569.2443; found: 569.2441.

[ClP(p-CF₃-BnNCH₂CH₂)₃N][Cl] **(12e-Cl⁺·Cl⁻)** White solid; yield: 62% (196 mg); mp 155°C. IR cm^{-1}: 2327, 2245, 1996, 1781, 1698, 1635, 1622, 1576, 1507, 1473, 1418, 1395, 1157, 1066,

816, 764, 573.

^{1}H NMR ($CDCl_3$, 300 MHz) δ = 7.63 (d, J = 6.0 Hz, 6H), 7.41 (d, J = 9.0 Hz, 6H), 4.76 (d, J = 15.0 Hz, 6H), 3.91 (q, J = 6.0 Hz, 6H), 3.53 (dt, J = 6.0 Hz, 12.0 Hz, 6H).

^{13}C NMR (CD_3CN, 75 MHz) δ = 144.0 (dd, J = 1.5 Hz, 4.5 Hz), 129.6 (d, J = 31.5 Hz), 128.3, 126.4 (q, J = 3.75 Hz), 125.4 (d, J = 270 Hz), 55.5 (d, J = 5.25 Hz), 46.4 (d, J = 9.0 Hz), 45.5 (d, J = 9.0 Hz).

^{31}P NMR ($CDCl_3$, 120 MHz) δ = –23.82. ^{19}F NMR ($CDCl_3$, 376 MHz) δ = –62.60. HRMS (ESI): *m/z* $[M]^+$ calcd for $C_{30}H_{30}N_4F_9ClP^+$ 612.1747; found: 612.1747.

Anions Metathesis In a flame-dried Schlenk flask were added dried acetonitrile (C = 0.1 mol.L^{-1}) and **12-Cl^{+}·Cl^{-}** (1.0 equiv.). A solution of $NaPF_6$ (1.4 equiv.) in dried acetonitrile (C = 0.26 mol.L^{-1}) was added dropwise, and the mixture was stirred for 2 h at room temperature. The solvent was evaporated under vacuum and dried acetone (C = 0.07 mol.L^{-1}) was added. White solid precipitate was observed. The supernatant was evaporated under vacuum to give pure **12-Cl^{+}·PF$_6^{-}$**.

[ClP(MeNCH$_2$CH$_2$)$_3$N][PF$_6$] **(12a-Cl^{+}·PF$_6^{-}$)** Beige solid; yield: 70% (105 mg); mp 250°C. IR cm^{-1}: 2945, 1489, 1394, 1254, 1144, 973, 122, 746, 556.

^{1}H NMR (CD_3CN, 300 MHz) δ = 3.37-3.25 (m, 6H), 3.21-3.14 (m, 6H), 2.90 (d, J = 15.0 Hz, 9H).

^{13}C NMR (CD_3CN, 75 MHz) δ = 46.8 (d, J_{PC} = 9.0 Hz), 46.3 (d, J_{PC} = 9.7 Hz), 39.7 (d, J_{PC} = 6.0 Hz). ^{31}P NMR (CD_3CN, 120 MHz) δ = –21.34, –144.61 (sept, $J_{P\text{-}F}$ = 697.2 Hz). ^{19}F NMR (CD_3CN, 376 MHz) δ = -71.64, -74.43. HRMS (ESI): *m/z* [M]$^{+}$ calcd for $C_9H_{21}N_4ClP^{+}$ 251.1187; found: 251.1187. X-Ray: the product was crystallized from Et_2O/CH_3CN. CCDC 2060857 contains the supplementary crystallographic data for this paper.

[ClP(iBuNCH$_2$CH$_2$)$_3$N][PF$_6$] **(12b-Cl^{+}·PF$_6^{-}$)** White solid; yield: 65% (169 mg); mp 177°C. IR cm^{-1}: 2960, 2928, 2872, 1466, 1390, 1368, 1313, 1212, 1176, 1114, 1076, 1058, 123, 780, 595, 556.

^{1}H NMR ($CDCl_3$, 400 MHz) δ = 3.29 (dt, J = 4.0 Hz, 16.0 Hz, 6H), 3.16 (td, J = 4.0 Hz, 8.0 Hz, 6H), 3.09 (dd, J = 4.0 Hz, 12.0 Hz, 6H), 2.01 (sept, J = 8.0 Hz, 3H), 0.94 (d, J = 8.0 Hz, 3H).

^{13}C NMR ($CDCl_3$, 75 MHz) δ = 58.9 (d, J_{PC} = 1.5 Hz), 47.4 (d, J_{PC} = 9.7 Hz), 45.5 (d, J_{PC} = 6.7 Hz), 28.6 (d, J_{PC} = 5.2 Hz), 20.2.

^{31}P NMR ($CDCl_3$, 120 MHz) δ = –4.32, –144.31 (sept, J_{PF} = 704.4 Hz). ^{19}F NMR ($CDCl_3$, 376 MHz) δ = –71.00, –73.52. HRMS (ESI): *m/z* [M + H]$^{+}$ calcd for $C_{18}H_{39}N_4PCl^{+}$ 377.2595; found: 377.2592.

[ClP(BnNCH$_2$CH$_2$)$_3$N][PF$_6$] **(12c-Cl^{+}·PF$_6^{-}$)** White solid; yield: 97% (252 mg); mp 137°C.IR/cm^{-1}: 3648, 2892, 1604, 1494, 1454, 1396, 1303, 1201, 1145, 1106, 1049, 949, 123, 760, 697, 606, 592, 510.

^{1}H NMR (CD_3CN, 500 MHz) δ = 7.44 -7.27 (m, 15H), 4.67 (d, J = 14.75 Hz, 6H), 3.35 (dt, J = 6.65 Hz, 12.85 Hz, 6H), 3.25 (td, J = 3.95 Hz, 6.4 Hz, 6H).

^{13}C NMR ($CDCl_3$, 75 MHz) δ = 136.9, 129.1, 128.1, 127.6, 55.5 (d, J_{PC} = 4.5 Hz), 45.1 (d, J_{PC} = 9.75 Hz), 44.1 (d, J_{PC} = 9.0 Hz).

^{31}P NMR ($CDCl_3$, 121 MHz) δ = –20.07, –144.28 (sept, J_{PF} = 710.65 Hz). ^{19}F NMR ($CDCl_3$,

376 MHz) δ = –70.56, –73.09. HRMS (ESI): *m/z* $[M]^+$ calcd for $C_{27}H_{33}ClN_4P^+$ 479.2126, found: 479.2131.

[ClP(p-OMe-BnNCH$_2$CH$_2$)$_3$N][PF$_6$] **(12d-Cl$^+$·PF$_6^-$)** Pale yellow solid; yield: 64% (119 mg); mp 260°C. IR/cm^{-1}: 2935, 2128, 1610, 1585, 1510, 1457, 1354, 1282, 1207, 1175, 1097, 951, 903, 829, 739, 657, 555, 518.

^{1}H NMR ($CDCl_3$, 300 MHz) δ = 7.22 (d, *J* = 8.6 Hz, 6H), 6.86 (d, *J* = 8.7 Hz, 6H), 4.56 (d, *J* = 14.2 Hz, 6H), 3.22 (dt, *J* = 12.8, 6.4 Hz, 6H), 3.08 (td, *J* = 3.0 Hz, 6.0 Hz, 6H).

^{13}C NMR ($CDCl_3$, 75 MHz) δ = 159.6, 129.3, 128.7 (d, *J* = 5.2 Hz), 114.4, 55.5, 54.8 (d, *J* = 4.5 Hz), 45.0 (d, *J* = 9.7 Hz), 43.8 (d, *J* = 9.0 Hz). ^{31}P NMR ($CDCl_3$, 120 MHz) δ = –19.04, –144.30 (sept, J_{PF} = 704.4 Hz). ^{19}F NMR ($CDCl_3$, 376 MHz) δ = –70.42, –72.94. HRMS (ESI): *m/z* $[M]^+$ calcd for $C_{30}H_{39}ClN_4O_3P^+$ 569.2443; found: 569.2442.

[ClP(p-CF$_3$-BnNCH$_2$CH$_2$)$_3$N][PF$_6$] **(12e-Cl$^+$·PF$_6^-$)** White solid; yield: 87% (201 mg); mp 227°C. IR cm^{-1} 3566, 2027, 1697, 1472, 1288, 1065, 1016, 935, 869, 846, 121, 765, 719, 658, 557.

^{1}H NMR (CD_3CN, 300 MHz) δ = 7.70 (d, *J* = 9.0 Hz, 6H), 7.50 (d, *J* = 6.0 Hz, 6H), 4.72 (d, *J* = 15.0 Hz, 6H), 3.51-3.37 (m, 12H), 3.53 (dt, *J* = 6.0 Hz, 12.0 Hz, 6H).

^{13}C NMR (CD_3CN, 100 MHz) δ = 143.8 (d, *J* = 4.0 Hz), 129.7 (d, *J* = 32.0 Hz), 126.5 (q, *J* = 4.0 Hz), 125.4 (d, *J* = 269.0 Hz), 55.5 (d, *J* = 5.0 Hz), 46.3 (d, *J* = 10.0 Hz), 45.4 (d, *J* = 9.0 Hz).

^{31}P NMR (CD_3CN, 120 MHz) δ = –22.50, –144.63 (sept., J_{PF} = 698.4 Hz). ^{19}F NMR (CD_3CN, 376 MHz) δ = –62.65, –62.71, –62.98, –70.08, –72.01. HRMS (ESI): *m/z* $[M]^+$ calcd for $C_{30}H_{30}N_4F_9ClP^+$ 612.1747; found: 612.1747. X-Ray: the product was crystallized from Et_2O/CH_3CN

[HP(p-OMe-BnNCH$_2$CH$_2$)$_3$N][PF$_6$] **12d-H$^+$·PF$_6^-$** In a round-bottomed flask were added deionized water (C = 0.17 mol/L), and **12d-H$^+$·Cl$^-$** (1.0 equiv.). The mixture was stirred and a solution of $NaPF_6$ (1.4 equiv.) in deionized water (C = 0.2 mol/L) was added dropwise. White solid precipitated instantaneously. The mixture was stirred for 2 h, then was filtered and washed by water to give pure compound.

White solid; yield: 95% (226 mg) ; mp 189°C.

IR cm^{-1} 2863, 1610, 1585, 1455, 1389, 1302, 1249, 1171, 1125, 1106, 1088, 1031, 945, 870, 759, 718, 657, 631, 557, 540.

^{1}H NMR ($CDCl_3$, 400 MHz) δ = 7.08 (d, *J* = 8.5 Hz, 6H), 6.87 (d, *J* = 8.5 Hz, 6H), 5.82 (d, *J* = 496.2 Hz, 1H), 4.10 (d, *J* = 17.1 Hz, 6H), 3.81 (s, 9H), 3.22 (dd, *J* = 4.0 Hz, 12.0 Hz, 6H), 3.05 (dt, *J* = 4.0 Hz, 12.0 Hz, 6H).

^{13}C NMR ($CDCl_3$, 75 MHz) δ = 159.4, 129.1, 128.9 (d, *J* = 5.25 Hz), 114.4, 55.4, 54.6 (d, *J* = 4.5 Hz), 45.2 (d, *J* = 9.75 Hz), 43.8 (d, *J* = 8.25 Hz).

^{31}P NMR ($CDCl_3$, 160 MHz) δ = -11.82, -144.25 (sept., J_{PF} = 711.2 Hz).

^{19}F NMR ($CDCl_3$, 376 MHz) δ = -71.24, -73.23.

HRMS (ESI) : *m/z* $[M]^+$ calcd for $C_{30}H_{40}N_4O_3P^+$ 535.2128; found : 535.2842.

[ClP(p-OMe-BnNCH$_2$CH$_2$)$_3$N][BAr^F] **12d-Cl$^+$·BAr^{F-}** In a flame-dried Schlenk flask were added dried acetonitrile (C = 0.1 mol.L^{-1}), and **12d-Cl$^+$·Cl$^-$** (1.0 equiv.). A solution of $NaBAr^F$ (1.2 equiv.) in dried acetonitrile (C = 0.26 mol.L^{-1}) was added dropwise, and the mixture was stirred for 2 h. The solvent was evaporated under vacuum and dried acetone (C = 0.07 mol.L^{-1}) was added. White solid precipitated was observed. The supernatant was evaporated under vacuum to give pure compound.

Colorless paste; yield: 41% (59 mg).

IR cm^{-1} 3568, 2936, 2032, 1657, 1584, 1473, 1450, 1285, 1175, 1097, 1068, 935, 859, 845, 769, 657, 556, 515.

^{1}H NMR (CD_3CN, 400 MHz) δ = 7.72-7.64 (m, 12H), 7.27 (d, *J* = 12.0 Hz, 6H), 4.58 (d, *J* = 16.0 Hz, 6H), 3.79 (s, 9H), 3.26 (dt, *J* = 4.0 Hz, 16.0 Hz, 6H), 3.13 (td, *J* = 4.0 Hz, 8.0 Hz, 6H).

^{13}C NMR (CD_3CN, 100 MHz) δ = 160.2, 135.7, 130.5 (d, J_{PC} = 6.0 Hz), 130.1 (q, J_{PC} = 3.0 Hz), 129.8, 129.5, 125.5 (d, J_{PC} = 270.0 Hz), 121.4, 118.6, 114.9, 55.9, 55.2 (d, J_{PC} = 4.0 Hz), 46.7 (d, J_{PC} = 9.0 Hz), 44.9 (d, J_{PC} = 8.0 Hz).

^{31}P NMR (CD_3CN, 160 MHz) δ = -17.43.

^{19}F NMR (CD_3CN, 376 MHz) δ = -63.24.

HRMS (ESI) : *m/z* $[M]^+$ calcd for $C_{30}H_{39}N_4O_3ClP^+$569.2443; found : 569.2441.

[FP(p-OMe-BnNCH$_2$CH$_2$)$_3$N][PF$_6$] **12d-F$^+$·PF$_6^-$** In a round flask, **12d-Cl$^+$.Cl$^-$** (1 equiv.) and CsF (6 equiv.) were added, acetonitrile (5 mL) as solvent to be introduced, reflux for 24 hours, the supernatant was evaporated under vacuum to give **12d-F$^+$·Cl$^-$**.[160] The counter-ion exchange to PF_6^- was performed using the method described to give **12d-F$^+$·PF$_6^-$**.

Colorless paste; yield: 29% (9 mg).

^{1}H NMR (CD_3CN, 300 MHz) δ = 7.18 (d, *J* = 8.6 Hz, 6H), 6.88 (d, *J* = 8.6 Hz, 6H), 4.16 (d, *J* = 11.3 Hz, 6H), 3.78 (s, 9H), 3.25-3.19 (m, 6H), 3.19-3.16 (m, 6H).

^{13}C NMR (CD_3CN, 75 MHz) δ = 160.0, 131.3 (d, *J* = 2.7 Hz), 129.9, 114.9, 55.9, 52.9 (dd, *J* = 4.6 Hz, 11.9 Hz), 47.3 (d, *J* = 10.6 Hz), 42.7 (d, *J* = 13.3 Hz).

^{31}P NMR (CD_3CN, 160 MHz) δ = -43.42 (d, *J* = 491.6 Hz), -144.62 (sept. *J* = 930.5 Hz).

[160] *A. D. Matthews, S. Prasad, N. D. Schley, K. J. Donald and Johnson, Inorg. Chem., 2019, **58**, 15912-15992.*

^{19}F NMR (CD_3CN, 376 MHz) δ = -70.43 (d, *J* = 982.4 Hz), -72.98 (d, *J* = 940.1 Hz).

***(4-(3-bromopropoxy)-3-methoxyphenyl)methanol* 95** In a round-dried bottom flask, vanillyl alcohol (10.0 g, 64.86 mmol) and potassium carbonate (10.0 g, 72.36 mmol) were dissolved in ethanol (500 mL), and 1, 3-dibromopropane (16.45 mL, 162.08 mmol) was added dropwise. The mixture was vigorously stirred and heated at 70 °C for 5 hours. The solvent was removed under reduced pressure, the crude residue was dissolved in CH_2Cl_2 (200 mL) and successively washed with 1 M NaOH solution (200 mL × 3). After 2 hours, the precipitate was filtered off on the sintered glass, the organic phase was dried by anhydrous Na_2SO_4 and CH_2Cl_2 was removed under reduced pressure to give brown oil. The crude compound was purified on silica gel by column chromatography using pure CH_2Cl_2 as eluent to give pure compound (12.85 g, 72%). White solid. T_m : 61 °C.

^{1}H NMR (400 MHz, $CDCl_3$): δ = 6.92 (d, *J* = 1.56 Hz, 1H), 6.90 – 6.12 (m, 2H), 4.60 (d, *J* = 4.8Hz, 2H), 4.14 (t, *J* = 6.0 Hz, 2H), 3.85 (s, 3H), 3.62 (t, *J* = 6.5 Hz, 2H), 2.35 (quint, *J* = 6.2 Hz, 2H), 1.82 (t, *J* = 5.44 Hz, 1H).

^{13}C NMR (101 MHz, $CDCl_3$): δ = 149.9, 147.9, 134.5, 119.6, 113.9, 111.2, 67.1, 65.3, 56.1, 32.5, 30.2. IR: cm^{-1} 3332, 2935, 2867, 2184, 1743, 1591, 1511, 1463, 1418, 1384, 1357, 1324, 1258, 1229, 1155, 1134, 1102, 1076, 1059, 1026, 915, 891, 653, 799, 761, 718, 761, 718, 646, 550.

HRMS (ESI): *m/z* $[M+Na]^+$ calcd for $C_{11}H_{15}BrO_3$, 297.0094; found at 297.0094.

***2-((4-(3-bromopropoxy)-3-methoxybenzyl)oxy)tetrahydro-2H-pyran* 96** In a round-dried bottom flask, **95** (3.0 g, 10.91 mmol) was dissolved in CH_2Cl_2 (80 mL), and catalytic amount of PPTS (274 mg, 1.09 mmol) was added. The mixture was vigorously stirred at room temperature for 16 hours. A solution of 1 M NaOH in distilled water (80 mL × 3) was added to extract the CH_2Cl_2. The combined organic phase was dried by anhydrous Na_2SO_4, then the solvent was removed under reduced pressure to give the yellow oil. The crude compound was purified by column chromatography on silica gel using pure CH_2Cl_2 as eluent to give the pure compound (3.12 g, 98%). Colorless oil.

^{1}H NMR (400 MHz, $CDCl_3$): δ = 6.94-6.12 (m, 3H), 4.72 (d, *J* = 11.6 Hz, 1H), 4.69 (t, *J* = 3.5 Hz, 1H), 4.44 (d, *J* = 11.7 Hz, 1H), 4.15 (t, *J* = 5.9 Hz, 2H), 3.97-3.89 (m, 1H), 3.87 (s, 3H), 3.63 (t, *J* = 6.4 Hz, 2H), 3.58-3.47 (m, 1H), 2.35 (quint, *J* = 6.2 Hz, 2H), 1.93-1.49 (m, 6H).

^{13}C NMR (101 MHz, $CDCl_3$): δ = 149.8, 147.9, 131.7, 120.7, 113.9, 112.2, 97.8, 68.9, 67.1, 62.5, 56.1, 32.6, 31.0, 30.3, 25.7, 19.7.

IR: cm^{-1} 2938, 2870, 1592, 1517, 1465, 1419, 1384, 1348, 1322, 1260, 1231, 1200, 1112, 1158, 1117, 1076, 1020, 975, 949, 931, 903, 868, 810, 766, 744, 547.
HRMS (ESI): *m/z* $[M+Na]^+$ calcd for $C_{16}H_{23}BrO_4$, 381.0669; found at 381.0669.

2-((4-(3-azidopropoxy)-3-methoxybenzyl)oxy)tetrahydro-2H-pyran **97** In a round-dried bottom flask, **96** (3.0 g, 8.35 mmol) was dissolved in DMF (50 mL), NaN_3 (1.09 g, 16.70 mmol) was added portion wise, the mixture was vigorously stirred and heated at 60 °C for 16 hours. The solvent was removed under reduced pressure, the crude residue was dissolved in CH_2Cl_2 (80 mL), then washed by 1 M NaOH solution (80 mL × 3). The combined organic layers were dried over anhydrous Na_2SO_4, then concentrated under vacuum to give the pure compound (2.47 g, 92%). Yellow oil. ^{1}H NMR (400 MHz, $CDCl_3$): δ = 6.97-6.79 (m, 3H), 4.72 (d, *J* = 11.6 Hz, 1H), 4.68 (dd, *J* = 3.1 Hz, 4.3 Hz, 1H), 4.44 (d, *J* = 11.7 Hz, 1H), 4.09 (t, *J* = 6.1 Hz, 2H), 3.99-3.89 (m, 1H), 3.86 (s, 3H), 3.54 (t, *J* = 6.7 Hz, 2H), 3.58-3.52 (m, 1H), 2.08 (quint, *J* = 6.2 Hz, 2H), 1.92-1.51 (m, 6H). ^{13}C NMR (101 MHz, $CDCl_3$): δ = 149.8, 147.8, 131.7, 120.7, 113.8, 112.1, 97.8, 68.9, 66.2, 62.4, 56.1, 48.4, 30.8, 28.9, 25.6, 19.6. IR: cm^{-1} 2940, 2871, 2093, 1746, 1677, 1592, 1513, 1465, 1420, 1385, 1347, 1321, 1200, 1112, 1159, 1117, 1076, 1054, 1021, 975, 949, 903, 868, 809, 731, 646, 584. HRMS (ESI): *m/z* $[M+Na]^+$ calcd for $C_{16}H_{23}N_3O_4$, 344.1578; found at 344.1578.

3-(2-methoxy-4-(((tetrahydro-2H-pyran-2-yl)oxy)methyl)phenoxy)propan-1-amine **98** In a round ice-cooled bottom flask, **97** (2 g, 6.22 mmol) was dissolved in THF (60 mL), PPh_3 (2.45 g, 9.34) was carefully added portion-wise. The mixture was allowed to warm at room temperature slowly for 36 hours. The solvent was removed under reduced pressure, the crude compound was dissolved in CH_2Cl_2 (70 mL), extracted by a solution of 1 M NaOH (70 mL × 3) in distilled water. The organic phase was dried over anhydrous Na_2SO_4, then concentrated under vacuum to give yellow oil. The crude compound was purified on silica gel by column chromatography using a mixture of CH_2Cl_2/MeOH (10:1) as eluent to give pure compound (1.31 g, 71%). Colorless oil.
^{1}H NMR (300 MHz, $CDCl_3$): δ = 6.94-6.66 (m, 3H), 4.65 (d, *J* = 11.7 Hz, 1H), 4.61 (dd, *J* = 1.2 Hz, 2.9 Hz, 1H), 4.37 (d, *J* = 11.7 Hz, 1H), 4.03 (t, *J* = 6.2 Hz, 2H), 3.90-3.81 (m, 1H), 3.79 (s, 3H), 3.52-3.43 (m, 1H), 2.86 (t, *J* = 6.6 Hz, 2H), 1.90 (quint, *J* = 6.4 Hz, 2H), 1.12 – 1.39 (m, 6H).
^{13}C NMR (75 MHz, $CDCl_3$): δ = 149.4, 147.8, 131.0, 120.5, 113.0, 111.8, 97.4, 68.7, 67.4, 62.2, 55.8, 39.3, 32.6, 30.5, 25.4, 19.4. IR: cm^{-1} 2939, 2870, 2196, 1592, 1513, 1465, 1420, 1385,

1348, 1322, 1261, 1231, 1200, 1112, 1159, 1116, 1075, 1020, 975, 946, 903, 868, 748, 732, 645, 547.

HRMS (ESI): *m/z* $[M+H]^+$ calcd for $C_{16}H_{25}NO_4$, 296.1857; found at 296.1857.

2,2',2''-nitrilotris(N-(3-(2-methoxy-4-(((tetrahydro-2H-pyran-2-yl)oxy)methyl)phenoxy)propyl) acetamide) **99** In a round ice-cooled round bottom flask, **98** (1.3 g, 4.40 mmol) was dissolved in THF (50 mL), DCC (1 g, 4.84 mmol) and HOBt (0.66 g, 4.84 mmol) was slowly added, respectively, then the ligand nitrilotriacetic acid (255 mg, 1.33 mmol) was added. The mixture was vigorously stirred and warmed to room temperature, then was heated at 50 °C for 16 hours. After removing the precipitate on sintered glass for several times, the solvent was removed under vacuum. The crude compound was dissolved in CH_2Cl_2 (50 mL), then was extracted by 1 M NaOH solution (50 mL × 3), filtered, the organic phase was dried over anhydrous Na_2SO_4, and was concentrated under vacuum to give the yellow oil. The crude compound was purified on silica gel column by chromatography using a mixture of CH_2Cl_2/EtOAc (30:1) as eluent to give pure compound (1.32 g, 97%). Light yellow oil.

^{1}H NMR (300MHz, $CDCl_3$): δ = 7.68 (t, *J* = 5.5 Hz, 3H), 6.92-6.84 (m, 6H), 6.81 (d, *J* = 8.1 Hz, 3H), 4.70 (d, *J* = 11.7 Hz, 3H), 4.67 (dd, *J* = 2.8 Hz, 4.3 Hz, 3H), 4.42 (d, *J* = 11.7 Hz, 3H), 4.04 (t, *J* = 6.0 Hz, 6H), 3.97-3.87 (m, 3H), 3.86 (s, 9H), 3.60-3.50 (m, 3H), 3.45 (q, *J* = 6.0 Hz, 6H), 3.36 (s, 6H), 1.99 (quint., *J* = 6.0 Hz, 6H), 1.91-1.47 (m, 18H).

^{13}C NMR (101 MHz, $CDCl_3$): δ = 170.7, 149.4, 147.7, 131.6, 120.7, 112.9, 111.9, 97.8, 68.9, 68.2, 62.5, 59.9, 56.1, 53.6, 37.8, 30.8, 29.0, 25.6, 19.7. IR: cm^{-1} 3296, 3007, 2943, 2874, 1750, 1658, 1592, 1513, 1465, 1452, 1384, 1348, 1262, 1232, 1215, 1201, 1159, 1135, 1118, 1075, 1022, 976, 950, 903, 868, 810, 744, 665, 596, 547.

HRMS (ESI): *m/z* $[M+Na]^+$ calcd for $C_{54}H_{78}N_4O_{15}$, 1045.5356; found at 1045.5356.

Hemicryptophane 93 Precursor **99** (1.0 g, 0.98 mmol) was dissolved in formic acid (1 L). The mixture was stirred vigorously and heated at 50 °C for 1 day. Then the solvent was removed under vacuum. The residue was dissolved in CH_2Cl_2 (50 mL) and was washed by 1 M NaOH solution (50 mL × 3). The organic phase was dried over anhydrous Na_2SO_4, then concentrated in vacuum to give yellow solid compound. The crude compound was purified on silica gel column by chromatography using a mixture solution of CH_2Cl_2/MeOH (15:1) as eluent to give the pure cage (294 mg, 42%). White solid. T_m : 157 °C.

^{1}H NMR (400 MHz, CD_2Cl_2): δ = 7.55 (s, 1H), 7.13 (t, *J* = 4.1 Hz, 1H), 7.02 (d, *J* = 8.5 Hz, 1H), 6.91 (s, 1H), 6.88 (s, 1H), 6.12 (s, 1H), 6.72 (d, *J* = 8.5 Hz, 1H), 6.48 (t, *J* = 4.1 Hz, 1H),

5.77 (t, *J* = 5.2 Hz, 1H), 4.74 (dd, *J* = 16.7, 13.6 Hz, 2H), 4.43 (d, *J* = 13.2 Hz, 1H), 4.26 – 4.04 (m, 5H), 4.02-3.94 (m, 1H), 3.93 (s, 3H), 3.80 (s, 3H), 3.79 (s, 3H), 3.54 (dd, *J* = 4.52 Hz, 19.2 Hz, 3H), 3.48-3.39 (m, 1H), 3.39 – 3.27 (m, 1H), 3.25 – 3.04 (m, 2H), 2.66 (d, *J* = 16.8 Hz, 1H), 2.58 (d, *J* = 5.5 Hz, 1H), 2.46 (d, *J* = 16.6 Hz, 1H), 2.37 (d; *J* = 16 Hz, 1H), 2.01 – 1.61 (m, 6H), 1.36 – 1.18 (m, 4H).

^{13}C NMR (101 MHz, DMSO): δ = 169.5, 169.4, 169.2, 149.7, 148.6, 147.5, 145.5, 144.8, 133.9, 133.8, 133.7, 132.6, 132.4, 131.1, 124.9, 118.2, 114.5, 113.5, 67.4, 66.9, 66.6, 60.3, 58.6, 55.7, 55.2, 35.4, 35.3, 35.0, 34.7, 30.9, 28.6, 28.2, 27.9, 27.6, 13.9, 8.1. IR cm-^{1}: 3296, 2918, 2849, 2436, 2229, 2184, 2148, 2053, 2031, 1735, 1654, 1597, 1576, 1517, 1412, 1463, 1445, 1401, 1378, 1337, 1263, 1215, 1158, 1133, 1081, 1035, 988, 964, 880, 801, 740, 701, 615.

HRMS (ESI): *m/z* $[M+Na]^+$ calcd for $C_{39}H_{48}N_4O_9$, 739.3313; found at 739.3312.

Hemicryptophane 94 Under atmosphere of argon, hemicryptophane **93** (294 mg, 0.41 mmol) was placed in a two-neck round bottom flask, and was dissolved in dry THF (10 mL), a 2 M BH_3SMe_2 solution in THF (2.05 mL) was added dropwise. The mixture was vigorously stirred and heated at 65 °C for 6 days. Then the reaction was cooled at room temperature, MeOH (7 mL) and 1 M HCl (1 mL) were added. Keeping the reaction mixture stirred and heated at 40 °C for another 1 day, the solvent was removed under reduced pressure. The crude was dissolved in $CHCl_3$ (10 mL), MeOH (7 mL) and 1 M HCl (1 mL) was added and the mixture was stirred at 60 °C for two days. The solvent was removed under reduced pressure and the residue was dissolved in CH_2Cl_2 (30 mL), extracted by 1 M NaOH solution (30 mL × 3), the organic phase was dried over anhydrous Na_2SO_4, the solvent was removed under vacuum to give brown oil. The crude compound was purified on silica gel by column chromatography by using CH_2Cl_2/MeOH/TEA (8:1:0.08) to give the pure cage (91 mg, 37%). White solid. T_m : 217°C.

^{1}H NMR (400 MHz, CD_2Cl_2): δ = 7.50 (s, 1H), 7.06 (d, *J* = 8.4 Hz, 1H), 6.87 (s, 1H), 6.84 (d, *J* = 8.4 Hz, 1H), 6.82 (s,1H), 6.79 (s,1H), 4.78 (d, *J* = 13.4 Hz, 1H), 4.70 (d, *J* = 13.7 Hz, 1H), 4.38 (d, *J* = 13.2 Hz, 1H), 4.27-4.01 (m, 6H), 3.91 (s, 3H), 3.79 (s, 3H), 3.75 (s, 3H), 3.55 (d, *J* = 13.8 Hz, 2H), 3.49 (d, *J* = 13.6 Hz, 2H), 2.55-1.91 (m, 20H), 1.82-1.59 (m, 6H).

^{13}C NMR (101 MHz, CD_2Cl_2): δ = 149.6, 149.3, 149.0, 148.6, 145.3, 145.1, 135.6, 134.7, 133.9, 133.1, 132.7, 131.8, 124.9, 117.2, 116.9, 115.7, 115.3, 113.1, 67.8, 66.9, 60.7, 56.3, 56.2, 53.33, 47.1, 46.9, 46.8, 46.6, 46.1, 45.9, 36.5, 30.1, 29.7. IR cm-^{1}: 2917, 2849, 2691, 2431, 2105, 1992, 1742, 1642, 1597, 1516, 1481, 1461, 1446, 1378, 1337, 1262, 1214, 1158, 1134, 1082, 1031, 964, 885, 800, 724, 699.

HRMS (ESI): *m/z* $[M+H]^+$ calcd for $C_{39}H_{54}N_4O_6$, 675.4114; found at 675.4114.

Hemicryptophane 94-PH=O In a two-neck round ice-cooled bottom flask, $PCl(NMe_2)_2$ (43 uL, 0.20 mmol) was dissolved in dry CH_2Cl_2 (10 mL), the mixture was vigorously stirred under atmosphere of argon for 30 minutes at 0 °C, then a solution of hemicryptophane **94** (91 mg, 0.13 mmol) in dry CH_2Cl_2 (10 mL) was added drop-wise. The mixture was heated at 40 °C for 2 days, the solvent was removed under vacuum, the crude compound was purified by silica gel column chromatography, using a mixture of CH_2Cl_2/MeOH (15 :1) as eluent to give pure compound as white solid (69 mg, 71 %, mp: 264 °C).

HRMS (ESI): *m/z* $[M+H]^+$ calcd for $C_{39}H_{53}N_4O_7P$, 721.3721; found at 721.3721.

IR cm-^{1}: 2926.74, 2851.93, 2546.55, 2441.58, 2387.35, 1604.25, 1513.43, 1482.52, 1462.41, 1447.86, 1401.47, 1373.72, 1345.27, 1263.14, 1213.72, 1160.61, 1135.91, 1081.94, 1035.39, 1002.80, 958.54, 915.12, 874.05, 129.70, 817.18, 743.27, 706.02, 613.07, 570.19, 554.52.

^{1}H NMR (400 MHz, CD_2Cl_2) δ=10.24 (s, 1H), 7.47 (s, 1H), 7.02 (d, *J* = 8.4 Hz, 1H), 6.87 (s, 1H), 6.82 (s, 1H), 6.79 (s, 1H), 6.74 (d, *J* = 8.4 Hz, 1H), 4.75 (d, *J* = 13.4 Hz, 1H), 4.62 (d, *J* = 13.6 Hz, 1H), 4.40 (d, *J* = 13.1 Hz, 1H), 4.36 – 4.22 (m, 3H), 4.18 (d, *J* = 13.2 Hz, 1H), 4.13 – 3.99 (m, 3H), 3.87 (s, 3H), 3.81 (s, 3H), 3.74 (s, 3H), 3.54 (d, *J* = 13.8 Hz, 1H), 3.47 (d, *J* = 13.6 Hz, 1H), 2.82–2.23 (m, 12H), 2.23 –1.96 (m, 3H), 1.76 (d, *J* = 14.0 Hz, 3H), 1.54–1.39 (m, 3H).

^{13}C NMR (101 MHz, CD_2Cl_2) δ 149.76, 148.89, 147.95, 143.08, 135.06, 134.65, 131.73, 124.92, 120.53, 118.54, 117.87, 114.46, 112.37, 67.40, 66.44, 60.20, 56.31, 55.77, 47.22, 46.48, 44.91, 44.45, 43.09, 36.12, 35.67, 29.66, 28.61, 28.03, 24.33, 22.67, 13.85.

Compound 105 In an ice-cooled round bottom flask, 4-hydroxybenzaldehyde (10 g, 81.89 mmol) was dissolved in *N*, *N*-Dimethylformamide (300 mL), then sodium hydride (3.93 g, 163.77 mmol) was added portion wise, chloromethyl methyl sulfide (8.23 mL, 98.26 mmol) The mixture was vigorously stirred and slowly warmed at room temperature for 4 hours. The solvent was extracted by ether for several times, then ether was removed under reduced pressure to give yellow oil. The crude compound was purified by silica gel column chromatography using petroleum ether / ethyl acetate (8:1) as eluent to give pure compound as a light-yellow oil (9.1 g, 61%).

HRMS (ESI): *m/z* $[M+Na]^+$ calcd for $C_9H_{10}O_2S$, 205.0297; found at 205.0297.

^{1}H NMR (400 MHz, $CDCl_3$) δ 9.90 (s, 1H), 7.98 – 7.75 (m, 2H), 7.18 – 6.94 (m, 2H), 5.22 (s, 2H), 2.27 (s, 3H).

^{13}C NMR (101 MHz, $CDCl_3$) δ 190.74, 162.06, 131.79, 130.64, 115.98, 76.71, 72.40, 67.71, 14.67, 13.79.

Compound 106 In a two-neck ice-cooled round bottom flask, **105** (6 g, 32.92 mmol) was added in dry dichloromethane (100 mL), sulfuryl chloride (2.93 mL, 36.22 mmol) was carefully added drop-wise. The mixture was vigorously stirred under atmosphere of argon at 0 °C and allowed to warm at room temperature slowly for 2 hours. The solvent was concentrated in vacuum to give a yellow oil (5.45 g, 97%), the compound was directly used in next step.

^{1}H NMR (400 MHz, $CDCl_3$) δ 9.94 (s, 1H), 7.90 (d, *J* = 8.8 Hz, 2H), 7.33 – 7.13 (m, 2H), 5.93 (s, 2H).

^{13}C NMR (101 MHz, $CDCl_3$) δ 190.68, 160.17, 135.42, 132.29, 131.93, 131.87, 131.84, 127.79, 116.21, 116.15, 115.67, 76.70, 76.51, 75.76, 71.21, 30.89.

Compound 107 In a two-neck round bottom flask, **106** (5 g, 29.31 mmol) was added in dry *N*,*N*-Dimethylformamide (100 mL), potassium carbonate (6.08 g, 43.97 mmol) and vanillyl alcohol (6.78 g, 43.96 mmol) was carefully added portion-wise. The mixture was vigorously stirred under atmosphere of argon at room temperature for 36 hours. The solvent was then removed under reduced pressure, the residue was dissolved in CH_2Cl_2 (150 mL), extracted by 1 M NaOH solution 150 mL × 3), the organic phase was dried by anhydrous Na_2SO_4, the solvent was concentrated in vacuum to give brown oil. Then the crude compound was purified by silica gel column chromatography using petroleum ether / ethyl acetate (1:1) to give the pure compound as white solid (4.31 g, 51%).

HRMS (ESI): *m/z* $[M+Na]^+$ calcd for $C_{16}H_{16}O_5$, 311.0893; found at 311.0893.

^{1}H NMR (300 MHz, $CDCl_3$) δ 9.90 (s, 1H), 7.84 (d, *J* = 8.8 Hz, 2H), 7.38 – 7.15 (m, 1H), 7.07 (d, *J* = 8.1 Hz, 2H), 6.96 (d, *J* = 2.0 Hz, 1H), 6.88 – 6.77 (m, 1H), 5.78 (s, 2H), 4.62 (d, *J* = 4.0 Hz, 2H), 3.84 (s, 3H).

^{13}C NMR (75 MHz, $CDCl_3$) δ 190.88, 161.89, 150.45, 144.96, 136.99, 131.90, 131.16, 119.29, 118.33, 116.52, 111.15, 91.77, 77.45, 77.23, 77.03, 76.60, 65.08, 55.88.

Compound 108 In a two-neck round bottom flask, **107** (4 g, 13.87 mmol) was added in dry dichloromethane (80 mL), a catalytic amount of scandium (III) triflate (612 mg, 1.39 mmol) was carefully added portion-wise. The mixture was vigorously stirred under atmosphere of argon and slowly heated at 40 °C for 24 hours. The solvent was then removed under reduced pressure, the residue was dissolved in CH_2Cl_2 (80 mL), extracted by 1 M NaOH solution 80 mL × 3), the organic phase was dried by anhydrous Na_2SO_4, the solvent was concentrated in vacuum to give brown oil, then the crude compound was purified by silica gel column chromatography using dichloromethane / ethyl acetate (20:1) to give the pure compound as

white solid (1.58 g, 42%).

HRMS (ESI): *m/z* $[M+Na]^+$ calcd for $C_{48}H_{42}O_{12,}$ 123.2566; found at 123.2566.

^1H NMR (300 MHz, $CDCl_3$) δ 9.91 (s, 1H), 7.91 – 7.76 (t, 2H), 7.27 – 7.14 (t, 2H), 7.08 (s, 1H), 6.78 (s, 1H), 5.75 (d, *J* = 7.2 Hz, 1H), 5.66 (d, *J* = 7.2 Hz, 1H), 4.71 (d, *J* = 13.7 Hz, 1H), 3.71 (s, 3H), 3.53 (d, *J* = 13.8 Hz, 1H).

^{13}C NMR (75 MHz, $CDCl_3$) δ 190.74, 162.02, 148.97, 144.43, 135.14, 131.87, 131.67, 131.24, 116.57, 113.85, 77.44, 77.01, 76.59, 56.00, 36.29.

Hemicryptophane 100 To a solution of precursor **CTV-108** (1.58 g, 1.95 mmol) in mixture chloroform / methanol (400 / 400 mL) was added a solution of tris (2-aminoethyl) amine (322 uL, 2.14 mmol) in mixture chloroform / methanol (100 /100 mL), the mixture was vigorously stirred in a round bottom flask at room temperature for overnight. Then the mixture was cooled at 0 °C, sodium borohydride (1.47 g, 38.97 mmol) was carefully added portion-wise, the mixture was stirred and slowly warmed at room temperature for 4 hours. The solvent was then removed under reduced pressure, the residue was dissolved in CH_2Cl_2 (100 mL), extracted by 1 M NaOH solution 100 mL × 3), the organic phase was dried by anhydrous Na_2SO_4, the solvent was concentrated in vacuum to give brown oil. The crude compound was purified by silica gel column chromatography by using dichloromethane / methanol / triethylamine (10:1:0.1) to give the cage as a white solid (691 mg, 39%).

HRMS (ESI): *m/z* $[M+2H]^+$ calcd for $C_{54}H_{60}N_4O_{9,}$ 455.2252; found at 455.2252.

^1H NMR (400 MHz, $CDCl_3$) δ 7.19 (s, 1H), 7.05 (d, *J* = 8.5 Hz, 2H), 6.91 (s, 1H), 6.89 – 6.85 (m, 2H), 5.12 (d, *J* = 7.4 Hz, 1H), 5.74 (d, *J* = 7.4 Hz, 1H), 4.74 (d, *J* = 13.6 Hz, 1H), 3.84 (s, 3H), 3.61 (s, 2H), 3.56 (d, *J* = 13.7 Hz, 1H), 2.62 – 2.34 (m, 4H).

^{13}C NMR (101 MHz, $CDCl_3$) δ 155.67, 147.57, 144.03, 134.18, 133.01, 131.52, 129.34, 116.61, 115.36, 113.73, 90.04, 77.32, 77.21, 77.01, 76.69, 56.34, 55.64, 53.78, 47.40, 36.25, 29.69.

Hemicryptophane-azaphosphatrane 102-H^+·Cl^- In an ice-cooled round bottom flask, bis(dimethylamino)chlorophosphine (64 uL, 0.42 mmol) was added carefully and dissolved in anhydrous dichloromethane (10 mL), the mixture was stirred vigorously under atmosphere of argon at 0 °C for 0.5 hour, then a solution of cage **100** (250 mg, 0.28 mmol) in anhydrous dichloromethane (10 mL) was added, the mixture was keeping stirred and slowly warm to room temperature, then heated at 40 °C for 1 day. The solvent was then removed under reduced pressure to give brown oil, the crude compound was purified by silica gel column chromatography by using dichloromethane / methanol (10:1) to give the pure compound as

white solid (238 mg, 89%).

^{1}H NMR (300 MHz, CDCl3) δ 7.40 (s, 1H), 6.94 (s, 1H), 6.49 – 6.36 (d, 2H), 6.23 – 6.13 (d, 2H), 5.77 (d, J = 6.5 Hz, 1H), 5.57 (d, J = 6.4 Hz, 1H), 4.12 (d, J = 13.7 Hz, 1H), 3.12 (s, 3H), 3.64 (d, J = 13.7 Hz, 1H), 3.42 – 3.12 (m, 4H).

^{13}C NMR (75 MHz, CDCl3) δ 155.43, 148.06, 143.74, 134.78, 133.94, 131.61, 128.89, 120.01, 118.58, 112.89, 93.36, 77.47, 77.04, 76.62, 55.27, 53.43, 50.50, 50.33, 47.58, 42.39, 36.22, 34.60.

^{31}P NMR (121 MHz, CDCl3) δ -30.16, -34.32.

^{31}P CPD NMR (121 MHz, CDCl3) δ -32.16.

Hemicryptophane 102 was not observed by using base potassium tert-butoxide.

Compound 110 In a round-dried bottom flask, **95** (5 g, 18.17 mmol) was dissolved in acetonitrile (100 mL), then a catalytic amount of scandium III triflate (447 mg, 9.09 mmol) was added. The mixture was vigorously stirred and heated at 80 °C for 36 hours. The solvent was removed under reduced pressure, the crude residue was dissolved in CH_2Cl_2 (150 mL) and successively washed by 1 M NaOH solution (150 mL × 3), the organic phase was dried by anhydrous Na_2SO_4 and CH_2Cl_2 was concentrated in vacuum to give brown oil. The crude compound was purified by silica gel column chromatography using pure CH_2Cl_2 as eluent to give pure compound as white solid (1.54 g, 33%)

HRMS (ESI): *m/z* $[M+Na]^+$ calcd for $C_{33}H_{39}Br_3O_6$, 795.0153; found at 795.0153

^{1}H NMR (300 MHz, $CDCl_3$) δ 6.91 (s, 1H), 6.85 (s, 1H), 4.76 (d, *J* = 13.7 Hz, 1H), 4.13 (td, *J* = 6.0, 1.3 Hz, 2H), 3.12 (s, 3H), 3.66 – 3.50 (m, 3H), 2.38 – 2.24 (m, 2H).

^{13}C NMR (75 MHz, $CDCl_3$) δ 148.51, 146.88, 132.68, 131.85, 115.96, 113.75, 67.11, 56.25, 36.46, 32.30, 30.40.

Compound 111 In a round-dried bottom flask, **110** (1.54 g, 2 mmol) was dissolved in *N*, *N*-dimethylformamide (30 mL), then hydroxybenzaldehyde (806 mg, 6.59 mmol) and cesium carbonate (2.15 g, 6.59 mmol) were added, respectively. The mixture was vigorously stirred and heated at 60 °C for 24 hours. The solvent was removed under reduced pressure, the crude residue was dissolved in CH_2Cl_2 (50 mL) and successively washed by 1 M NaOH solution (50 mL × 3), the organic phase was dried by anhydrous Na_2SO_4 and CH_2Cl_2 was concentrated in vacuum to give brown oil. The crude compound was purified by silica gel column chromatography using dichloromethane/ethyl acetate (20:1) as eluent to give the pure

compound as white solid (1.56 g, 87%).

HRMS (ESI): *m/z* $[M+Na]^+$ calcd for $C_{54}H_{54}O_{12,}$ 971.3505; found at 917.3505

^{1}H NMR (400 MHz, $CDCl_3$) δ 9.86 (s, 1H), 7.91 – 7.65 (d, 2H), 6.97 (d, *J* = 8.7 Hz, 2H), 6.87 (s, 1H), 6.80 (s, 1H), 4.73 (d, *J* = 13.8 Hz, 1H), 4.29 – 4.19 (m, 2H), 4.14 (dt, *J* = 9.8, 6.0 Hz, 2H), 3.75 (s, 3H), 3.51 (d, *J* = 13.8 Hz, 1H), 2.28 (p, *J* = 6.0 Hz, 2H).

^{13}C NMR (75 MHz, $CDCl_3$) δ 190.74, 171.12, 163.89, 148.34, 146.91, 132.53, 131.96, 129.99, 115.62, 114.74, 113.82, 65.68, 64.89, 60.38, 56.15, 36.44, 29.70, 29.11, 21.04, 14.21.

Hemicryptophane 101 To a solution of precursor **CTV-111** (1.56 g, 1.74 mmol) in mixture chloroform / methanol (400 / 400 mL) was added a solution of tris (2-aminoethyl) amine (322 uL, 2.14 mmol) in mixture chloroform / methanol (100 /100 mL), the mixture was vigorously stirred in a round bottom flask at room temperature for overnight. Then the mixture was cooled at 0 °C, sodium borohydride (1.47 g, 38.97 mmol) was carefully added portion-wise, the mixture was stirred and slowly warmed at room temperature for 4 hours. The solvent was then removed under reduced pressure, the residue was dissolved in CH_2Cl_2 (100 mL), extracted by 1 M NaOH solution 100 mL × 3), the organic phase was dried by anhydrous Na_2SO_4, the solvent was concentrated in vacuum to give brown oil. The crude compound was purified by silica gel column chromatography using dichloromethane / methanol / triethylamine (10:1:0.1) to give the pure compound as white solid (744 mg, 43%).

HRMS (ESI): *m/z* $[M+H]^+$ calcd for $C_{60}H_{72}N_4O_{9,}$ 993.5376; found at 993.5376.

^{1}H NMR (400 MHz, CD_2Cl_2) δ 7.10 – 7.03 (m, 2H), 6.89 – 6.76 (m, 2H), 6.72 – 6.63 (m, 2H), 4.72 (d, *J* = 13.8 Hz, 1H), 4.20 – 4.03 (m, 2H), 3.97 (t, *J* = 6.2 Hz, 2H), 3.84 – 3.71 (s, 3H), 3.56 – 3.47 (m, 2H), 2.64 – 2.47 (m, 4H), 2.25 – 2.11 (m, 2H).

^{13}C NMR (101 MHz, CD_2Cl_2) δ 157.94, 148.33, 147.21, 132.13, 131.93, 128.88, 115.10, 114.14, 114.05, 65.37, 64.35, 56.35, 53.92, 53.85, 53.65, 53.59, 53.38, 53.31, 53.11, 52.93, 52.84, 47.80, 36.00, 29.14.

Hemicryptophane-azaphosphatrane 103-H^+·Cl^- In an ice-cooled round bottom flask, bis(dimethylamino)chlorophosphine (64 uL, 0.42 mmol) was added carefully and dissolved in anhydrous dichloromethane (10 mL), the mixture was stirred vigorously under atmosphere of argon at 0 °C for 0.5 hour, then a solution of hemicryptophane **101** (278 mg, 0.28 mmol) in anhydrous dichloromethane (10 mL) was added, the mixture was keeping stirred and slowly warm to room temperature, then heated at 40 °C for 1 day. The solvent was then removed under reduced pressure to give brown oil, the crude compound was purified by silica gel column

chromatography by using dichloromethane / methanol (10:1) to give the pure azaphosphatrane compound as white solid (249 mg, 84%).

HRMS (ESI): *m/z* $[M]^+$ calcd for $C_{60}H_{70}N_4O_9P^+$, 1021.4874; found at 1021.4874.

^{1}H NMR (300 MHz, $CDCl_3$) δ 6.94 – 6.12 (s, 2H), 6.76 – 6.61 (d, 4H), 4.68 (d, *J* = 13.7 Hz, 1H), 4.08 (ttd, *J* = 14.9, 9.6, 4.8 Hz, 4H), 3.87 – 3.78 (s, 3H), 3.74 – 3.60 (d, 1H), 3.49 – 3.43 (m, 2H), 3.26 – 3.12 (m, 2H), 2.36 – 2.10 (m, 2H), 1.87 (s, 2H).

^{13}C NMR (75 MHz, $CDCl_3$) δ 158.65, 147.53, 147.27, 131.91, 131.39, 129.35, 128.09, 114.60, 113.98, 113.18, 76.61, 65.85, 63.87, 63.51, 56.48, 36.31, 29.37, 15.26.

^{31}P NMR CPD (162 MHz, $CDCl_3$) δ -23.72.

^{31}P NMR (162 MHz, $CDCl_3$) δ -22.18, -25.37.

Hemicryptophane 103-PH=O Same procedure with **hemicryptophane 103-H^+·Cl^-**

^{1}H NMR (400 MHz, $CDCl_3$) δ=10.52 (s, 1H), 10.36 (s, 1H), 7.60 (d, *J* = 8.6 Hz, 1H), 7.11 (d, *J* = 8.5 Hz, 1H), 6.90 (d, *J* = 8.5 Hz, 1H), 6.81 (d, *J* = 3.9 Hz, 1H), 6.79 (s, 1H), 6.79 – 6.74 (m, 2H), 6.74 (d, *J* = 2.1 Hz, 1H), 6.71 (s, 1H), 6.69 (d, *J* = 2.4 Hz, 1H), 6.67 (s, 1H), 4.71 (dd, *J* = 14.0, 4.4 Hz, 2H), 4.28 (td, *J* = 9.7, 3.8 Hz, 1H), 4.14 (ddd, *J* = 16.2, 8.0, 3.2 Hz, 6H), 4.11 – 4.03 (m, 3H), 4.05 – 3.93 (m, 3H), 3.85 (s, 3H), 3.81 (s, 3H), 3.74 (s, 3H), 3.56 (d, *J* = 9.4 Hz, 1H), 3.49 (dd, *J* = 13.7, 7.8 Hz, 2H), 3.12 – 2.12 (m, 6H), 2.12 – 2.59 (m, 6H), 2.55 – 2.43 (m, 6H), 2.35 – 2.20 (m, 6H).

^{13}C NMR (75 MHz, $CDCl_3$) δ=159.16, 158.39, 148.04, 147.53, 147.49, 147.39, 147.31, 147.15, 132.36, 132.23, 132.09, 132.01, 131.47, 131.31, 129.55, 128.66, 128.19, 127.79, 123.27, 114.82, 114.53, 114.46, 114.38, 114.27, 114.21, 113.74, 113.26, 113.05, 64.86, 64.39, 56.89, 56.76, 56.51, 47.02, 45.89, 36.33, 29.30, 29.05, 28.89, 8.65.

^{31}P NMR (162 MHz, $CDCl_3$) δ=15.05.

^{31}P NMR (121 MHz, $CDCl_3$) δ 15.02 (d, *J* = 632.8 Hz).

Hemicryptophane 103 Azaphosphatrane **101-H^+·Cl^-** (150 mg, 0.14 mmol) was placed in a Schlenk tube, and dissolved in anhydrous tetrahydrofuran (3 mL), then potassium tert-butoxide (32 mg, 0.28 mmol) was added carefully. The mixture was stirred under atmosphere of argon at room temperature for 2 hours. The solvent was removed in vacuum and then anhydrous toluene was added (3 mL), the mixture was stirred at room temperature for an additional 0.5 hour, then Fritted glass was used to filter the suspension under argon, the filtrate was kept and the solvent was removed under vacuum to give pure compound as light-yellow solid (123 mg, 85%).

^{1}H NMR (300 MHz, Tol) δ 7.09 – 7.00 (s, 2H), 6.12 – 6.59 (d, 4H), 4.63 (d, *J* = 13.5 Hz, 1H), 4.00 – 3.76 (m, 4H), 3.61 – 3.53 (s, 3H), 3.49 (s, 2H), 3.41 (d, *J* = 13.6 Hz, 1H), 2.93 – 2.84 (m, 2H), 2.78 (t, *J* = 5.1 Hz, 2H), 2.01 (dtd, *J* = 17.6, 9.3, 4.7 Hz, 2H).
^{13}C NMR (75 MHz, Tol) δ 158.07, 148.64, 148.01, 137.40, 137.10, 133.21, 132.28, 132.14, 127.91, 127.88, 127.59, 127.56, 127.27, 127.25, 124.74, 124.42, 115.05, 114.05, 64.78, 64.04, 56.00, 36.16, 29.67, 19.52, 19.27.
^{31}P NMR CPD (121 MHz, Tol) δ =115.57.

2-((4-chlorophenyl)(hydroxy)methyl)cyclopent-2-en-1-one 4-Chlorbenzaldehyde (42 mg, 0.3 mmol) was placed in an oven-dried 5 mL Schlenk tube, and dissolved in anhydrous dichloromethane (1 mL), then 2-cyclopenten-1-one (76 uL, 0.9 mmol) was introduced, a solution of **103** (30 mg, 0.03 mmol) in anhydrous dichloromethane (1 mL) was added drop-wise, the mixture was stirred under atmosphere of argon at room temperature, then was followed by addition of titanium chloride solution in anhydrous dichloromethane (1 M) (0.3 mL, 0.3 mmol). The mixture was stirred for 0.5 hour and then was quenched by saturated aqueous $NaHCO_3$ solution (3.0 mL), the mixture was stirred for an additional 0.5 hour. Then, the inorganic precipitate was filtered through Celite. The organic phase was dried over Na_2SO_4, filtered and evaporated under vacuum to give the crude product, the crude compound was purified by silica gel column chromatography using petroleum ether / ethyl acetate (2.5:1) to give pure product as yellow wax (47 mg, 72%).
^{1}H NMR (400 MHz, $CDCl_3$) δ 7.23 (s, 4H), 7.20 (m, 1H), 5.43 (s, 1H), 3.63 (s, 1H), 2.50 (d, *J* = 4.3 Hz, 2H), 2.36 (d, *J* = 7.9 Hz, 2H).
^{13}C NMR (101 MHz, $CDCl_3$) δ 209.48, 159.51, 147.48, 139.94, 133.53, 128.61, 127.76, 76.77, 69.10, 35.23, 26.70.

2-((4-chlorophenyl)(hydroxy)methyl)cyclohex-2-en-1-one 4-Chlorbenzaldehyde (42 mg, 0.3 mmol) was placed in an oven-dried 5 mL Schlenk tube, and dissolved in anhydrous dichloromethane (1 mL), then 1-Cyclohex-2-enone (90 uL, 0.9 mmol) was introduced, a solution of **103** (30 mg, 0.03 mmol) in anhydrous dichloromethane (1 mL) was added drop-wise, the mixture was stirred under atmosphere of argon at room temperature, then was followed by addition of titanium chloride solution in anhydrous dichloromethane (1 M) (0.3 mL, 0.3 mmol). The mixture was stirred for 0.5 hour and then was quenched by saturated aqueous $NaHCO_3$ solution (3.0 mL), the mixture was stirred for an additional 0.5 hour. Then, the inorganic precipitate was filtered through Celite. The organic phase was dried over Na_2SO_4,

filtered and evaporated under vacuum to give the crude product, the crude compound was purified by silica gel column chromatography using petroleum ether / ethyl acetate (2:1) to give pure product as yellow wax (50 mg, 71%).

^{1}H NMR (400 MHz, $CDCl_3$) δ 7.26 (s, 4H), 6.72 (s, 1H), 5.48 (s, 1H), 3.48 (s, 1H), 2.47 – 2.32 (m, 4H), 2.03 – 1.89 (m, 2H).

^{13}C NMR (101 MHz, $CDCl_3$) δ 200.24, 158.66, 147.40, 147.28, 140.82, 133.18, 129.96, 127.86, 114.05, 71.88, 56.50, 38.52, 22.47.

2-(hydroxy(p-tolyl)methyl)cyclohex-2-en-1-one 4-Methylbenzaldehyde (36 mg, 0.3 mmol) was placed in an oven-dried 5 mL Schlenk tube, and dissolved in anhydrous dichloromethane (1 mL), then 1-Cyclohex-2-enone (90 uL, 0.9 mmol) was introduced, a solution of **103** (30 mg, 0.03 mmol) in anhydrous dichloromethane (1 mL) was added drop-wise, the mixture was stirred under atmosphere of argon at room temperature, then was followed by addition of titanium chloride solution in anhydrous dichloromethane (1 M) (0.3 mL, 0.3 mmol). The mixture was stirred for 0.5 hour and then was quenched by saturated aqueous $NaHCO_3$ solution (3.0 mL), the mixture was stirred for an additional 0.5 hour. Then, the inorganic precipitate was filtered through Celite. The organic phase was dried over Na_2SO_4, filtered and evaporated under vacuum to give the crude product, the crude compound was purified by silica gel column chromatography using petroleum ether / ethyl acetate (5:1) to give pure product as a yellow wax (42 mg, 66%).

^{1}H NMR (400 MHz, $CDCl_3$) δ 7.21 – 7.13 (m, 2H), 7.13 – 7.00 (m, 2H), 6.68 (td, *J* = 4.2, 1.1 Hz, 1H), 5.48 – 5.42 (s, 1H), 3.29 (d, *J* = 5.3 Hz, 1H), 2.42 – 2.32 (m, 4H), 2.26 (s, 3H), 1.99 – 1.85 (m, 2H).

^{13}C NMR (101 MHz, $CDCl_3$) δ 200.41, 147.13, 141.16, 138.72, 137.14, 129.01, 126.39, 76.69, 72.46, 38.60, 25.76, 22.54, 21.10.

Crystallographic data

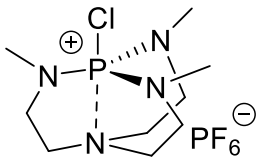

[ClP(MeNCH$_2$CH$_2$)$_3$N][PF$_6$] (12a-Cl$^+$.PF$_6^-$). X-Ray: the product was crystallized from Et$_2$O/CH$_3$CN. CCDC 2060857 contains the supplementary crystallographic data for this paper. (Table S1)

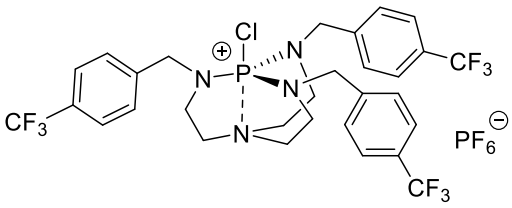

[ClP(*p*-CF$_3$-BnNCH$_2$CH$_2$)$_3$N][PF$_6$] (12e-Cl$^+$.PF$_6^-$) X-Ray: product was crystallized from Et$_2$O/CH$_3$CN. CCDC 2060875 contains supplementary crystallographic data for this paper. (Table S2)

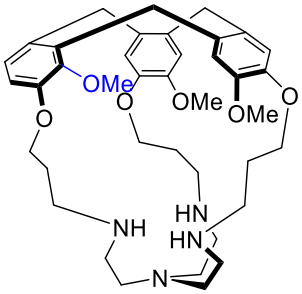

Hemicryptophane 93 Single crystal $C_{39}H_{54}N_4O_6$ was crystalized by slow diffusion of CH_2Cl_2, CCDC 2092998 contains the supplementary crystallographic data for this paper. (Table S3)

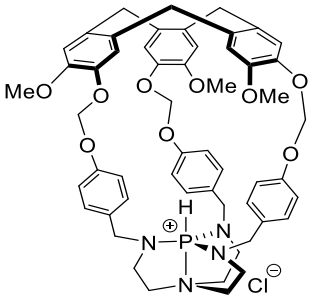

Hemicryptophane 102-H$^+$.Cl$^-$ Single crystal **C$_{58}$H$_{68}$ClN$_4$O$_{10}$P** was crystalized by slow diffusion of CH_2Cl_2, CCDC 2093016 contains the supplementary crystallographic data for this paper. (Table S3)

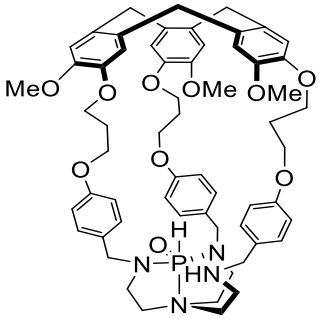

Hemicryptophane 103-PH=O Single crystal **C$_{61}$H$_{66.6}$Br$_{0.6}$Cl$_3$N$_4$O$_{10}$P** was crystalized by slow diffusion of CH_2Cl_2, CCDC 2099451 contains the supplementary crystallographic data for this paper. (Table S5)

Table S1

Empirical formula	$C_9H_{21}ClF_6N_4P_2$
Formula weight	396.69
Temperature/K	180.01(10)
Crystal system	trigonal
Space group	R3
a/Å	9.0049(7)
b/Å	9.0049(7)
c/Å	17.2073(11)
α/°	90
β/°	90
γ/°	120
Volume/Å^3	1208.4(2)
Z	3
ρcalcg/cm^3	1.635
μ/mm-1	4.594
F(000)	612.0
Crystal size/mm^3	0.2 × 0.14 × 0.05
Radiation	Cu Kα (λ = 1.54184)
2Θ range for data collection/°	12.462 to 141.498
Index ranges	-10 ⩽ h ⩽ 10, -9 ⩽ k ⩽ 10, -20 ⩽ l ⩽ 20
Reflections collected	1942
Independent reflections	1012 [Rint = 0.0239, Rsigma = 0.0262]
Data/restraints/parameters	1012/2/68
Goodness-of-fit on F^2	1.113
Final R indexes [I>=2σ (I)]	R_1 = 0.0589, wR_2 = 0.1663
Final R indexes [all data]	R_1 = 0.0596, wR_2 = 0.1677
Largest diff. peak/hole / e Å^{-3}	0.54/-0.65

Table S2

Empirical formula	$C_{30}H_{30}ClF_{15}N_4P_2$
Formula weight	828.97
Temperature/K	295
Crystal system	triclinic
Space group	P-1
a/Å	9.9667(4)
b/Å	10.7222(5)
c/Å	16.8376(7)
α/°	80.786(4)
β/°	81.175(4)
γ/°	80.644(4)
Volume/Å^3	1737.45(13)
Z	2
ρcalcg/cm3	1.585
μ/mm-1	2.864
F(000)	840.0
Crystal size/mm^3	0.15 × 0.15 × 0.05
Radiation	Cu Kα (λ = 1.54184)
2Θ range for data collection/°	5.364 to 145.406
Index ranges	-12 ⩽ h ⩽ 12, -8 ⩽ k ⩽ 12, -17 ⩽ l ⩽ 20
Reflections collected	15154
Independent reflections	6733 [Rint = 0.0350, Rsigma = 0.0386]
Data/restraints/parameters	6733/36/496
Goodness-of-fit on F2	1.042
Final R indexes [I>=2σ (I)]	R1 = 0.0601, wR_2 = 0.1660
Final R indexes [all data]	R1 = 0.0671, wR_2 = 0.1767
Largest diff. peak/hole / e Å^{-3}	0.59/-0.41

Table S3

Empirical formula	$C_{39}H_{57}Cl_3N_4O_6$
Formula weight	784.23
Temperature/K	295
Crystal system	monoclinic
Space group	C2/c
a/Å	32.0703(12)
b/Å	15.3700(11)
c/Å	21.3754(8)
α/°	90
β/°	92.017(3)
γ/°	90
Volume/Å^3	10529.8(9)
Z	8
ρ_{calc}g/cm^3	0.989
μ/mm^{-1}	1.883
F(000)	3344.0
Crystal size/mm^3	0.4 × 0.22 × 0.14
Radiation	Cu Kα (λ = 1.54184)
2Θ range for data collection/°	7.55 to 136.5
Index ranges	-37 ⩽ h ⩽ 38, -9 ⩽ k ⩽ 18, -25 ⩽ l ⩽ 25
Reflections collected	23778
Independent reflections	9576 [R_{int} = 0.0536, R_{sigma} = 0.0690]
Data/restraints/parameters	9576/87/473
Goodness-of-fit on F^2	1.173
Final R indexes [I>=2σ (I)]	R_1 = 0.0959, wR_2 = 0.2406
Final R indexes [all data]	R_1 = 0.1592, wR_2 = 0.2913
Largest diff. peak/hole / e Å^{-3}	0.31/-0.28

Table S4

Empirical formula	$C_{58}H_{68}ClN_4O_{10}P$
Formula weight	1047.58
Temperature/K	180.01(10)
Crystal system	triclinic
Space group	P-1
a/Å	10.2610(2)
b/Å	10.87103(19)
c/Å	26.4434(4)
α/°	82.7150(14)
β/°	86.3036(16)
γ/°	77.2137(17)
Volume/Å^3	2851.32(10)
Z	2
ρ_{calc}g/cm^3	1.220
μ/mm^{-1}	1.340
F(000)	1112.0
Crystal size/mm^3	0.24 × 0.22 × 0.06
Radiation	Cu Kα (λ = 1.54184)
2Θ range for data collection/°	6.744 to 141.766
Index ranges	-12 ⩽ h ⩽ 12, -13 ⩽ k ⩽ 13, -32 ⩽ l ⩽ 32
Reflections collected	49135
Independent reflections	10867 [R_{int} = 0.0415, R_{sigma} = 0.0260]
Data/restraints/parameters	10867/16/690
Goodness-of-fit on F^2	1.048
Final R indexes [I>=2σ (I)]	R_1 = 0.0641, wR_2 = 0.1779
Final R indexes [all data]	R_1 = 0.0717, wR_2 = 0.1845
Largest diff. peak/hole / e Å^{-3}	1.26/-0.59

Table S5

Empirical formula	$C_{61}H_{66.6}Br_{0.6}Cl_3N_4O_{10}P$
Formula weight	1201.04
Temperature/K	153.01(10)
Crystal system	monoclinic
Space group	$P2_1/n$
a/Å	12.4213(8)
b/Å	29.5258(19)
c/Å	17.9736(8)
α/°	90
β/°	102.414(6)
γ/°	90
Volume/Å^3	6437.7(7)
Z	4
ρ_{calc}g/cm^3	1.239
μ/mm^{-1}	2.419
F(000)	2510.0
Crystal size/mm^3	0.16 × 0.08 × 0.04
Radiation	Cu Kα (λ = 1.54184)
2Θ range for data collection/°	5.858 to 141.642
Index ranges	-13 ⩽ h ⩽ 15, -33 ⩽ k ⩽ 35, -21 ⩽ l ⩽ 20
Reflections collected	29490
Independent reflections	11984 [R_{int} = 0.0899, R_{sigma} = 0.1362]
Data/restraints/parameters	11984/56/757
Goodness-of-fit on F^2	1.135
Final R indexes [I>=2σ (I)]	R_1 = 0.1294, wR_2 = 0.2712
Final R indexes [all data]	R_1 = 0.2146, wR_2 = 0.3175
Largest diff. peak/hole / e Å^{-3}	0.53/-0.41

Determination of rate constants of proton exchange of 103-H^+

Table S6 Proton transfer kinetic data between **103**-H^+ and **103** (**12a** as monitor**)**

	t(min)	[**103**]	[**103**-H^+]	[**12a**-H^+]	[**12a**]	[**103**]/[**103**-H^+]	d([**103**]/[**103**-H^+])/dt	(1+[**103**]/[**103**-H^+])	[**12a**-H^+]/[**12a**]	$k_1K_e/K_a^{\mathbf{12a}\text{-}H^+}$
1	0	0.8791	5.1547	3.3261	18.0362	0.170543388	-	1.170543388	0.184412459	-
2	30	1.0141	7.6105	5.4794	27.5649	0.133250115	0.000781901	1.133250115	0.198781784	0.000137152
3	60	0.0715	0.3288	0.263	1.2295	0.217457421	0.001361967	1.217457421	0.213908093	0.000239299
4	90	0.0675	0.314	0.2787	1.2281	0.214968153	0.000773014	1.214968153	0.226935917	0.000144386
5	120	0.0796	0.3017	0.2875	1.2192	0.26312825	0.001394787	1.26312825	0.235810367	0.000260243
6	150	0.0844	0.2826	0.2977	1.1809	0.298655343	0.001481176	1.298655343	0.252095859	0.000287527
7	180	1.8574	5.2661	5.7805	23.0259	0.352708126	0.001344158	1.352708126	0.25104339	0.000249456
8	210	1.8955	4.9973	5.8713	22.0822	0.379304825	0.001005577	1.379304825	0.265812124	0.000193842
9	240	0.1045	0.253	0.3176	1.1688	0.413043478	0.001711712	1.413043478	0.271731691	0.00032918
10	270	2.2723	4.7142	6.1381	21.9193	0.482011794	0.002335643	1.482011794	0.280031753	0.000441329
11	300	2.2478	4.0634	5.8139	20.0513	0.553182064	0.001052017	1.553182064	0.289951275	0.000196393
12	330	2.1566	3.9561	5.9179	19.8868	0.545132123	0.001394391	1.545132123	0.297579299	0.000268548
13	360	2.547	3.9994	6.2663	20.2325	0.636845527	0.00162535	1.636845527	0.309714568	0.00030754
14	390	2.1678	3.3732	5.6442	17.9871	0.64265386	0.00125138	1.64265386	0.313791551	0.000239048
15	420	0.151	0.2121	0.3646	1.1543	0.711921236	0.00142173	1.711921236	0.315862427	0.000262319
16	450	2.3093	3.1723	5.7199	17.8746	0.727957633	0.001933399	1.727957633	0.320001566	0.000358047
17	480	2.6647	3.2185	6.267	18.9661	0.827932267	0.002488504	1.827932267	0.330431665	0.000449842
18	510	0.1644	0.1874	0.3737	1.1224	0.877267876	0.00232931	1.877267876	0.332947256	0.00041312
19	540	2.8723	2.9682	6.1574	18.2002	0.967690856	0.002008543	1.967690856	0.331214964	0.000345339
20	570	2.8771	2.8125	6.2613	18.1298	0.997780475	0.001347088	1.997780475	0.345359574	0.000232873
21	600	2.9219	2.7867	6.3152	18.0553	1.048516166	0.002732266	2.048516166	0.349769874	0.000466515
22	630	3.043	2.6194	6.2539	17.2318	1.161716424	0.001425204	2.161716424	0.362927843	0.000239276
23	660	2.991	2.6375	6.5362	18.0737	1.134028436	0.002910767	2.134028436	0.361641501	0.000493271
24	690	3.0441	2.2779	5.9077	16.0721	1.336362439	0.003806461	2.336362439	0.367574866	0.000598862
26	750	2.8877	2.2432	6.2449	16.8988	1.287312767	0.001059781	2.287312767	0.36954695	0.000171222
27	780	3.0853	2.1636	6.0147	16.1186	1.426002958	0.003658205	2.426002958	0.373152755	0.000562682
28	810	3.0778	2.0426	6.2022	15.9919	1.506805052	0.001054464	2.506805052	0.387123841	0.000163139
29	840	2.9635	1.9899	6.3054	16.0508	1.489270818	0.002360166	2.489270818	0.392840232	0.000372466

Defining $X_i=\dfrac{k_1K_e}{K_a^{PH^+@\mathbf{12a}}}$ (i=1,2,3,…,29.)

so $\sum_{i=1}^{29} X_i = 0.008422915$ $\bar{X}= 0.00031196$

According to

$$\frac{d\left(\dfrac{[P@\mathbf{103}]}{[PH^+@\mathbf{103}]}\right)}{dt}=\frac{k_1K_e}{K_a^{PH^+@\mathbf{12a}}}\times\frac{[P@\mathbf{12a}](1+[P@\mathbf{103}]/[PH^+@\mathbf{103}])}{[PH^+@\mathbf{12a}]}$$

$$\frac{k_1 K_e}{K_a^{PH^+}@\mathbf{12a}} = \frac{\bar{X}}{60} = 5.2\times10^{-6}\ \ L\cdot mol^{-}s^{-}$$

with $K_e = 10^{-32.2}$ $K_a^{PH^+}@\mathbf{103} = 4.77\times10^{-33}$

$$k_1 = 1.04\times10^{-6}$$

$$k_{-1} = 1.37\times10^{-6}$$

Analytical chiral HPLC separation

Analytical chiral HPLC separation for hemicryptophane 93

• The sample **93** is dissolved in dichloromethane, injected on the chiral columns, and detected with an UV detector at 280 nm. The flow-rate is 1 mL/min.

Column	Mobile Phase	t1	k1	t2	k2	α	Rs
Chiralpak IF	Heptane/ ethanol + triethylamine 0.5% / dichloromethane	4.81	0.63	6.27	1.13	1.79	4.27

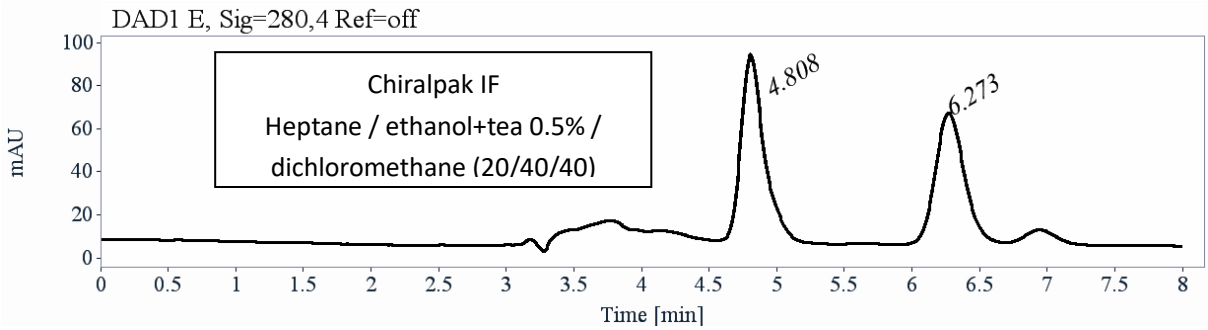

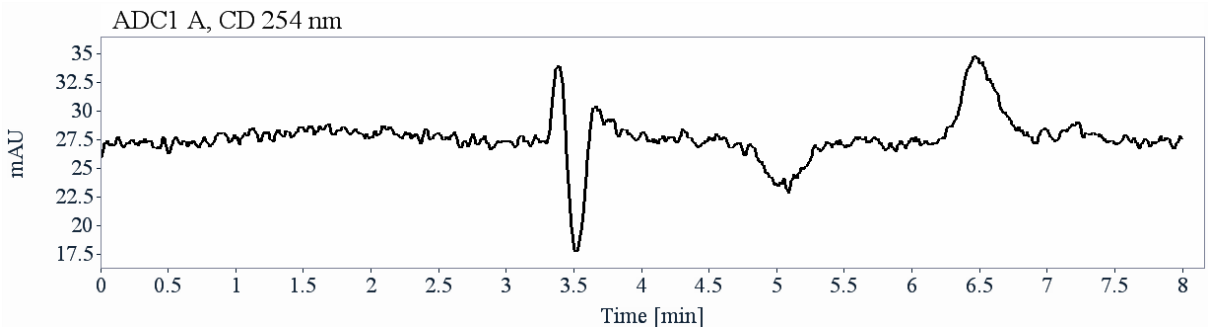

RT [min]	Area	Area%	Capacity Factor	Enantioselectivity	Resolution (USP)
4.81	1047	53.78	0.63		
6.27	900	46.22	1.13	1.79	4.27
Sum	1947	100.00			

Preparative separation for hemicryptophane 93

• Sample preparation: About 70 mg of compound **93** are dissolved in 3 mL of dichloromethane.

• Chromatographic conditions: Chiralpak IF (250 x 10 mm), Hexane / ethanol + tea 0.5% / dichloromethane (20/40/40) as mobile phase, flow-rate = 5 mL/min, UV detection at 254 nm.

• Injections (stacked): 15 times 200 uL, every 5.5 minutes.

• First fraction: 12 mg of the first eluted with ee > 99.5 %

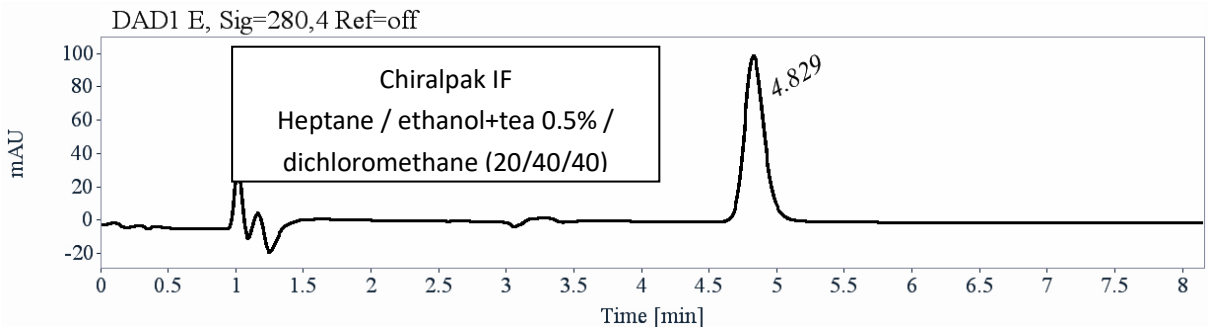

RT [min]	Area	Area%
4.12	1042	100.00
Sum	1042	100.00

• Second fraction: 11 mg of the second eluted with ee > 99.5 %

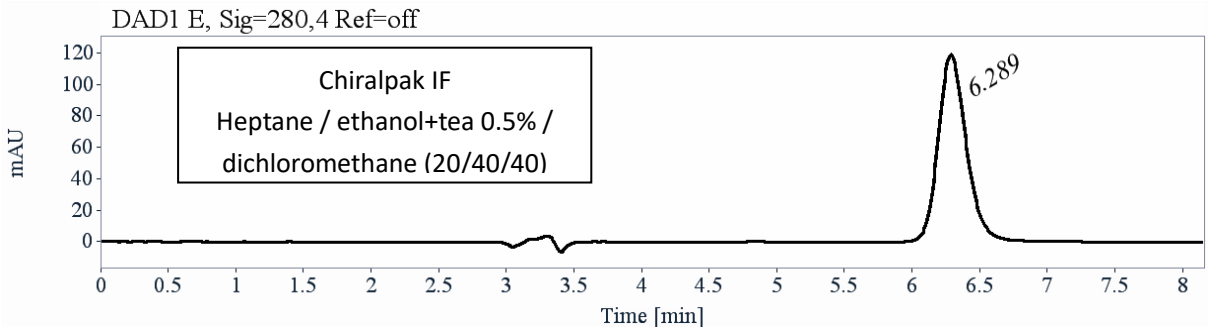

Optical rotations

Optical rotations were measured on a 241 Perkin-Elmer polarimeter with a mercury lamp (589, 578, 546, 436 and 405 nm) and a double-jacketed 10 cm cell at 25°C.

λ (nm)	first eluted on Chiralpak IF α_λ^{25} (CH_2Cl_2, c =0.15)	second eluted on Chiralpak IF α_λ^{25} (CH_2Cl_2, c =0.18)
589	- 8.5	+ 8.5
578	- 9	+ 9
546	- 11	+ 11
436	- 17.5	+ 17.5
405	- 23	+ 23

Assignment of the stereodescriptor for hemicryptophane 93

Based on the methodology described by Prelog for C_3 CTV units, the stereodescriptor *M* or *P* can be assigned for this C_1 symmetrical CTV.[161] As equivalent with this CTV presenting a C_1 symmetry. The CIP rules allow for determining the priority of one pair. In the case of this C_1 symmetrical CTV, atom c has to be chosen and then the conformation around bonds b–c and the torsion angles τ [e–d–b–f] has to be selected, according to CIP classification. Thus, this spatial arrangement correspond to a stereodescriptor *M* has to be used for this spatial arrangement.

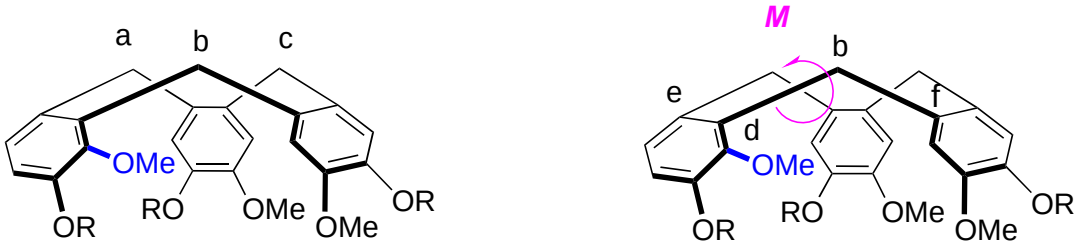

[161] *Collet, A.; Gabard, J.; Jacques, J.; Cesario, M.; Guilhem, J.; Pascard, C. J. Chem. Soc. Perkin 1* ***1981****, 0, 1630.*

Analytical chiral HPLC separation for 94-boc

• The sample is dissolved in dichloromethane, injected on the chiral columns, and detected with an UV detector at 254 nm, a circular dichroism detector at 254 nm. The flow-rate is 1 mL/min.

Column	Mobile Phase	t1	k1	t2	k2	α	Rs
Chiralpak ID	Heptane/ ethanol + triethylamine 0.1% / dichloromethane (60/20/20)	7.99 (-)	1.71	10.12 (+)	2.43	1.42	3.39

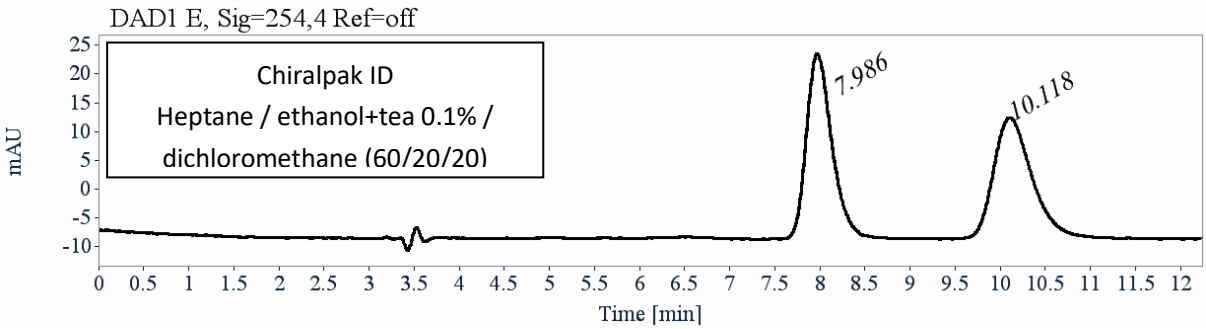

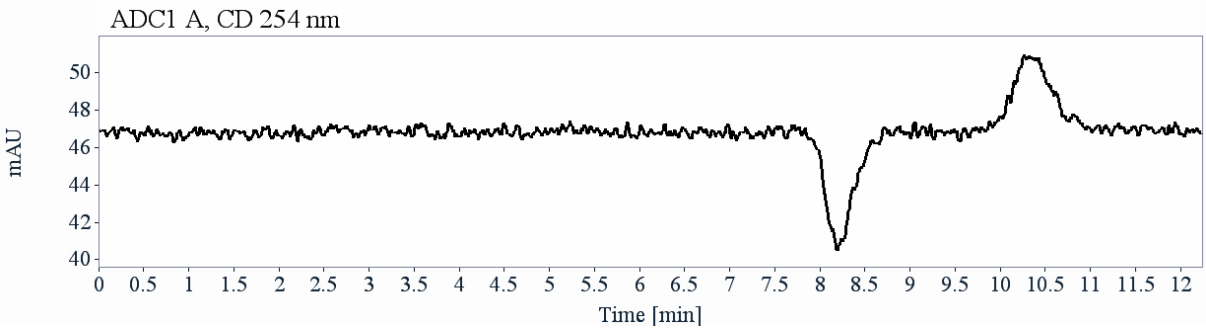

RT [min]	Area	Area%	Capacity Factor	Enantioselectivity	Resolution (USP)
7.99	635	50.22	1.71		
10.12	630	49.78	2.43	1.42	3.39
Sum	1265	100.00			

Preparative separation for compound 94-boc:

• Sample preparation: About 60 mg of compound **94-boc** are dissolved in 1.7 mL of dichloromethane.

• Chromatographic conditions: Chiralpak ID (250 x 10 mm), hexane / ethanol + tea 0.1% / dichloromethane (60/20/20) as mobile phase, flow-rate = 5 mL/min, UV detection at 254 nm.

• Injections (stacked): 17 times 100 □L, every 11 minutes.

• First fraction: 27 mg of the first eluted with ee > 99.5%

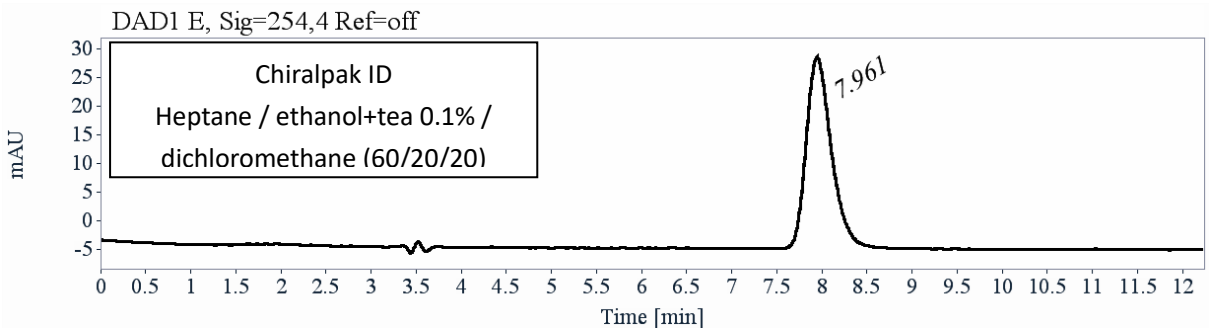

RT [min]	Area	Area%
7.96	651	100.00
Sum	651	100.00

• Second fraction: 27 mg of the second eluted with ee > 99.5%

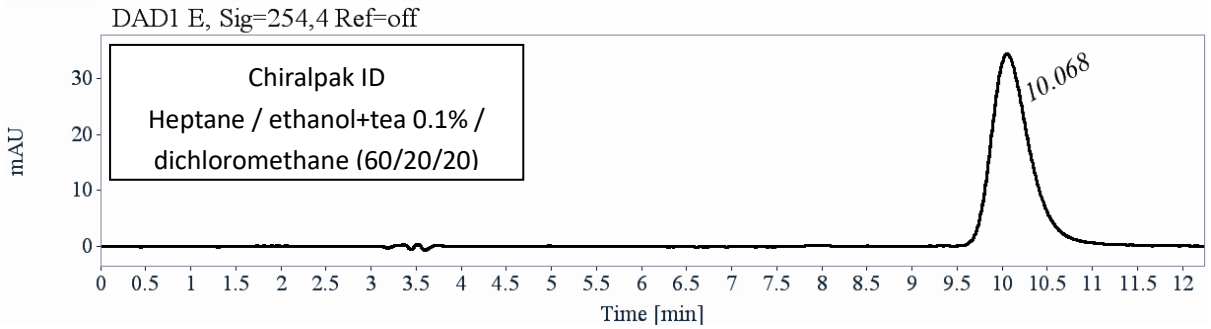

RT [min]	Area	Area%
10.07	1016	100.00
Sum	1016	100.00

Optical rotations

Optical rotations were measured on a Jasco P-2000 polarimeter with a halogen lamp (589, 578, 546, 436, 405, 365 and 325 nm), in a 10 cm cell, thermostated at 25°C with a Peltier controlled cell holder.

λ (nm)	first eluted on α_λ^{25} (CH_2Cl_2, c =0.12)	second eluted α_λ^{25} (CH_2Cl_2, c =0.17)
589	+140	-140
578	+147	-147
546	+172	-172
436	+306	-306
405	+391	-391
365	+571	-571
325	+793	-793

Analytical chiral HPLC separation for 94-PH=O

• The sample is dissolved in dichloromethane, injected on the chiral column, and detected with an UV detector at 254 and 280 nm. The flow-rate is 1 mL/min.

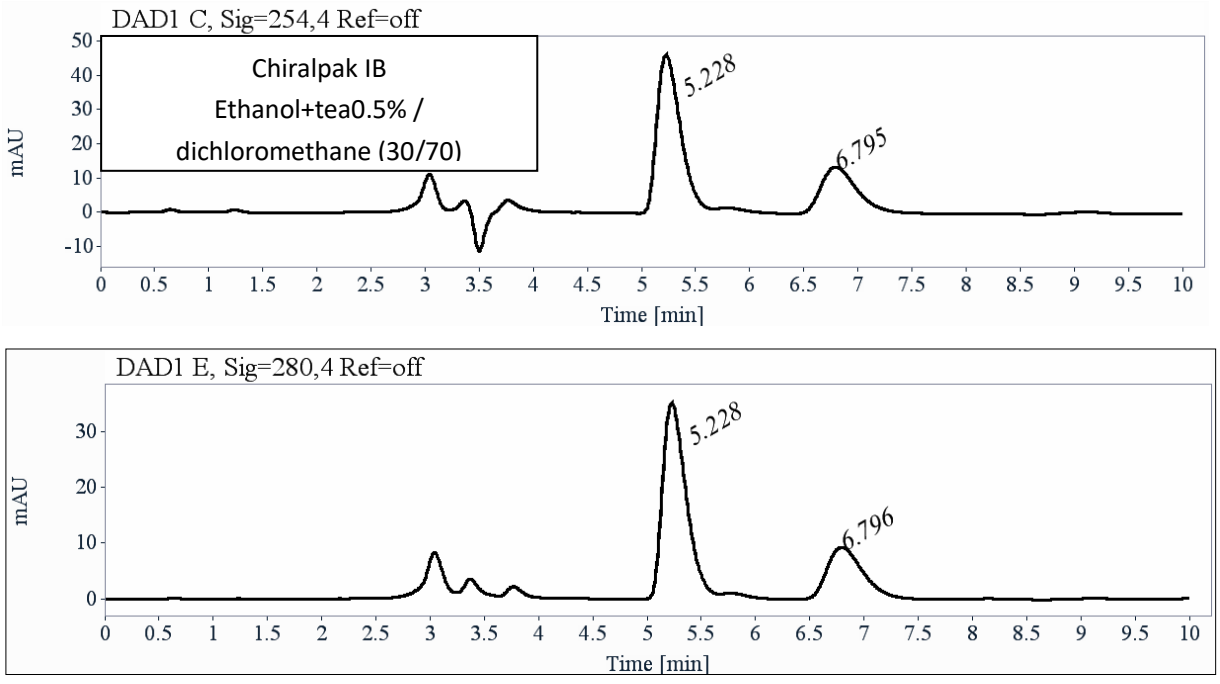

RT [min]	Area	Area%	Capacity Factor
5.23	708	68.62	0.77
6.80	324	31.38	1.30

Sum	1032	100.00	
RT [min]	**Area**	**Area%**	**Capacity Factor**
5.23	535	71.00	0.77
6.80	219	29.00	1.30
Sum	754	100.00	

Preparative separation for 94-PH=O

• Sample preparation: About 58 mg of compound **94-PH=O** are dissolved in 2.15 mL of a mixture of dichloromethane and ethanol (70/30).

• Chromatographic conditions: Chiralpak IB (250 x 10 mm), Ethanol+tea0.5% / dichloromethane (30/70) as mobile phase, flow-rate = 5 mL/min, UV detection at 270 nm.

• Injections (stacked): 55 times 40 uL, every 5 minutes.

• First fraction: 16 mg **94-PH=O-FR1**

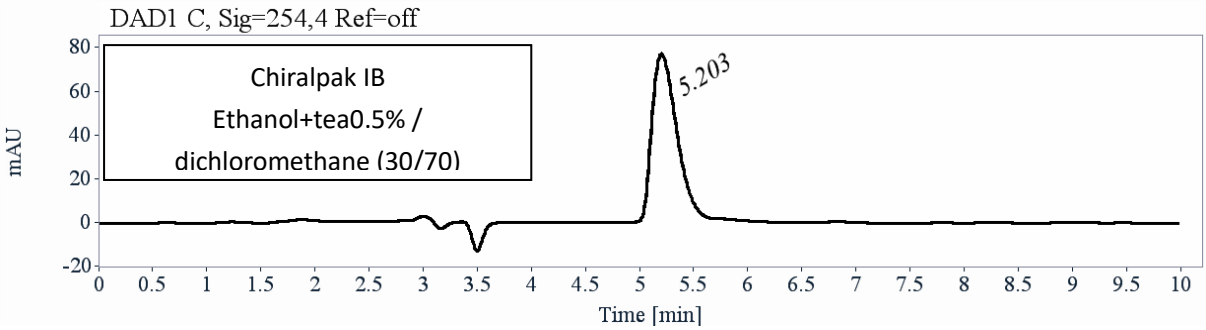

• Second fraction: 12 mg **94-PH=O-FR2**

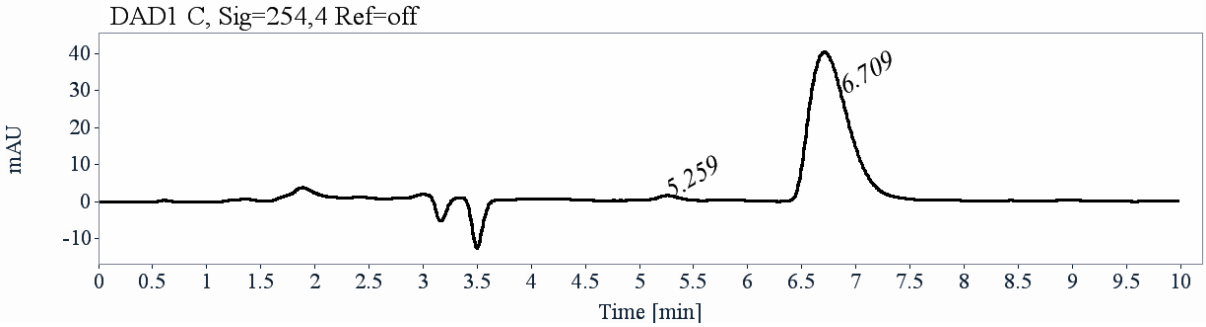

Analytical chiral HPLC separation for CTV 108

• The sample is dissolved in dichloromethane, injected on the chiral columns, and detected with an UV detector at 254 nm and a polarimetric detector. The flow-rate is 1 mL/min.

Column	Mobile Phase	t1	k1	t2	k2	α	Rs
Chiralpak IG	Hexane /ethanol / dichloromethane (40/30/30)	7.26 (+)	1.46	8.78 (-)	1.98	1.35	2.76

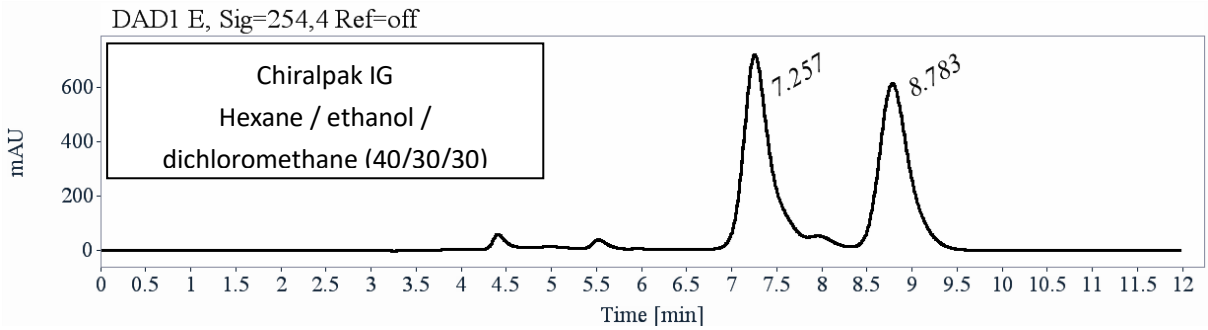

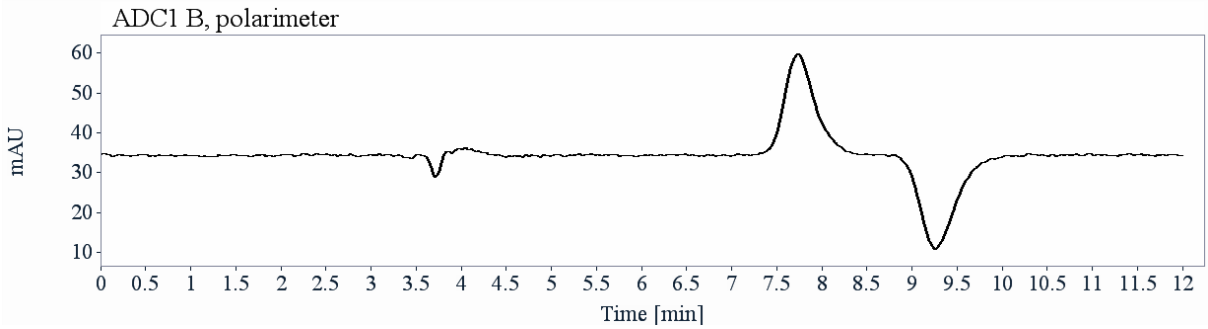

RT [min]	Area	Area%	Capacity Factor	Enantioselectivity	Resolution (USP)
7.26	15202	51.21	1.46		
8.78	14412	48.79	1.98	1.35	2.76
Sum	29684	100.00			

Preparative separation for CTV 108

• Sample preparation: About 300 mg of compound **CTV 108** are dissolved in 5 mL of a mixture of dichloromethane, ethanol and hexane (60/20/20).

• Chromatographic conditions: Chiralpak IG (250 x 10 mm), hexane / ethanol / dichloromethane (40/30/30) as mobile phase, flow-rate = 5 mL/min, UV detection at 254 nm.

• Injections (stacked): 100 times 50 uL, every 4 minutes.

• First fraction: 125 mg of the first eluted with ee > 98.5 %

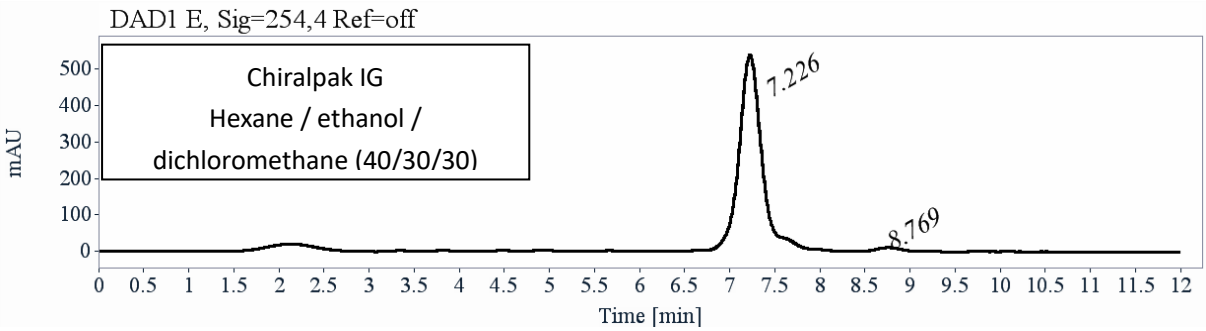

RT [min]	Area	Area%
7.23	9609	99.28
8.77	70	0.72
Sum	9679	100.00

• Second fraction: 110 mg of the second eluted with ee > 99 %

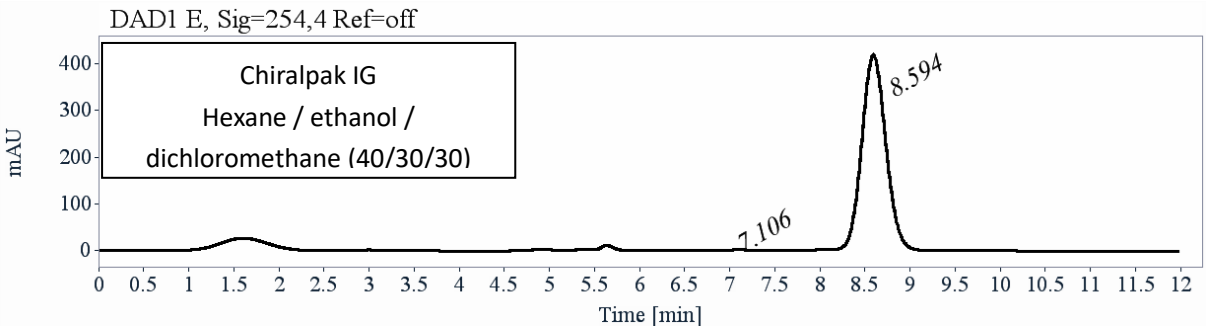

RT [min]	Area	Area%
7.11	35	0.44
8.59	7905	99.56
Sum	7940	100.00

Analytical chiral HPLC separation for CTV 111

• The sample is dissolved in dichloromethane, injected on the chiral column, and detected with an UV detector at 254 nm and a polarimetric detector. The flow-rate is 1 mL/min.

Column	Mobile Phase	t1	k1	t2	k2	α	Rs
Chiralpak IF	Ethanol / dichloromethane(50/50)	4.79 (+)	0.62	6.20 (-)	1.10	1.76	4.17

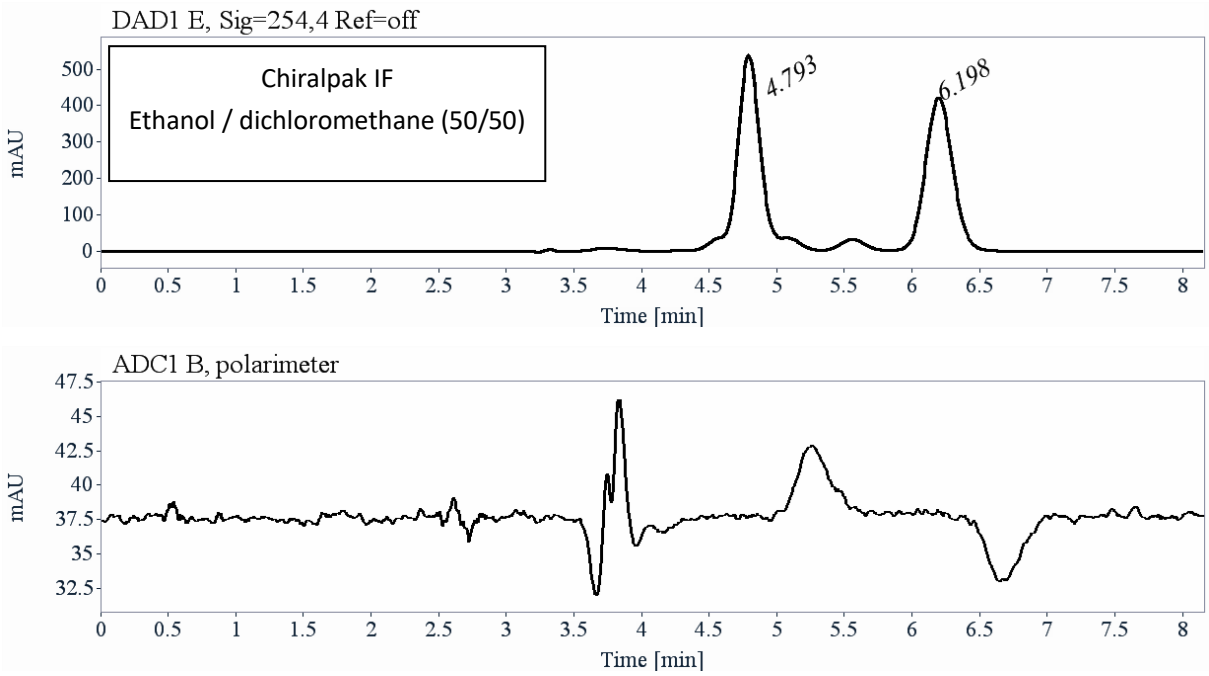

RT [min]	Area	Area%	Capacity Factor	Enantioselectivity	Resolution (USP)
4.79	6071	50.31	0.62		
6.20	5995	49.69	1.10	1.76	4.17
Sum	12067	100.00			

Preparative separation for CTV-111

• Sample preparation: About 470 mg of compound **CTV-111** are dissolved in 10 mL of a mixture of dichloromethane and ethanol (50/50).

• Chromatographic conditions: Chiralpak IF (250 x 10 mm), ethanol / dichloromethane (50/50) as mobile phase, flow-rate = 5 mL/min, UV detection at 310 nm.

• Injections (stacked): 125 times 80 uL, every 4 minutes.

• First fraction: 180 mg of the first eluted with ee > 99.5 %

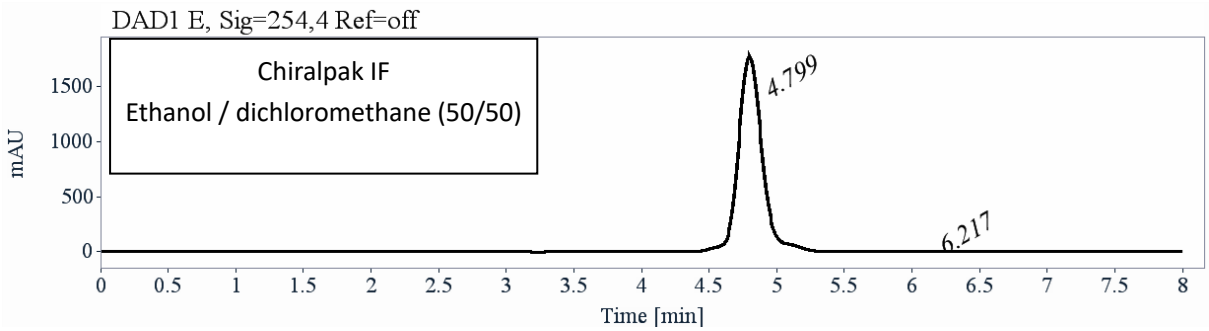

RT [min]	Area	Area%
4.80	21753	99.87
6.22	28	0.13
Sum	21781	100.00

• Second fraction: 180 mg of the second eluted with ee > 99 %

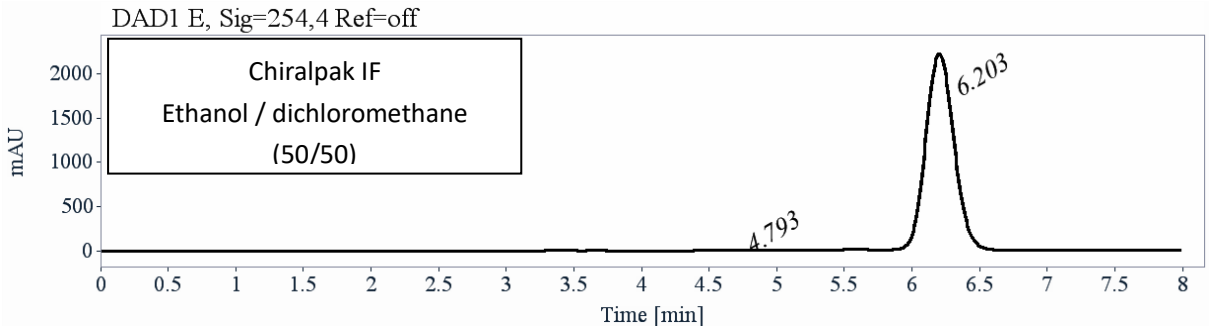

RT [min]	Area	Area%
4.79	100	0.30
6.20	32691	99.70
Sum	32791	100.00

Titration experiments

A solution of host **12-Cl$^+$.PF$_6^-$** (5.0 mM in CD_3CN, 500 µL) was titrated in NMR tubes with aliquots of a concentrated solution (50 mM in CD_3CN) of halide anions. The shifts of $N_{eq}CH_2$ protons of the hosts signals were measured after each addition and plotted as a function of the guest/host ratio ([G]/[H]). The association constant K_a was obtained by nonlinear least-squares fitting of these plots using the BINDFIT program.

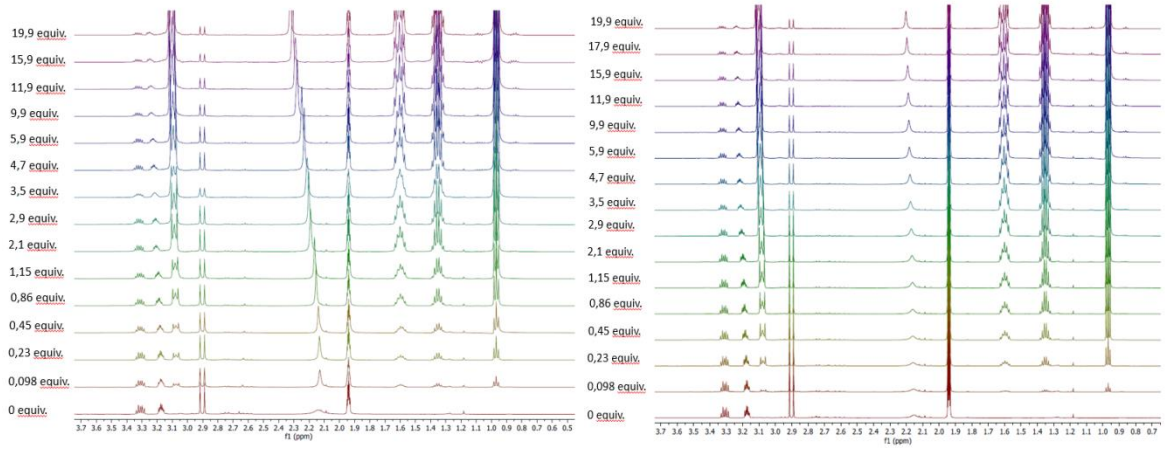

Figure S1 ^{1}H NMR (CD_3CN, 500 MHz, 300 K) spectra of [**12a-Cl$^+$.PF$_6^-$**] = 5 mM for several additions of a concentrated solution [*n*-Bu_4N^+ Cl^-] = 50 mM.

Figure S2 ^{1}H NMR (CD_3CN, 600 MHz, 300 K) spectra of [**12a-Cl$^+$.PF$_6^-$**] = 5 mM for several additions of a concentrated solution [*n*-Bu_4N^+ Br^-] = 50 mM.

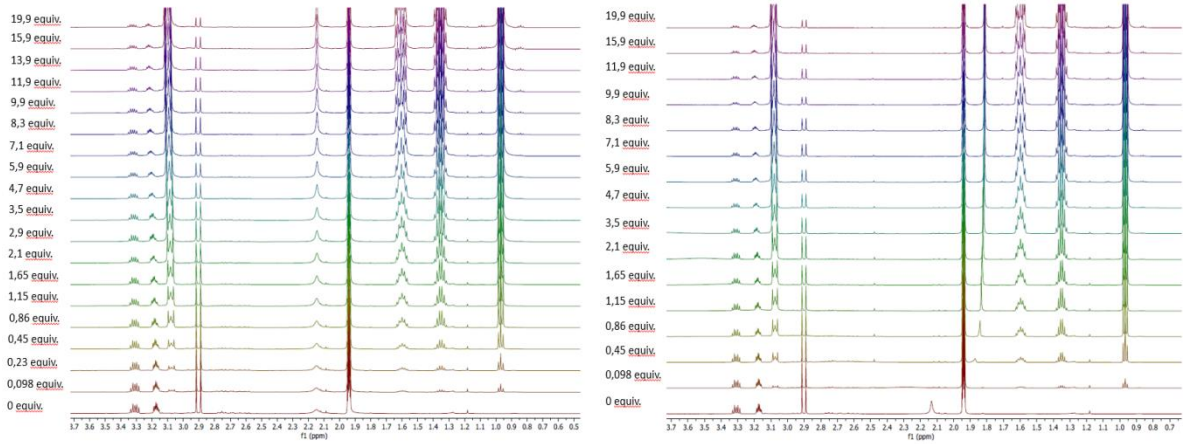

Figure S3 ^{1}H NMR (CD_3CN, 500 MHz, 300 K) spectra of [**12a-Cl$^+$.PF$_6^-$**] = 5 mM for several additions of a concentrated solution [*n*-Bu_4N^+ I^-] = 50 mM.

Figure S4 ^{1}H NMR (CD_3CN, 500 MHz, 300 K) spectra of [**12a-Cl$^+$.PF$_6^-$**] = 5 mM for several additions of a concentrated solution [*n*-Bu_4N^+ AcO^-] = 50 mM.

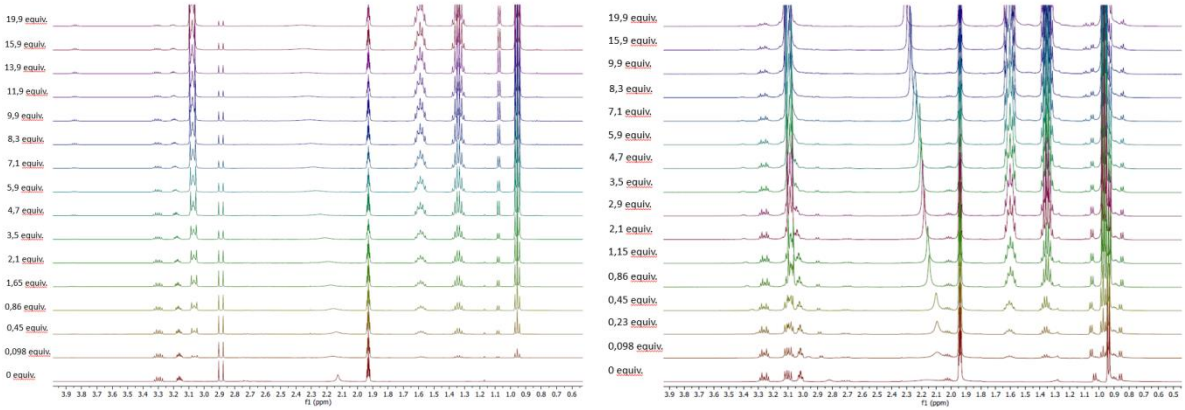

Figure S5 ^{1}H NMR (CD_3CN, 500 MHz, 300 K) spectra of [**12a-Cl$^+$.PF$_6^-$**] = 5 mM for several additions of a concentrated solution [*n*-Bu_4N^+ CN^-] = 50 mM

Figure S6 ^{1}H NMR (CD_3CN, 500 MHz, 300 K) spectra of [**12b-Cl$^+$.PF$_6^-$**] = 5 mM for several additions of a concentrated solution [*n*-Bu_4N^+ Cl^-] = 50 mM.

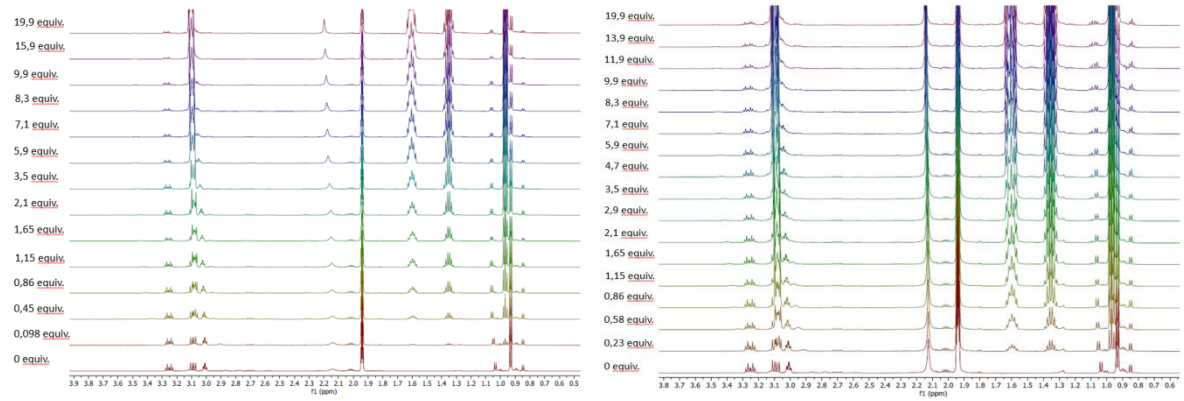

Figure S7 ^{1}H NMR (CD_3CN, 600 MHz, 300 K) spectra of [**12b-Cl$^+$.PF$_6^-$**] = 5 mM for several additions of a concentrated solution [*n*-Bu_4N^+ Br^-] = 50 mM.

Figure S8 ^{1}H NMR (CD_3CN, 500 MHz, 300 K) spectra of [**12b-Cl$^+$.PF$_6^-$**] = 5 mM for several additions of a concentrated solution [*n*-Bu_4N^+ I^-] = 50 mM.

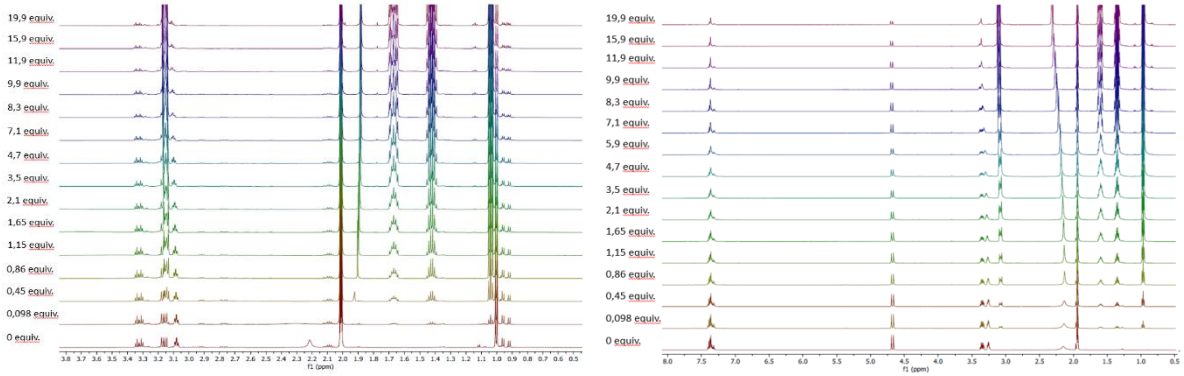

Figure S9 ^{1}H NMR (CD_3CN, 600 MHz, 300 K) spectra of [**12b-Cl$^+$.PF$_6^-$**] = 5 mM for several additions of a concentrated solution [*n*-Bu_4N^+ AcO^-] = 50 mM.

Figure S10 ^{1}H NMR (CD_3CN, 500 MHz, 300 K) spectra of [**12c-Cl$^+$.PF$_6^-$**] = 5 mM for several additions of a concentrated solution [*n*-Bu_4N^+ Cl^-] = 50 mM.

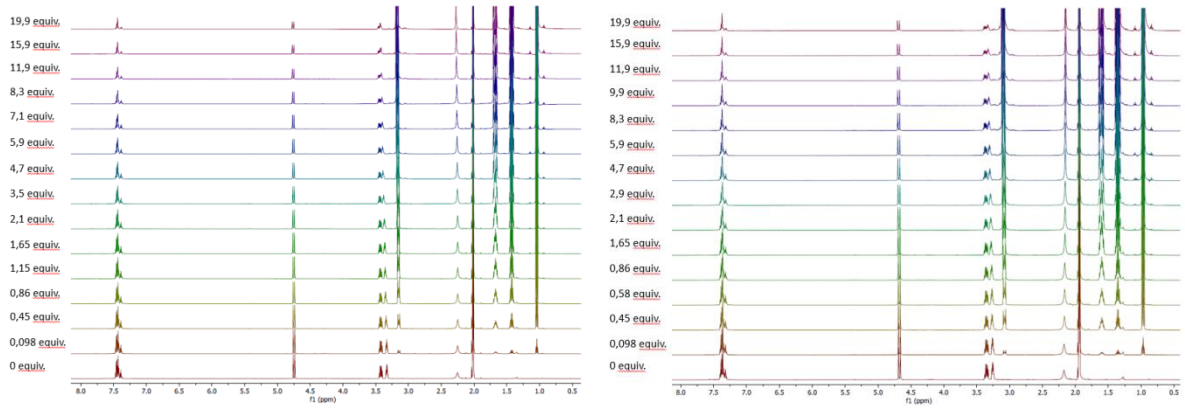

Figure S11 ^{1}H NMR (CD_3CN, 600 MHz, 300 K) spectra of [**12c-Cl$^+$.PF$_6^-$**] = 5 mM for several additions of a concentrated solution [*n*-Bu_4N^+ Br^-] = 50 mM.

Figure S12 ^{1}H NMR (CD_3CN, 500 MHz, 300 K) spectra of [**12c-Cl$^+$.PF$_6^-$**] = 5 mM for several additions of a concentrated solution [*n*-Bu_4N^+ I^-] = 50 mM.

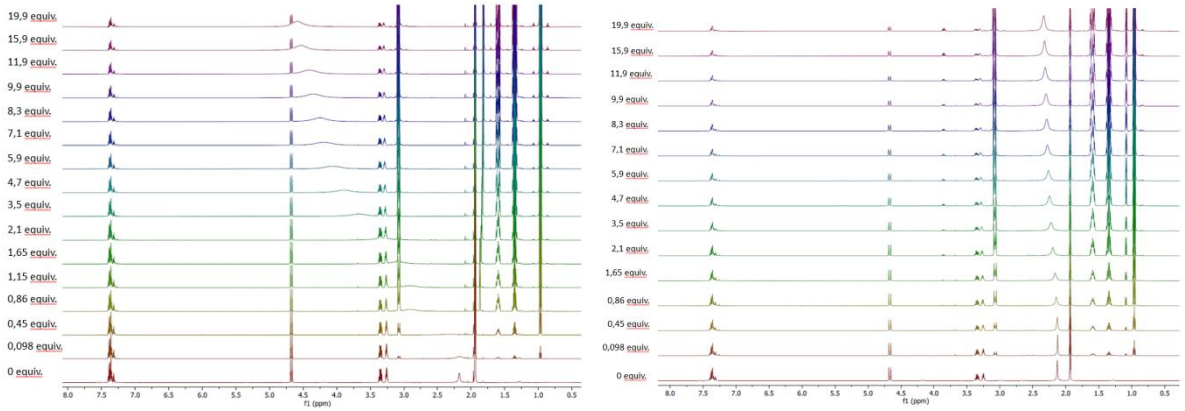

Figure S13 ^{1}H NMR (CD_3CN, 600 MHz, 300 K) spectra of [**12c-Cl$^+$.PF$_6^-$**] = 5 mM for several additions of a concentrated solution [*n*-Bu_4N^+ AcO^-] = 50 mM.

Figure S14 ^{1}H NMR (CD_3CN, 600 MHz, 300 K) spectra of [**12c-Cl$^+$.PF$_6^-$**] = 5 mM for several additions of a concentrated solution [*n*-Bu_4N^+ CN^-] = 50 mM.

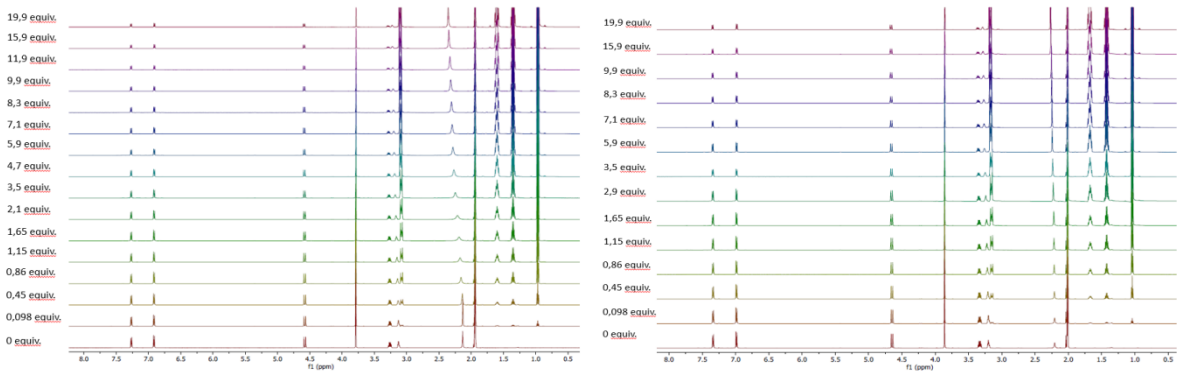

Figure S15 ^{1}H NMR (CD_3CN, 600 MHz, 300 K) spectra of [**12d-Cl$^+$.PF$_6^-$**] = 5 mM for several additions of a concentrated solution [*n*-Bu_4N^+ Cl^-] = 50 mM.

Figure S16 ^{1}H NMR (CD_3CN, 600 MHz, 300 K) spectra of [**12d-Cl$^+$.PF$_6^-$**] = 5 mM for several additions of a concentrated solution [*n*-Bu_4N^+ Br^-] = 50 mM.

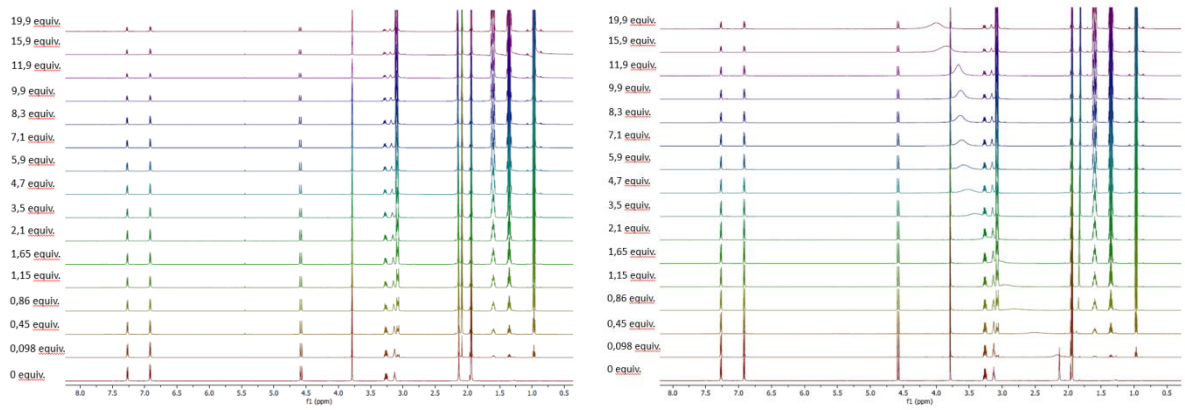

Figure S17 ^{1}H NMR (CD_3CN, 600 MHz, 300 K) spectra of [**12d-Cl$^+$.PF$_6^-$**] = 5 mM for several additions of a concentrated solution [n-Bu_4N^+ I^-] = 50 mM.

Figure S8 ^{1}H NMR (CD_3CN, 600 MHz, 300 K) spectra of [**12d-Cl$^+$.PF$_6^-$**] = 5 mM for several additions of a concentrated solution [n-Bu_4N^+ AcO^-] = 50 mM.

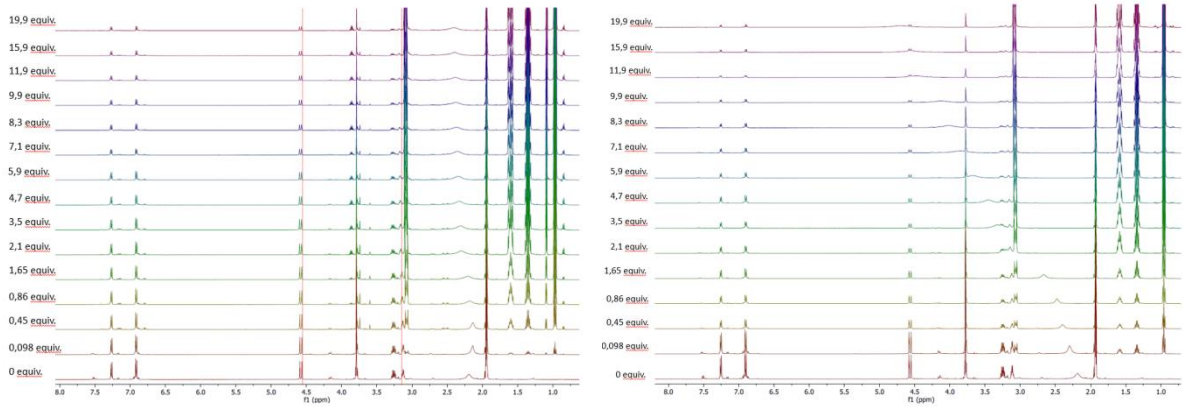

Figure S19 ^{1}H NMR (CD_3CN, 600 MHz, 300 K) spectra of [**12d-Cl$^+$.PF$_6^-$**] = 5 mM for several additions of a concentrated solution [*n*-Bu_4N^+ CN^-] = 50 mM.

Figure S20 ^{1}H NMR (CD_3CN, 600 MHz, 300 K) spectra of [**12d-Cl$^+$.PF$_6^-$**] = 5 mM for several additions of a concentrated solution [*n*-Bu_4N^+ HSO_4^-] = 50 mM.

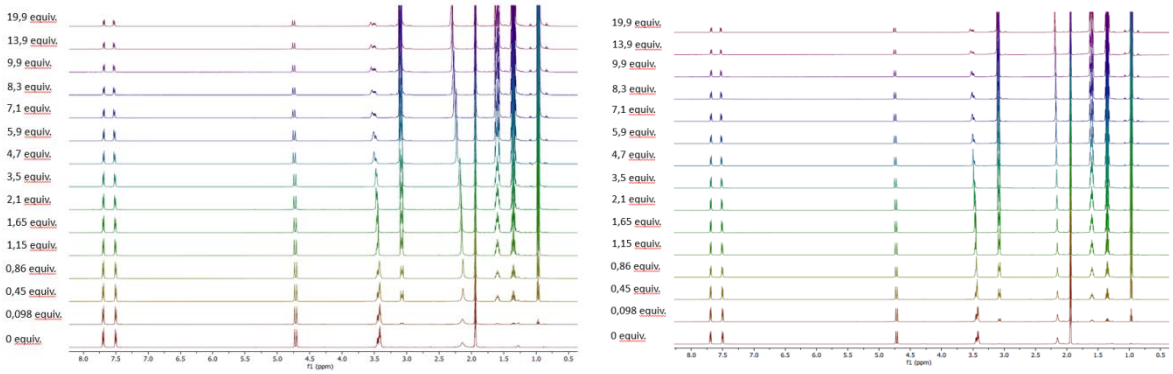

Figure S21 ^{1}H NMR (CD_3CN, 500 MHz, 300 K) spectra of [**12e-Cl$^+$.PF$_6^-$**] = 5 mM for several additions of a concentrated solution [*n*-Bu_4N^+ Cl^-] = 50 mM.

Figure S22 ^{1}H NMR (CD_3CN, 600 MHz, 300 K) spectra of [**12e-Cl$^+$.PF$_6^-$**] = 5 mM for several additions of a concentrated solution [*n*-Bu_4N^+ Br^-] = 50 mM.

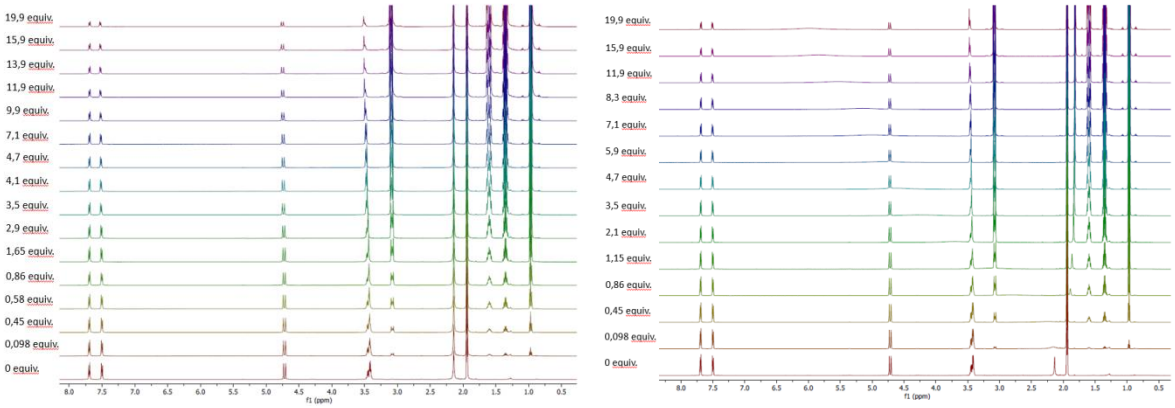

Figure S23 ^{1}H NMR (CD_3CN, 500 MHz, 300 K) spectra of [**12e-Cl$^+$.PF$_6^-$**] = 5 mM for several additions of a concentrated solution [*n*-Bu_4N^+ I^-] = 50 mM.

Figure S24 ^{1}H NMR (CD_3CN, 600 MHz, 300 K) spectra of [**12e-Cl$^+$.PF$_6^-$**] = 5 mM for several additions of a concentrated solution [*n*-Bu_4N^+ AcO^-] = 50 mM.

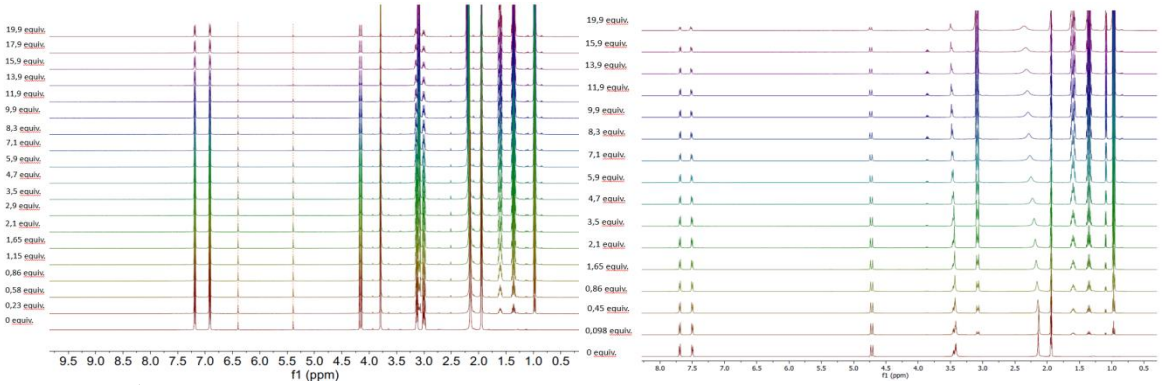

Figure S25 ^{1}H NMR (CD_3CN, 600 MHz, 300 K) spectra of [**12e-Cl$^+$.PF$_6^-$**] = 5 mM for several additions of a concentrated solution [*n*-Bu_4N^+ CN^-] = 50 mM.

Figure 26 ^{1}H NMR (CD_3CN, 600 MHz, 300 K) spectra of [**12d-Cl$^+$.BAr^F $^-$**] = 5 mM for several additions of a concentrated solution [n-Bu_4N^+ Cl^-] = 50 mM.

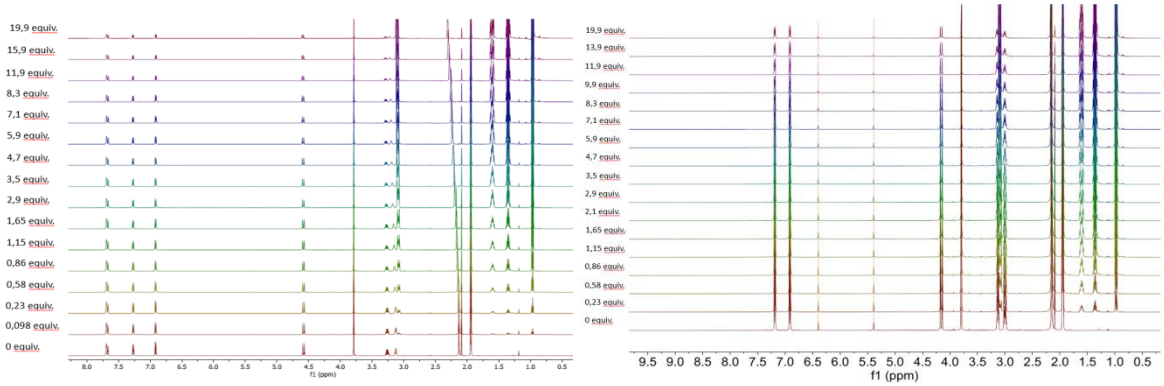

Figure S27 ^{1}H NMR (CD_3CN, 500 MHz, 300 K) spectra of [**12d-H$^+$.PF$_6^-$**] = 5 mM for several additions of a concentrated solution [n-Bu_4N^+·Cl^-] = 50 mM.

Figure S28 ^{1}H NMR (CD_3CN, 500 MHz, 300 K) spectra of [**12d-H$^+$.PF$_6^-$**] = 5 mM for several additions of a concentrated solution [n-Bu_4N^+ Br^-] = 50 mM.

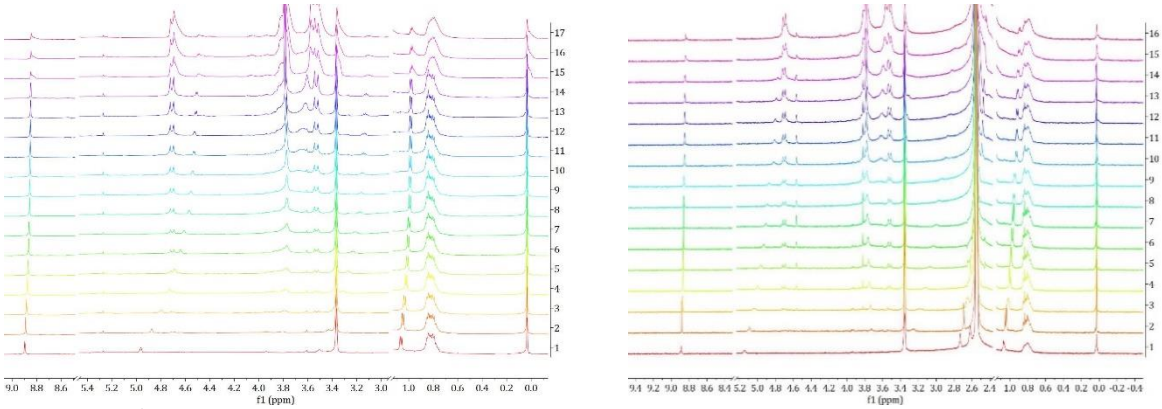

Figure S29 ^{1}H NMR spectroscopy (500 MHz, 300 K, $CDCl_3$/MeOH 95:5) titration of hemicryptophane (*M*)-**100** [C_G=5 mM] towards norephedrine [C_H=0.5 mM] (as picrate salt).

Figure S30 ^{1}H NMR spectroscopy (500 MHz, 300 K, $CDCl_3$/MeOH 95:5) titration of hemicryptophane (*M*)-**100** [C_G=5 mM] towards ephedrine [C_H=0.5 mM] (as picrate salt).

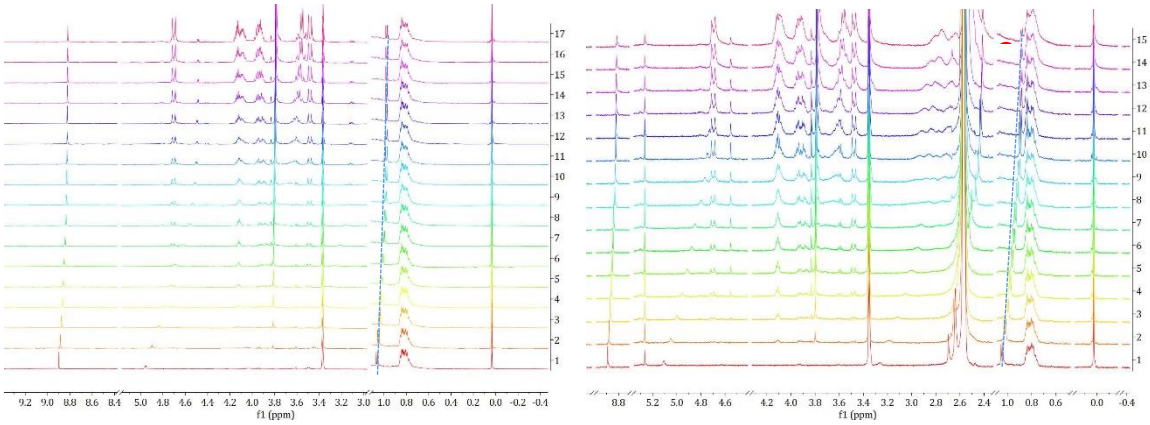

Figure S31 ^{1}H NMR spectroscopy (500 MHz, 300 K, $CDCl_3$/MeOH 95:5) titration of hemicryptophane *(M)*-**101** [C_G=5 mM] towards norephedrine [C_H=0.5 mM] (as picrate salt).

Figure S32 ^{1}H NMR spectroscopy (500 MHz, 300 K, $CDCl_3$/MeOH 95:5) titration of hemicryptophane *(M)*-**101** [C_G=5 mM] towards ephedrine [C_H=0.5 mM] (as picrate salt).

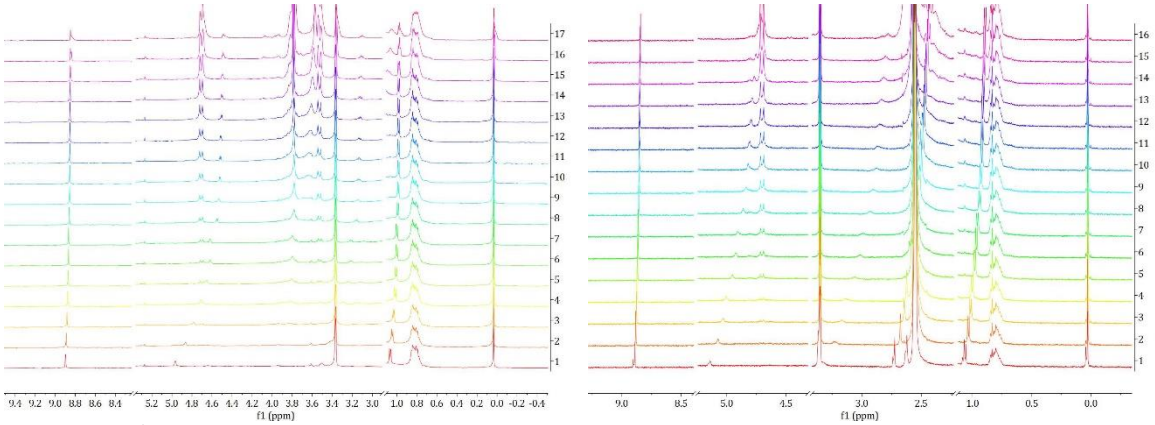

Figure S33 ^{1}H NMR spectroscopy (500 MHz, 300 K, $CDCl_3$/MeOH 95:5) titration of hemicryptophane (*P*)-**100** [C_G=5 mM] towards norephedrine [C_H=0.5 mM] (as picrate salt).

Figure S34 ^{1}H NMR spectroscopy (500 MHz, 300 K, $CDCl_3$/MeOH 95:5) titration of hemicryptophane (*P*)-**100** [C_G=5 mM] towards ephedrine [C_H=0.5 mM] (as picrate salt).

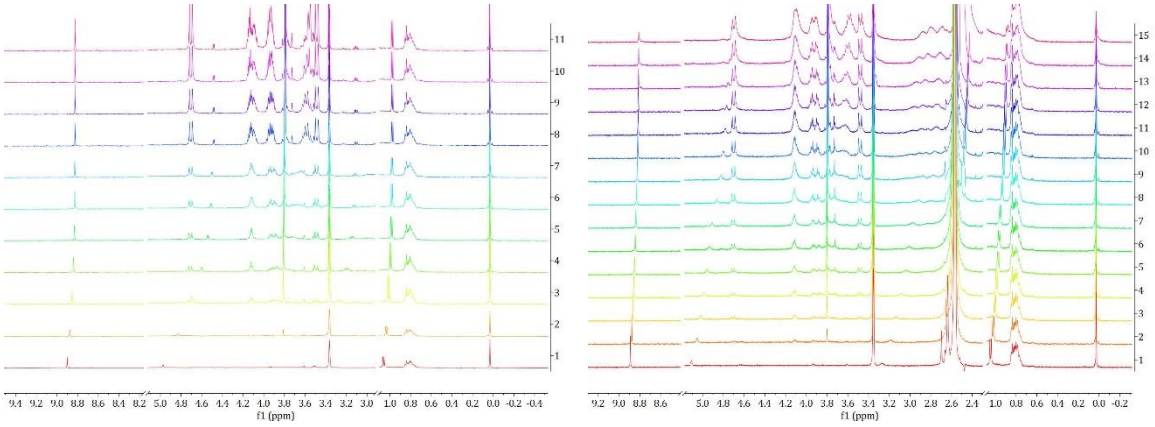

Figure S35 ^{1}H NMR spectroscopy (500 MHz, 300 K, $CDCl_3$/MeOH 95:5) titration of hemicryptophane *(P)*-**101** [C_G=5 mM] towards norephedrine [C_H=0.5 mM] (as picrate salt).

Figure S36 ^{1}H NMR spectroscopy (500 MHz, 300 K, $CDCl_3$/MeOH 95:5) titration of hemicryptophane *(P)*-**101** [C_G=5 mM] towards ephedrine [C_H=0.5 mM] (as picrate salt).

NMR spectra

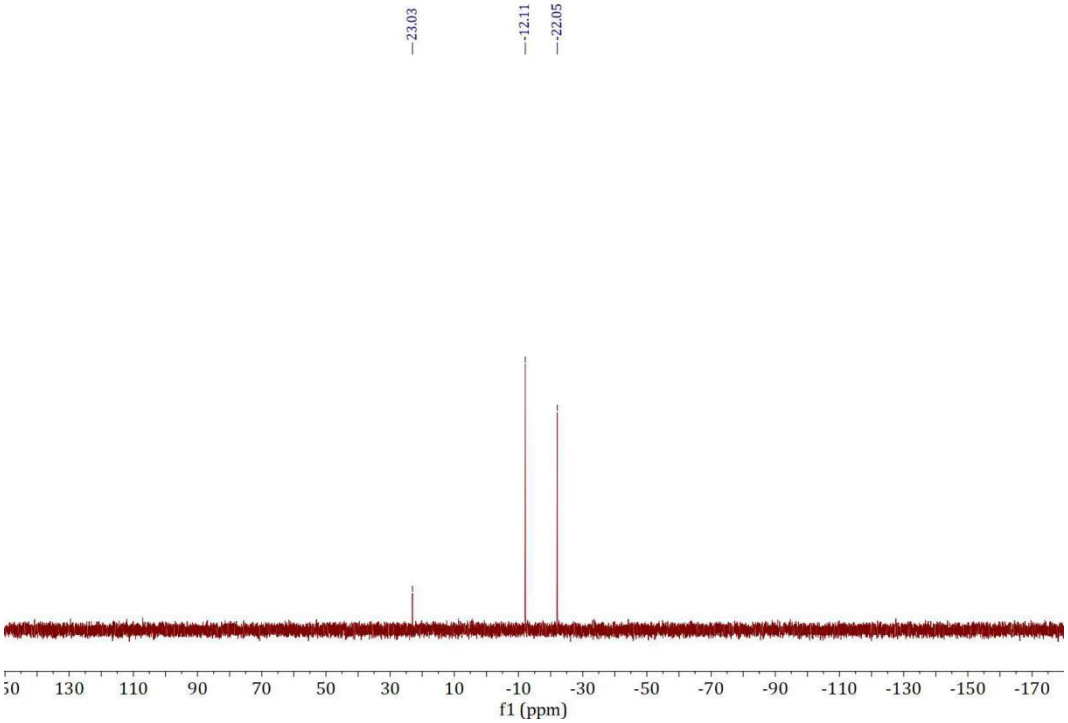

Figure S37 ^{31}P NMR (120 MHz, $CDCl_3$) of reaction between **12d** and chloroimidazolium **89**. The signal at -22.04 ppm correspond to **12d-Cl**$^+$ whereas that -12.11 ppm to **12d-H**$^+$ (probably because of water traces in the NMR solvent).

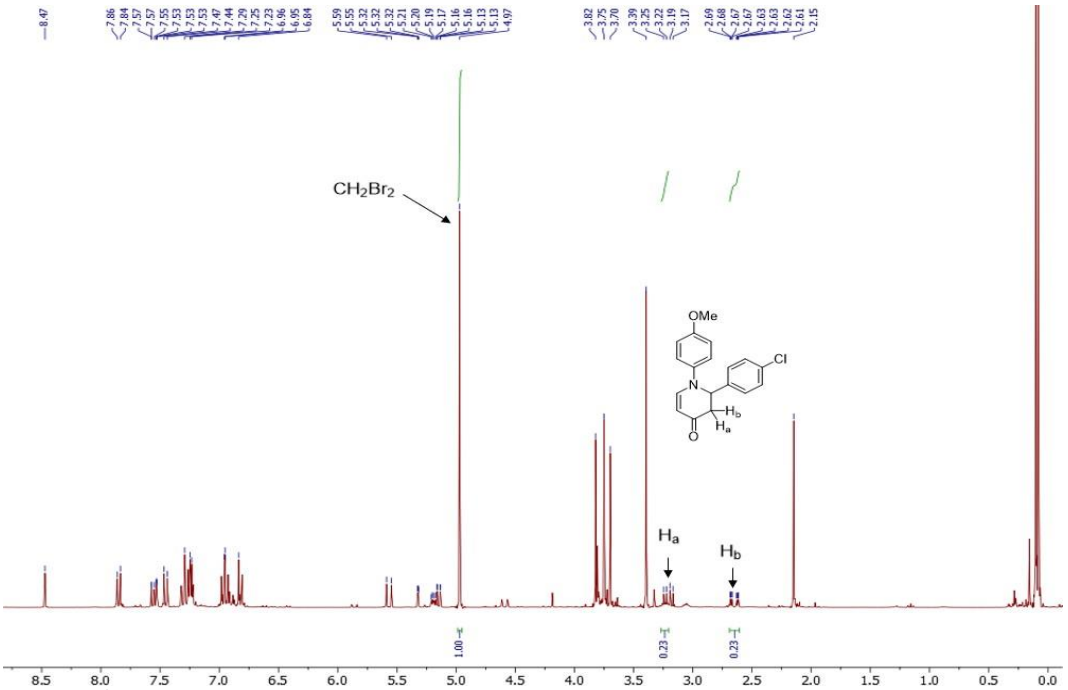

Figure S38 ^1H NMR (300 MHz, CD_2Cl_2) of the Aza-Diels-Alder reaction catalyzed by **12d-Cl**$^+$·PF_6^-. CH_2Br_2 was used as internal standard (integral ((δ 3.21 + δ 2.65) : δ 4.97) = 0.46 : 1 = 46 % yield).

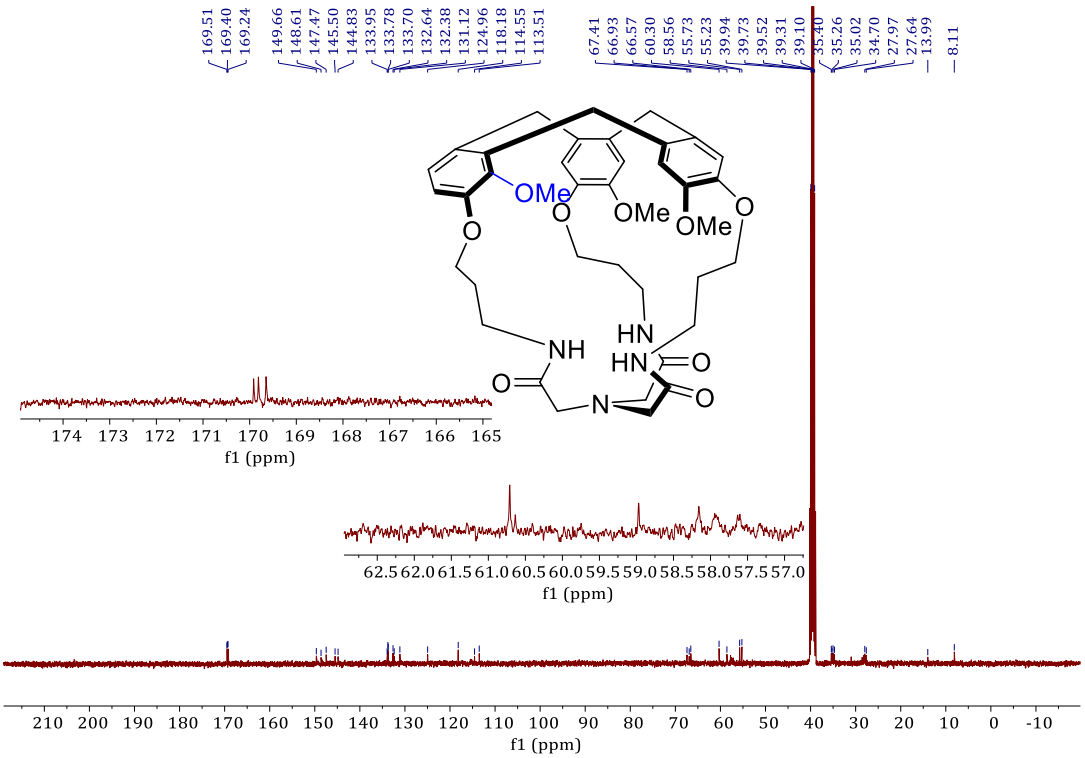

Figure S39 ^{13}C NMR (101 MHz, $(CD_3)_2SO$) spectrum of hemicryptophane **93.**

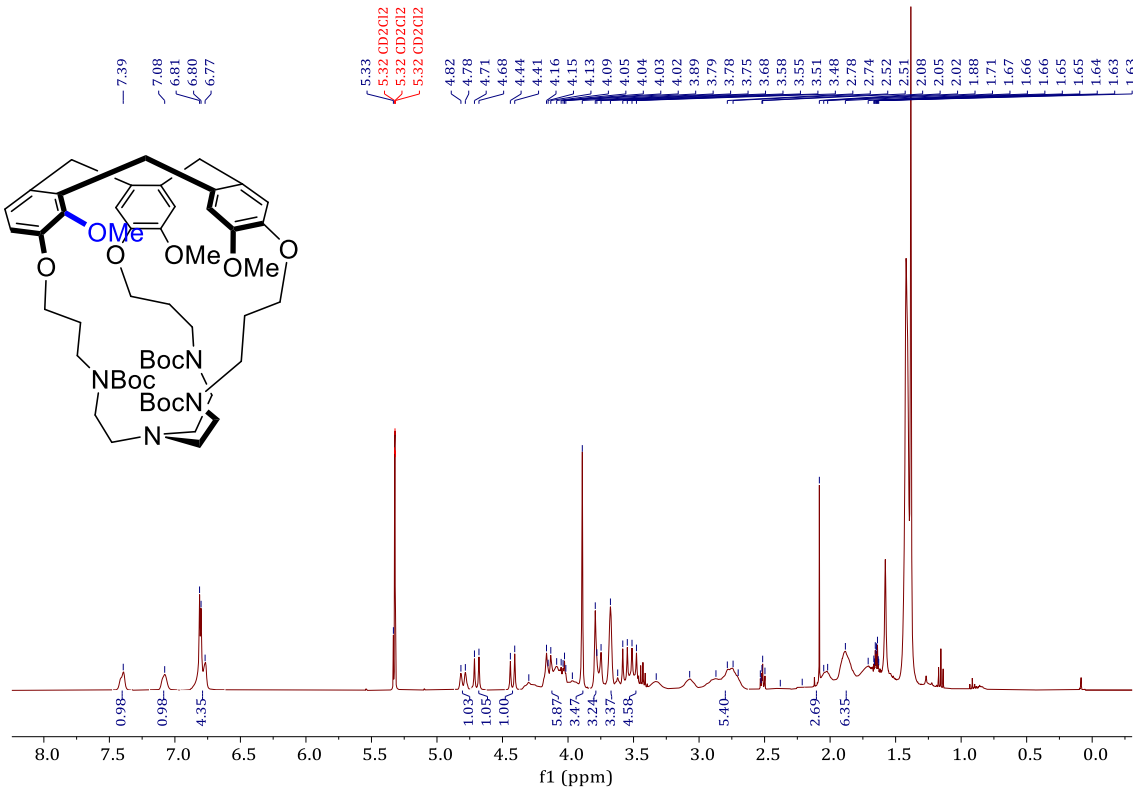

Figure S40 ^{1}H NMR (400 MHz, CD_2Cl_2) spectrum of hemicryptophane **94-Boc.**

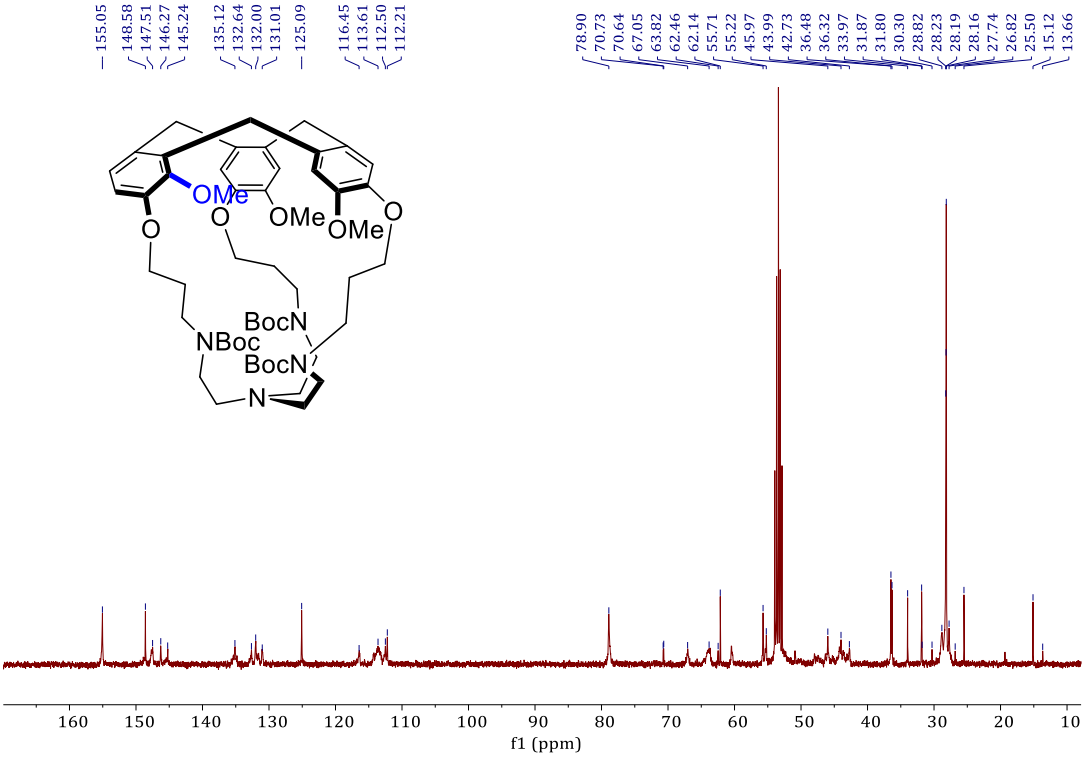

Figure S41 ^{13}C NMR (101 MHz, CD_2Cl_2) spectrum of hemicryptophane**94-Boc.**

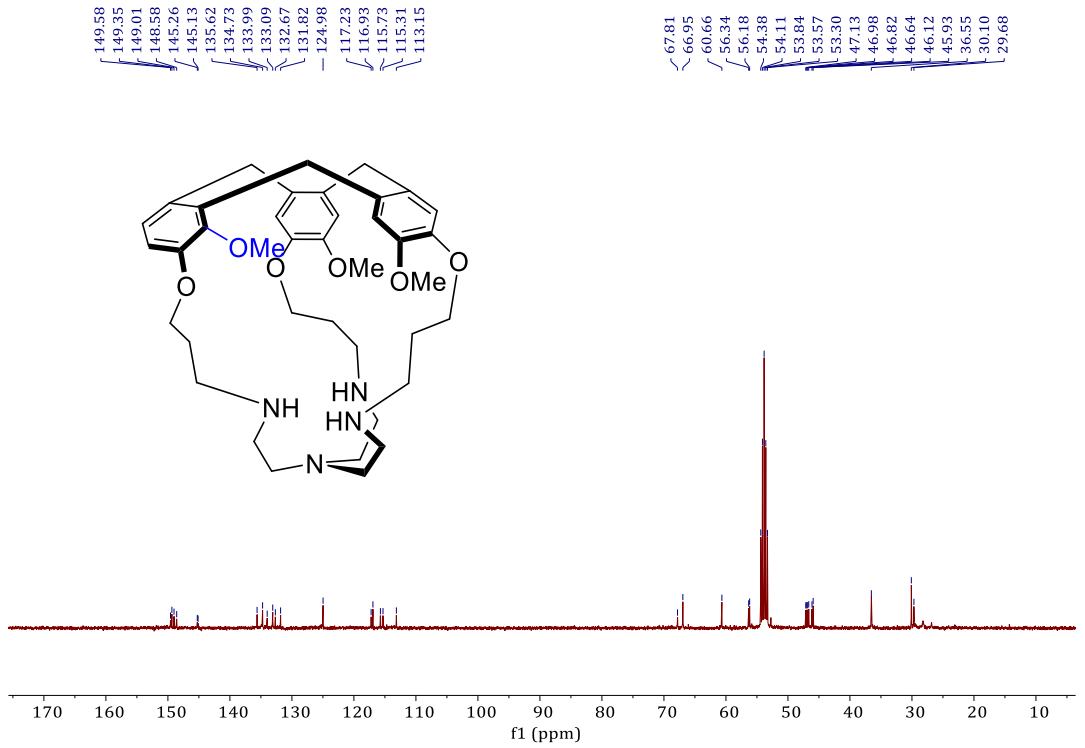

Figure S42 ^{13}C NMR (101 MHz, CD_2Cl_2) spectrum of hemicryptophane **94.**

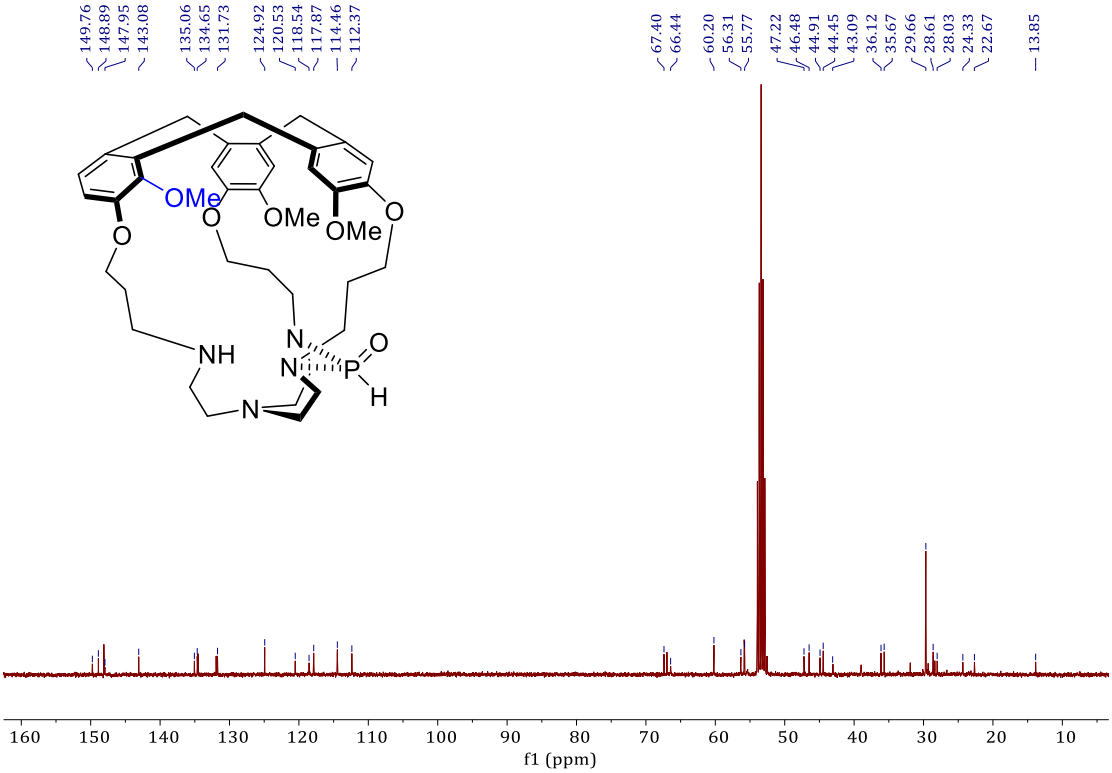

Figure43 ^{13}C NMR (101 MHz, $(CD_3)_2SO$) spectrum of hemicryptophane **94-PH=O.**

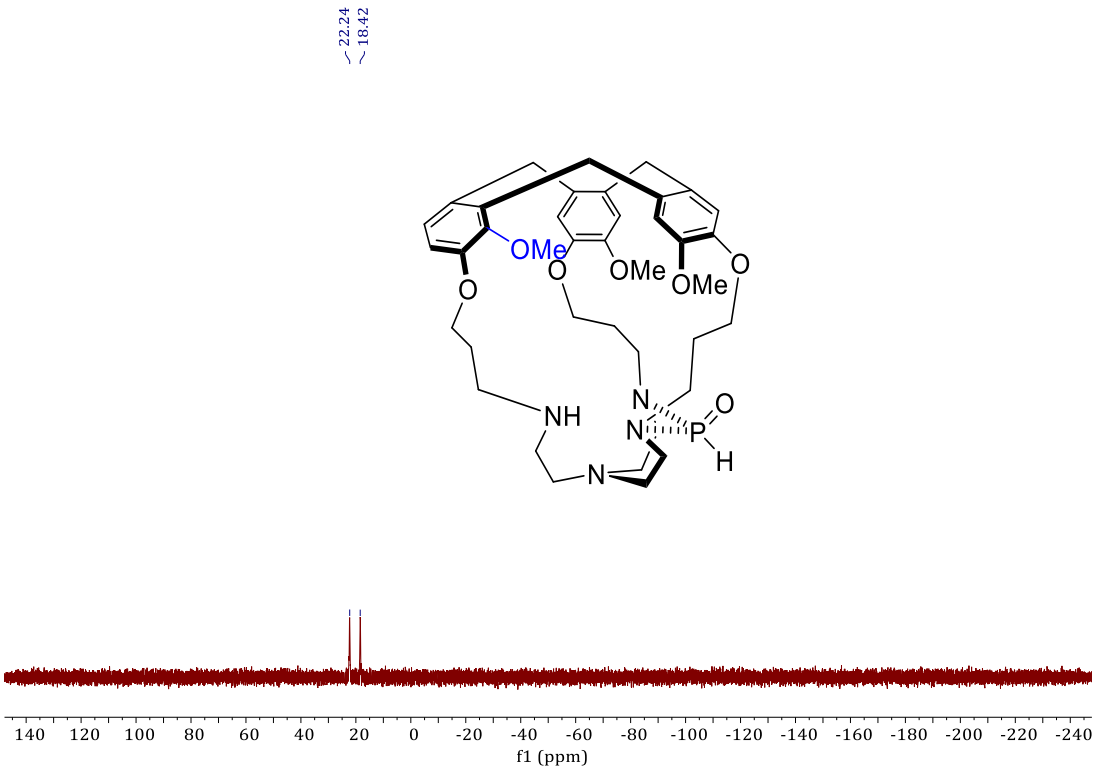

Figure S44 ^{31}P NMR (121 MHz, $CDCl_3$) spectrum of **94-PH=O.**

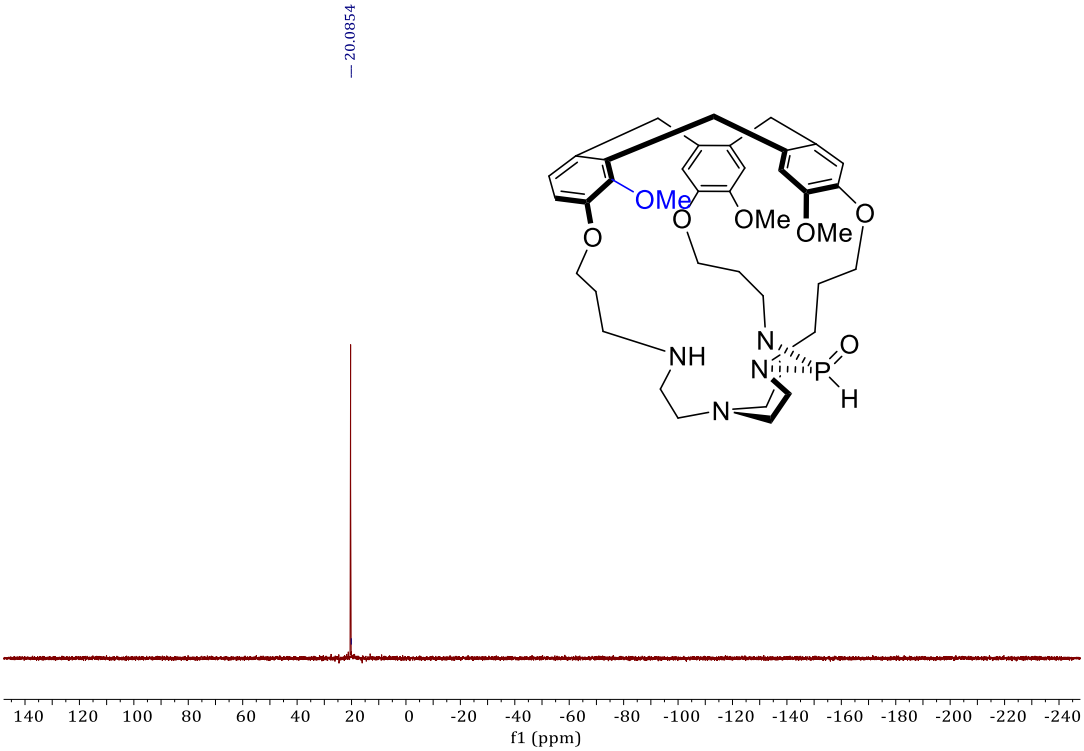

Figure S45 ^{31}P CPD NMR (121 MHz, $CDCl_3$) spectrum of **94-PH=O.**

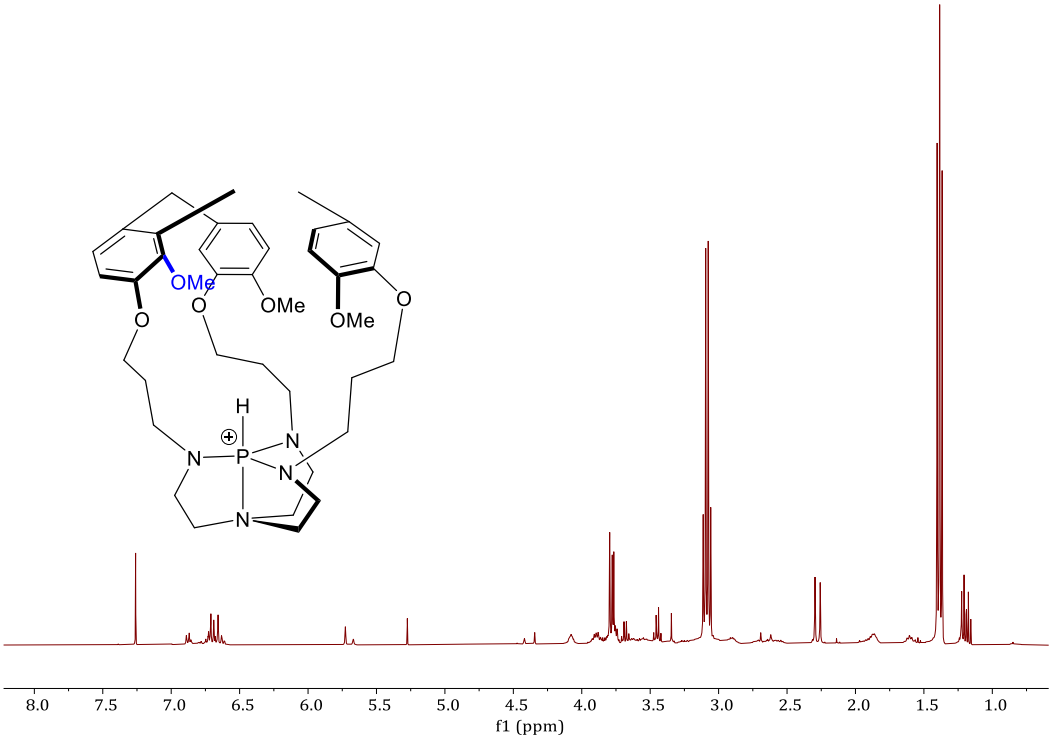

Figure S46 ^{1}H NMR (400 MHz, CD_2Cl_2) spectrum of hemicryptophane **CTV-opened 94-H$^+$.**

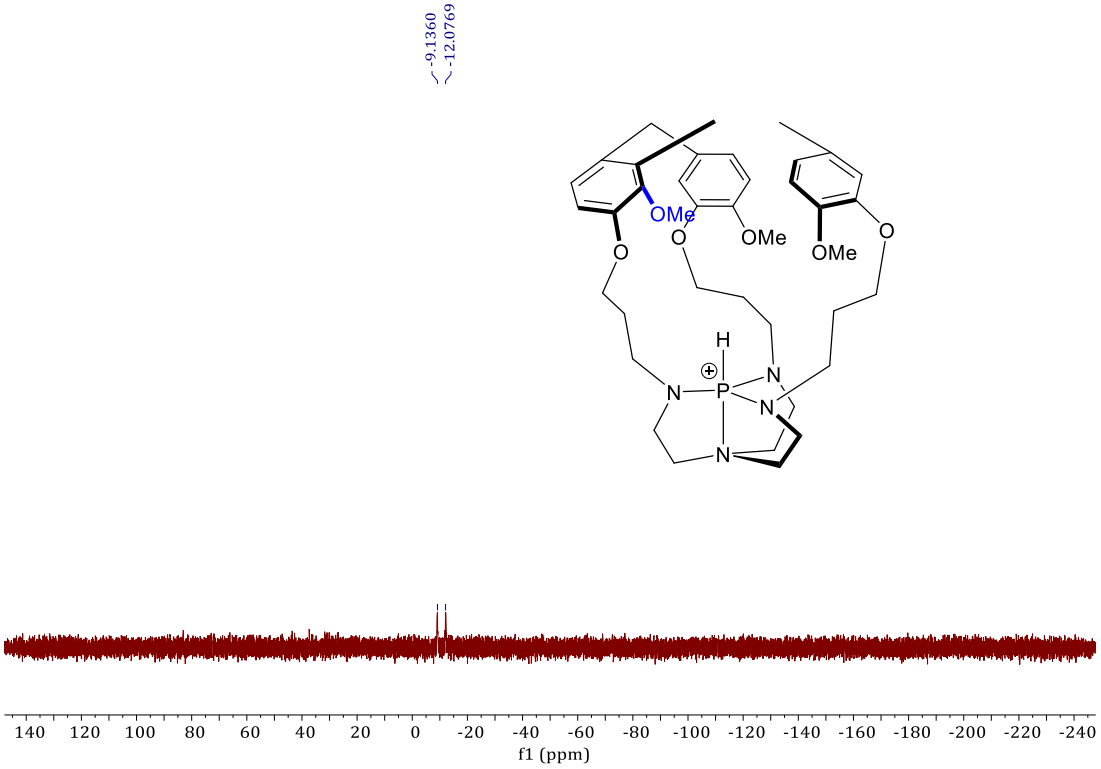

Figure S47 ^{31}P CPD NMR (121 MHz, $CDCl_3$) spectrum of **CTV-opened 94-H$^+$.**

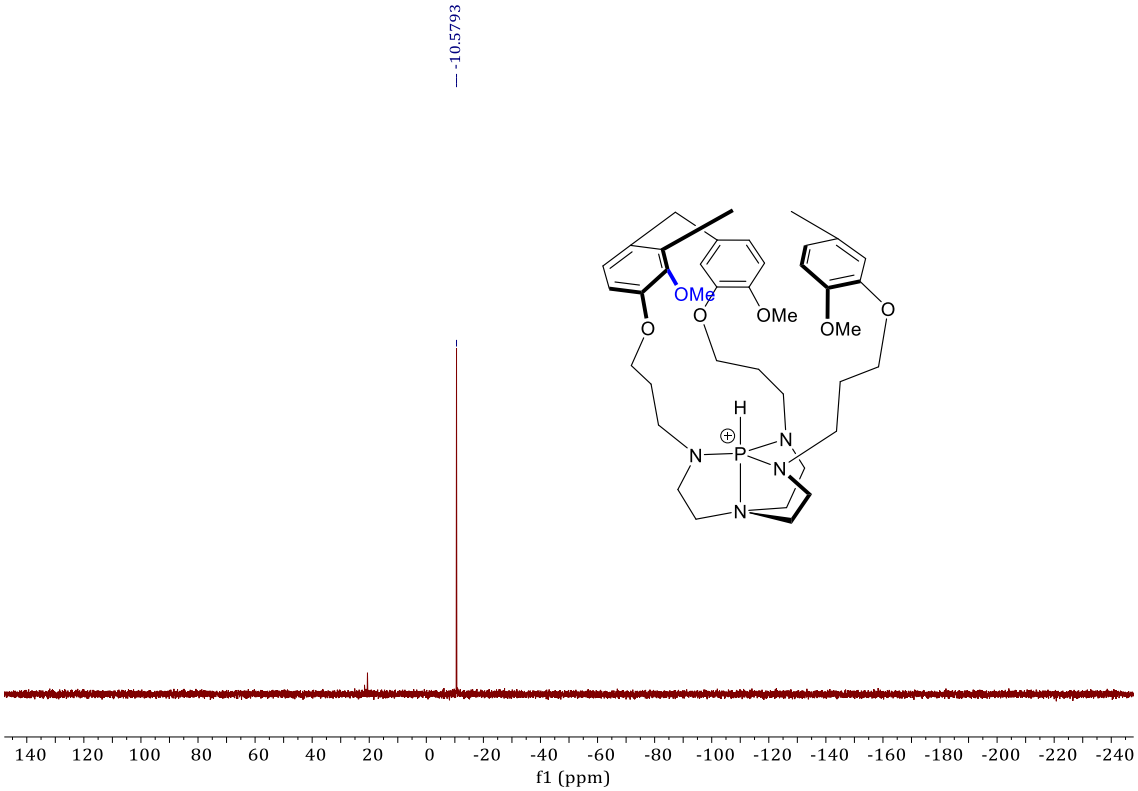

Figure S48 ^{31}P NMR (121 MHz, $CDCl_3$) spectrum of **CTV-opened 94-H$^+$.**

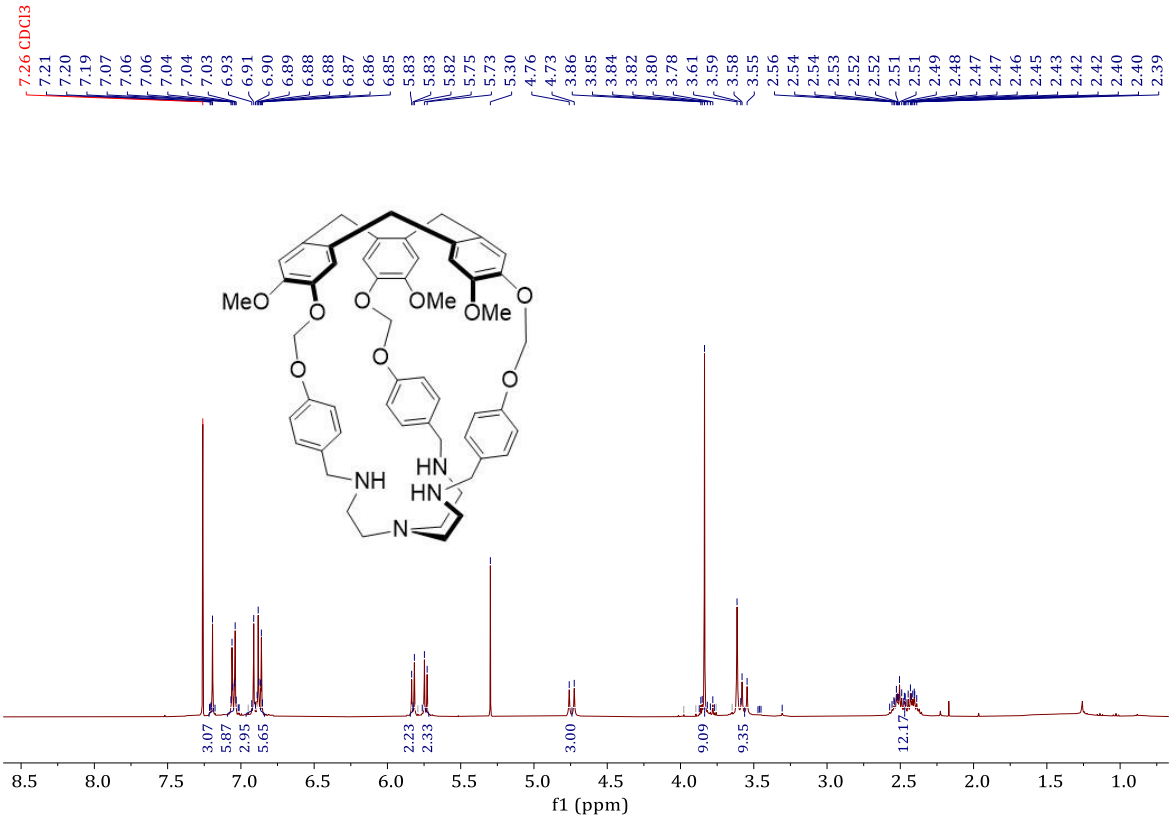

Figure S49 ^{1}H NMR (400 MHz, CD_2Cl_2) spectrum of hemicryptophane **100.**

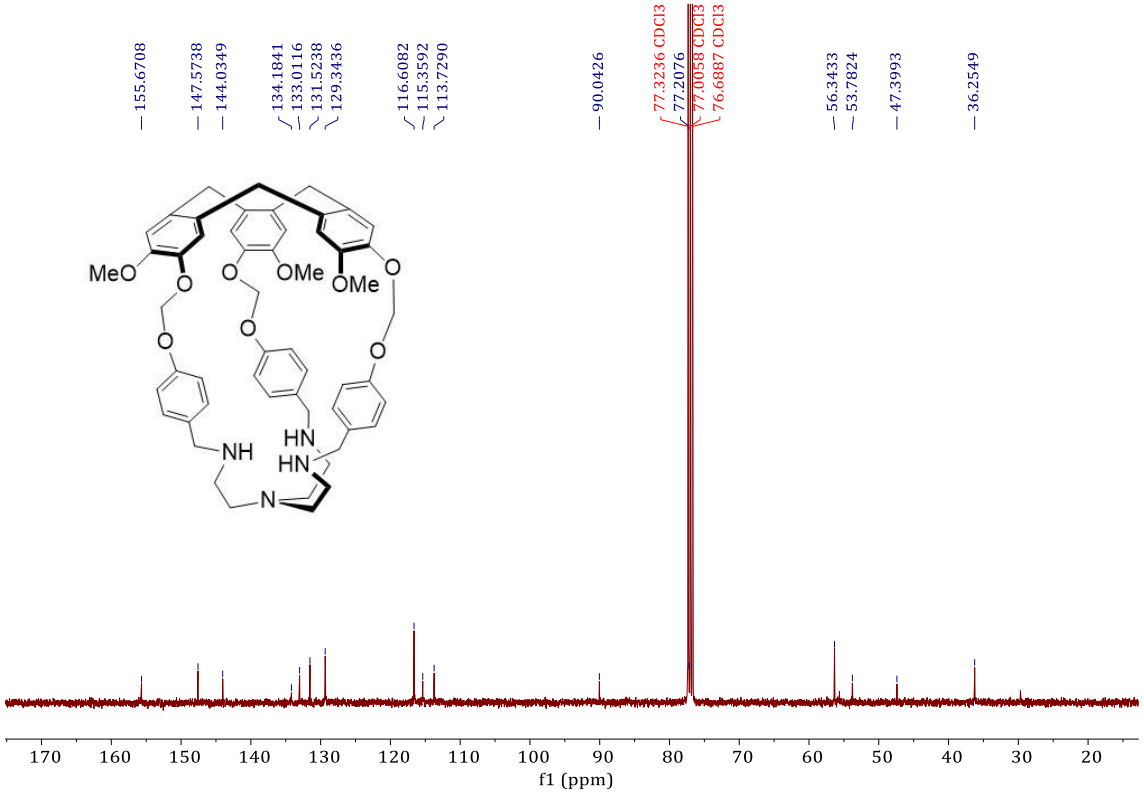

Figure S50 ^{13}C NMR (101 MHz, CD_2Cl_2) spectrum of hemicryptophane **100.**

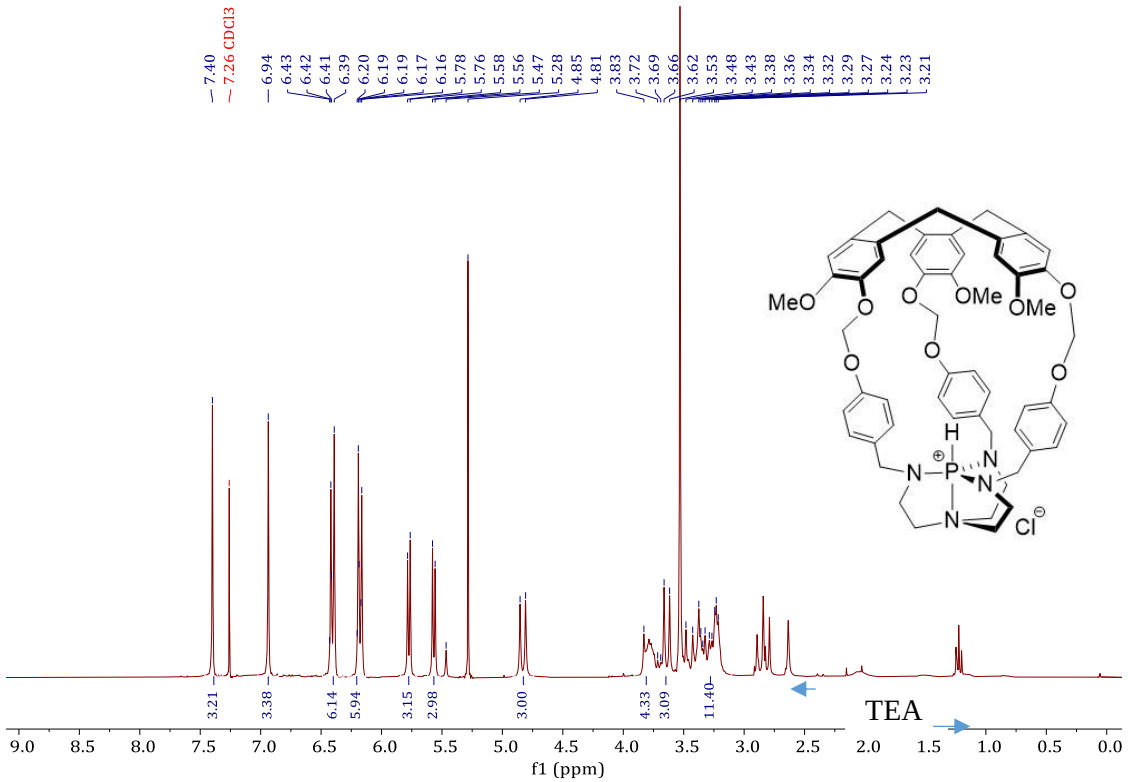

Figure S51 ^{1}H NMR (300 MHz, $CDCl_3$) spectrum of **102-H^{+}·Cl^{-}**.

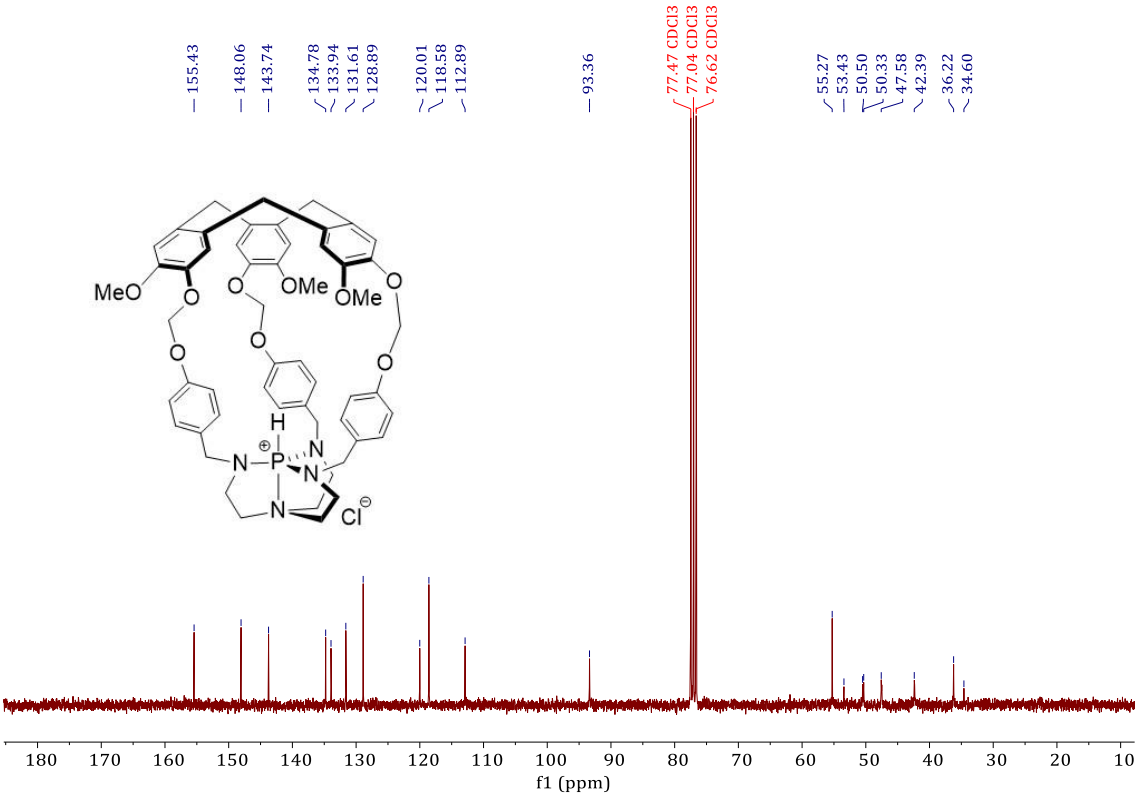

Figure S52 ^{1}C NMR (75 MHz, $CDCl_3$) spectrum of **102-H^{+}·Cl^{-}**.

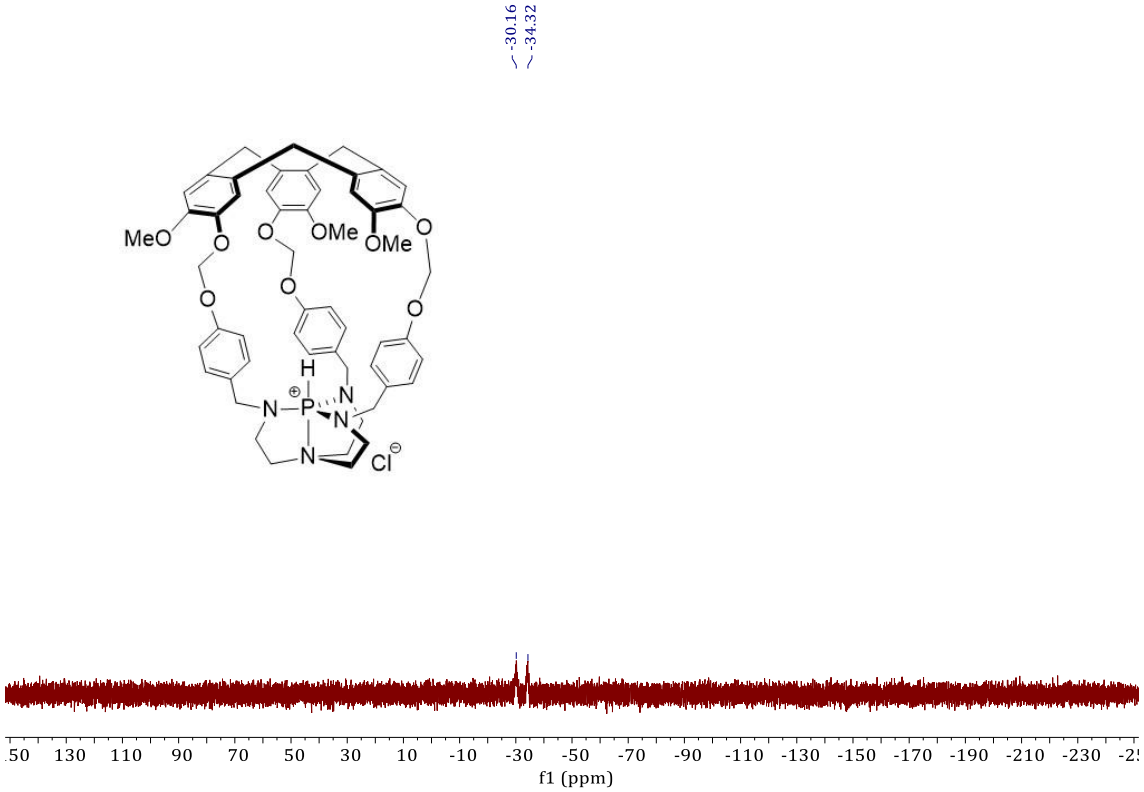

Figure S53 ^{31}P NMR (121 MHz, $CDCl_3$) spectrum of **102-H$^+$·Cl$^-$**.

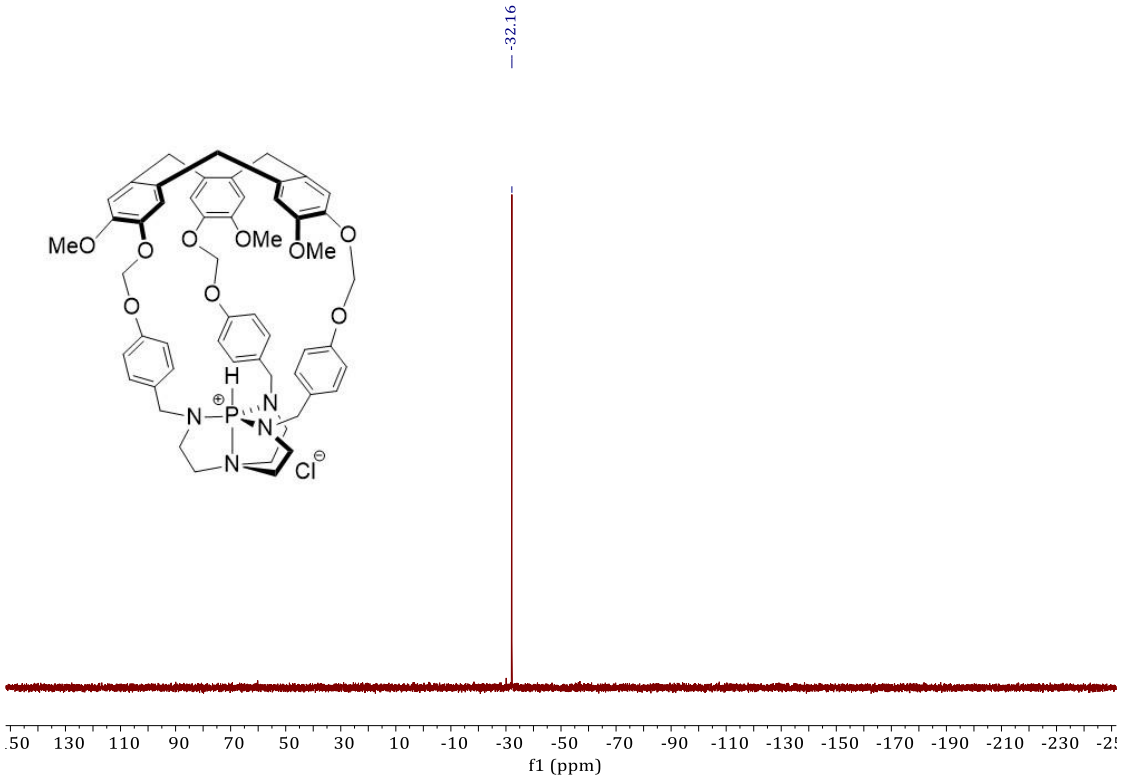

Figure S54 ^{31}P CPD NMR (121 MHz, $CDCl_3$) spectrum of **102-H$^+$·Cl$^-$**.

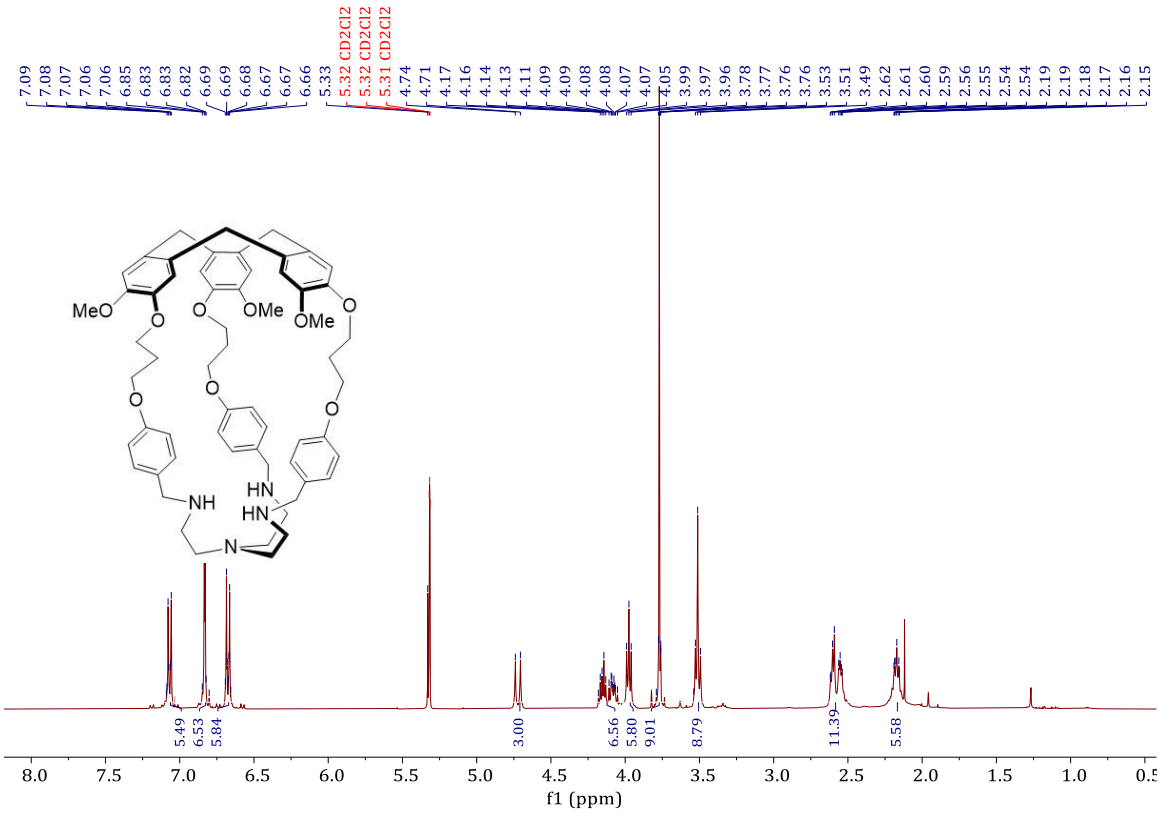

Figure S55 ^{1}H NMR (400 MHz, CD_2Cl_2) spectrum of hemicryptophane **101.**

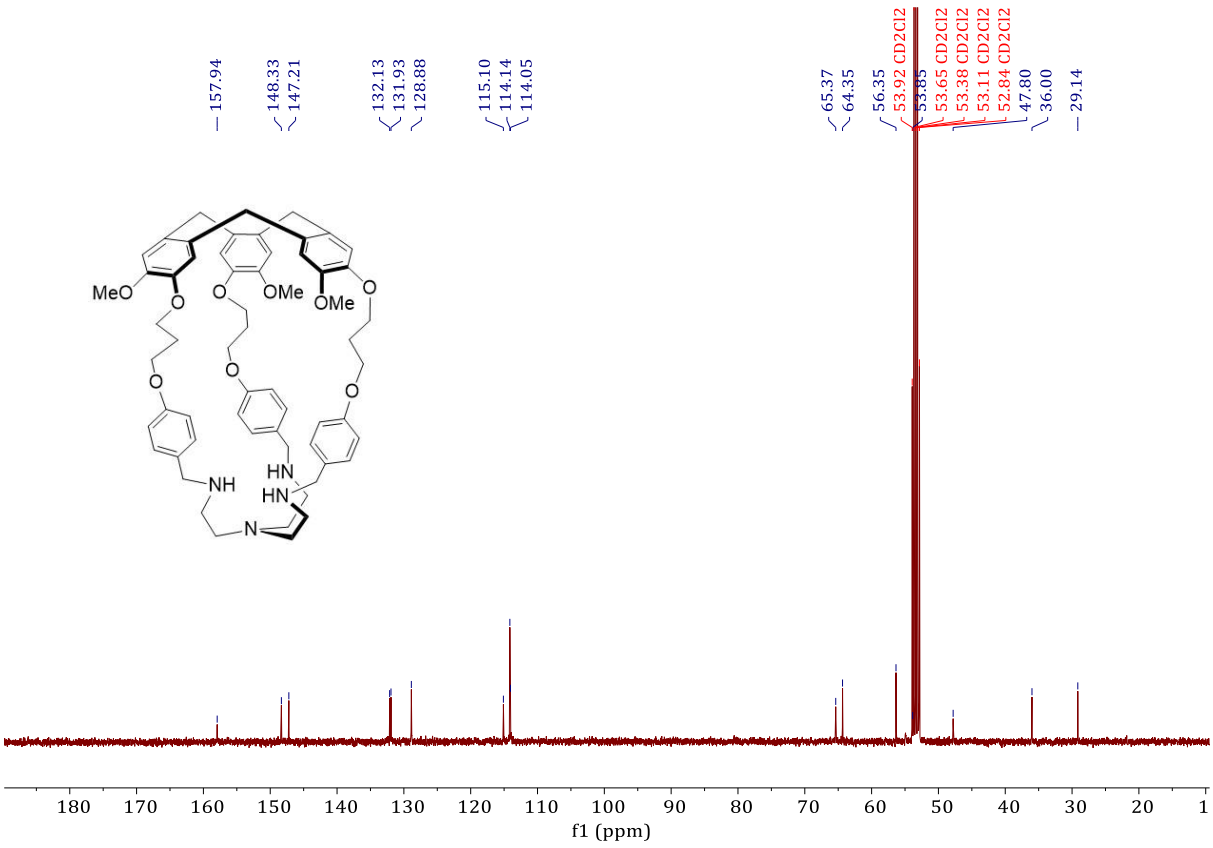

Figure S56 ^{13}C NMR (101 MHz, CD_2Cl_2) spectrum of hemicryptophane **101**

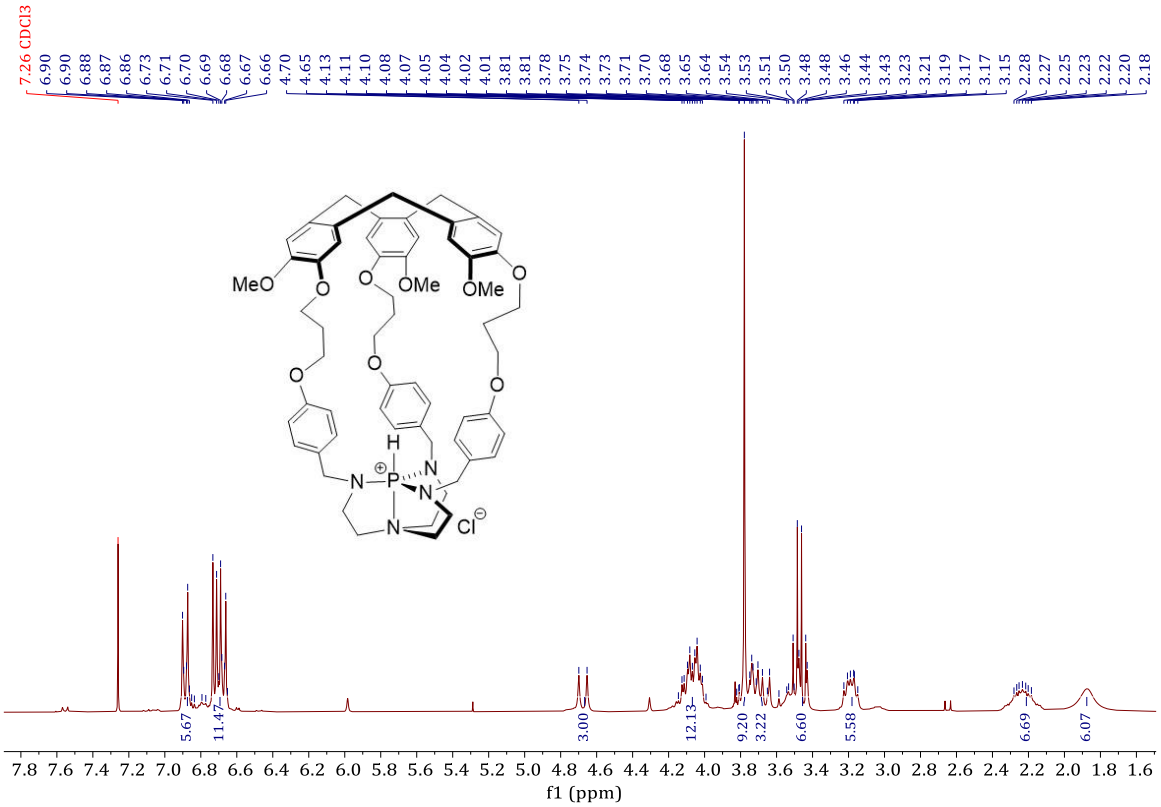

Figure S57 ^{1}H NMR (300 MHz, CD_2Cl_2) spectrum of **103-H^{+}·Cl^{-}.**

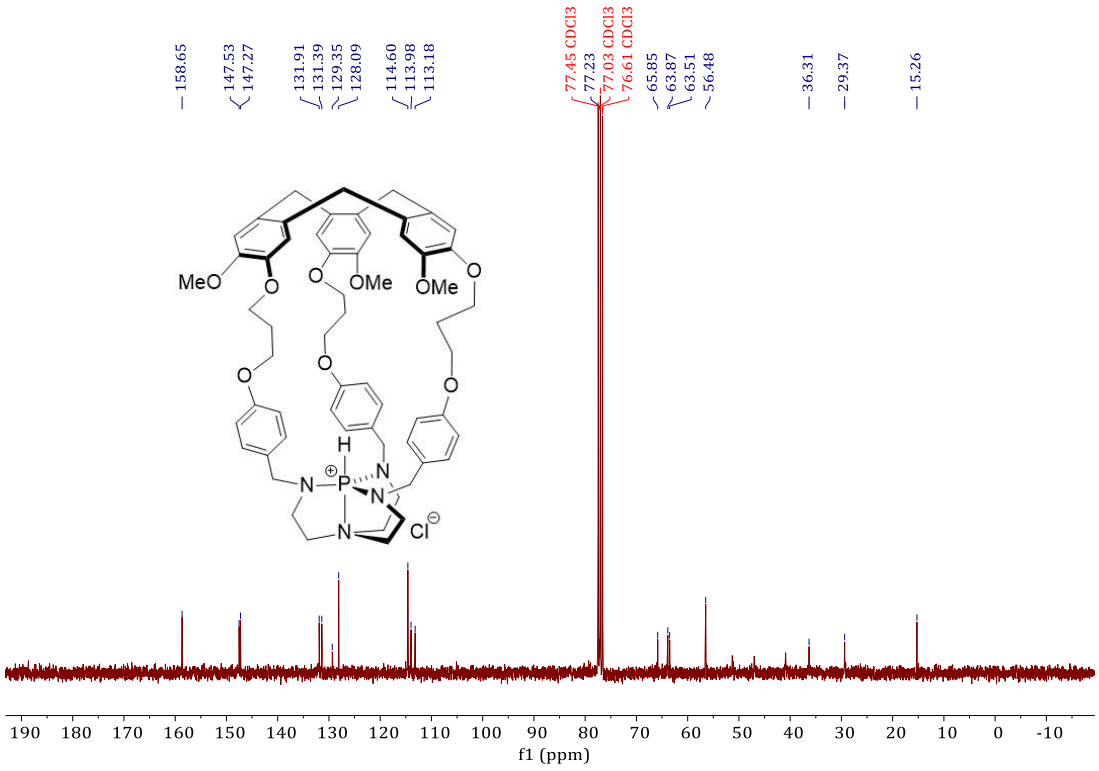

Figure S58 ^{13}C NMR (75 MHz, CD_2Cl_2) spectrum of **103-H^{+}·Cl^{-}.**

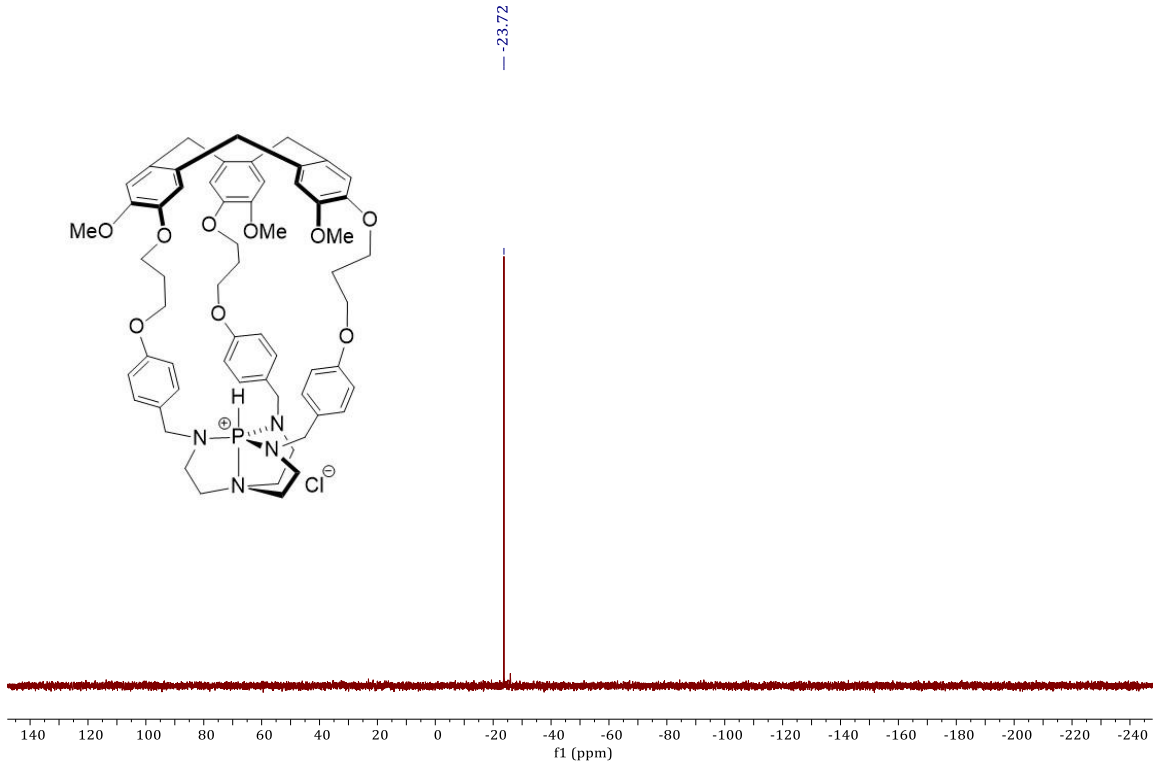

Figure S59 ^{31}P CPD NMR (162 MHz, $CDCl_3$) spectrum of **103-H$^+$·Cl$^-$.**

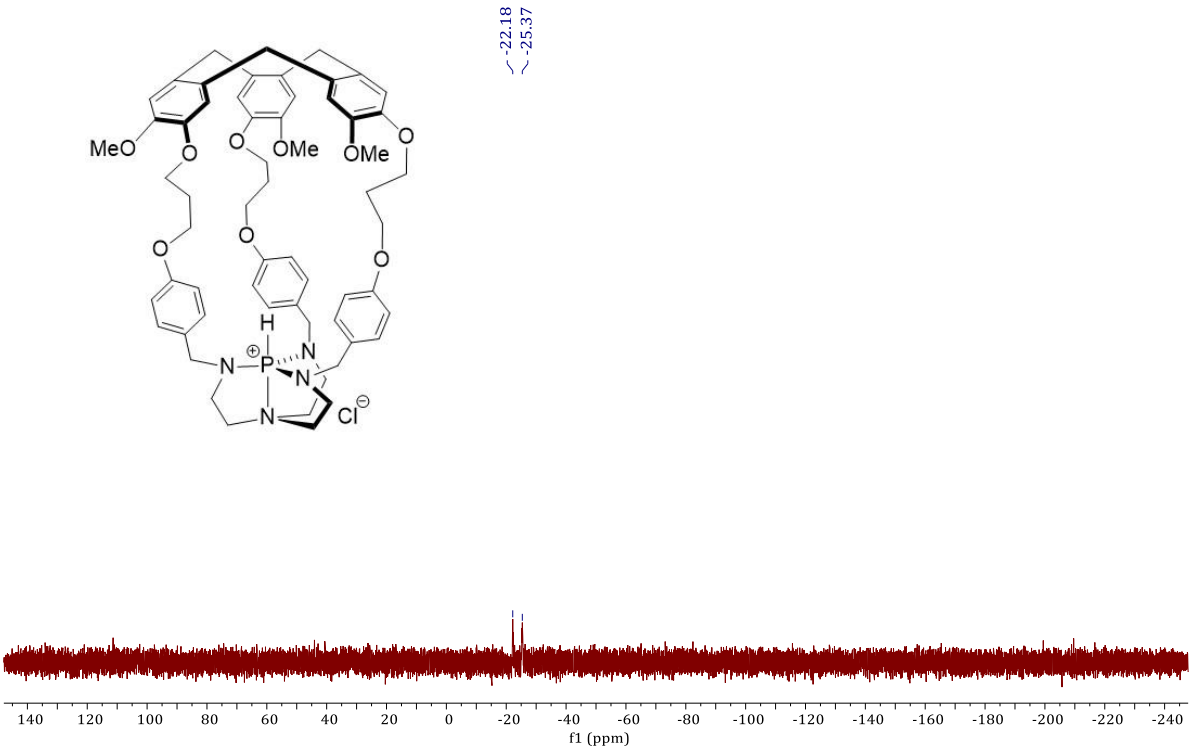

Figure S60 ^{31}P NMR (162 MHz, $CDCl_3$) spectrum of **103-H$^+$·Cl$^-$.**

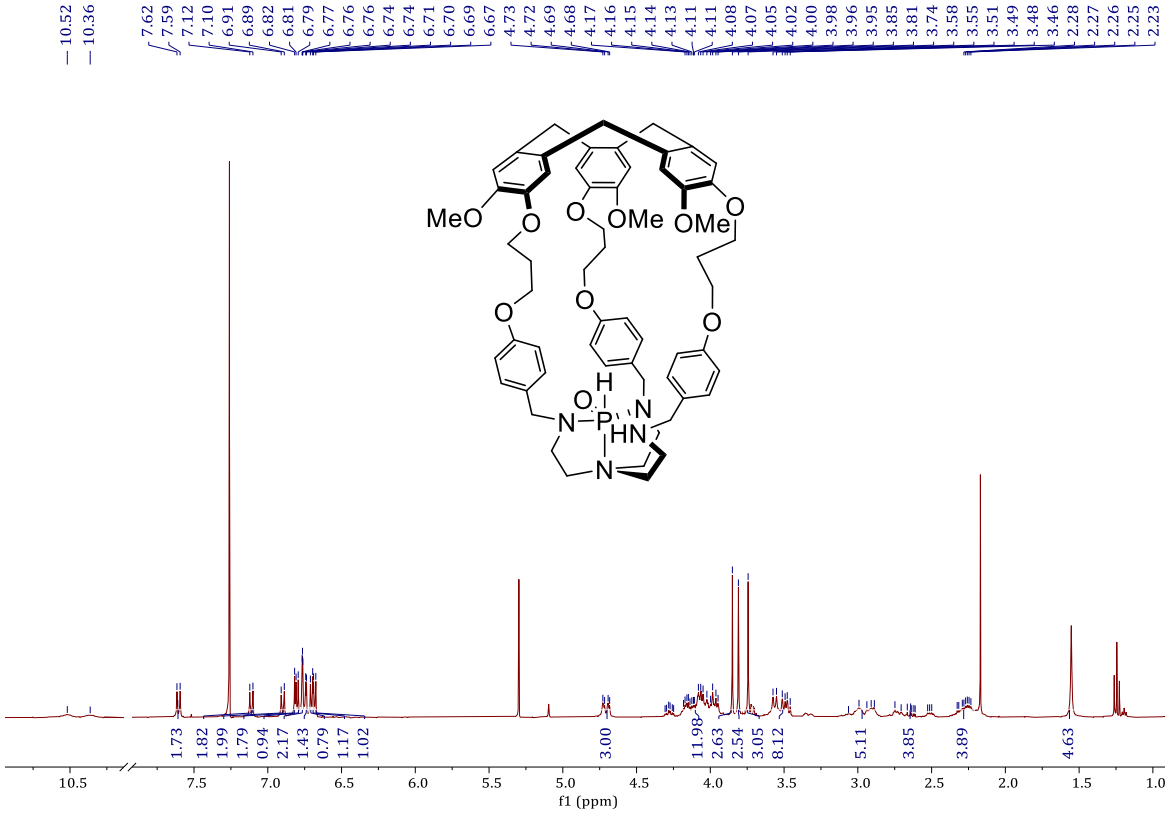

Figure S61 ^{1}H NMR (400 MHz, CD_2Cl_2) spectrum of **103-PH=O.**

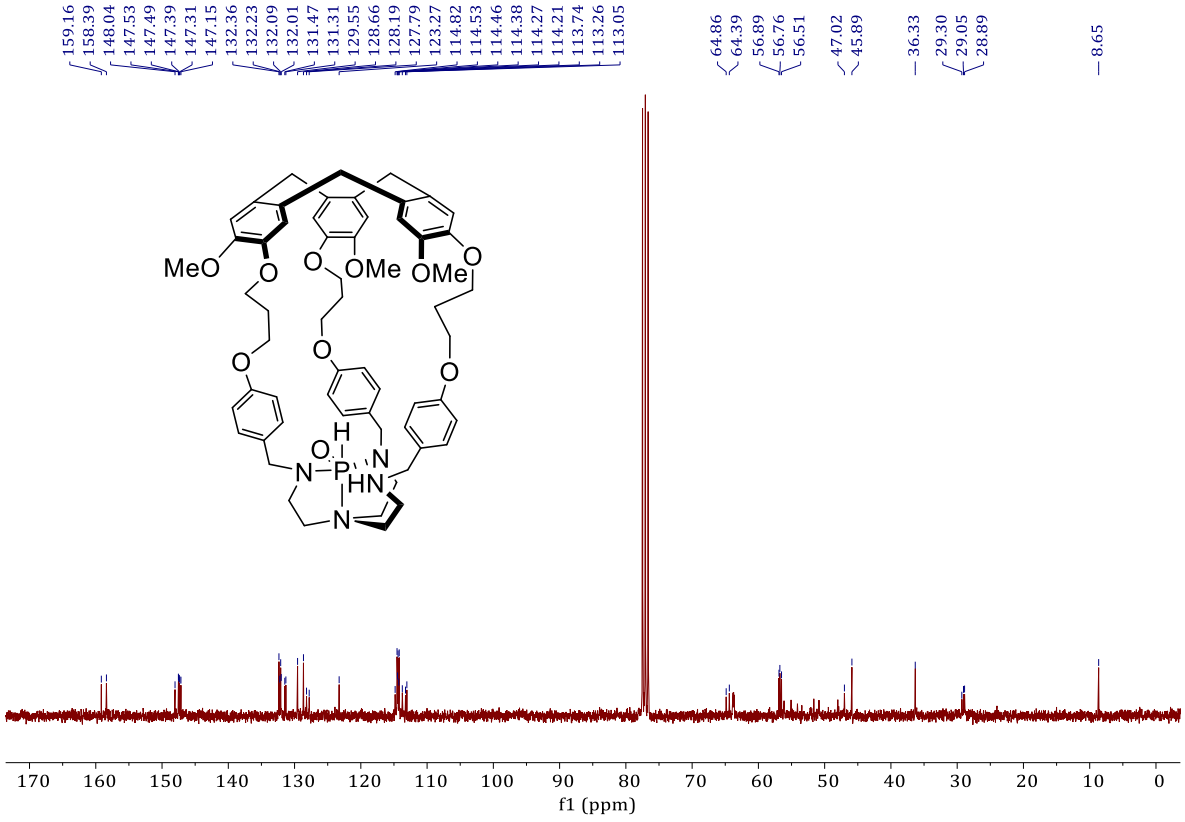

Figure S62^{13}C NMR (101 MHz, CD_2Cl_2) spectrum of **103-PH=O.**

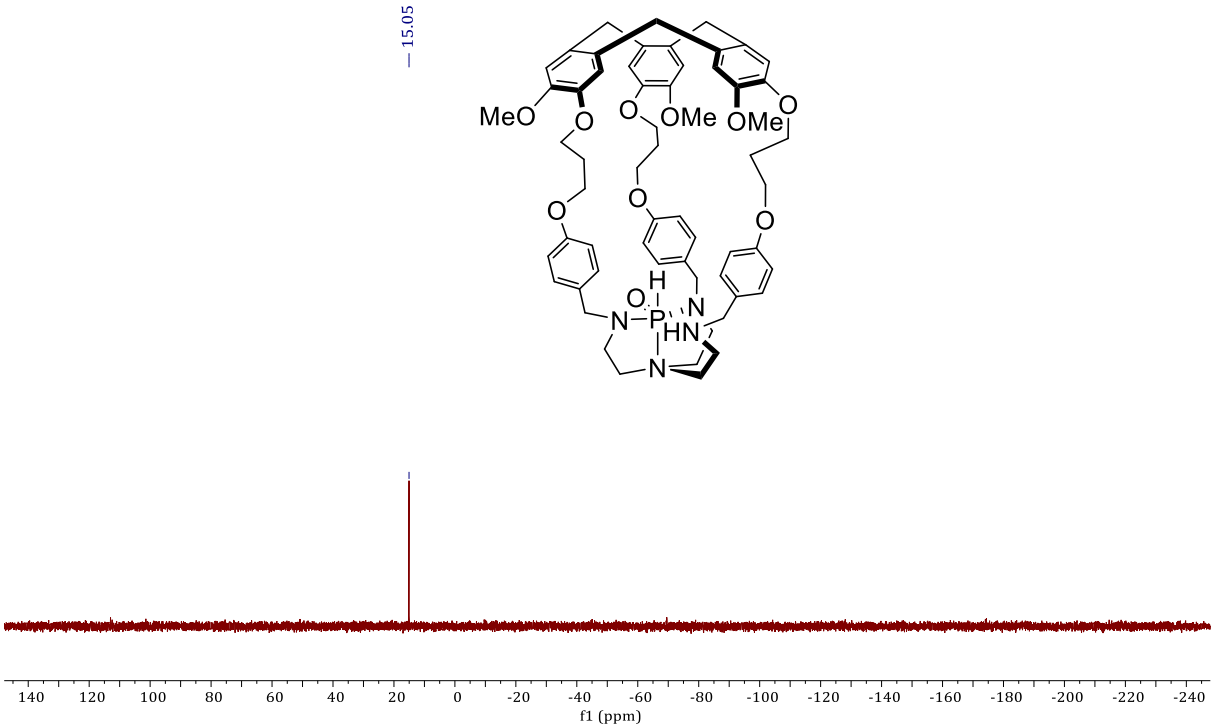

Figure S63 ^{31}P CPD NMR (162 MHz, $CDCl_3$) spectrum of **103-PH=O.**

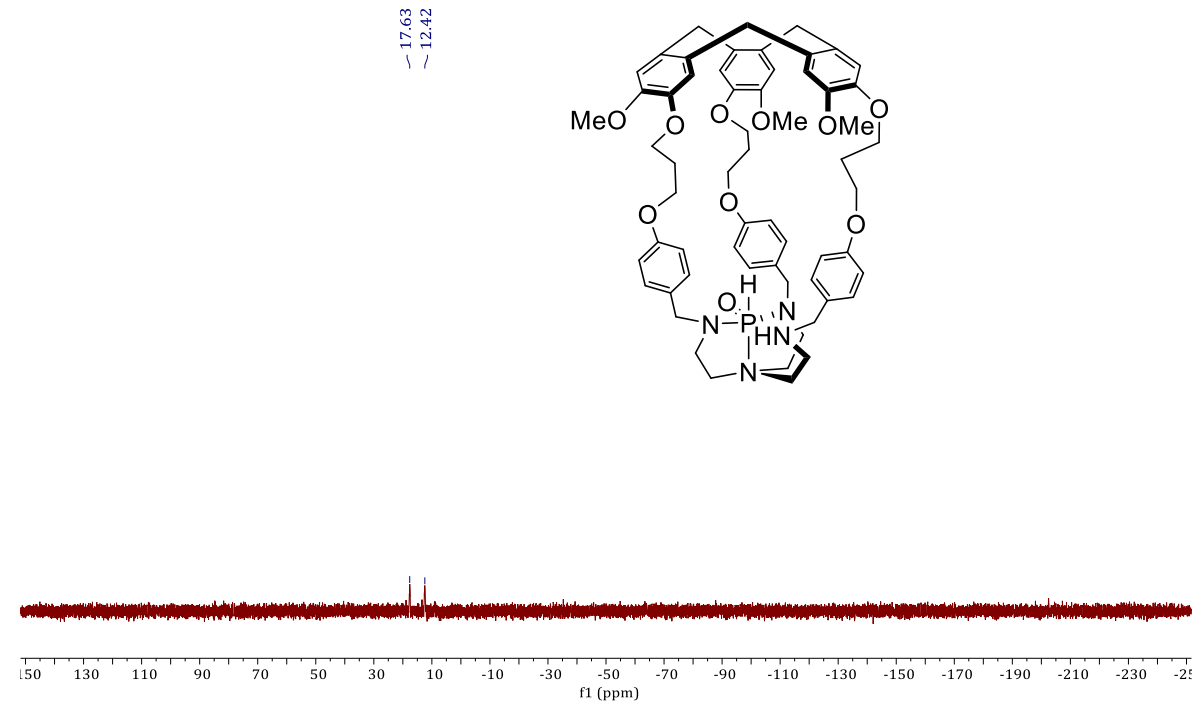

Figure S64 ^{31}P NMR (162 MHz, $CDCl_3$) spectrum of **103-PH=O**.

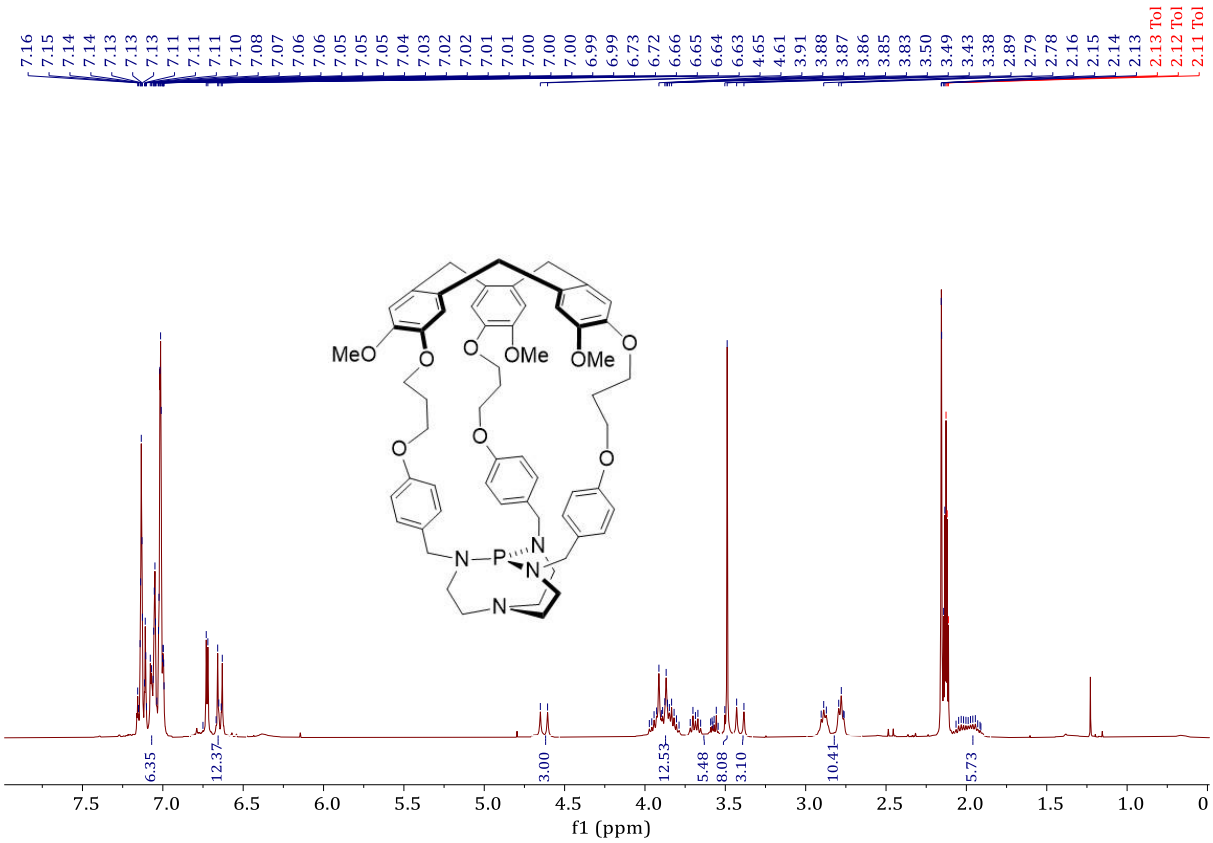

Figure S65 ^{1}H NMR (162 MHz, Toluene) spectrum of hemicryptophane **103.**

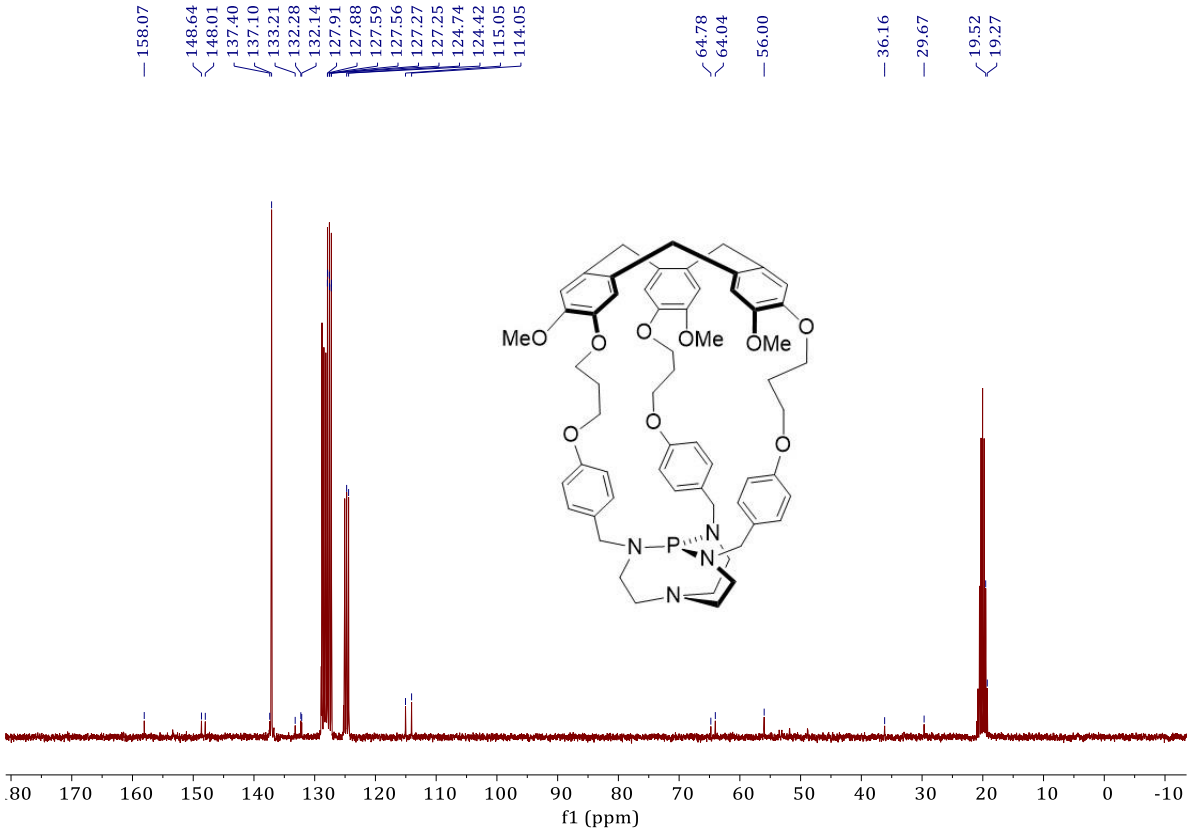

Figure 66 ^{13}C NMR (101 MHz, toluene) spectrum of hemicryptophane **103.**

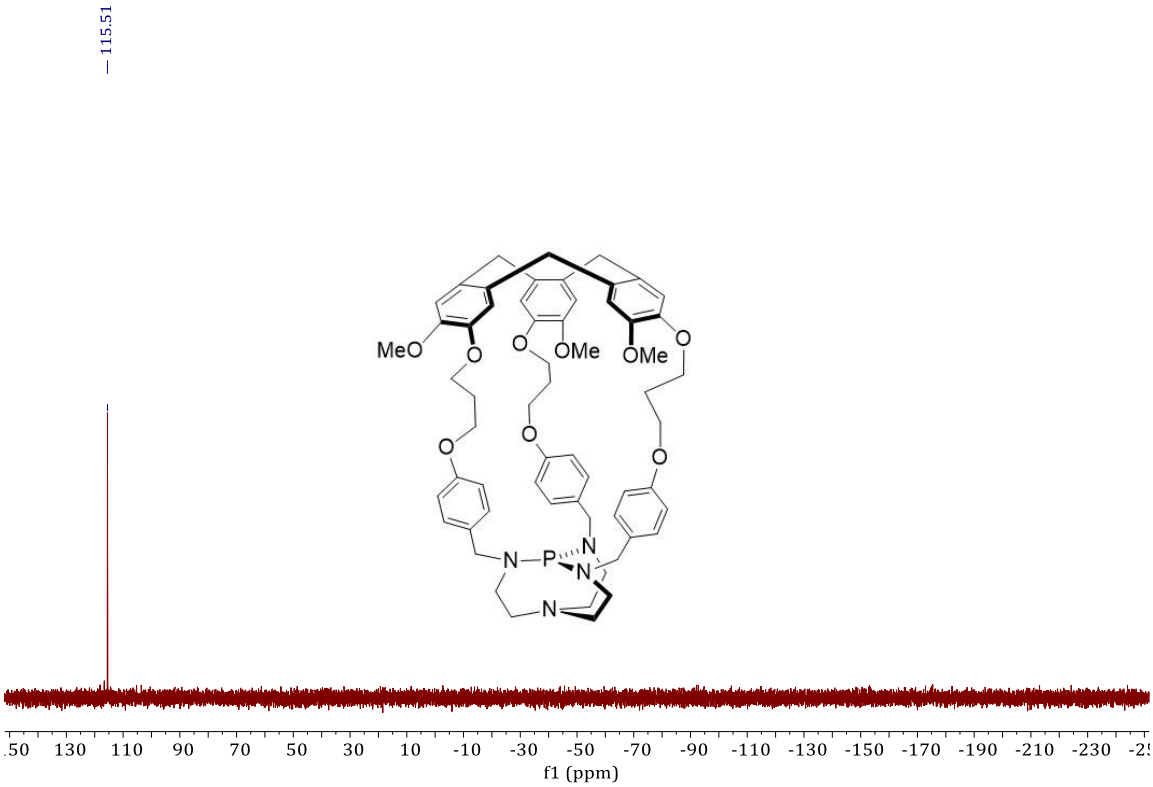

Figure S67 ^{31}P CPD NMR (121 MHz, $CDCl_3$) spectrum of **103.**

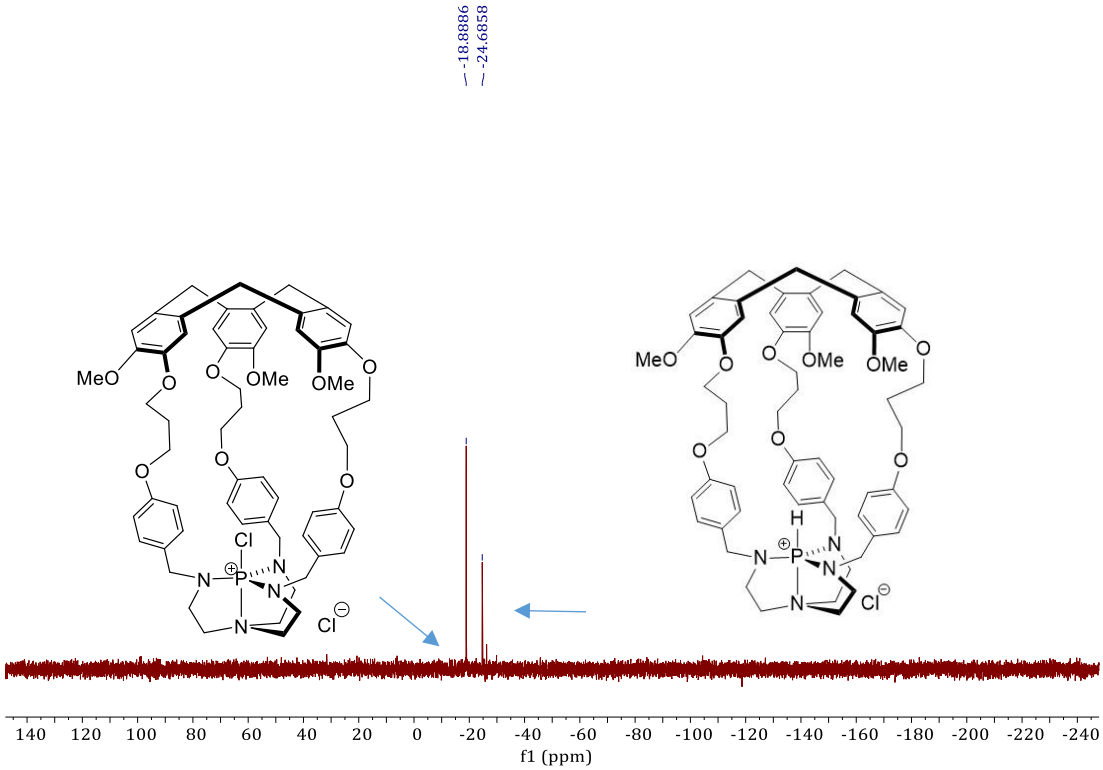

Figure S68 ^{31}P CPD NMR (121 MHz, $CDCl_3$) spectrum of MBH reaction.

RESUME Dans cette étude, nous nous concentrons sur les dérivés d'Azaphosphatranes : études sur leurs propriétés de donneurs de liaisons halogènes, leurs comportements en tant que paires de Lewis/Bronsted frustrées confinées et leurs propriétés de reconnaissance chirale. Tout d'abord, nous avons synthétisé les chloroazaphosphatranes avec différents groupes substituants, et discuté de leurs constantes de liaison. Ensuite, nous avons synthétisé deux hémicryptophanes qui contiennent des cavités rigides, nous avons discuté de la chiralité inhérente et des résultats de la réactivité. Enfin, nous avons synthétisé deux autres hémicryptophanes pour discuter de leurs propriétés de reconnaissance envers les neurotransmetteurs, et nous nous sommes également concentrés sur les études thermodynamiques et cinétiques, nous avons finalement calculé la valeur du pKa, et les constantes de vitesse. En outre, nous avons discuté d'un véritable système FLP en présence de $TiCl_4$.

MOTS-CLES Chimie supramoléculaire, Hémicryptophanes, Chloroazaphosphatranes, Catalyse en milieu confiné, Complexes énantiopures, Contrôle de la chiralité

ABSTRACT In this study, we focus on the Azaphosphatranes derivatives: studies on their halogen-bond donor properties, their behaviors as confined Frustrated Lewis/Bronsted Pairs and their chiral recognition properties. Firstly, we synthesized the chloroazaphosphatranes with various substituent groups, and discussed their binding constants. Then we synthesized two hemicryptophanes which contain rigid cavities, we discussed the inherent chirality and the reactivity outcome. Last, we synthesized two other hemicryptophanes to discuss their recognition properties toward neurotransmitters, and also we focus on the thermodynamic and kinetic studies, we finally calculated the value of pKa, and the rate constants. Besides, we discussed a true FLP system in the presence of $TiCl_4$.

KEYWORDS Supramolecular chemistry, Hemicryptophanes, Chloroazaphosphatranes, Catalysis in confined space, Enantiopures complexes, Chirality control